# A LOWER UPPER-BOUND APPROACH TO SOME METAL FORMING PROBLEMS

A THESIS

Presented to

The Faculty of the Graduate Division

by

Vijay Nagpal

In Partial Fulfillment

of the Requirements for the Degree

Doctor of Philosophy

in the School of Mechanical Engineering

Georgia Institute of Technology

August, 1974

A LOWER UPPER-BOUND APPROACH TO SOME

METAL FORMING PROBLEMS

APPROVED:

Chairman,
Dr. E. E. Underwood, Chairman, M.E.

Dr. J. M. Bradford, M.E.

Dr. David Kalish, M.E.

Dr. J. M. Anderson, E. S. M.

Dr. E. Starke, Ch.E.

Date June 7, 1974

## ACKNOWLEDGMENTS

I wish to express my appreciation to all those individuals who have encouraged, helped and guided me in doing this research. I am indebted to the late Dr. W. R. Clough, who suggested the topic of this thesis and also encouraged me in achieving my professional goals. His untimely death during the course of this study was a great personal loss. I am also gratefully indebted to Dr. E. E. Underwood, who served as my thesis advisor after Dr. Clough's death and under whose guidance this thesis was completed. I wish also to thank the other members of my thesis committee, Drs. J. M. Bradford, D. Kalish, J. M. Anderson, and E. Starke, for their review of this work.

I would like to dedicate this thesis to my wife Kamini and to my parents for their continued love, encouragement, and patience in the pursuance of my education.

TABLE OF CONTENTS

# LIST OF ILLUSTRATIONS

Figure Page

# LIST OF TABLES

## SUMMARY

In this thesis, a generalized analytical upper bound approach to the solution of some metal forming problems is proposed. The approach allows variations in the assumed kinematically admissible models in order to yield lower upper-bounds on forming pressures. The analysis presents a method for selecting a general kinematically admissible model for any metal forming problem. This method uses the characteristic features of a flow function. The admissible models are obtained in terms of some arbitrary functions or constants through which the models can be varied independently of the kinematic conditions. General expressions for the upper bound on average forming pressures are obtained and then minimized to yield lower upper-bounds. Such solutions are obtained for the following metal forming problems:

1. Extrusion through arbitrarily shaped dies based on plane strain and axisymmetric conditions. The solution of the plane strain case is extended to include an upper bound analysis of ironing of cups in the deep drawing process.

2. Forging of rectangular and cylindrical workpieces based on plane strain and axisymmetric conditions, respectively.

The analyses show that many of the upper bound solutions proposed by others for the above problems are only special cases of the general models obtained from the flow function concepts used in this work. Comparison of numerical results with existing theoretical solutions and experimental work indicates that the proposed upper-bound approach is capable of predicting

closely the forming loads and also the deformation characteristics of the processes analyzed.

# CHAPTER I

# INTRODUCTION

## Definition of the Problem

This research investigates some metal forming problems with an analytic upper bound approach which allows variations in the assumed kinematically admissible models for the processes with the purpose of obtaining better upper bound solutions. The research devises an approach for the formulation of a general kinematically admissible model for any metal forming process. Specific problems are then analyzed using the concepts of the proposed upper bound approach. The following problems are treated:

1. Steady state extrusion or drawing of a rigid-perfectly plastic material through any arbitrarily shaped die. Both plane strain and axisymmetric flows are considered. The die profile is not originally defined and thus the analysis is applicable to all possible die shapes. The process of ironing of cups in deep drawing is analyzed as an extension of the plane strain problem.

2. Cold forging of rectangular and cylindrical workpieces based on plane strain and axisymmetric conditions, respectively. The material of the workpiece is again assumed to be rigid-perfectly plastic.

## Review of the Literature

### General

The mechanics of the deformation occurring in most metal forming

processes is very complex and becomes even more so if the many metallurgical variables affecting the work material are taken into account. All theoretical methods of solving metal forming problems are based on simplified assumptions regarding material properties and process conditions. Metallurgical variables such as grain size, internal defects like dislocations, nonhomogeneities in structure, etc. are normally neglected in most all classical methods of solution. The problem is thus treated purely from a continuum mechanics point of view. Further approximations are made to simplify the solutions. Where possible, the effects of temperature and strain rate are neglected as these can not be adequately taken into account in plasticity theory with the present state of knowledge.

Even with all these assumptions, mathematically exact solutions can be obtained for only a few problems where symmetry or the homogeneity of deformation simplifies the formulation. Metal forming problems such as extrusion of a rod through a curved die or forging under frictional conditions which involve nonhomogeneous deformation usually require further simplification and therefore further approximations regarding material properties are made. Anisotropy of the material undergoing deformation is neglected and in many cases even the strain hardening is not accounted for and the material is assumed to be perfectly plastic. Clearly these assumptions limit the usefulness of solutions for real materials, yet of necessity these assumptions must be made if any solution at all is desired. It is quite common to account for these material properties in an approximate manner after the solution is obtained. Most metal forming problems involving nonhomogeneous deformation

still defy exact solution and are thus treated by various approximate methods.

The General Problem. The solution of a general problem of plastic deformation involves a solution of the following:

(a) The static equilibrium equations

$$\frac{\partial \sigma_{ij}}{\partial x_j} + X_i = 0 \tag{1.1}$$

where $\sigma_{ij}$ is the stress tensor and $X_i$ is the body force per unit volume. In the absence of body forces, there are six unknown stress components in these three equilibrium conditions.

(b) The instantaneous yield condition. One of the simplest is the von Mises yield condition

$$\sigma'_{ij}\,\sigma'_{ij} = 2k^2 \tag{1.2}$$

where $\sigma'_{ij}$ is the deviatoric stress tensor and k is the yield stress in shear.

(c) The six plasticity equations. Most commonly used are the Prandtl-Reuss equations

$$d\epsilon'_{ij} = \frac{3}{2}\sigma'_{ij}\frac{d\bar{\epsilon}^{*p}}{\bar{\sigma}^*} + \frac{d\sigma'_{ij}}{2G} \tag{1.3}$$

where $\epsilon'_{ij}$ is the deviatoric strain tensor, $\bar{\sigma}^*$ and $\bar{\epsilon}^*$ are the effective stress and strain respectively, and G is the modulus of rigidity. The six equations (1.3) can be written in terms of displacement (u,v,w) and the

stress components.

There are thus ten unknowns and ten independent equations and an exact solution is theoretically possible. However, except when some simplifications can be made from symmetry or other considerations, no general method exists by which solution may be obtained for all metal forming problems.

Plane Strain Deformation. The general problem of plastic deformation is greatly simplified if deformation occurs under plane strain conditions. A state of plane strain is defined by the properties that the flow is everywhere parallel to a given plane, say the (x,y) plane, and that the motion is independent of z. The set of equations (1.1), (1.2) and (1.3) reduce to the following five equations with five unknowns for plane strain deformation of an isotropic rigid-perfectly plastic material [1].

Equilibrium equations:

$$\frac{\partial \sigma_{xx}}{\partial x} + \frac{\partial \sigma_{yx}}{\partial y} = 0$$
$$\frac{\partial \sigma_{yx}}{\partial x} + \frac{\partial \sigma_{yy}}{\partial y} = 0 \qquad (1.4)$$

Yield criterion:

$$(\sigma_{xx} - \sigma_{yy})^2 + 4\sigma_{xy}^2 = 4k^2 \qquad (1.5)$$

Velocity equations:

$$\frac{\partial \dot{u}_x}{\partial x} + \frac{\partial \dot{u}_y}{\partial y} = 0 \qquad (1.6)$$

$$\frac{2\sigma_{xy}}{\sigma_{xx}-\sigma_{yy}} = \frac{\partial\dot{U}_x/\partial y + \partial\dot{U}_y/\partial x}{\partial\dot{U}_x/\partial x - \partial\dot{U}_y/\partial y} \tag{1.7}$$

$(\dot{U}_x, \dot{U}_y)$ are the components of velocity in x and y directions respectively. Most problems which have been solved exactly fall under the category of plane strain deformation. A general theory, the so called 'Slip-Line Field Theory' has been developed to solve problems involving homogeneous as well as nonhomogeneous plane strain deformation of a rigid-perfectly plastic material.

Axisymmetric Deformation. If a cylindrical coordinate system $(r,\theta,z)$ is chosen to represent axisymmetric deformation with z as the axis of symmetry, then the stress and velocity are independent of $\theta$, and are functions only of r,z and the time. The flow is confined to meridian planes. The set of equations (1.1), (1.2) and (1.3) reduce to the following seven equations with seven unknowns, when the elastic strains are neglected.

Equilibrium equations:

$$\frac{\partial\sigma_{rr}}{\partial r} + \frac{\partial\sigma_{rz}}{\partial z} + \frac{\sigma_{rr}-\sigma_{\theta\theta}}{r} = 0$$

$$\frac{\partial\sigma_{rz}}{\partial r} + \frac{\partial\sigma_{zz}}{\partial z} + \frac{\sigma_{rz}}{r} = 0 \tag{1.8}$$

Yield criterion of von Mises:

$$(\sigma_{rr}-\sigma_{\theta\theta})^2 + (\sigma_{\theta\theta}-\sigma_{zz})^2 + (\sigma_{zz}-\sigma_{rr})^2 + 6\sigma_{rz}^2 = 6K^2 \tag{1.9}$$

Levy-Mises relations:

$$\dot{\epsilon}_{rr} = \frac{\partial \dot{U}_r}{\partial r} = \dot{\lambda}\left(2\sigma_{rr} - \sigma_{\theta\theta} - \sigma_{zz}\right)$$

$$\dot{\epsilon}_{\theta\theta} = \frac{\dot{U}_r}{r} = \dot{\lambda}\left(2\sigma_{\theta\theta} - \sigma_{zz} - \sigma_{rr}\right) \qquad (1.10)$$

$$\dot{\epsilon}_{zz} = \frac{\partial \dot{U}_z}{\partial z} = \dot{\lambda}\left(2\sigma_{zz} - \sigma_{rr} - \sigma_{\theta\theta}\right)$$

$$2\dot{\epsilon}_{rz} = \left(\frac{\partial \dot{U}_r}{\partial z} + \frac{\partial \dot{U}_z}{\partial r}\right) = 6\dot{\lambda}\sigma_{rz}$$

where $(\dot{U}_r, \dot{U}_\theta, \dot{U}_z)$ are the velocity components in r, $\theta$ and z directions, $\dot{\epsilon}_{ij}$ is the strain rate tensor and $\dot{\lambda}$ is a positive quantity related to the effective stress and strain. Whereas the theory of plane strain is well developed and the method of solving specific problems is well understood, there is at present nothing similar for axial symmetry. It is, for example, not clear how to construct, in principle, the solution of mixed boundary-value problems such as cone indentation or wire drawing.

Methods of Solution of Forming Problems

Slip-Line Field Theory. In many metal forming processes where material undergoes large plastic strains, elastic strains can safely be neglected. The material can thus be treated as rigid-plastic. Nonhomogeneous plane strain deformation of a rigid-perfectly plastic material can be treated by slip-line field theory. It has been shown that equations (1.4) to (1.7) of plane strain deformation are hyperbolic and the

characteristics are lines of maximum shear stress called slip-lines [1]. Methods are available for the construction of slip line nets for various boundary-value problems. From a knowledge of the stress state at any point on a slip line, the stress state of other points along the slip line may be computed through the use of a set of relationships first derived by Hencky [2]. The velocity distribution for the slip-line field may also be determined through a similar set of relations proposed by Geiringer [3].

Slip line theory has been used extensively for plane strain deformation [1]. The analysis is generally limited to the behavior of a rigid plastic, non-workhardening material when temperature and strain rate effects are neglected. Attempts [4] have been made to include work-hardening of material in the framework of the theory but still no general procedures have been developed to solve problems of forming strain hardening materials. Aside from the idealizing assumptions made concerning the work material, slip line solutions lack uniqueness and more than one solution fits a particular set of boundary conditions [5]. In addition, most slip line solutions are incomplete, i.e., while the rate of plastic work may have been determined to be positive throughout the deforming regions, the stress state in the assumed rigid regions has not been examined [6].

Slip line theory is strictly applicable only to plane strain deformation. Attempts [7] have been made to solve axisymmetric problems by assuming an artificial yield condition suggested first by Haar and von Karman which makes the equations analogous to the plane strain equations. Shield [8] has shown, however, that when the Tresca yield

criterion and associated flow rule are employed, the governing equations are kinematically or statically determinate in character. The statically determinate case arises when the heuristic hypothesis of Haar and von Karman is satisfied. The stress and velocity fields are then hyperbolic with identical families of characteristics. The equations along slip lines are however more difficult to handle compared to those for plane strain and are generally employed in their finite difference form. Except for some simple problems, slip line theory has not been applied successfully to solution of axisymmetric problems.

Visioplasticity Method. Thomsen and co-workers [9,10] have developed a visioplasticity technique which consists of analyzing the distortion of grids inscribed on a plane of symmetry using the differential equations governing plastic flow. The velocity components, strain rate and stress distribution are obtained from the experimentally determined flow lines by the use of a computer technique [11]. The visioplasticity method supplies all the required information about the mechanics of the process and can be applied to both plane strain and axisymmetric deformation problems. However, the usefulness of this method is limited by the fact that an experiment must be performed first before a solution can be obtained.

Slab Method. One of the earlier methods which is still commonly employed to solve metal forming problems is the slab method. Sachs[12] and Siebel [13] apparently were the authors who introduced it. Here, equilibrium of a slab of the deforming body is considered assuming a simplified stress distribution for the slab. The governing equations are solved and an approximate solution for the forming forces is obtained.

The slab method has been used extensively to obtain approximate solutions to many metal forming problems [6]. The method is simple but the assumption of simplified stress introduces errors of unknown magnitude. Also, since it is generally assumed that friction forces do not affect the internal stress distribution in the slab, this method tends to give erroneous results for problems involving high frictional forces.

Finite Element Method. Very recently finite element method has been pressed into use to solve some metal forming problems [14,15]. In many forming problems, the geometrical configuration of the deforming body changes continuously during the process and these changes in shape can be determined only by following the path of deformation. Where further deformation maintains the original geometry, slip-line field theory can be used to provide solution to plane strain deformation. Where the original geometry is not maintained, a step by step solution may be required for problems involving large plastic deformations. The finite element method, which also provides only an approximate solution, can successfully be applied to such problems.

Upper Bound Method. Because of the difficulty of obtaining exact solutions to metal forming problems, extremum principles are being used increasingly to solve metal forming problems [16]. From the extremum principles are derived the Limit-Load theorems [17-19] which form the basis for the upper bound and the lower bound methods of solving plasticity problems. These methods, as the names suggest, are used to obtain upper bounds and lower bounds on the required quantity of interest, which is usually the power required to form or the average forming pressure.

In the lower bound method, a statically admissible stress field

which satisfies equilibrium and yield conditions is assumed for the deforming body. No attempt is made to satisfy velocity or strain rate conditions. The power required to form the material, when obtained from the assumed fictitious admissible stress field, gives a lower bound on the actual power. Some applications of this method are given in References [16,20].

The upper bound method, which is of main interest to this work, is based on one of the Limit-Load Theorems now commonly known as the Upper Bound Theorem. The theorem was formulated by Prager and Hodge [17] and later modified by Drucker, et al. [18,19] to include velocity discontinuities. Hill [1,22], however, had published certain work principles from which this theorem was deducible. For a rigid-perfectly plastic material, the theorem reads:

Among all kinematically admissible strain rate fields $\dot{\varepsilon}_{ij}^{*}$ , the actual one minimizes the expression

$$J^{*} = \frac{2}{\sqrt{3}} \sigma_o \int_V \sqrt{\tfrac{1}{2} \dot{\varepsilon}_{ij}^{*} \dot{\varepsilon}_{ij}^{*}} \, dV + \int_{S_T} \tau \, |\Delta v^{*}| \, dS_T^{*} - \int_{S_T} T_i v_i^{*} \, dS \qquad (1.11)$$

$J^{*}$ is the upper bound on power, V is the volume of the deforming zone, $\tau$ is the shear stress, $S_T$ is the surface of velocity discontinuity, $\Delta v^{*}$ is the tangential velocity discontinuity along $S_T$, $T_i$ are external tractions, $v_i^{*}$ are velocities and $S_T$ is the surface over which the tractions are exerted. The first term of expression (1.11) represents the internal power for deformation over the volume of the deforming body. The second term includes the shear power over surfaces of velocity discontinuity including the boundary between tool and the material. The

last term covers the power supplied by predetermined body tractions.

In the upper bound method, the approach to solve any steady state problem is to select a kinematically admissible velocity field ($v_i^*$) or strain rate field ($\dot{\varepsilon}_{ij}^*$) by dividing the deforming body in different zones which may be separated by surfaces of tangential velocity discontinuity ($S_r^*$). In principle, therefore, one constructs a solution by assuming an admissible deformation model and obtains from it upper bounds on certain quantities by the use of Upper Bound Theorem. Since stress conditions are not necessarily satisfied, there are, in general, infinite admissible velocity fields for any problem. According to the Upper Bound Theorem, among these admissible velocity fields, the actual one yields the minimum upper bound on power required. It is generally not feasible to get the exact solution by upper bound method but a close approximate solution can be obtained by trying different kinematically admissible velocity fields and selecting the one which yields the lowest upper bound.

Numerous applications of the upper bound method to metal forming problems have appeared in the literature in recent years [16]. A number of approaches which differ primarily in the selection of admissible velocity fields have been presented. Hill [21] gave an upper bound solution for drawing through wedge shaped dies by dividing the deforming body into rigid blocks with straight surfaces of velocity discontinuity as shown in Figure 1. Green [23] and Johnson [24-26] used the same method in a number of solutions to other plane strain forming problems. Later Kudo [27] modified this approach and introduced the concept of dividing the body into unit deformation blocks, obtaining lower upper-bounds by changing the shape and number of these unit blocks. These solutions have

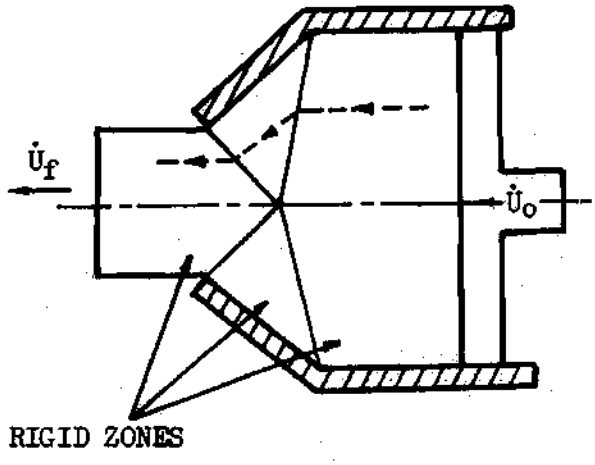


Figure 1. Assumed Rigid Zones for Extrusion through Symmetrical Wedge-Shaped Die. (After Hill [21])

the drawback that the assumed mode of deformation is, in most cases, not realistic and even though a good approximation to applied power may be obtained, the approximation to actual strain rates is poor [28]. Another drawback is that the upper bounds on power are restricted by the assumption that the deforming body consists only of rigid blocks separated by plane surfaces of velocity discontinuity.

Kudo [29] extended the concept of the unit rectangular deforming region to the analysis of axisymmetric forming problems and introduced the unit cylindrical region. He obtained upper bound solutions using parallel-velocity fields and triangular-velocity fields consisting of straight conical discontinuity surfaces. Kobayashi [20,30] suggested curved discontinuity surfaces for the unit regions which resulted in better upper bounds for some axisymmetric problems. Velocity patterns in kobayashi's analyses were selected by assuming a constant axial velocity component or a radial velocity component of form $\dot{U}_r=Ar^m$ for the deforming body. A and m are some constants.

Stepanskii [31] presented a different upper bound approach for plane strain extrusion through wedge shaped dies. He assumed a continuous radial velocity field for the plastic zone in terms of an arbitrary admissible function. By optimizing this function by variational techniques, he obtained lower upper-bounds[1] and curved shapes for the boundaries separating plastic zone from rigid zones (see Figure 2). Zimerman and Avitzur [32] extended Stepanskii's analysis to include a

---

1. The use of term "lower upper-bound" is preferred to "minimum upper bound" because the minimum is, in these cases, restricted by the form of velocity field assumed and is not the absolute minimum.

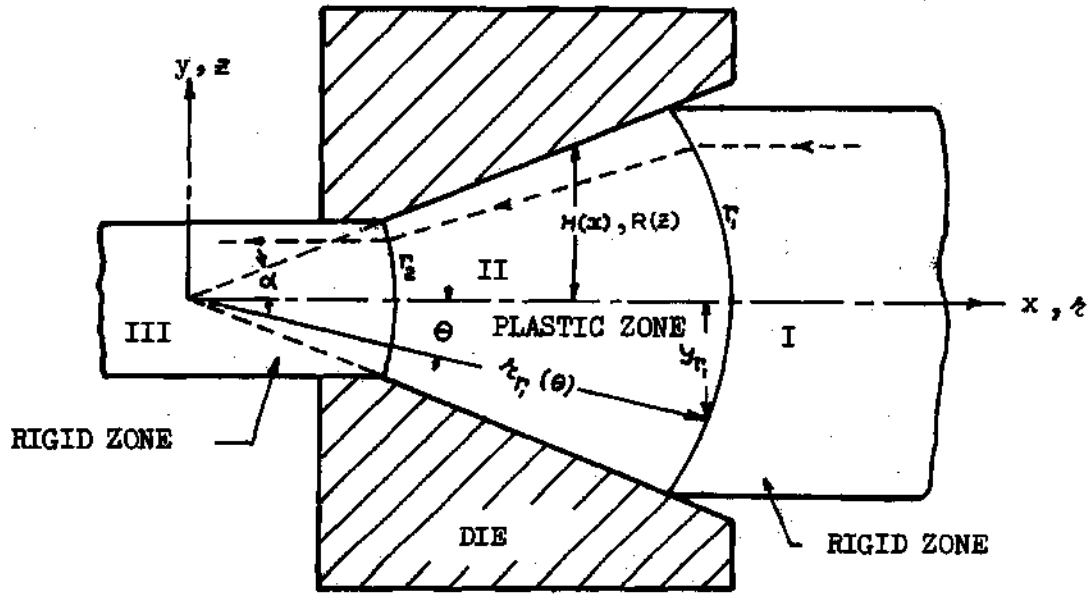


Figure 2. Flow through Wedge-Shaped Die (After Stepanskii [31])

lower upper-bound solution for axisymmetric extrusion through a conical die. Comparison with experimental data shows that the assumption of a continuous velocity field with curved plastic zone boundaries gives a better approximation to the actual strain rate field [28]. The above solutions assumed a radial velocity field and are, therefore, applicable only to flow through straight converging dies. Avitzur [16] has derived upper bound solutions for other forming problems assuming a continuous velocity field for the plastic zone. Most of his solutions are not general upper bound solutions in the sense that no attempt is made to determine lower upper-bounds.

All of the above cited work on upper bound solutions considered only straight tools or dies. In general, these approaches cannot be extended to the solution of problems involving curved tools or dies. Johnson [33] obtained upper bound solutions to plane strain extrusion through circular dies by dividing the deforming body into rigid blocks with circular surfaces of velocity discontinuity. His solutions are applicable only to flow through circular dies under plane strain conditions. Also the upper bounds are restricted by the assumption that the deforming body consists only of rigid blocks separated by circular surfaces of velocity discontinuity. Chen and Ling [34] and Chen [35] presented a method of selecting continuous admissible velocity field for the plastic zone by use of a stream function and obtained upper bound solutions for extrusion through some special curved dies. Recently Chang and Choi [36] extended their analyses to the case of extrusion through any curved die. In these solutions, no attempt was made to determine lower upper-bounds.

From the above brief review of the literature, it is apparent that the upper bound approach, which assumes a continuous velocity field for the plastic zone, gives more realistic solutions. However, no general solutions, which allow minimization of upper bounds, have been presented for metal flow through curved dies. Also most of the other solutions to metal forming problems involving flat tools or dies are restricted in their analysis by a priori assumptions regarding the shape of boundaries or the velocity field of the plastic zone.

## Objectives

The main aim of this proposed investigation is to devise an analytical approach which allows formulation of lower upper-bound solutions for some metal forming problems involving curved and straight tools and which does not restrict a priori the shape of boundaries or the velocity field. Using the proposed approach, specific metal forming problems stated under "Definition of the Problem" are analyzed.

## Some Metal Forming Problems

A brief description of the forming problems investigated in this research along with a review of the existing work that has been done in the literature is now presented.

### Steady State Plane Strain Flow through An Arbitrarily Shaped Die

The problem investigated here is the steady state flow of a billet of rigid-perfectly plastic material through a die of arbitrary shape, when the deformation occurs under plane strain conditions (see Figure 3). The interest is to determine theoretically the pressure required for deformation and the effects of parameters such as shape of the die, length

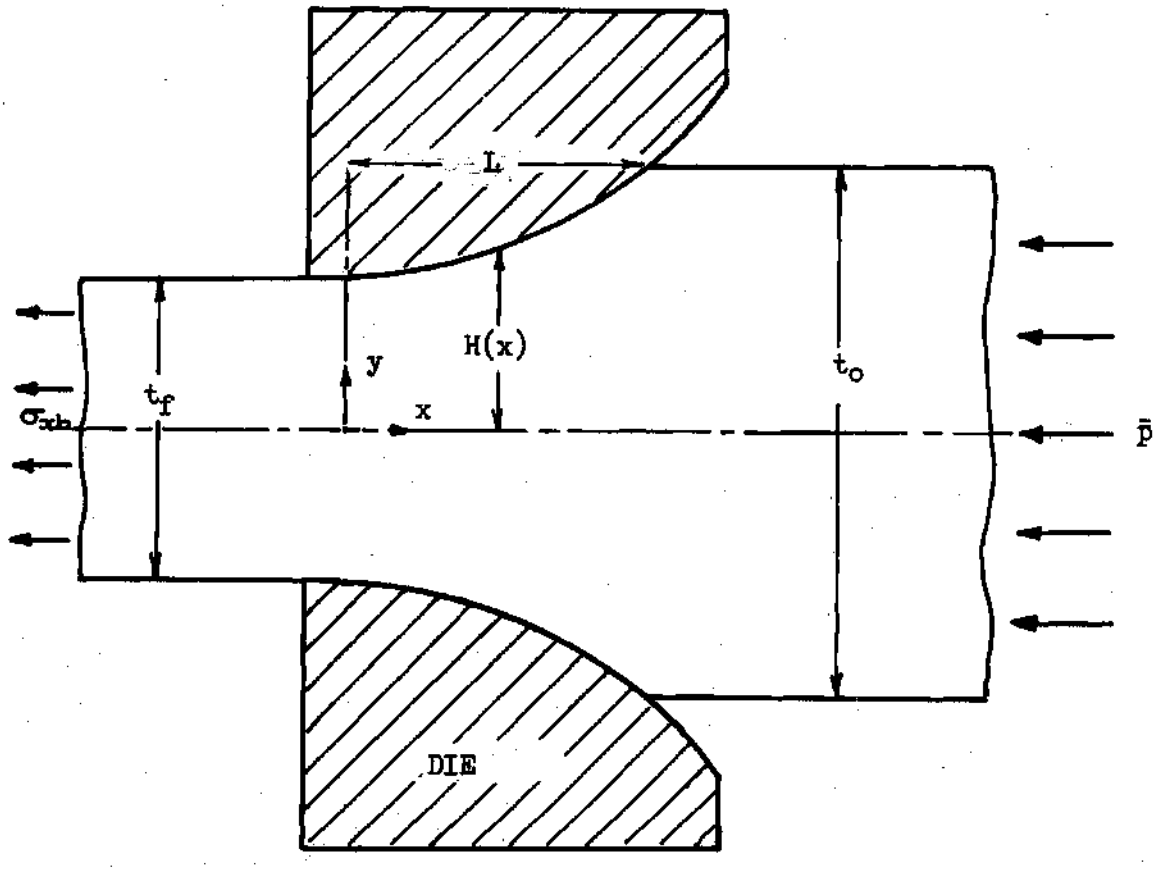


Figure 3. Flow through An Arbitrarily Shaped Die

of the die, reduction in thickness of billet, friction at die surfaces, etc., on forming pressure and deformation of the material.

The flow of a rigid-perfectly plastic material through wedge shaped dies has been analyzed extensively. Hill [1] constructed the first slip-line field for the sheet-drawing process which satisfied both stress and velocity requirements and adequately accounted for inhomogeneous deformation. The effect of friction and modification of the slip-line field for certain reductions have been discussed by Hill and Green [37]. Stepanskii [31] proposed a generalized upper bound solution for the problem of extrusion through wedge shaped dies. Using a special velocity field, Avitzur, et al. [38] present a simple but comprehensive upper bound solution which depicts the effect of various process parameters and the characteristics of the flow of the material. In the latter two quoted works, the authors assumed surfaces of tangential velocity discontinuity in constructing kinematically admissible models. Using the flow function concept and by superimposing basic flow patterns, Lambert and co-workers [28] derived kinematically admissible velocity fields without any tangential velocity discontinuity. Shabaik, et al. [39] analyzed extrusion through wedge dies using potential flow theory which also utilized a model without velocity discontinuities.

The construction of slip-line fields for drawing or extrusion through curved dies is difficult to develop because the boundary conditions are very complex. Sokolovskii [40] has given a detailed account of how to solve the problem of strip drawing or extrusion through a frictionless die of arbitrary contour for certain reductions. The solution formulated requires a discontinuity to exist in the tangential component

of velocity across certain slip planes. Johnson and Hilliar [41] , Kronsjö and Mellor [42],and Sowerby, Johnson and Samanta [43] have proposed slip-line field solution for extrusion through convex and concave dies. In their solutions, however, the die shapes are not fixed a priori and are obtained only after the velocity diagrams have been constructed. Samanta [44] was probably the first to propose slip-line fields for drawing through cosine die where the die shape is fixed before a solution is obtained. Numerical construction of such slip-line fields involves heavy computational work in order to evaluate the effects of various process variables.

No general upper bound solution has been offered for drawing or extrusion through curved dies. As stated earlier, Johnson [33] proposed upper bound solutions for circular dies using circular surfaces of tangential velocity discontinuity. His solution, however, cannot be extended to dies of other shapes. Chen [35] presented simple upper bound solutions for extrusion through cosine, elliptic and hyperbolic dies. Chang and Choi [36] extended Chen's analysis to the general case of any curved die. In their solution, the boundaries are assumed a priori to be vertical surfaces. Simple velocity fields are assumed for the plastic zone which are not affected by the frictional conditions at the die surface. The expression for upper bound on pressure cannot be varied independent of velocity conditions to yield lower upper-bounds and a close approximate solution thus is not obtained for all process conditions.

The intent here is to present a generalized upper-bound solution which allows the upper bound on pressure to be minimized. Moreover, this solution should give the best approximate deformation model for any given

set of process variables so that the effects of these variables on deformation process may be studied.

Steady State Axisymmetric Flow through Arbitrarily Shaped Die

The problem investigated is the steady state flow of a rod of rigid-perfectly plastic material through a die of arbitrary shape when the deformation occurs under axisymmetric conditions. The interest here is to determine theoretically the pressure required for deformation and the effect of parameters such as shape of the die, length of the die, reduction in area and friction at the die surface on pressure and the deformation of the material.

Whereas the slip-line field method has been applied with great facility to solutions for flow through dies under plane strain conditions, solutions treating axisymmetric flow are not forthcoming primarily because the basic equations are not hyperbolic and slip lines are not the characteristics in this case if the von Mises yield condition and associated flow rule is assumed. When the Tresca yield criterion and associated flow rule is applied, the resulting equations along slip lines are more complex and the construction of the slip line net is quite difficult. One of the metal forming problems analyzed by slip-line field theory is the construction of ideal die profiles for the frictionless drawing process where the additional condition of streamlined flow is available. Assuming the Haar and von Karman hypothesis, Sortais and Kobayashi [46] presented die profiles which eliminate as much redundant work as possible. Richmond and Morrison [47] obtained streamlined dies of minimum length for the same problem. Slip line solutions for flow through curved dies where the shape is fixed to begin with have not been proposed.

For the particular case of flow through conical dies, upper bound solutions have been suggested [48-52,20,31,32]. Special note is given to the generalized upper bound solution presented by Zimerman and Avitzur [32] which adequately accounted for the effect of process variables. Flow through curved dies has not been treated extensively mainly because of the difficulty in forming a kinematically admissible model. Only recently, some authors [34,36,53] have presented simple upper bound solutions for axisymmetric extrusion of a rod through curved dies. Chen and Ling [34] were probably the first to analyze flow through a curved die. They presented solutions for cosine, elliptic and hyperbolic dies. Their analysis was extended by Chang and Choi [36] to the general case of a curved die of arbitrary shape. Samanta [53] used similar approach to analyze flow through a convex die. These authors in their respective analyses considered only some particular velocity fields and assumed fixed location and shape for the boundaries of the plastic zone. Such solutions have the drawback that the upper bound on forming pressure cannot be minimized to yield better bounds. Also, their solutions are not likely to give a close approximation to the actual flow field because the velocity field assumed in the analysis is not affected by interfacial friction at the die surface. Experimental data [54], however, show a strong dependence of flow field on friction conditions.

The intent in this portion of the research is to propose a theoretical generalized upper bound solution for the problem of steady state extrusion or drawing of a rigid-perfectly plastic material through a die of arbitrary shape. Moreover, this solution should predict the effects of various process variables such as reduction, shape and length

of die,and friction at die surfaces on the forming pressure and the deformation of the material.

Ironing of Cups in Deep Drawing

In an ordinary deep drawing process, the clearance between the punch and the die is usually about 130 to 150 percent of the thickness of the blank. However, when the clearance is smaller than the above range, a forced reduction in the thickness of the cup wall occurs during the process (see Figure 4). This is regarded as ironing of cups in the deep drawing process.

The process of simple deep drawing when no ironing takes place has been analyzed extensively and the literature is replete with an unusually large number of analyses. These range from the solution given by Chung and Swift [54] for a non-workhardening, isotropic material to the more complex picture of an anisotropic work-hardening blank as studied by Chiang and Kobayashi [55]and by Ray and Berry [56]. A solution which accounts for material characteristics and the effect of redundant work and die-profile friction has recently been presented by Berry and Pope [57]. On the other hand, the process of simple ironing of prior drawn cups has been analyzed. Hill [1] presented a slip-line field solution assuming the ironing process to be occurring under plane strain conditions. Barlow [58] and Alexander [59] analyzed this process using a slab method. Due to the similarity of ironing of prior drawn cups to tube drawing with a fixed mandrel, the upper bound method can also be used to analyze this process [16].

In spite of the fact that both of the principal processes that occur simultaneously during ironing in deep drawing have been studied

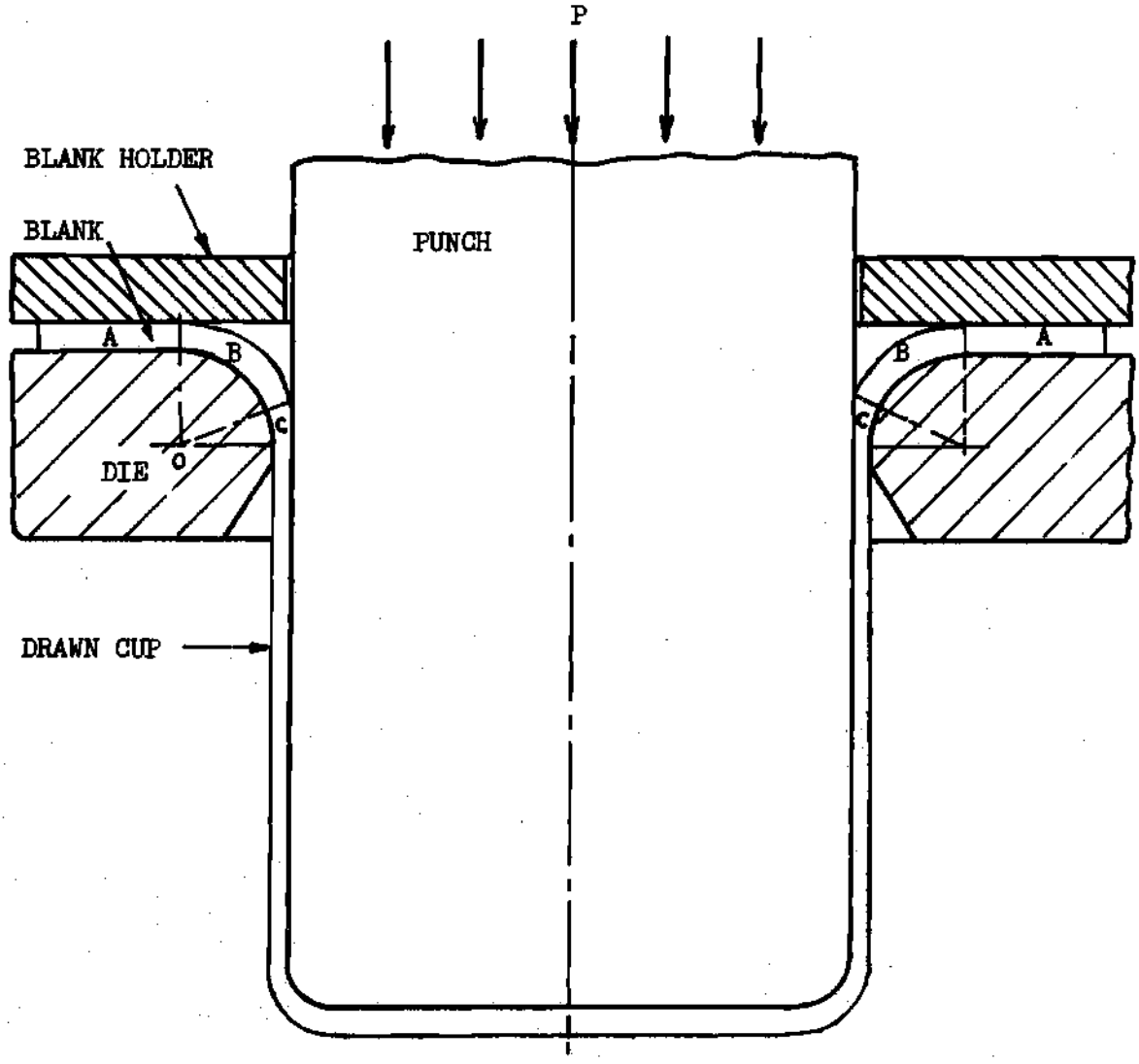


Figure 4. Deep Drawing with Simultaneous Ironing

separately, no suitable theoretical analysis has been proposed for the combined process. Previous theoretical analyses presented by others [58-60] regarded the simultaneous ironing process equivalent to tube drawing with initial tension caused by the drawing resistance over the flange. The deformation of material in ironing of cups, however, is quite different from tube drawing, as pointed by Kasuga, et al. [60]. In simultaneous ironing, the material bends over the die radius before a reduction in its thickness takes place as shown in Figure 9 of Reference [60] (reproduced and marked Figure 5 here). The material at the entry, therefore, has an initial curvature and forced reduction of this initially curved material takes place in the ironing of cups in the deep drawing process. No theoretical analysis has been presented which takes into account the curvature of the material before its thickness is reduced.

The intent of the investigation here is to analyze the process of simultaneous ironing of cups in the deep drawing process using a generalized upper bound approach so that the effects of process variables such as reduction in thickness by ironing, radius of the die, and friction may be evaluated. Radial drawing of the blank over the flange and its bending over the die profile in tension has been analyzed by others and is not treated here.

Plane Strain Forging

The problem to be investigated here is the open die forging of a rectangular block under plane strain conditions (see Figure 6). The purpose is to determine the effects of such process parameters such as the width to thickness ratio (w/t) of the block, friction at platen surfaces, etc., on the forging loads. Only the case where flat platens

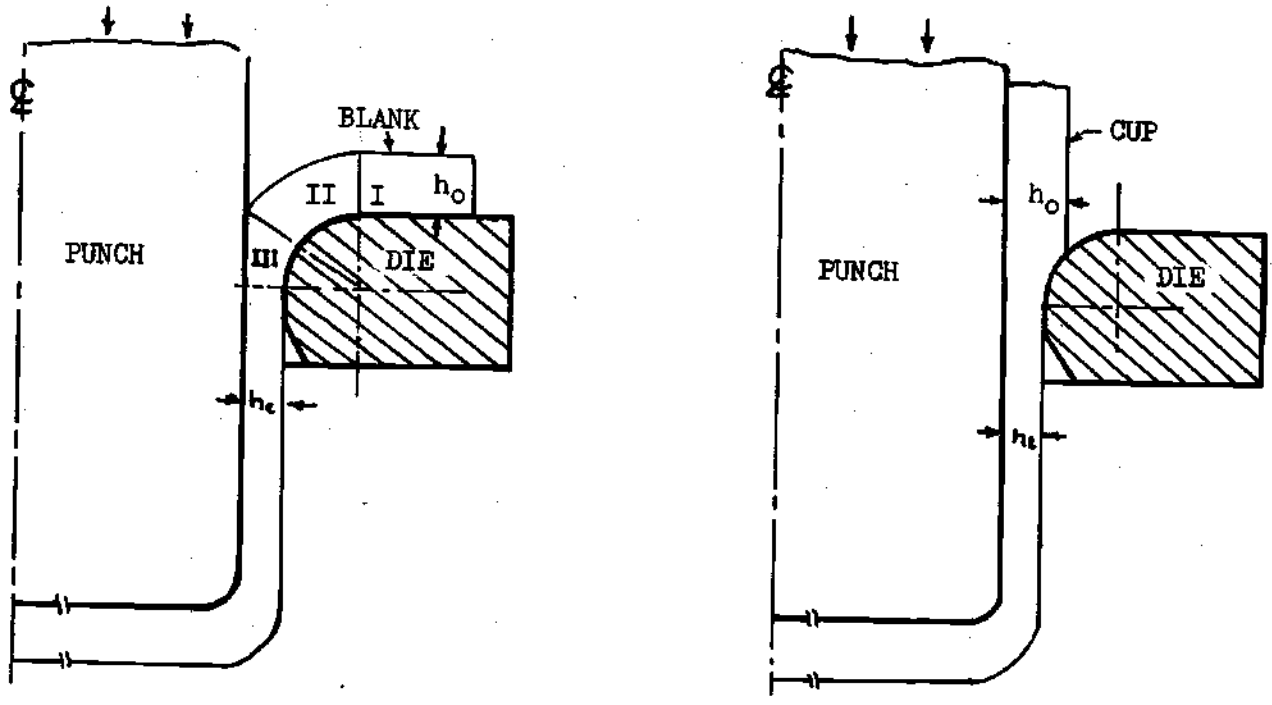


(a) Simultaneous Process

(b) Separated Process

Figure 5. Difference in Deformation in (a) Simultaneous Process of Ironing of Cups in Deep Drawing and (b) Separated Process in which Thickness of Cups is Reduced after Deep Drawing

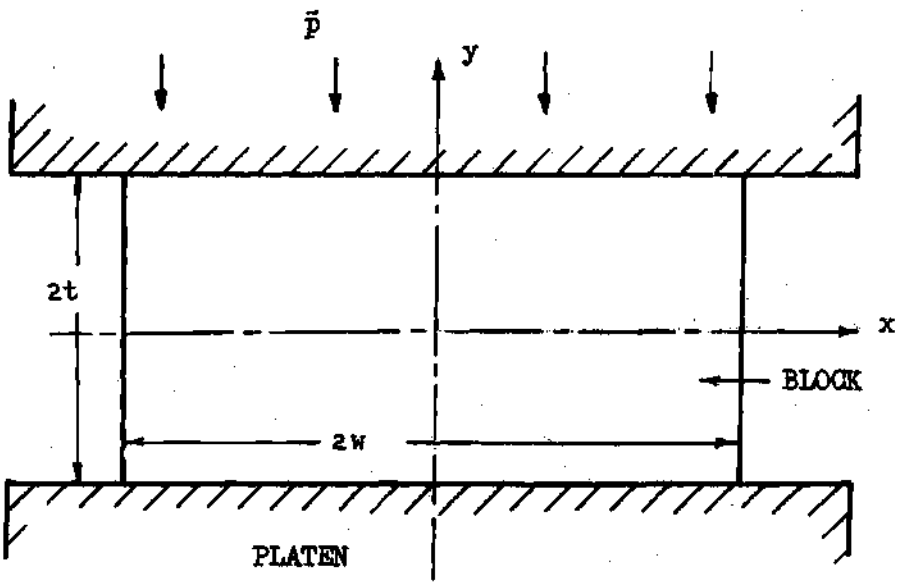


Figure 6. Forging of a Rectangular Block

overlap the rectangular block is investigated. The following review of the literature is restricted only to this case.

The problem of forging (compressing) a rectangular block of metal between rough parallel dies or platens was first investigated by Prandtl [61] who deduced that the slip lines were cycloids. The problem was later reconsidered by Hill, et al. [62] who showed that Prandtl's solution is only valid when the material and the die are of infinite width. A simple account of their work is given in Hill's book [1]. According to Hill, a slip-line field of the shape shown in Figure 7a is valid for compression of a rectangular block between perfectly rough overlapping platens for $w/t \geq 3.64$. For w/t between 3.64 and 6.72, the average pressure $\bar{p}$ over the platens at the yield point is found to depend on w/t ratio very nearly according to

$$\frac{\bar{p}}{2k} = \frac{3}{4} + \frac{1}{4}\frac{w}{t} \qquad (\text{for } w/t \geq 1) \qquad (1.12)$$

For compression between perfectly rough platens, when the w/t ratio lies between 3.64 and 1.00, a slip-line field as shown in Figure 7b is applicable. In this case, the rigid or dead zone between the block and the platens extends over whole width of the block. The right angle triangular region to the left of OA is stressed in pure compression and is displaced as a rigid whole. The solution continues to hold throughout subsequent compression so that, as remarked by Hill [1] , rather surprisingly there is no barrelling. The slip-line field solutions of Hill and co-workers do not explain bulging of free surfaces.

Alexander [63] presented slip line solutions for integral width

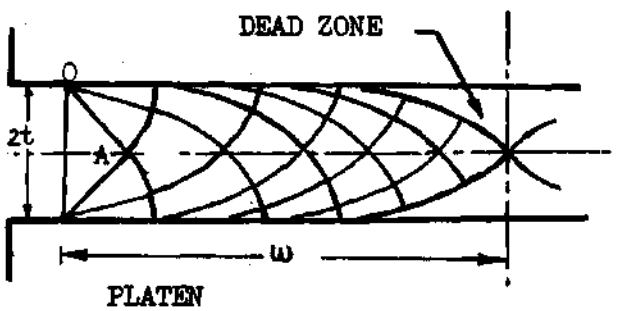


(a) Slip-Line Field Net for $w/t \geq 3.64$

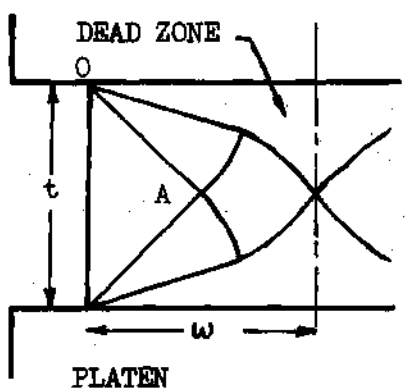


(b) Slip-Line Field Net for $1 \leq w/t \leq 3.64$

Figure 7. Slip-Line Solutions for Plane Strain Forging (After Hill [1])

to thickness ratios considering the effect of Coulomb friction at the faces of the parallel platens. He observed that for coefficients of Coulomb friction greater than 0.39, the yield shear stress is always attained along the complete zone of contact. Bishop [64] reviewed the work done by Hill and others and defined the range of friction coefficients in which a particular slip-line field solution is applicable. According to Bishop, the forging pressure is 2k for all coefficients of friction when $w/t \leq 1.0$. k is the yield stress in pure shear.

From the above review of slip-line field solutions, it is apparent that exact slip line solutions can be obtained in principle for all ranges of w/t ratios and frictional conditions. The slip line solutions, however, fail to account for barrelling which is indeed known to occur when the platens are not frictionless [65]. Siebel [66] has suggested a slip line solution which accounts for barrelling. However to justify his solution, it is necessary to assume that the coefficient of Coulomb friction ($\mu$) drops severely near the edge and may even become negative. Negative $\mu$, i.e., radially outward frictional shear stress, is not observed experimentally [65].

Because of the heavy computation work involved in constructing slip lines for each set of process parameters, approximate solutions have been proposed. Stone and Greenberger [67] and Hoffman and Sachs [68] presented solutions using the slab method. Due to the assumption of a simplified stress state, their solutions give reasonable approximations to exact solution only when coefficient of friction ($\mu$) is small. Hill obtained a simple upper bound solution by dividing the forging into unit rigid zones separated by straight surfaces of velocity discontinuity.

His work is reported by Green [23]. A similar approach was used by Kudo [27] and Johnson [24] in their analyses of upper bound solutions to the plane strain forging process. It may be noted that bulging of free surfaces is not accounted for by these solutions. Avitzur [16] presented an upper bound solution which takes into account the bulging effect. The velocity field assumed in his analysis, however, does not satisfy all of the physical boundary and continuity conditions. Also the form of velocity field does not truly represent the bulging shape of free surfaces. His analysis therefore can be improved.

The purpose of this investigation is to present a generalized upper bound solution which includes bulging and gives close upper bounds on pressure required to forge.

Axisymmetric Forging

The problem investigated is the forging of a cylindrical workpiece of rigid-perfectly plastic material under axisymmetric conditions. The purpose is to determine the effects of process parameters such as diameter to thickness ratio of the workpiece, friction at platen surfaces, etc., on the load required to forge. Only the case when flat platens overlap the cylindrical workpiece is treated.

No mathematically exact slip-line field solutions have been proposed for this problem. Slab method [6] has been used to analyze this problem, which gives a reasonable approximate solution when the coefficient of friction is small. The upper bound approach has been used by Kudo [29] and Kobayashi [20,30] in finding average forging pressures. In their analyses, the deforming regions are assumed to be homogeneous, i.e., the cylindrical surface remains cylindrical during deformation. In practice,

the free surface bulges or barrels out as a result of friction at die-platen interface. The radial component of velocity at the surfaces in contact with the platens is smaller than the radial component in the central plane of the cylindrical workpiece. The bulging effect is taken into account in analysis proposed by Avitzur [16] who showed that when friction exists at the die surfaces in contact with workpiece, a velocity field which accounts for bulging gives lower upper-bounds on forging pressure. Liu [69] later pointed out that in Avitzur's analysis, the velocity field assumed does not satisfy all of the physical boundary and continuity conditions. He suggested a different velocity field which resulted in lower upper-bounds on forging loads compared to Avitzur's solution. In their respective analyses, Avitzur and Liu assumed a certain class of admissible velocity fields. Their upper bound solutions are therefore restricted by the forms of velocity field assumed and hence can be improved. The intent of proposed work is to present a more generalized upper bound treatment of this problem of axisymmetric forging.

# CHAPTER II

## A GENERAL UPPER BOUND APPROACH

Solution of any metal forming problem by upper bound method requires, as a first step, that a kinematically admissible velocity field be selected for the process. For the velocity field to be kinematically admissible, it must satisfy the incompressibility condition, velocity boundary conditions and continuity requirement across any surface of tangential velocity discontinuity. To simplify selection, the deforming body is usually divided into different zones and admissible velocity fields are determined for each zone. In effect, therefore, one first forms a kinematically admissible model for the problem. Since stress conditions are not necessarily satisfied, there are, in general, an infinite number of such admissible models. In this Chapter, an approach for selecting a general admissible model for any plane strain or axi-symmetric metal forming problem is described. The general model includes many different admissible models and thus allows formulation of a general upper bound solution.

### Assumptions

In the present work, certain assumptions regarding material properties and processes are made which are common to all the problems considered. These are:

1. The solid subjected to deformation is isotropic and homogeneous. This analysis treats only the materials which exhibit identical properties

in all directions. Phenomena like the Bauschinger effect and hysteresis loop in unloading and loading which arise due to non-uniformity on a microscopic scale are disregarded. Size effects due to grain size, inclusions, etc., are also neglected.

2. The solid is rigid-perfectly plastic and obeys von Mises stress-strain rate laws. The assumption that the material is rigid or non-deforming below the yield point is, in effect, equivalent to neglecting elastic deformations. All the metal forming problems considered in this work involve the unconstrained plastic flow of an elastic-plastic material in which the elastic part of strains are small compared with the plastic part and may be neglected when considering the stress and velocity distribution [70]. Consequently the use of the rigid-plastic model is justified. No plastic volume change occurs and therefore, the solid is also incompressible. The assumption of a perfectly plastic solid or a non-strain hardening solid is indeed a mathematical simplification. The effect of work-hardening can be incorporated with certain assumptions only at the expense of heavy computational work.

3. Temperature and time effects are considered negligible. With the present knowledge, the effect of these parameters cannot be adequately incorporated in mathematical formulations of plasticity of solids [1]. This analysis is therefore valid only at temperatures for which recovery, creep and thermal phenomena generally can be neglected.

4. The tools deforming the solid are considered rigid and non-deforming. The dies and tools used in metal forming processes treated here are usually made of high strength materials. Their deformation is small compared to that of the material and therefore can be neglected.

5. The inertia effects are neglected and the problems are treated as quasi-static. This assumption is justified since in the problems considered here, the solid is usually deformed at low deformation rates. Inertia forces due to plastic flow at these velocities are small compared to other forces and therefore can be neglected [70].

6. Steady state processes only are considered.

It may be stated here that not all of the above assumptions, including the material properties, need to be made in the formulation of a deformation model. A complete upper bound analysis, however, uses all the stated assumptions.

Formulation of General Kinematically Admissible Model

The two basic classes of problems which shall be analyzed are those occurring under

1. Plane strain conditions
2. Axisymmetric conditions

As the basic equations are different, each class is dealt with separately. While each metal forming process deforms the material differently, there are actually only a few 'kinds' of velocity boundary conditions that are encountered in most forming problems. In this section, the flow of a body under these different kinds of velocity conditions is discussed. Some ideas are developed and later applied to form kinematically admissible models for specific forming problems. Of importance is that a uniform treatment can be applied to obtain a kinematic model for any forming problem. First, flow under plane strain conditions is treated.

Plane Strain Deformation

Consider a body D undergoing plane plastic deformation in x-y plane under steady state conditions (Figure 8). The flow is independent of the z direction. The body of solid is subjected to various kinds of velocity boundary conditions as follows. $\Gamma_s$ is known surface of a stationary tool which imposes the condition that the velocity of D normal to its surface be zero. $\Gamma_b$ is the boundary separating body D from another body $D_2$. It is assumed here that surface $\Gamma_b$ is not defined by the problem except that it passes through points Q and R. Since plane strain deformation in x-y plane is being considered, one can talk of surfaces as lines and their intersections as points. Volume constancy requires that the normal velocity across boundary $\Gamma_b$ be continuous. However, a tangential velocity discontinuity can occur along this surface. Surface $\Gamma_m$ is the known shape of a moving tool and again continuity demands that at this surface, the components of velocities of body D and the tool normal to $\Gamma_m$ be equal. The free surface $\Gamma_f$ does not impose any condition on the velocity field of body D. The foregoing are the velocity boundary conditions most commonly encountered in metal forming problems.

For any velocity field in body D to be kinematically admissible, it must satisfy all boundary conditions as well as the incompressibility condition. To formulate a general upper bound solution, it is necessary to first find a general kinematically admissible velocity field for body D which is not completely defined by these admissibility conditions. At first, the problem seems difficult and indeed a complete solution cannot be obtained unless the tool shapes are explicitly known. But in the following section, a method of approach is advanced which greatly simplifies the problem and which in general can be used to solve any

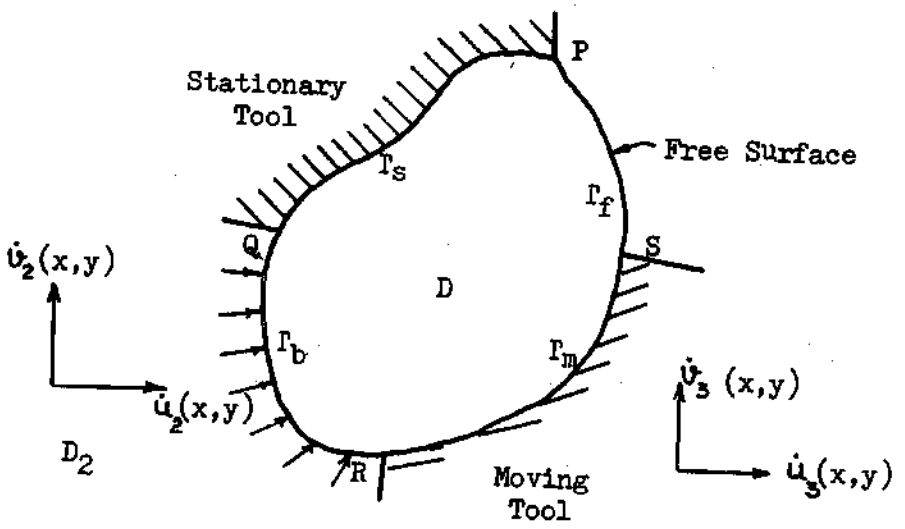


Figure 8. Deformation of a Body under Certain Prescribed Velocity Boundary Conditions

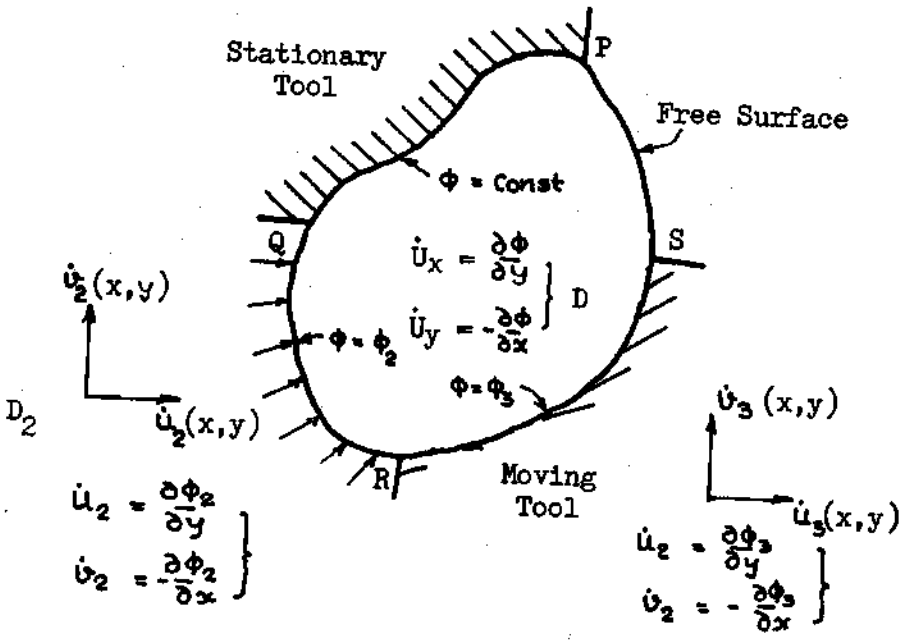


Figure 9. Boundary Conditions on the Flow Function Corresponding to the Prescribed Velocity Boundary Conditions

specific metal forming problem when the tool shapes are known. The method uses the concept of flow function.

Flow Function Concept. The incompressibility condition for plane strain deformation of body D is

$$\frac{\partial \dot{U}_x}{\partial x} + \frac{\partial \dot{U}_y}{\partial y} = 0 \qquad (2.1)$$

where $(\dot{U}_x, \dot{U}_y)$ are components of the velocity field in body D in the x and y directions of a rectangular coordinate system. The mathematical form of equation (2.1) suggests that there exists a function $\phi(x,y)$, called the flow function or the stream function, such that

$$\dot{U}_x = \frac{\partial \Phi}{\partial y} , \qquad \dot{U}_y = -\frac{\partial \phi}{\partial x} \qquad (2.2)$$

Therefore, if an admissible flow function $\phi(x,y)$ can be found, then the velocity field obtained from it would always satisfy the incompressibility condition. Of importance is the introduction of flow function $\phi$ as it reduces the number of unknowns from two, $\dot{U}_x$ and $\dot{U}_y$, to one $(\phi)$, and in addition, makes certain that the incompressibility condition is satisfied. Admissibility conditions on the velocity field are now transformed to yield corresponding conditions on the flow function. It will become apparent later that this transformation further simplifies the problem.

A basic property of the flow function is that $\phi(x,y)$ = Constant represents the equation of a streamline. Since the tangent to a streamline or flowline at any point represents the direction of the resultant velocity of the particle at that point, the velocity normal to a

streamline is zero. The velocity boundary condition at surface $\Gamma_s$ of the stationary tool can be satisfied by assuming a flow function that is constant along this surface, i.e., by taking surface $\Gamma_s$ to be a streamline.

Continuity at boundary $\Gamma_b$ requires that the normal velocities of D and $D_2$ at any point on $\Gamma_b$ be equal. This is expressed by the equation

$$\text{At} \quad y = y_{\Gamma_b}: \quad (\dot{u}_2 \sin\theta - \dot{v}_2 \cos\theta) - (\dot{u}_x \sin\theta - \dot{u}_y \cos\theta) = 0 \tag{2.3}$$

$$\text{where} \qquad \tan\theta = \frac{dy_{\Gamma_b}}{dx}$$

$(\dot{u}_2, \dot{v}_2)$ are components of the velocity field of $D_2$ in the x and y directions respectively and $y = y_{\Gamma_b}$ is the equation of $\Gamma_b$. Let $\phi_2(x,y)$ be the corresponding flow function in $D_2$. Substituting for the velocity components in terms of $\phi$ and $\phi_2$ in equation (2.3) and rearranging, one obtains along $\Gamma_b$

$$\frac{\partial \phi}{\partial y} dy + \frac{\partial \phi}{\partial x} dx - \frac{\partial \phi_2}{\partial y} dy - \frac{\partial \phi_2}{\partial x} dx = 0 \tag{2.4}$$

On integrating,

$$\text{At} \quad y = y_{\Gamma_b}: \qquad \phi(x,y) = \phi_2(x,y) + \text{Constant} \tag{2.5}$$

Since the constant can be included in $\phi_2$ without affecting the velocity field, equation (2.5) may be written, without loss of generality, as

$$\text{At} \quad y = y_{\Gamma_b}: \qquad \Phi(x,y) = \Phi_2(x,y) \tag{2.6}$$

Similarly, continuity requires that

$$\text{At} \quad y = y_{\Gamma_m}: \qquad \Phi(x,y) = \Phi_3(x,y) \tag{2.7}$$

where $\Phi_3(x,y)$ is the flow function defining the velocity of the moving tool. Figure 9 shows all the boundary conditions on the flow function $\Phi$ that must be satisfied in order for it to be kinematically admissible. It is important to realize that since the shape of boundary $\Gamma_b$ is not defined, the condition (2.6) can always be satisfied by letting $\Gamma_b$ be represented by this equation (2.6). Thus the original problem of finding a velocity field is now simplified to finding a flow function $\Phi(x,y)$ which satisfies the boundary conditions

$$\left.\begin{aligned} &\Phi(x,y) = \text{Const} \quad \text{at} \quad y = y_{\Gamma_s} \\ &\Phi(x,y) = \Phi_3(x,y) \quad \text{at} \quad y = y_{\Gamma_m} \end{aligned}\right\} \tag{2.8}$$

Clearly when the surfaces $\Gamma_m$ and $\Gamma_b$ are explicitly known, it is not difficult to find a general kinematically admissible flow function which would satisfy these conditions and yet is not completely defined by them.

The concept of a general kinematically admissible flow function is logical. The form of incompressibility equation (2.1) guarantees the existence of a flow function. Corresponding to any unique and exact solution, there would exist a unique and exact flow function. This exact flow function would necessarily be kinematically as well as

statically admissible. When stress conditions are not satisfied, it is logical to conceive that this exact and unique flow function would take the form of a general kinematically admissible flow function which becomes unique only when the stress conditions are satisfied. In this general upper bound approach, we are interested in finding this general flow function. Admissible kinematic models shall now be derived for some specific metal forming problems by using the flow function analysis.

Extrusion through Arbitrarily Shaped Die. Consider a deforming body of material subjected to a combination of the already considered 'kinds' of velocity boundary conditions as shown in Figure 10a. The body is bounded on two sides by stationary tools and on other two sides by surfaces $\Gamma_{b_1}$ and $\Gamma_{b_2}$ which separate it from some other bodies $D_1$ and $D_2$. We are interested here in finding a velocity field for D when the flow functions $\phi_1$ and $\phi_2$ for $D_1$ and $D_2$ respectively are known and are given to be

$$\phi_1 = \dot{U}_o\, y \tag{2.9}$$

and

$$\phi_2 = \dot{U}_f\, y \tag{2.10}$$

$\dot{U}_o$ and $\dot{U}_f$ are some constants. These equations imply that the velocity field $(\dot{u}_1, \dot{v}_1)$ for $D_1$ is

$$\dot{u}_1 = \dot{U}_o \quad , \quad \dot{v}_1 = 0 \tag{2.11}$$

and the velocity field $(\dot{u}_2, \dot{v}_2)$ for $D_2$ is

$$\dot{u}_2 = \dot{U}_f \quad , \quad \dot{v}_2 = 0 \tag{2.12}$$

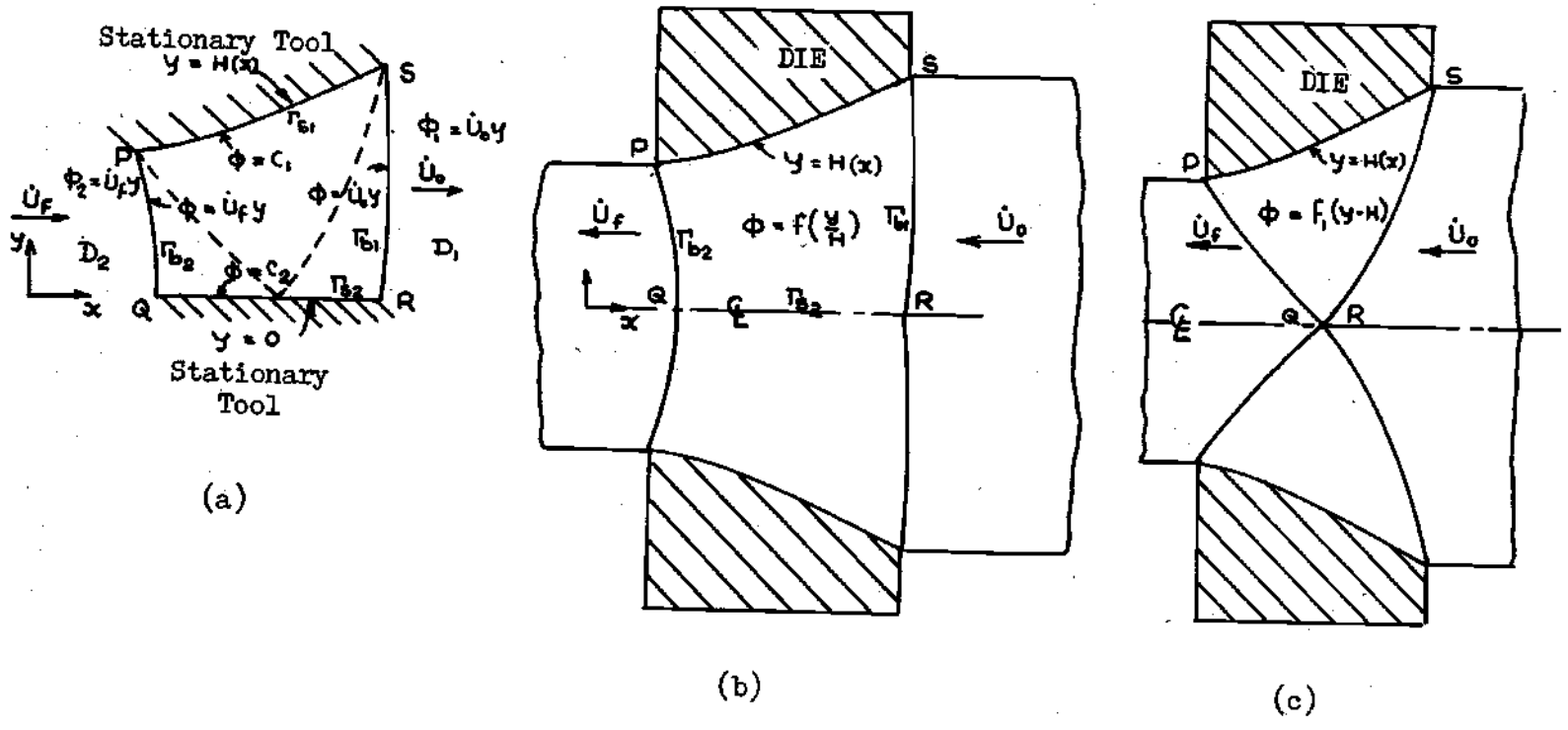


Figure 10. Admissible Models for Plane Strain Extrusion through Arbitrarily Shaped Die

The physical interpretation of equations (2.11) and (2.12) is that bodies $D_1$ and $D_2$ are rigid and are moving with uniform velocities in the x direction. Continuity requires that at surfaces

$$\Gamma_{b_1}: \qquad \phi(x,y) = \dot{U}_o\, y \tag{2.13}$$

$$\Gamma_{b_2}: \qquad \phi(x,y) = \dot{U}_f\, y \tag{2.14}$$

$$\Gamma_{s_1}: \qquad \phi(x,y) = C_1 \tag{2.15}$$

and $$\Gamma_{s_2}: \qquad \phi(x,y) = C_2 \tag{2.16}$$

$C_1$ and $C_2$ are constants. $\Gamma_{b_1}$ and $\Gamma_{b_2}$ have not been defined by the problem and thus conditions (2.13) and (2.14) can always be satisfied by letting the surfaces $\Gamma_{b_1}$ and $\Gamma_{b_2}$ be represented by these equations in the kinematic model. With suitable choice of origin of coordinate system, let the tool surface be represented by the equation

$$y = H(x) \tag{2.17}$$

where H(x) is some function of x and let $\Gamma_{s_2}$ be represented by equation

$$y = 0 \tag{2.18}$$

A general kinematically admissible velocity field for D can be selected by choosing a flow function of the form

$$\phi(x,y) = f(\eta) \tag{2.19}$$

where $\eta(x,y) = y/H(x)$

$f(\eta)$ is some function of $\eta$. It can be easily verified that this flow function satisfies the conditions (2.15) and (2.16). Thus a general admissible velocity field for D is

$$\dot{U}_x = f'(\eta)\frac{\partial \eta}{\partial y} \quad , \quad \dot{U}_y = -f'(\eta)\frac{\partial \eta}{\partial x} \tag{2.20}$$

This velocity field together with boundaries represented by equations (2.13) and (2.14) forms a general kinematically admissible model which satisfies all kinematic conditions.

The model investigated can be used to describe extrusion of a sheet through any arbitrarily shaped die shown in Figure 10b. In the extrusion process, material enters as a rigid body, is plastically deformed as it passes through the die and then leaves the die as a rigid body again. Boundaries $\Gamma_{b1}$ and $\Gamma_{b2}$ together with the die profile boundary define the zone in which the material is plastically deformed. Due to symmetry, no material passes through the extrusion axis which therefore can be treated as a rigid stationary boundary. Each half of this symmetrical extrusion process presents the same situation as considered in the body shown in Figure 10a. The general velocity field given by equation (2.20) together with boundaries given by equations (2.13) and (2.14) forms a general kinematically admissible model for the extrusion process. It may be noted that the flow function $\phi$ and hence the velocity field is not completely defined since the function $f(\eta)$ can be any function of $\eta$.

It is evident that in the model, the shapes of boundaries $\Gamma_{b1}$ and

$T_{b2}$ of the plastic zone can be freely chosen. Only the points at which these meet the die profile are fixed; however, where these meet the extrusion axis is not fixed. It is possible in practice that for certain process parameters such as reduction ratios and lengths of die, these boundaries meet at one point on the extrusion axis. In that situation, the condition that $\phi$ = Constant at y = 0 does not apply as the plastic zone PQRS no longer covers a finite portion of the boundary y = 0. An admissible flow function for this case is

$$\phi(x,y) = f_1(\eta_1) \tag{2.21}$$

where $\eta_1(x,y) = y - H(x)$

$f_1$ is any function of $\eta_1$. The admissible model is shown in Figure 10c.

Ironing of Cups in Deep Drawing. Consider the same problem discussed in the previous section with a slight difference. The flow function $\phi_1$ for velocity in $D_1$ is now given to be

$$\phi_1 = -\frac{\omega}{2}\left[(a-y)^2 + x^2\right] \tag{2.22}$$

This gives the velocity field in $D_1$

$$\begin{aligned} \dot{u}_1 &= \frac{\partial \phi_1}{\partial y} = \omega(a-y) \\ \dot{v}_1 &= -\frac{\partial \phi_1}{\partial x} = \omega x \end{aligned} \tag{2.23}$$

Note that the velocity field given by equation (2.23) represents a rigid

body rotation. As before, an admissible flow function $\phi$ for the deforming body D is

$$\phi(x,y) = f(y/H(x))$$

If the tool boundary $\Gamma_{s_1}$ has a circular contour , the deformation model in Figure 11a can be used to describe the process of drawing of an initially curved sheet as shown in Figure 11b. The entering sheet has an initial radius of curvature and thus a rigid rotation about the center of the circular die. This curved material gets plastically deformed in zone II between the dies and then leaves again as a rigid body. The deformation model, Figure 11a, can also represent the bimetallic plane strain extrusion process shown in Figure 11c. If the ironing of cups in a deep drawing process is considered as occurring under plane strain conditions, then this process is very similar to drawing of a initially curved sheet. Model 11a can be used to analyze this process.

Plane Strain Forging. So far problems involving only rigid stationary tools have been considered. Problems involving moving tools can be analyzed in a similar manner with one notable difference. For moving tools, the boundary between tool and material is fixed by the geometry of the problem provided no dead zone is assumed at the tool surface. Continuity requirement must then be satisfied at the tool boundary. In case a dead zone is assumed, continuity does not impose any restriction on flow function and can in general be satisfied by choosing a suitable shape for the dead zone surface.

To illustrate the above remarks, consider the deformation of a

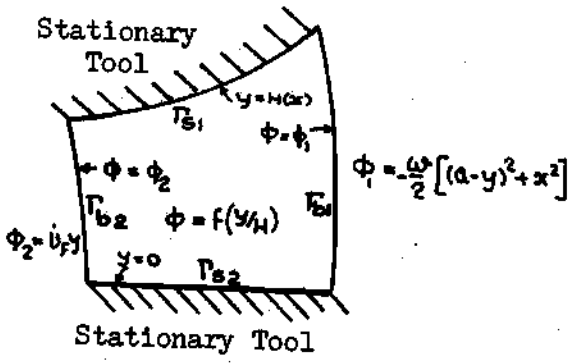


(a) Deforming Body

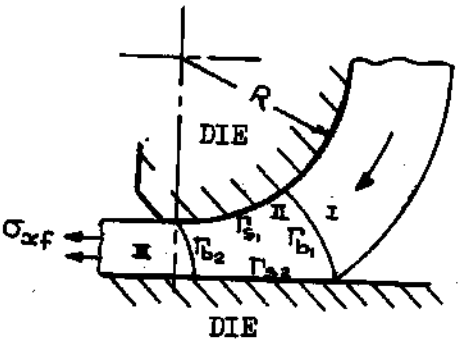


(b) Drawing of Initially Curved Sheet

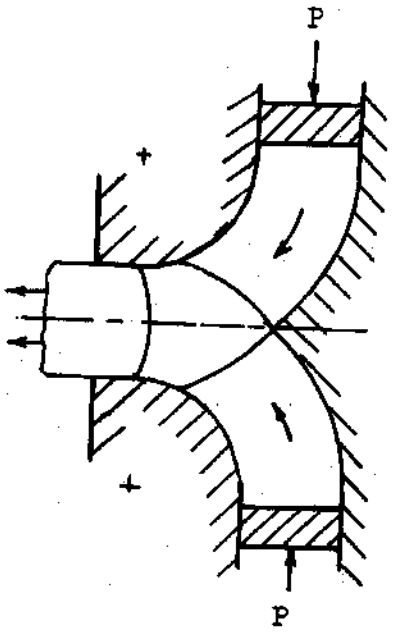


(c) Bi-metallic Extrusion

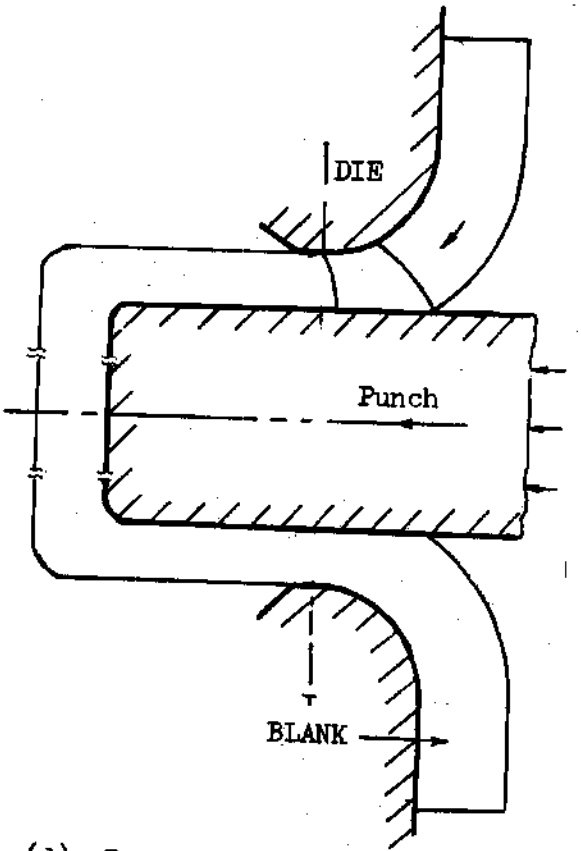


(d) Ironing of Cups in Deep Drawing

Figure 11. Deformation Model and Its Application to Various Processes

body due to a moving tool as shown in Figure 12a. An admissible flow function $\phi(x,y)$ for D must satisfy the following conditions

$$\phi(x,y) = 0 \quad \text{at} \quad y = 0 \tag{2.24}$$

$$\phi(x,y) = 0 \quad \text{at} \quad x = 0 \tag{2.25}$$

$$\text{and} \quad \phi(x,y) = \dot{U} x \quad \text{at} \quad y = y_p \tag{2.26}$$

Now if boundary $\Gamma$ is not defined, only equations (2.24) and (2.25) need to be satisfied. A general flow function which satisfies these conditions is

$$\phi(x,y) = h(x)\,g(y) \tag{2.27}$$

$$\text{where} \quad h(x) = 0 \quad \text{at} \quad x = 0$$

$$g(y) = 0 \quad \text{at} \quad y = 0 \tag{2.28}$$

$h(x)$ and $g(y)$ are some functions of x and y respectively. It is seen that this deformation model can represent plane strain forging when a dead zone is assumed, as shown in Figure 12b. In forging of rectangular strips, the top platen move down towards the bottom platen and in so doing presses the rectangular strip. Due to symmetry, no material passes through the x and y axes and thus these surfaces can be treated as rigid stationary boundaries. The flow function given by equation (2.27), together with dead

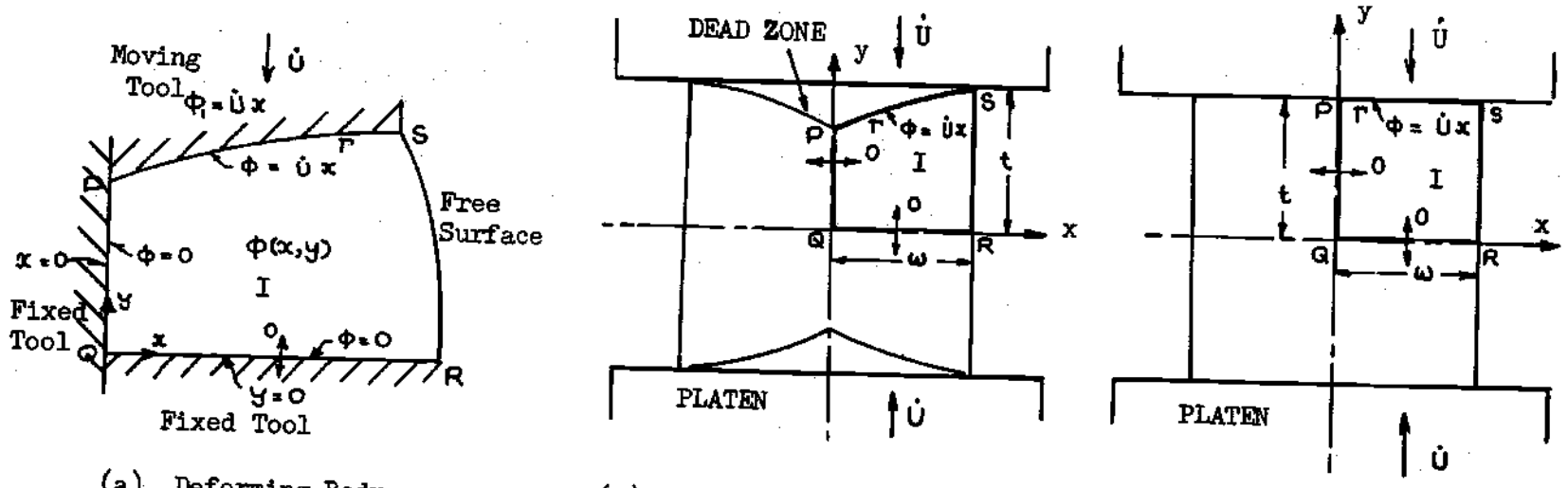


(a) Deforming Body

(b) Plane Strain Forging- With Dead Zone

(c) Plane Strain Forging- Without Dead Zone

Figure 12. Kinematically Admissible Deformation Models for Plane Strain Forging

zone of shape given by equation (2.26), forms a general kinematically admissible model for this process.

In case no dead zone is assumed, boundary $\Gamma$ shall necessarily be $y = t$ and equation (2.26) must be satisfied at this surface. It can be readily verified that an admissible flow function for this case is

$$\phi(x,y) = \dot{U} \frac{g(y)}{g(t)} x \qquad (2.29)$$

where $g(y) = 0$ at $y = 0$

In the foregoing discussion, it is shown how the flow function concept can be used advantageously to describe, kinematically, some metal forming processes occurring under plane strain conditions. The detailed analysis is presented later in the following Chapters. In addition to the problems discussed, the flow function analysis can be used to obtain admissible deformation models for many other problems such as direct and indirect extrusion, piercing, machining, etc. In general, it can be applied to any metal forming problem to simplify selection of a kinematically admissible velocity field.

Axisymmetric Deformation

Axisymmetric deformation can be treated in a similar manner as plane strain deformation. Concept of flow function can again be used to analyze problems involving various 'kinds' of velocity boundary conditions encountered in metal forming processes. As before, a general problem is first posed and an approach to its solution is described. Specific problems are then analyzed using the concepts developed.

Consider deformation of an axisymmetric body D, using a cylindrical coordinate system $(r,\theta,z)$. Since the incremental displacements are independent of the $\theta$ direction, it is sufficient to analyze the deformation in a meridian plane. Due to axial symmetry, only the upper half of body D in meridian plane is shown in Figure 13. The body is bounded by surfaces $\Gamma_{S_1}$, $\Gamma_m$, $\Gamma_f$ and $\Gamma_b$ which impose certain prescribed velocity boundary conditions. The stationary tool imposes the condition that the velocity of D normal to the surface $\Gamma_{S_1}$ be zero. $\Gamma_b$ is any surface separating bodies D and $D_2$. Continuity requires that the velocity component normal to this surface be continuous. $\Gamma_m$ is the known shape of a moving tool and continuity demands that the velocity of D normal to this surface should be equal to the velocity of the tool normal to it. The free surface $\Gamma_f$ does not restrict the velocity field in D. No material passes through the axis of symmetry and, therefore, it may be treated as a rigid boundary. The velocity of body D normal to the axis of symmetry should be zero. In addition to these boundary conditions, the incompressibility condition must be satisfied by the velocity field for body D. The problem posed here is to determine a general kinematically admissible velocity field for body D which is not completely defined by kinematic conditions. As in the plane strain case, the flow function concept shall be utilized to simplify the problem.

Flow Function Concept. The incompressibility condition for axisymmetric deformation is

$$\frac{\partial \dot{U}_r}{\partial r} + \frac{\dot{U}_r}{r} + \frac{\partial \dot{U}_z}{\partial z} = 0 \qquad (2.30)$$

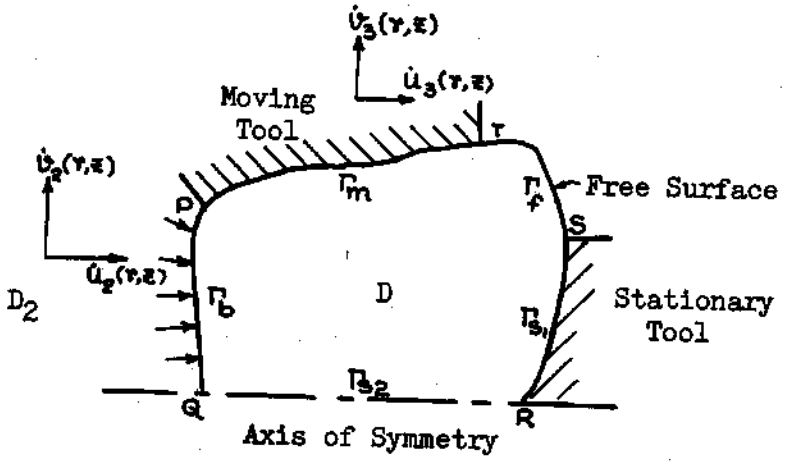


Figure 13. Deformation of An Axisymmetric Body under Prescribed Velocity Boundary Conditions

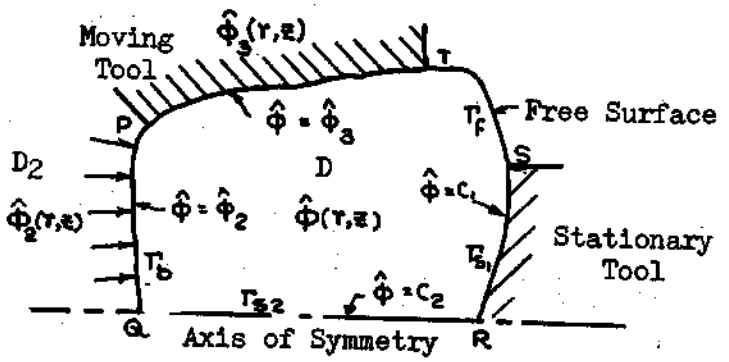


Figure 14. Boundary Conditions on the Flow Function Corresponding to the Prescribed Velocity Boundary Conditions

where $(\dot{U}_r, \dot{U}_z)$ are components of velocity field in the body D in the r and z directions of a cylindrical coordinate system. The mathematical form of equation (2.30) suggests that there exists a function $\hat{\phi}(r,z)$, called flow function, such that

$$\dot{U}_r = -\frac{1}{2\pi r}\frac{\partial\hat{\phi}}{\partial z} \qquad (2.31)$$

$$\dot{U}_z = \frac{1}{2\pi r}\frac{\partial\hat{\phi}}{\partial r} \quad , \quad \dot{U}_\theta = 0$$

The incompressibility condition will always be satisfied if a flow function $\hat{\phi}(r,z)$ which describes the deformation of body D can be determined. Thus the introduction of a flow function reduces the number of unknowns from two, $\dot{U}_r$ and $\dot{U}_z$ , to one, namely $\hat{\phi}$. Furthermore, incompressibility condition (2.30) is necessarily satisfied. Admissibility conditions on the flow function shall now be derived from the velocity boundary conditions.

One basic property of the flow function is that $\hat{\phi}(r,z)$ = Const represents the equation of a streamline or flowline. The velocity boundary condition at surface $\Gamma_{s_1}$ of a stationary tool can be satisfied by taking a flow function that is constant along this surface, i.e., by making $\Gamma_{s_1}$ a streamline. Continuity at the boundary $\Gamma_b$ requires that the normal velocity of D and $D_2$ should match. Resolving the components of velocity of these bodies in a direction perpendicular to surface $\Gamma_b$ and equating, yields

$$\text{At} \quad r = r_{\Gamma_b} : \quad (\dot{u}_2 \sin\beta - \dot{v}_2 \cos\beta) - (\dot{U}_z \sin\beta - \dot{U}_r \cos\beta) = 0$$

$$\text{where} \quad \tan\beta = \frac{dr_{\Gamma_b}}{dz}$$

$(\dot{u}_2, \dot{v}_2)$ are the components of the velocity field in $D_2$ in r and z directions, respectively, and $r = r_{\Gamma_b}$ is the equation of the boundary $\Gamma_b$. Let $\hat{\Phi}_2(r,z)$ be the corresponding flow function in $D_2$. Substituting for velocity components in terms of $\hat{\Phi}$ and $\hat{\Phi}_2$ and rearranging, one obtains along $\Gamma_b$

$$\frac{1}{r}\frac{\partial\hat{\Phi}}{\partial r}dr + \frac{1}{r}\frac{\partial\hat{\Phi}}{\partial z}dz - \frac{1}{r}\frac{\partial\hat{\Phi}_2}{\partial r}dr - \frac{1}{r}\frac{\partial\hat{\Phi}_2}{\partial z}dz = 0$$

On integrating

$$\hat{\Phi}(r,z) = \hat{\Phi}_2(r,z) \quad , \quad \text{at} \quad r = r_{\Gamma_b} \qquad (2.32)$$

The constant of integration is included in the definition of flow function $\hat{\Phi}_2$ as this does not affect the velocity field. Similarly from continuity requirement at the moving tool surface $\Gamma_m$

$$\hat{\Phi}(r,z) = \hat{\Phi}_3(r,z) \quad \text{at} \quad r = r_{\Gamma_m} \qquad (2.33)$$

$\hat{\Phi}_3(r,z)$ is the flow function defining the velocity of the moving tool.

While equations (2.32) and (2.33) look similar, these actually impose different types of restrictions on the flow function. The tool shape $\Gamma_m$ is defined by the geometry of the problem and, therefore, equation (2.33) needs to be satisfied at this surface. The shape of boundary $\Gamma_b$, on the other hand, is not defined and therefore equation (2.32) can be satisfied simply by letting shape of boundary $\Gamma_b$ be represented by this equation (2.32). The original problem is thus reduced to finding an admissible flow function $\hat{\Phi}(r,z)$ which satisfies the conditions

$$\hat{\Phi}(r,z) = C_1 \quad \text{at} \quad r = r_{\Gamma_{s1}} \tag{2.34}$$

$$\hat{\Phi}(r,z) = C_2 \quad \text{at} \quad r = r_{\Gamma_{s2}} \tag{2.35}$$

$$\hat{\Phi}(r,z) = \hat{\Phi}_3 \quad \text{at} \quad r = r_{\Gamma_m} \tag{2.36}$$

The problem cannot be solved further without knowing the shapes of the surfaces $\Gamma_m$, and $\Gamma_{s1}$. The selection of a general flow function, however, is not difficult when the shapes are explicitly known. Kinematic admissible models shall now be derived for some specific metal forming problems using the flow function concept.

Extrusion through Arbitrarily Shaped Die. Consider an axisymmetric deforming body subjected to velocity boundary conditions shown in Figure 15a. The body D is bounded by the stationary tool surface and by surfaces $\Gamma_{b1}$ and $\Gamma_{b2}$ which separate it from some other bodies $D_1$ and $D_2$. The problem is to find a general kinematically admissible velocity field for

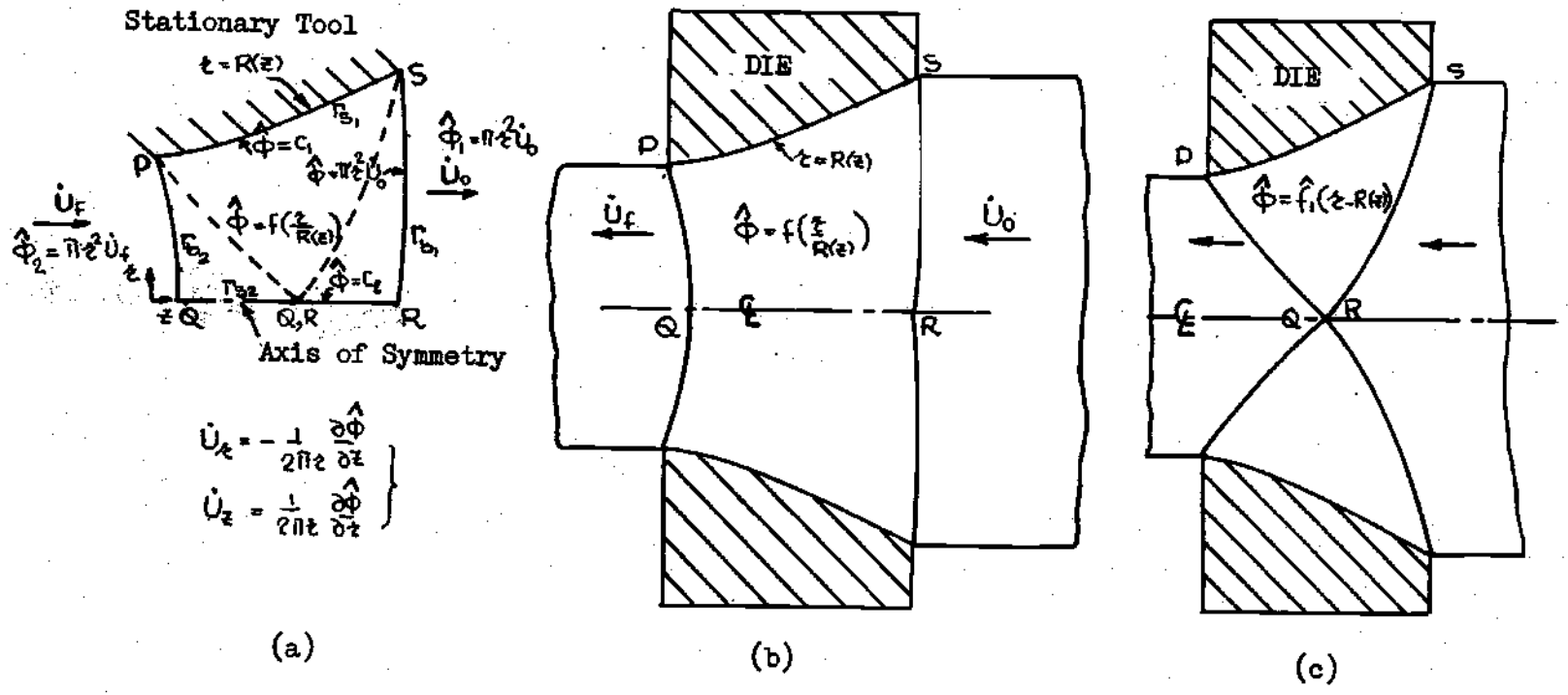


Figure 15. Admissible Models for Axisymmetric Extrusion through An Arbitrarily Shaped Die

D when the flow functions for the velocity fields in $D_1$ and $D_2$ are known to be

$$\hat{\Phi}_1 = \pi \dot{U}_o r^2$$
$$\hat{\Phi}_2 = \pi \dot{U}_f r^2 \tag{2.37}$$

$\dot{U}_o$ and $\dot{U}_f$ are constants. These equations imply that the velocity field $(\dot{u}_1, \dot{v}_1)$ for $D_1$ is

$$\dot{u}_1 = \dot{U}_o \quad , \quad \dot{v}_1 = 0 \tag{2.38}$$

and the velocity field $(\dot{u}_2, \dot{v}_2)$ for $D_2$ is

$$\dot{u}_2 = \dot{U}_f \quad , \quad \dot{v}_2 = 0 \tag{2.39}$$

The physical interpretation of equations (2.38) and (2.39) is that $D_1$ and $D_2$ are rigid and are moving with uniform velocities in the z direction. Due to axial symmetry, only the upper half of the body needs to be considered. Admissibility conditions on the flow function $\hat{\Phi}(r,z)$ for the deforming body D are

$$T_{b_1} : \qquad \hat{\Phi}(r,z) = \pi r^2 \dot{U}_o \tag{2.40}$$

$$\Gamma_{b_2} : \quad \hat{\Phi}(r,z) = \pi r^2 \dot{U}_f \tag{2.41}$$

$$\Gamma_{s1} : \quad \hat{\Phi}(r,z) = C_1 \tag{2.42}$$

$$\Gamma_{s2} : \quad \hat{\Phi}(r,z) = C_2 \tag{2.43}$$

where $C_1$ and $C_2$ are constants. $\Gamma_{b1}$ and $\Gamma_{b2}$ have not been defined by the problem and thus conditions (2.40) and (2.41) can always be satisfied by letting surfaces $\Gamma_{b1}$ and $\Gamma_{b2}$ be represented by these equations. Let the tool surface $\Gamma_{s1}$ be represented by the equation

$$r = R(z) \tag{2.44}$$

where R(z) is some function of z and $\Gamma_{b2}$ by the equation

$$r = 0 \tag{2.45}$$

A general kinematically admissible flow function for D is

$$\hat{\Phi}(r,z) = \hat{f}(\hat{\eta}) \tag{2.46}$$

where $\hat{\eta}(r,z) = r/R(z)$

and $\hat{f}(\hat{\eta})$ is some function of $\hat{\eta}$. It can be easily checked that this flow function $\hat{\phi}(r,z)$ satisfies the conditions (2.42) and (2.43) and is therefore kinematically admissible. Using equations (2.31) and (2.46), the general velocity field for D is

$$\left.\begin{aligned} \dot{U}_r &= -\frac{1}{2\pi r}\,\hat{f}'(\hat{\eta})\,\frac{\partial\hat{\eta}}{\partial z} \\ \dot{U}_z &= \frac{1}{2\pi r}\,\hat{f}'(\hat{\eta})\,\frac{\partial\hat{\eta}}{\partial r} \end{aligned}\right\} \qquad (2.47)$$

This velocity field together with boundaries represented by equations (2.40) and (2.41) forms a general kinematically admissible model. It is important to realize that the flow function has not been completely defined. It can be any function of $\hat{\eta}$, i.e., $(r/R(z))$, and therefore represents an infinite number of different admissible flow functions.

The model investigated can also be used to describe the extrusion of a rod through an arbitrarily shaped die shown in Figure 15b. In the extrusion process, the rod enters as a rigid body, gets plastically deformed as it passes through the die, and then leaves the die as a rigid body again. It is apparent that this process presents the same velocity conditions as considered in Figure 15a. The general velocity field given by equation (2.47), together with the plastic zone boundaries given by equations (2.40) and (2.41), forms a general kinematically admissible model for the axisymmetric extrusion of a rod through an arbitrarily shaped

die.

The extrusion process does not define the shapes of boundaries $\Gamma_{b_1}$ and $\Gamma_{b_2}$ nor the points at which these meet the extrusion axis. For certain reduction ratios and lengths of die, it is possible that the boundaries meet at one point on the extrusion axis. In that situation, the condition that $\hat{\phi}(r,z) = C_2$ at $r = 0$ does not apply as the plastic zone no longer covers a finite portion of the boundary $r = 0$. A general admissible flow function for this situation is

$$\hat{\phi}(r,z) = \hat{F}_1(\hat{\eta}_1) \tag{2.48}$$

where $\hat{\eta}_1 = [\, r^2 - R^2(z)\,]$

The admissible model is shown in Figure 15c.

Axisymmetric Forging

The problem of forging a cylindrical workpiece by moving dies can be treated in a similar manner as plane strain forging. The problem involves a velocity boundary condition imposed by a moving tool. Continuity requirement must be satisfied at the surface of the moving tool provided no dead zone is assumed at the surface. It is obvious that if a dead zone is assumed, the continuity requirement would have to be satisfied at the material-dead zone boundary. Since the shape of dead zone is not defined by the problem, the velocity boundary condition can always be satisfied by choosing a suitable shape for the dead zone.

Consider the deformation of a body due to a moving tool as shown in Figure 16a. The admissibility conditions on flow function $\hat{\phi}(r,z)$ for D are

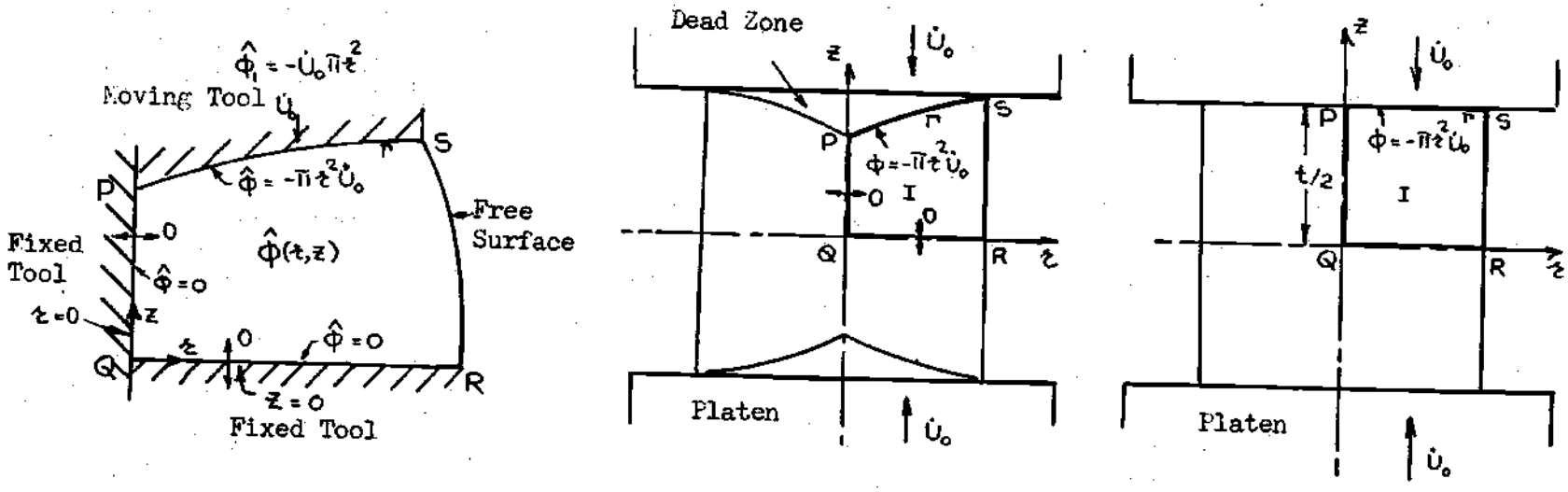


(a) Deforming Body

(b) Axisymmetric Forging --With Dead Zone

(c) Axisymmetric Forging - Without Dead Zone

Figure 16. Kinematically Admissible Deformation Models for Axisymmetric Forging Process.

$$\hat{\phi}(r,z) = 0 \quad \text{at} \quad r = 0 \tag{2.49}$$

$$\hat{\phi}(r,z) = 0 \quad \text{at} \quad z = 0 \tag{2.50}$$

$$\text{and} \quad \hat{\phi}(r,z) = -\pi r^2 \dot{U}_0 \quad \text{at} \quad r = r_f \tag{2.51}$$

If the shape of the boundary $\Gamma$ is not defined, only conditions (2.49) and (2.50) need to be satisfied. A general flow function which satisfies (2.49) and (2.50) is

$$\hat{\phi}(r,z) = \hat{h}(r)\,\hat{g}(z) \tag{2.52}$$

$$\left.\begin{aligned} \text{where} \quad \hat{h}(r) &= 0 \quad \text{at} \quad r = 0 \\ \hat{g}(z) &= 0 \quad \text{at} \quad z = 0 \end{aligned}\right\} \tag{2.53}$$

The problem considered can be used to form a kinematically admissible model for axisymmetric forging of a cylindrical workpiece when a dead zone forms at the tool surface, as shown in Figure 16b. The tools (platens) move towards each other and in doing so compress the cylindrical workpiece. Due to symmetry, the axes r and z act as rigid stationary tools. The flow

function given by equations (2.52) and (2.53) defines an admissible velocity field and this together with the shape of the dead zone given by equation (2.51) defines an admissible deformation model for the axisymmetric forging.

In case no dead zone is assumed, equation (2.51) needs to be satisfied at the tool-material interface given by equation z = t. This imposes an additional restriction on the flow function. It can be easily verified that an admissible flow function, when no dead zone is formed, is

$$\hat{\phi}(r,z) = -\dot{U}_0 \pi r^2 \frac{\hat{g}(z)}{\hat{g}(t)} + \text{Const} \qquad (2.54)$$

In addition to the problems discussed, the concept of flow function can be used to form kinematically admissible models for other axisymmetric metal forming problems such as direct and indirect extrusion of a rod, piercing, tube drawing etc.

## Lower Upper-Bound Solution

After a kinematically admissible velocity field is selected for any problem, the next step in its solution involves determination of the upper bound on forming pressure from consideration of rate of energy consumption. In this analysis, a general expression for the upper bound on power required shall be derived from the general kinematically admissible velocity field. Since the velocity field and some of the boundaries of plastic zones in a kinematic model for the process are obtained in terms of general flow function, the upper bound in effect shall be obtained as a function of the assumed flow function. Hill's principle of complimentary

minimum energy states that the exact strain rate field requires the minimum rate of energy dissipation. The exact flow function derived from the exact strain rate field therefore by principle would yield the minimum upper bound. The approach used here would give an exact solution if the most general kinematically admissible flow function which includes all possible flow functions including the actual one is used to form the upper bound on power; moreover, this upper bound must be minimized with respect to the flow function to yield the exact flow function and the exact power. Analytical formulation of the upper bound, however, requires a closed form expression for the flow function, whereas, except for some trivial problems, most general flow function cannot be obtained in closed form. Some generality therefore is lost when a general flow function in closed form is assumed which does not include all the possible admissible flow functions. For some problems, numerical computation may require that the assumed flow function be further restricted. Thus the upper bound approach proposed here will not form the most general upper bound solution and will not give the absolute minimum upper bound, but instead, will form a solution which yields lower upper-bounds. In this thesis, this approach of minimizing the upper bound using a flow function which is general in the sense that it is not completely defined by kinematic conditions but restricted to allow analytical formulation is termed a 'Lower Upper-Bound Approach'.

# CHAPTER III

## PLANE STRAIN EXTRUSION THROUGH ARBITRARILY SHAPED DIE

In this Chapter, direct steady state extrusion of a billet through a die of arbitrary shape is analyzed. Indirect extrusion and strip drawing operations are also performed with similar dies as used in direct extrusion. Similar flow patterns can be assumed and therefore the present analysis can be extended easily to analyze these processes as well.

### General Deformation Model

In Chapter II, two different kinematically admissible deformation models were derived for this problem of plane strain extrusion through arbitrarily shaped die (see Figure 10). In the model shown in Figure 10b, the deformation zone extends over a finite portion of the extrusion axis. From the existing slip-field solutions for flow through wedge shaped dies [1], it appears that the assumption of such a deformation model would be appropriate for the process conditions when the ratio of the length of the die to initial thickness of the billet ($\ell$), and the reduction of thickness (RA) is large. The other deformation model which assumes a triangular plastic zone as shown in Figure 10c would seem to be more suitable when $\ell$ and (RA) are small. In this work, special features of both these general deformation models are discussed. Lower upper-bound solution and the results are, however, obtained with the assumption of the second deformation model (Figure 10c). As shown later, with this model a closed form expression for general upper-bound on extrusion pressure is obtained which greatly

simplifies the computation work. Also the solution shows promise of analyzing another very important industrial problem not solved yet, namely, the determination of the most efficient die profiles for plane strain extrusion and drawing under frictional conditions. Special features of the first deformation model shall now be discussed.

Deformation Model for Long Dies

The general kinematically admissible deformation model is shown in full detail in Figure 17. Due to symmetry, only the upper half of the deformation process is considered. The die profile is represented by the equation

$$y = H(x) \tag{3.1}$$

$$\text{and} \qquad H(0) = t_f/2 \ , \quad H(L) = t_o/2$$

where $t_o$ is the initial thickness of the billet and $t_f$ is its final thickness. The die profile function H(x) is continuous and also has continuous first and second derivatives in the range considered. As discussed later, the analysis can be extended to die shapes that do not have a continuous slope and/or curvature.

In the admissible deformation model, the deforming billet is divided into three zones. In zone I, the undeformed region, a rigid body motion in the negative x direction is described by a uniform velocity $\dot{U}_o$ and in zone III, the already deformed region, no further deformation occurs and the rigid body motion is described by a uniform velocity $\dot{U}_f$ in

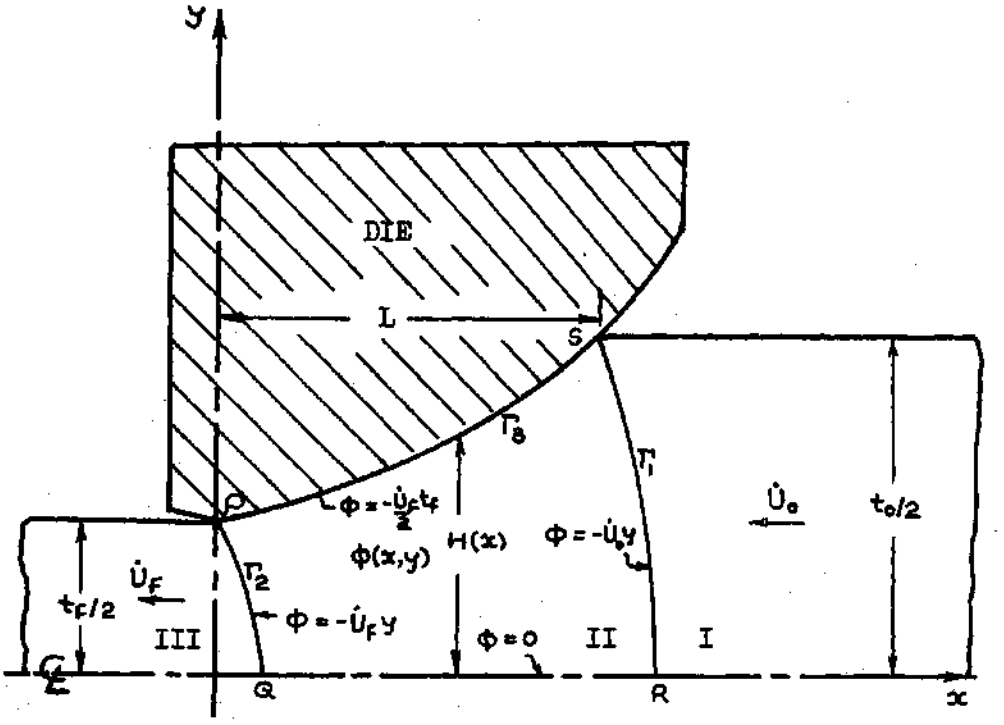


Figure 17. Admissible Deformation Model for Plane Strain Extrusion through An Arbitrarily Shaped Die of Large Dimensionless Length ($L/t_o$)

the negative x direction. Because of volume constancy

$$\dot{U}_f = \dot{U}_o \frac{t_o}{t_f} \tag{3.2}$$

As derived in Chapter II, a general kinematically admissible velocity field for zone II is

$$\left.\begin{aligned} \dot{U}_x &= f'(\eta)\frac{\partial \eta}{\partial y} = f'(\eta)\frac{1}{H(x)} \\ \dot{U}_y &= -f'(\eta)\frac{\partial \eta}{\partial x} = f'(\eta)\frac{y}{H^2(x)}H'(x) \end{aligned}\right\} \tag{3.3}$$

$$\text{where} \quad \phi = f(\eta) \quad \text{and} \quad \eta = \frac{y}{H(x)} \tag{3.4}$$

$\Phi$ is the flow function. The corresponding admissible boundaries $\Gamma_1$ and $\Gamma_2$ of the plastic zone are represented by

$$\Gamma_1 : \quad f(\eta) = -\dot{U}_o\, y \quad \text{at} \quad y = y_{\Gamma_1}(x) \tag{3.5}$$

$$\Gamma_2 : \quad f(\eta) = -\dot{U}_f\, y \quad \text{at} \quad y = y_{\Gamma_2}(x) \tag{3.6}$$

The general velocity field can also be represented as a function

of the shape of boundaries $\Gamma_1$ and $\Gamma_2$ of plastic zone II. To accomplish this, differentiate equations (3.5) and (3.6) and obtain

$$f'(\eta) = -\dot{U}_0 \frac{dy}{d\eta} \quad \text{at} \quad y = y_{\Gamma_1} \tag{3.7}$$

$$F'(\eta) = -\dot{U}_f \frac{dy}{d\eta} \quad \text{at} \quad y = y_{\Gamma_2} \tag{3.8}$$

Equations (3.7) and (3.8) represent the boundary conditions on the flow function $f(\eta)$ for zone II. Also flow function $f(\eta)$ can only be a function of $\eta$. An admissible flow function which satisfies equations (3.7) and (3.8) is

$$F'(\eta) = -\dot{U}_0 \frac{dy_{\Gamma_1}}{d\eta}$$

$$\text{or} \qquad F'(\eta) = -\dot{U}_f \frac{dy_{\Gamma_2}}{d\eta} \tag{3.9}$$

Substituting equation (3.9) in equation (3.3), the general velocity field for zone II is represented as a function of the shape of boundary $\Gamma_1$ as

$$\dot{U}_x = \left(-\dot{U}_0 \frac{dy_{\Gamma_1}}{d\eta}\right) \frac{1}{H(x)} \tag{3.10}$$

$$\dot{U}_y = \left(-\dot{U}_o \frac{dy_{\Gamma_1}}{d\eta}\right) \frac{y}{H^2(x)} H'(x)$$

where $y = y_{\Gamma_1}(x)$ is the equation of boundary of $\Gamma_1$. From equation(3.9),it is obvious that the two boundaries $\Gamma_1$ and $\Gamma_2$ are related by the expression

$$\frac{y_{\Gamma_1}}{y_{\Gamma_2}} = \frac{\dot{U}_f}{\dot{U}_o} \tag{3.11}$$

The above relation can be derived independently from the incompressibility condition. Some interesting special cases of the above general model shall be considered next.

Particular Deformation Model When $f'(\eta)$ is a Constant. Consider the special case when

$$f'(\eta) = \text{Constant}$$

$$\text{or} \qquad f(\eta) = \left(-\frac{\dot{U}_o t_o}{2}\right) \frac{y}{H(x)} = \left(-\frac{\dot{U}_f t_f}{2}\right) \frac{y}{H(x)} \tag{3.12}$$

Substituting for $f(\eta)$ in equations (3.5) and (3.6), the plastic zone boundaries $\Gamma_1$ and $\Gamma_2$ for this particular case become

$$\Gamma_1: \qquad H(x) = t_o/2 \quad \text{or} \quad x = L \tag{3.13}$$

$$T_2: \quad H(x) = t_f/2 \quad \text{or} \quad x = 0 \tag{3.14}$$

The boundaries thus become vertical surfaces. Substituting for $f(\eta)$ in equation (3.3), the velocity field for this special case is

$$\left.\begin{aligned} \dot{U}_x &= -\frac{1}{H(x)} \\ \dot{U}_y &= -\frac{y}{H^2(x)} H'(x) \end{aligned}\right\} \quad \text{for } \dot{U}_o \equiv 1, t_o/2 = 1 \tag{3.15}$$

The foregoing velocity field is the same as proposed by Chang and Choi [36] for extrusion through any curved die. Thus the velocity field and the deformation model assumed by these authors is only a special case of the more general kinematic model proposed here.

Model For Extrusion through Wedge-Shaped Die. Consider the case when the die has a wedge shape as shown in Figure 2. The apex of the wedge is taken as the origin of the coordinate axes. The die profile is represented in this case by

$$y = H(x) = x \tan\alpha \tag{3.16}$$

Substituting for H(x) in equation (3.10) gives the velocity field in zone II

$$\dot{U}_x = \left(-\dot{U}_o \frac{dy_\eta}{d\eta}\right) \frac{1}{x \tan\alpha}$$

$$\dot{U}_y = \left( -\dot{U}_o \frac{dy_\eta}{d\eta} \right) \frac{y}{x^2 \tan\alpha}$$

where $\eta(x,y) = \frac{y}{x \tan\alpha}$

The following rule is used to transform into a cylindrical coordinate system $(r,\theta,z)$

$$x = r\cos\theta \ , \quad y = r\sin\theta$$

The velocity field becomes

$$\dot{U}_x = -\dot{U}_o \frac{d}{d\theta}(r_{\Gamma_i}\sin\theta) \frac{d\theta}{d\eta} \cdot \frac{1}{r\cos\theta \tan\alpha}$$

$$\dot{U}_y = -\dot{U}_o \frac{d}{d\theta}(r_{\Gamma_i}\sin\theta) \frac{d\theta}{d\eta} \frac{\sin\theta}{r\cos^2\theta \tan\alpha}$$

where $r = r_{\Gamma_i}(\theta)$ is the equation of the boundary $\Gamma_i$.

Now

$$\frac{d\theta}{d\eta} = 1/\left(\frac{d\eta}{d\theta}\right) = \frac{\tan\alpha}{\sec^2\theta}$$

The velocity field thus simplifies to

$$\dot{U}_x = -\dot{U}_0 \cos\theta \cdot \frac{1}{r} \frac{d}{d\theta}(r_{\Gamma_1} \sin\theta)$$

$$\dot{U}_y = -\dot{U}_0 \sin\theta \cdot \frac{1}{r} \frac{d}{d\theta}(r_{\Gamma_1} \sin\theta) \qquad (3.17)$$

From equation (3.17), one can obtain

$$\frac{\dot{U}_y}{\dot{U}_x} = \tan\theta$$

Thus the resultant velocity is purely radial and is given by

$$\dot{U}_r = \sqrt{\dot{U}_x^2 + \dot{U}_y^2} = -\frac{\dot{U}_0}{r} \frac{d}{d\theta}(r_{\Gamma_1} \sin\theta) \qquad (3.18)$$

and $\dot{U}_\theta = 0$

The foregoing velocity field is the same as suggested by Stepanskii [31] who derived it from a different approach. If it is assumed that $r_{\Gamma_1}$ is not a function of $\theta$, the boundaries $\Gamma_1$ and $\Gamma_2$ become cylindrical surfaces and the velocity field given by equation (3.18) reduces to

$$\dot{U}_r = -\frac{\dot{U}_o}{r} r_1 \cos\theta$$

$$\dot{U}_\theta = 0 \qquad (3.19)$$

$r_1$ is a constant. Avitzur et al. [38] used this special velocity field in their solution for the problem of extrusion through wedge shaped dies. The proposed general deformation model (see Figure 17) thus extends Stepanskii's model for extrusion through a conical die to the general case of extrusion through an arbitrarily shaped die. Analyses by Chang and Choi [36] and Avitzur et al. [38] turn out to be only special cases of the proposed general deformation model.

Deformation Model for Short Dies

The proposed model for extrusion through an arbitrarily shaped die of short length($L/t_o$) is shown in Figure 18 in full detail. As derived in Chapter II, a general admissible velocity field for zone II is

$$\dot{U}_x = \frac{\partial\phi}{\partial y} = -g'(\theta)$$

$$\dot{U}_y = -\frac{\partial\phi}{\partial x} = -g'(\theta)\, H'(x) \qquad (3.20)$$

where $\phi(x,y) = g(\theta)$ , $\theta(x,y) = H(x) - y$ (3.21)

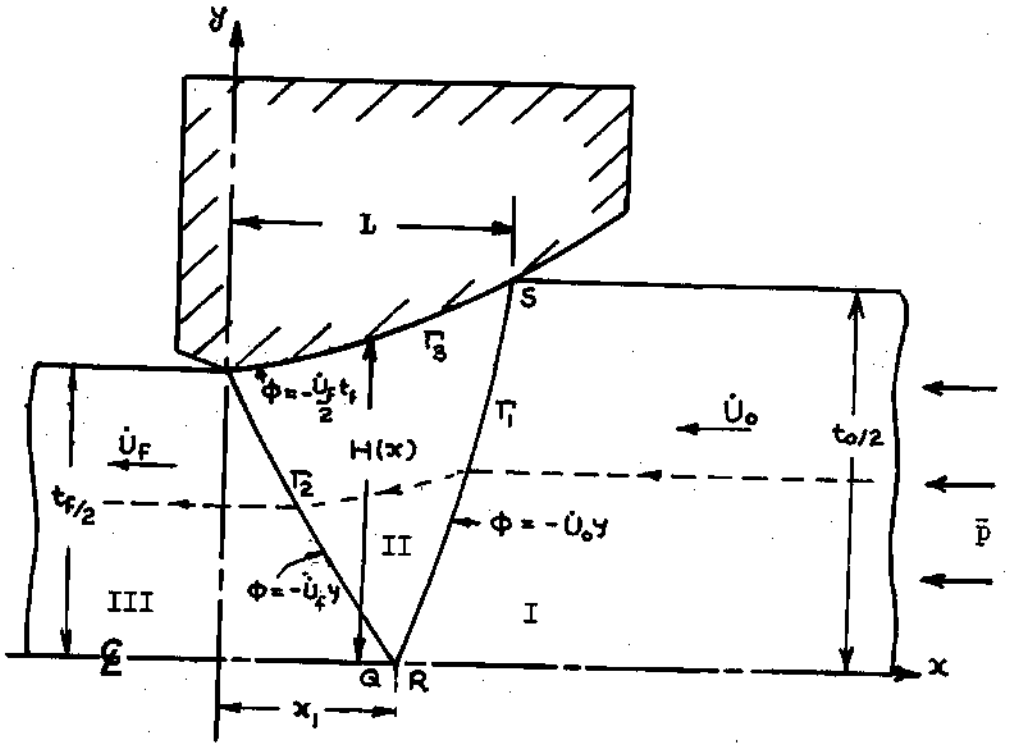


Figure 18. Admissible Deformation Model for Plane Strain Extrusion through An Arbitrarily Shaped Die of Small Dimensionless Length ($L/t_o$)

$g(\phi)$ is any function of $\phi$ . The equation of the flow lines is given by

$$g(\phi) = \text{Constant}$$

$$\text{or} \qquad \phi(x,y) = H(x) - y = \text{Const.} \tag{3.22}$$

The equation (3.22) implies that all the streamlines have the same shape as the die in zone II. The choice of an arbitrary function $g$ changes the constant in equation (3.22) and thereby shifts up or down all the streamlines except the ones along the die surfaces. The plastic zone boundaries are represented by

$$\Gamma_1: \qquad g(\phi) = -\dot{U}_0 y \quad \text{at} \quad y = y_{\Gamma_1}(x) \tag{3.23}$$

$$\Gamma_2: \qquad g(\phi) = -\dot{U}_f y \quad \text{at} \quad y = y_{\Gamma_2}(x) \tag{3.24}$$

A necessary requirement for the admissibility of this model is that the boundaries $\Gamma_1$ and $\Gamma_2$ meet at one point along the extrusion axis. Applying the conditions that $\Gamma_1$ and $\Gamma_2$ meet the extrusion axis at say $Q(x_1, 0)$ and $R(x_2, 0)$ respectively, one obtains from equations (3.23) and (3.24)

$$g(x_1, 0) = 0 \tag{3.25}$$

$$\text{and} \qquad g(x_2, 0) = 0 \tag{3.26}$$

Clearly the above relations are satisfied when

$$\left.\begin{aligned} g(x_1, 0) &= 0 \\ \text{and} \qquad x_1 &= x_2 \end{aligned}\right\} \tag{3.27}$$

Also along the die surface ($y = H(x)$)

$$\phi(x,y) = -\dot{U}_f\, t_f/2$$

$$\therefore \quad g(\theta)\Big|_{\theta=0} = g(0) = -\dot{U}_f\, t_f/2 \tag{3.28}$$

Thus a kinematically admissible model is formed when the flow function assumed for zone II is

$$\phi(x,y) = g(\theta) \tag{3.29}$$

where $\theta(x,y) = H(x) - y$, $g(x_1, 0) = 0$, $g(\theta)\Big|_{H(x)=y} = g(0) = -\frac{\dot{U}_f t_f}{2}$

An interesting result is obtained on considering the special case of extrusion through a wedge-shaped die. The die profile is then represented by

$$y = H(x) = t_f/2 + x\tan\alpha$$

where $\alpha$ is the half wedge angle. Let the flow function be

$$\Phi(x,y) = \frac{\dot{U}_f t_f}{2} \frac{(H(x)-y)}{H(x_1)} - \frac{\dot{U}_f t_f}{2}$$

This flow function is only a special case of the general kinematically admissible flow function given by equation (3.29). Substituting for $\Phi(x,y)$, $H(x)$ and $H(x_1)$ in equation (3.24) and simplifying, one obtains the following equation for boundary $\Gamma_2$

$$\Gamma_2 : \qquad y = t_f \left( 1 - \frac{x}{x_1} \right)$$

which is an equation of a straight line. Proceeding in a similar manner, it can be shown that boundary $\Gamma_1$ also is a straight line. From the velocity field, the following strain rate field is derived for zone II

$$\dot{\epsilon}_{xx} = \dot{\epsilon}_{yy} = \dot{\epsilon}_{xy} = 0$$

where $\dot{\epsilon}_{ij}$ is the strain rate tensor. Since all the strain components are zero, zone II in this particular case is nondeforming and is rigid. This model was first suggested by Hill [21], who derived it from an entirely different approach of using a hodograph (velocity diagram). He divided the deforming body into rigid zones separated by straight surfaces of velocity discontinuity. His approach can be applied only to tools with straight boundaries, e.g., wedge shaped dies. The proposed approach of using flow function can be applied to curved as well as straight tools. A more

general deformation model is thus derived here which gives Hill's analysis as a special case.

## Lower Upper-Bound Analysis

From the general kinematically admissible model, that particular model is to be selected which results in a minimum upper bound on the extrusion pressure. Since the entire kinematic model is defined by the flow function, the problem thus is to find the extremizing flow function. The expression for extrusion pressure is however too complex to allow determination of exact flow function. An approximate solution to this variational problem is sought here. In present analysis, the actual flow function is approximated by a linear combination of known functions $\beta^i$

$$\Phi(x,y) = \sum_{i=0}^{N} a_i \beta^i \qquad (3.30)$$

$$\text{where} \quad \beta = H(x) - y \,, \quad a_0 = -\dot{U}_f t_f/2 \,, \quad \sum_{i=0}^{N} a_i H(x_i)^i = 0$$

The coefficients $a_i$ are constants and are determined such that the upper bound on extrusion pressure is a minimum. It should be noted here that this choice of flow function automatically implies that the boundaries of the plastic zone meet at one point on the extrusion axis. To further simplify and obtain a closed form solution, all constants $a_i$ except $a_0$ and $a_1$ are assumed equal to zero. Thus the assumed flow function is

$$\Phi(x,y) = -\frac{\dot{U}_f t_f}{2}\left[1 - \frac{1}{H(x_i)}\left(H(x) - y\right)\right] \qquad (3.31)$$

This flow function is kinematically admissible and has an arbitrary parameter $x_1$ which can be varied independently of the kinematic conditions.

Upper Bound On Extrusion Pressure

From the assumed flow function, one obtains

Velocity field in zone II:

$$\dot{U}_x = \frac{\partial \Phi}{\partial y} = -\frac{\dot{U}_f t_f}{2} \cdot \frac{1}{H(x_1)}$$

$$\dot{U}_y = -\frac{\partial \Phi}{\partial x} = -\frac{\dot{U}_f t_f}{2} \cdot \frac{H'(x)}{H(x_1)} \qquad (3.32)$$

Boundaries of plastic zone:

From equations (3.23), (3.24) and (3.31)

$$\Gamma_1: \qquad y_{\Gamma_1} = t_o \frac{H(x_1) - H(x)}{2H(x_1) - t_o}$$

$$\Gamma_2: \qquad y_{\Gamma_2} = t_f \frac{H(x_1) - H(x)}{2H(x_1) - t_f}$$

To nondimensionalize, let

$$2y/t_o = \psi \;,\; 2x/t_o = \xi \;,\; 2H(x)/t_o = h(\xi) \;,\; t_f/t_o = h_f$$

$$2L/t_o = \ell \;,\; 2x_1/t_o = \ell_1 \;,\; H'(x) = h'(\xi) \;,\; H''(x) = 2h''(\xi)/t_o \qquad (3.33)$$

$$\Gamma_1 : \quad \psi_{\Gamma_1} = \frac{h(s) - h(\ell_1)}{1 - h(\ell_1)}$$

$$\Gamma_2 : \quad \psi_{\Gamma_2} = h_f \frac{h(\ell_1) - h(s)}{h_1(\ell_1) - h_f} \tag{3.34}$$

Strain rate field in zone II:

$$\dot{\epsilon}_{xx} = \frac{\partial \dot{U}_x}{\partial x} = 0$$

$$\dot{\epsilon}_{yy} = \frac{\partial \dot{U}_y}{\partial y} = 0 \tag{3.35}$$

$$\dot{\epsilon}_{xy} = \frac{1}{2}\left(\frac{\partial \dot{U}_x}{\partial y} + \frac{\partial \dot{U}_y}{\partial x}\right) = -\left(\dot{U}_f t_f/2\right) \frac{H''(x)}{2 H(x_i)}$$

It may be noted that the incompressibility condition ( $\dot{\epsilon}_{xx} + \dot{\epsilon}_{yy} = 0$ ) is satisfied and the zone II is undergoing pure shear in x-y direction.

Internal power of deformation ($\dot{W}_i$) :

The internal power of deformation in zone I and zone III is zero as these zones are rigid and nondeforming. In zone II, the rate of energy dissipation ($\dot{W}_i$) for the upper half of the deforming body is

$$\dot{W}_i = \frac{2}{\sqrt{3}} \sigma_0 \iint \sqrt{\frac{1}{2} \dot{\epsilon}_{ij} \dot{\epsilon}_{ij}}\, dx\, dy \tag{3.36}$$

Substituting for strain rates

$$\dot{W}_i = \frac{\sigma_o}{\sqrt{3}} \left(\frac{\dot{U}_f t_f}{2}\right) \frac{1}{H(x_1)} \left| \left[ \int_0^{x_1} H''(x)\,dx \int_{y_{\Gamma_2}}^{H(x)} dy + \int_{x_1}^{L} H''(x)\,dx \int_{y_{\Gamma_1}}^{H(x)} dy \right] \right|$$

or

$$\frac{\dot{W}_i}{\sigma_o/\sqrt{3}\,(\dot{U}_f t_f/2)} = \frac{1}{h(\ell_1)} \left| \left[ \int_0^{\ell_1} h''(\varsigma)\,d\varsigma \int_{\psi_{\Gamma_2}}^{h(\varsigma)} d\psi + \int_{\ell_1}^{\ell} h''(\varsigma)\,d\varsigma \int_{\psi_{\Gamma_1}}^{h(\varsigma)} d\psi \right] \right|$$

for $0 < x_1 < L$

Upon integrating and simplifying, one obtains

$$\frac{W_i}{(\sigma_o/\sqrt{3})(\dot{U}_f t_f/2)} = \left| \left\{ h_f \left[ \frac{h'(0) - h'(\ell_1)}{h(\ell_1) - h_f} \right] + \left[ \frac{h'(\ell_1) - h'(\ell)}{h(\ell_1) - 1} \right] + \int_0^{\ell_1} \frac{h''(\varsigma)\,h(\varsigma)}{h(\ell_1) - h_f}\,d\varsigma + \int_{\ell_1}^{\ell} \frac{h''(\varsigma)\,h(\varsigma)}{h(\ell_1) - 1}\,d\varsigma \right\} \right| \qquad (3.37)$$

An alternative form for equation (3.37) is

$$\frac{W_i}{(\sigma_o/\sqrt{3})(\dot{U}_f t_f/2)} = \left| \left\{ \int_{\ell_1}^{\ell} \frac{h'^2(\varsigma)}{1 - h(\ell_1)}\,d\varsigma - \int_0^{\ell_1} \frac{h'^2(\varsigma)}{h(\ell_1) - h_f}\,d\varsigma \right\} \right| \qquad (3.38)$$

Shear power loss over entrance boundary $\Gamma_1$ :

The shear power loss ($\dot{W}_{s_{\Gamma_1}}$) due to tangential velocity discontinuity along $\Gamma_1$ is

$$W_{s_{\Gamma_1}} = \int_{S_{\Gamma_1}} T_i \,|\Delta v_i|\, ds \qquad (3.39)$$

The shear stress $\tau_i$ at the surface is not more than the shear stress in yield ( $\sigma_o/\sqrt{3}$ ). The tangential velocity discontinuity $\Delta v_i$ is given by

$$\Delta v_i = (\dot{U}_x + \dot{U}_o)\frac{dx}{ds} + \dot{U}_y \frac{dy}{ds} \quad \text{at} \quad y = y_{\tau_i}$$

Substituting for $\dot{U}_x$, $\dot{U}_y$ and $\Delta v_i$ , and nondimensionalizing

$$\dot{W}_{s_{\tau_i}} = \frac{\sigma_o}{\sqrt{3}} \left| \left\{ \int_{x_i}^{L} \left( -\frac{\dot{U}_o t_o}{2} \cdot \frac{1}{H(x_i)} + \dot{U}_o \right) dx \right. \right.$$

$$\left. \left. + \int_0^{t_o/2} -\frac{\dot{U}_o t_o}{2} \frac{H'(x)}{H(x_i)} dy \right\} \right|$$

$$\text{or} \quad \dot{W}_{s_{\tau_i}} = \frac{\sigma_o}{\sqrt{3}} \frac{\dot{U}_f t_f}{2} \left| \left\{ \int_{\ell_i}^{\ell} \left( -\frac{1}{h(\ell_i)} + 1 \right) d\xi + \int_0^1 \frac{h'(\xi)}{h(\ell_i)} d\psi \right\} \right|$$

Integration is along the boundary $\tau_i$ where

$$\psi = \frac{h(\ell_i) - h(\xi)}{h(\ell_i) - 1}$$

$$\text{or} \quad d\psi = -\frac{h'(\xi)}{h(\ell_i) - 1} d\xi$$

By substituting for $d\psi$ in the expression for $\dot{W}_{s_{\tau_i}}$ , one obtains upon simplification

$$\frac{\dot{W}_{s_{\tau_i}}}{(\sigma_o/\sqrt{3})(\dot{U}_f t_f/2)} = \left| \left\{ \frac{h(\ell_i)-1}{h(\ell_i)} (\ell - \ell_i) + \frac{1}{h(\ell_i)[h(\ell_i)-1]} \int_{\ell_i}^{\ell} h'^2(\xi)\, d\xi \right\} \right| \quad (3.40)$$

Shear power loss over exit boundary $\Gamma_2$ :

The shear power loss ($\dot{W}_{S_{\Gamma_2}}$) due to the tangential velocity discontinuity along $\Gamma_2$ is

$$\dot{W}_{S_{\Gamma_2}} = \int_{S_{\Gamma_2}} \tau_2 |\Delta v_2| \, ds$$

Proceeding in a similar manner as for the shear power loss along $\Gamma_1$ , the following expression for shear power loss over the exit boundary $\Gamma_2$ is obtained

$$\frac{\dot{W}_{S_{\Gamma_2}}}{(\sigma_0/\sqrt{3})(\bar{v}_f t_f/2)} = \left| \left\{ \frac{h(\ell_1)-h_f}{h_f h(\ell_1)} \ell_1 + \frac{h_f}{h(\ell_1)[h(\ell_1)-h_f]} \int_0^{\ell_1} h^2(s) \, ds \right\} \right| \tag{3.41}$$

Friction power loss over die surface:

The friction at the die surface is taken into account by assuming a constant shear stress $\tau_3$ at die surface. Let

$$\tau_3 = m_3 (\sigma_0/\sqrt{3})$$

where $m_3$ is called the friction index. The rate of energy dissipation at the die surface is

$$\dot{W}_{S_{\Gamma_3}} = \int (m_3 \sigma_0/\sqrt{3}) |\Delta v_3| \, ds$$

The tangential velocity discontinuity $\Delta v_3$ is given by

$$\Delta v_3 = \sqrt{\dot{U}_x^2 + \dot{U}_y^2} \quad \text{at} \quad y = H(x)$$

Substituting for $\dot{U}_x$ and $\dot{U}_y$

$$\Delta v_3 = \dot{U}_f \frac{t_f}{2} \cdot \frac{1}{H(x_1)} \sqrt{1 + H'^2(x)}$$

The incremental area ds is

$$ds = [dx^2 + dy^2]^{1/2} \quad \text{at} \quad y = H(x)$$

$$= dx \sqrt{1 + H'^2(x)}$$

Substituting, one obtains upon simplification

$$\frac{\dot{W}_{sr_3}}{(\sigma_o/\sqrt{3})(\dot{U}_f t_f/2)} = m_3 \frac{1}{h(\ell_1)} \left| \left\{ \ell + \int_0^{\ell} h'^2(s)\, ds \right\} \right| \qquad (3.42)$$

According to the Upper Bound Theorem, the sum of the rates of energy dissipation derived from a kinematically admissible model will always be in excess of the actual rate at which energy is supplied. The two rates will be equal only for a mathematically exact model, that is for one that is kinematically as well as statically admissible. Now the applied power J is given by

$$J = \bar{p}_a \dot{U}_o t_o \qquad (3.43)$$

where $\tilde{p}_a$ is the applied mean extrusion pressure. An upper bound on J termed $J^*$ is thus given by the equation

$$J^* = 2(\dot{W}_i + \dot{W}_{S_{T_1}} + \dot{W}_{S_{T_2}} + \dot{W}_{S_{T_3}})$$

The right hand side of the equation represents the sum of the rates of energy dissipation derived from the assumed kinematic model. Substituting for the various terms, one obtains the following expression for the upper bound on reduced extrusion pressure ($\tilde{p}/(2\sigma_0/\sqrt{3})$)

$$\frac{\tilde{p}}{2\sigma_0/\sqrt{3}} = \frac{1}{2}\left|\left\{\frac{I_2(\ell,\ell_1)}{1-h(\ell_1)} - \frac{I(\ell_1)}{h(\ell_1)-h_f}\right\}\right| \qquad (3.44)$$

$$+ \frac{1}{2}\left|\left\{\frac{1-h(\ell_1)}{h(\ell_1)}(\ell-\ell_1) + \frac{I_2(\ell,\ell_1)}{h(\ell_1)[1-h(\ell_1)]}\right\}\right|$$

$$+ \frac{1}{2}\left|\left\{\frac{h(\ell_1)-h_f}{h_f\,h(\ell_1)}\ell_1 + \frac{h_f\,I_1(\ell_1)}{h(\ell_1)[h(\ell_1)-h_f]}\right\}\right|$$

$$+ \frac{1}{2}\left|\left\{\frac{m_3}{h(\ell_1)}[\ell + I_3(\ell)]\right\}\right| \qquad (0<\ell_1<\ell)$$

where $I_1(\ell_1) = \int_0^{\ell_1} h'^2(s)\,ds$, $I_2(\ell,\ell_1) = \int_{\ell_1}^{\ell} h'^2(s)\,ds$, $I_3(\ell) = \int_0^{\ell} h'^2(s)\,ds$

For a given set of process parameters $(h_f, \ell, m_3)$, the upper bound on $\tilde{p}_a$ $(\bar{p})$ is obtained as a function of an arbitrary parameter $\ell_1$. This parameter represents the location of the point at which the boundaries of the plastic zone meet the extrusion axis. Varying $\ell_1$ results in shifting of the plastic zone and thus in the alteration of the kinematically admissible model. Different upper bounds on $\bar{p}_a$ are obtained corresponding to the different values of $\ell_1$ and the least upper-bound gives the best approximation to the actual extrusion pressure. The kinematic model which results in least upper bound presents the best approximation to the actual deformation occurring in the extrusion process for the given set of process parameters.

A computer program was written to obtain the least upper bound on extrusion pressure for a given set of process parameters $(\ell, h_f, m_3)$ by varying the arbitrary parameter $\ell_1$. Details of this computer program are given in Appendix A. Numerical results for four types of dies, namely, wedge-shaped, cosine, elliptic and hyperbolic, were obtained.

Dies

Wedge-Shaped Die. The die profile is represented by

$$\psi = h(s) = h_f + s\tan\alpha \qquad (3.45)$$

It can easily be checked that all the strain rates components in zone II are zero and thus region II is rigid. Substituting for $h(s)$ and its first and second derivatives in equation (3.44) gives

$$\frac{\bar{p}}{(\sigma_0/\sqrt{3})} = \left(\frac{1}{h_f + \ell_1\tan\alpha}\right)\left[(\ell-\ell_1)\left\{1-(h_f+\ell_1\tan\alpha)\right.\right. +$$

$$+ \frac{\tan^2\alpha}{1-(h_f+\ell_1\tan\alpha)}\Big\} + (\ell_1\tan\alpha)\left\{\frac{\ell_1}{h_f} + \frac{h_f}{\ell_1}\right\}$$

$$+ m_3\ell\left\{1+\tan^2\alpha\right\}\Big] \qquad (3.46)$$

It can be easily verified that the above equation is the same as the expression given by Thomsen , et al. [6] who derived it using a hodograph technique.

Cosine Die. The cosine die considered here has a zero entrance and a zero exit angle. The die profile is represented by

$$\psi = h(s) = \frac{h_f+1}{2} - \frac{1-h_f}{2}\cos\left(\frac{\pi s}{\ell}\right) \qquad (3.47)$$

The upper bound on extrusion pressure is given by equation (3.44) with

$$I_1(\ell_1) = \left[\left(\frac{1-h_f}{2}\right)\frac{\pi}{\ell}\right]^2\left\{\frac{\ell_1}{2} - \frac{\ell}{4\pi}\sin\left(\frac{2\pi\ell_1}{\ell}\right)\right\}$$

$$I_2(\ell,\ell_1) = \left[\left(\frac{1-h_f}{2}\right)\frac{\pi}{\ell}\right]^2\left\{\frac{\ell-\ell_1}{2} + \frac{\ell}{4\pi}\sin\left(\frac{2\pi\ell_1}{\ell}\right)\right\} \qquad (3.48)$$

and $$I_3(\ell) = \left[\left(\frac{1-h_f}{2}\right)\frac{\pi}{\ell}\right]^2\frac{\ell}{2}$$

Elliptic Die. The elliptic die considered here has a zero entrance angle but a non-zero exit angle. The profile is

$$\Psi = h(s) = \sqrt{1-\left(\frac{1-h_f^2}{\ell^2}\right)(\ell-s)^2} \qquad (3.49)$$

Expression (3.44) gives the upper bound on pressure with $I_1(\ell_1)$, $I_2(\ell,\ell_1)$ and $I_3(\ell)$ defined as

$$I_1(\ell_1) = B\left[-\ell_1 + \frac{1}{2\sqrt{B}} \ln\left\{\left(\frac{1-(\ell-\ell_1)\sqrt{B}}{1+(\ell-\ell_1)\sqrt{B}}\right)\left(\frac{1+\ell\sqrt{B}}{1-\ell\sqrt{B}}\right)\right\}\right]$$

$$I_2(\ell,\ell_1) = B\left[-(\ell-\ell_1) + \frac{1}{2\sqrt{B}} \ln\left\{\frac{1+(\ell-\ell_1)\sqrt{B}}{1-(\ell-\ell_1)\sqrt{B}}\right\}\right] \qquad (3.50)$$

$$I_3(\ell) = I(\ell_1) + I(\ell,\ell_1) \quad , \text{ and } \quad B = \frac{1-h_f^2}{\ell^2}$$

Hyperbolic Die. The hyperbolic die considered here has a zero exit angle and a non-zero (finite) entrance angle. The die profile is represented by

$$\Psi = h(s) = \sqrt{h_f^2 + \left(\frac{1-h_f^2}{\ell^2}\right)s^2} \qquad (3.51)$$

The upper bound on extrusion pressure is given by equation (3.44) with $I_1(\ell_1)$, $I_2(\ell,\ell_1)$ and $I_3(\ell)$ defined as

$$I_1(\ell_1) = B\left[\ell_1 - \frac{h_f}{\sqrt{B}} \tan^{-1}\left(\frac{\ell_1\sqrt{B}}{h_f}\right)\right]$$

$$I_2(\ell,\ell_1) = B\left[(\ell-\ell_1) - \frac{h_f}{\sqrt{B}}\left\{\tan^{-1}\left(\frac{\ell\sqrt{B}}{h_f}\right) - \tan^{-1}\left(\frac{\ell_1\sqrt{B}}{h_f}\right)\right\}\right]$$

$$I_3(\ell) = I_1(\ell_1) + I_2(\ell,\ell_1)$$

$$\text{where} \quad B = (1-h_f^2)/\ell^2 \qquad (3.52)$$

The die profiles and the shapes of plastic zone boundaries are shown in Figure 19. From equations (3.44), (3.46), (3.48), (3.50) and (3.52) one can observe that a closed form expression is obtained for a general upper-bound on extrusion pressure for the particular dies considered. Numerical results can thus be readily obtained. They are presented next.

Results

Effect of Parameter $\ell_1$. Figure 20 shows typical variations in the upper bound on reduced extrusion pressures with parameter $\ell_1$ for a cosine die when the reduction is 50%. For a frictionless die ($m_3 = 0$), the upper bound goes through a minimum and is least for a certain optimal value of $\ell_1$ ($\ell^1_{opt}$). The shape of the plastic zone II defined by $\ell^1_{opt}$ gives the best approximate model for the extrusion process occurring under the considered process variables ($h_f, m_3$).

When friction is present at the die surface, a greater pressure is required to extrude the material. The upper bound on extrusion pressure

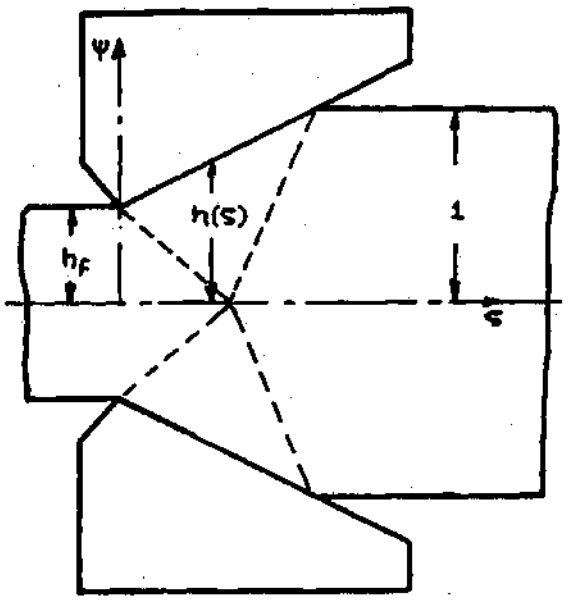


WEDGE SHAPED DIE

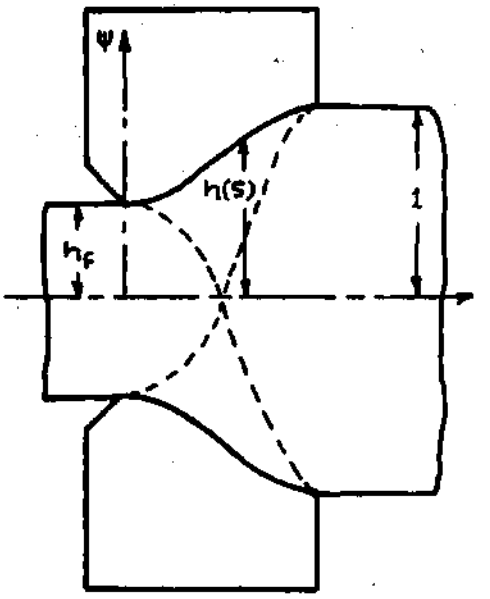


COSINE DIE

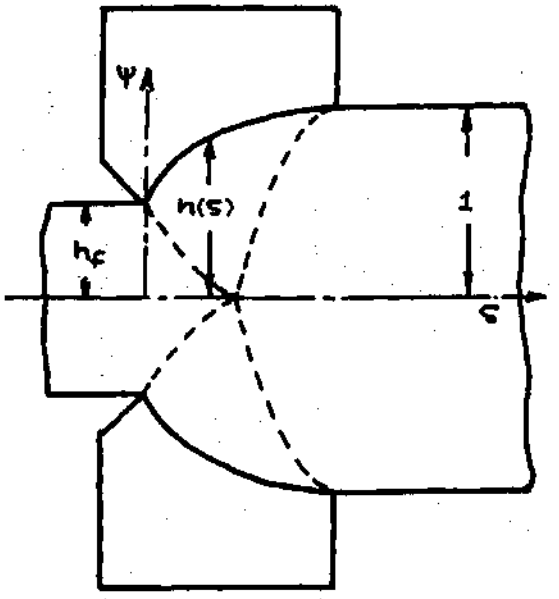


ELLIPTIC DIE

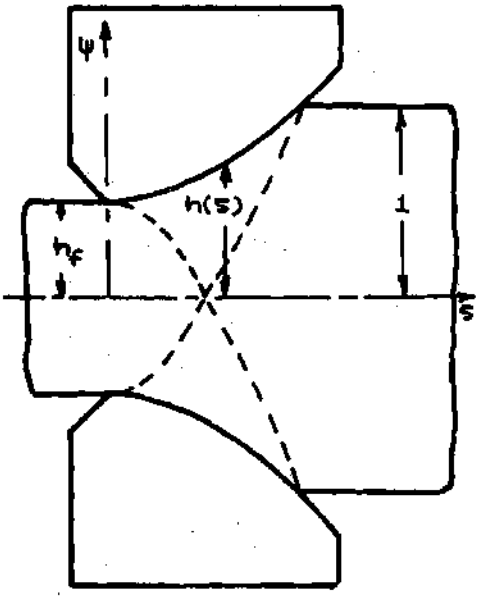


HYPERBOLIC DIE

**Figure 19.** Particular Die Shapes Analyzed. ( Dotted Lines Show the Shapes of the Plastic Zone Boundaries)

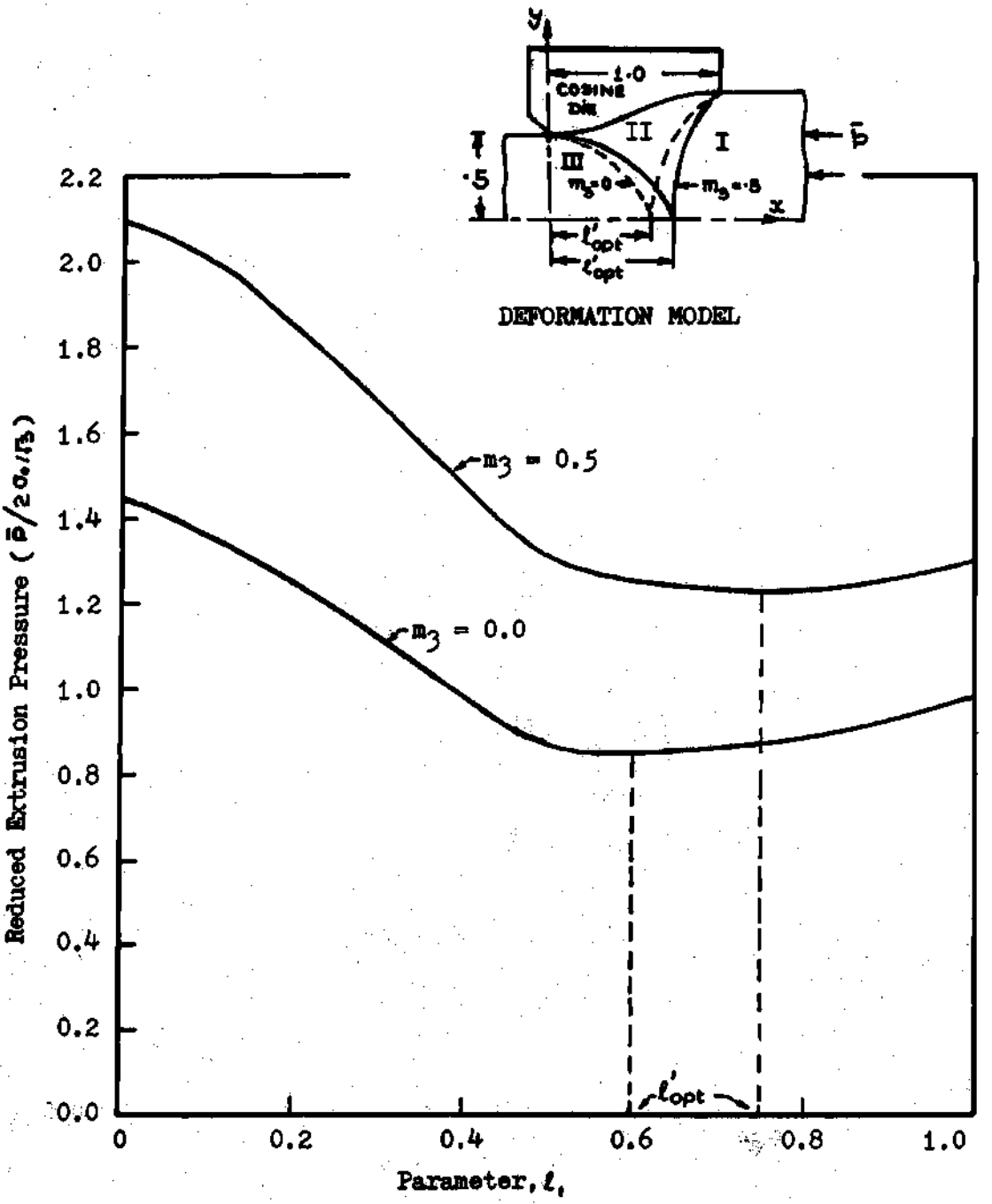


Figure 20. Variation of Upper Bound on Reduced Extrusion Pressure with Parameter $\ell_1$

still shows a similar variation with the parameter $\ell_1$ and a minimum in the upper bound is again obtained for a certain value of $\ell_1$. The value of optimal $\ell_1$ obtained under frictional conditions is greater than the optimal value of $\ell_1$ for a frictionless process. The effect of friction on the deformation model is thus to move the plastic zone in a direction opposite to the material flow. From slip-line field theory, one would expect, qualitatively, such an effect of friction on the deformation model [72]. For the elliptic, hyperbolic and wedge shaped dies, a similar variation of upper bound on reduced extrusion pressure with $\ell_1$ was observed.

Least Upper Bounds. Figures 21 and 22 show, for various dies, the least upper-bounds obtained as a function of percent reduction, which is defined as

$$RA\,\% = \left(\frac{t_o - t_f}{t_o}\right) \times 100$$

$$\text{or} \qquad RA\,\% = (1 - h_f) \times 100 \tag{3.53}$$

The dimensionless length ($\ell$) of the dies is equal to unity. The effect of friction at the die surface is indicated by plotting extrusion pressure as a function of reduction for different die friction indices ($m_3$). As one might expect, the results show an increase in extrusion pressure with reduction and / or friction at the die surface. From expression (3.44), it is obvious that the contribution due to friction becomes larger for longer dies. Comparison of numerical values shows that when $\ell = 1$, wedge shaped dies require the least extrusion pressure for a given reduction,

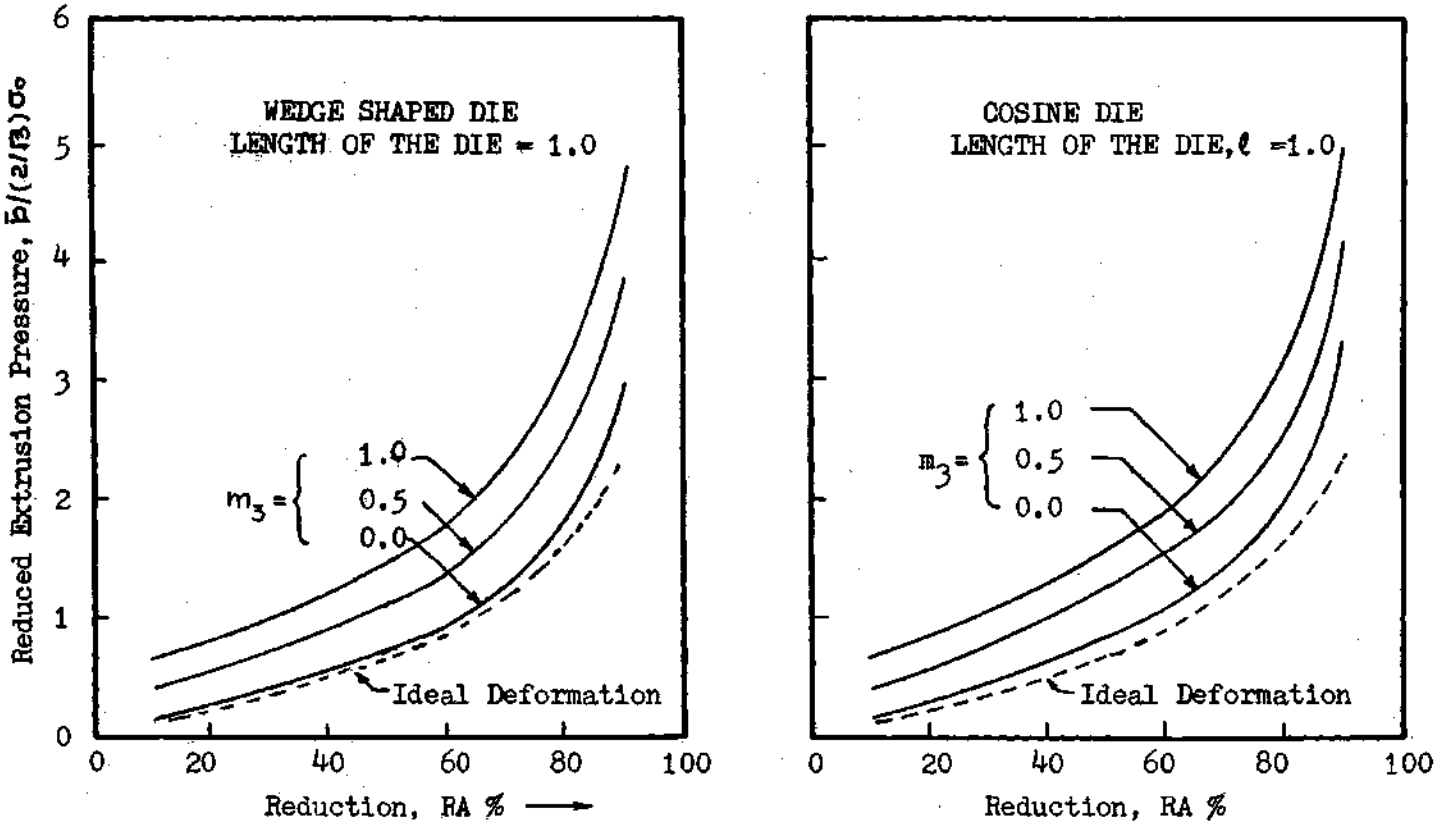


Figure 21. Reduced Extrusion Pressure VS Percent Reduction (RA)

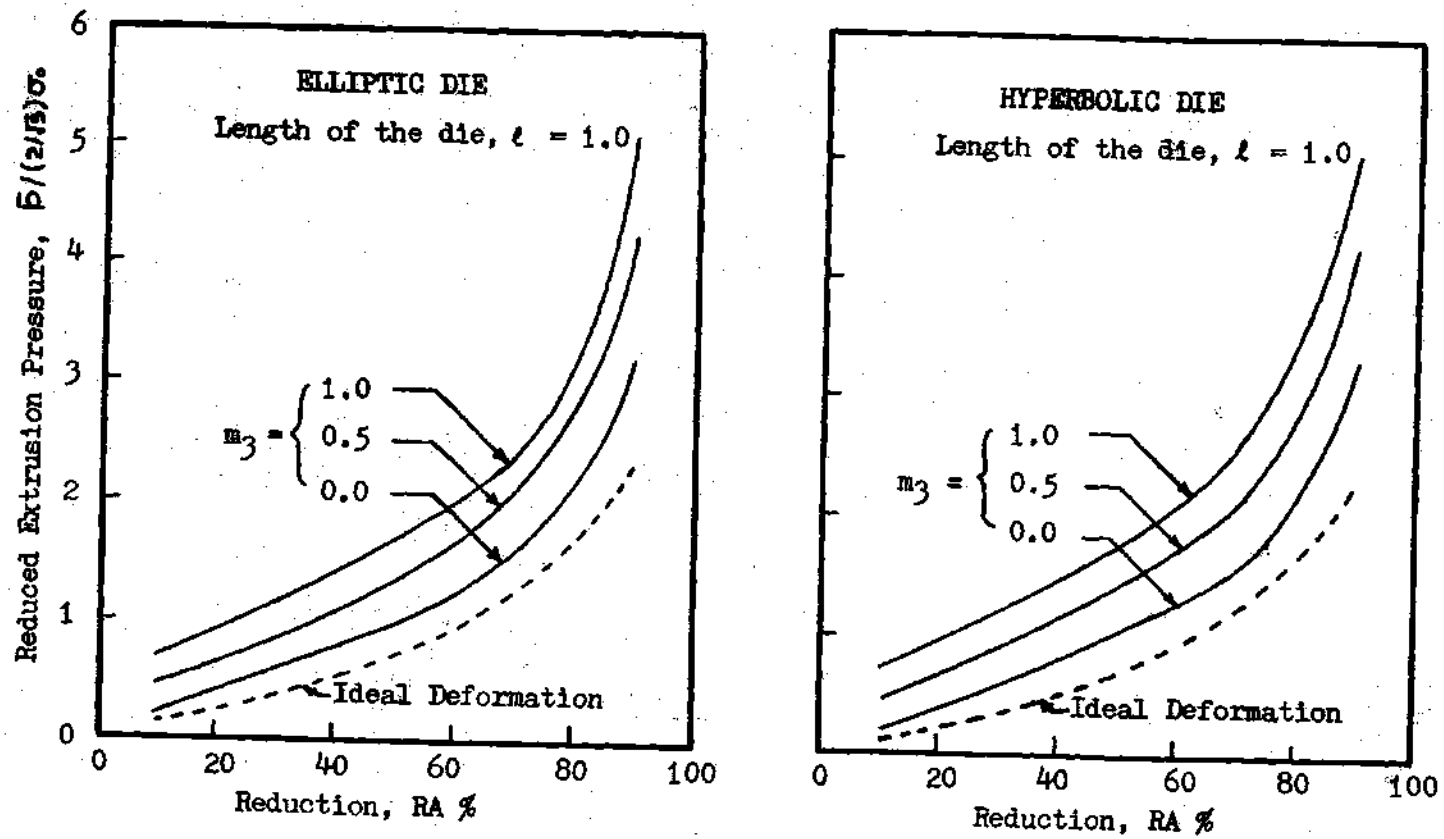


Figure 22. Reduced Extrusion Pressure VS Percent Reduction (RA)

cosine dies require higher pressure than wedge shaped dies, elliptic dies require higher than cosine, and hyperbolic dies require the highest extrusion pressure.

For a given reduction, the pressure required to deform the material ideally, e.g. under uniaxial tensile loading, is also shown in Figures 21 and 22. The ideal pressures are given by the relation

$$\frac{p_{ideal}}{2\sigma_o/\sqrt{3}} = \ln\left(\frac{1}{h_f}\right) \tag{3.54}$$

The difference between the actual extrusion pressure and the ideal pressure is an index of the additional redundant power needed over and above the minimum power required for homogeneous deformation. This difference is used normally to represent the inefficiency of any die. The redundancy of a die is normally defined [34] as

$$\text{Redundancy } \% = \left(\frac{p_{actual}}{p_{ideal}} - 1\right) \times 100 \tag{3.55}$$

Using the least upper bound in place of actual pressure, the redundancy is plotted in Figure 23 for various dies when $\ell = 1$. The redundancy is least for wedge shaped dies and highest for hyperbolic dies. Figure 24 shows the dependence when $\ell = 2$. The wedge shaped dies show the least redundancy up to about 70% reduction. Above this reduction, the elliptic dies show better efficiency. It is important to realize that the actual redundancy of these dies will be less than the values plotted in Figures 23 and 24 because the least upper bound value is used in place of the actual

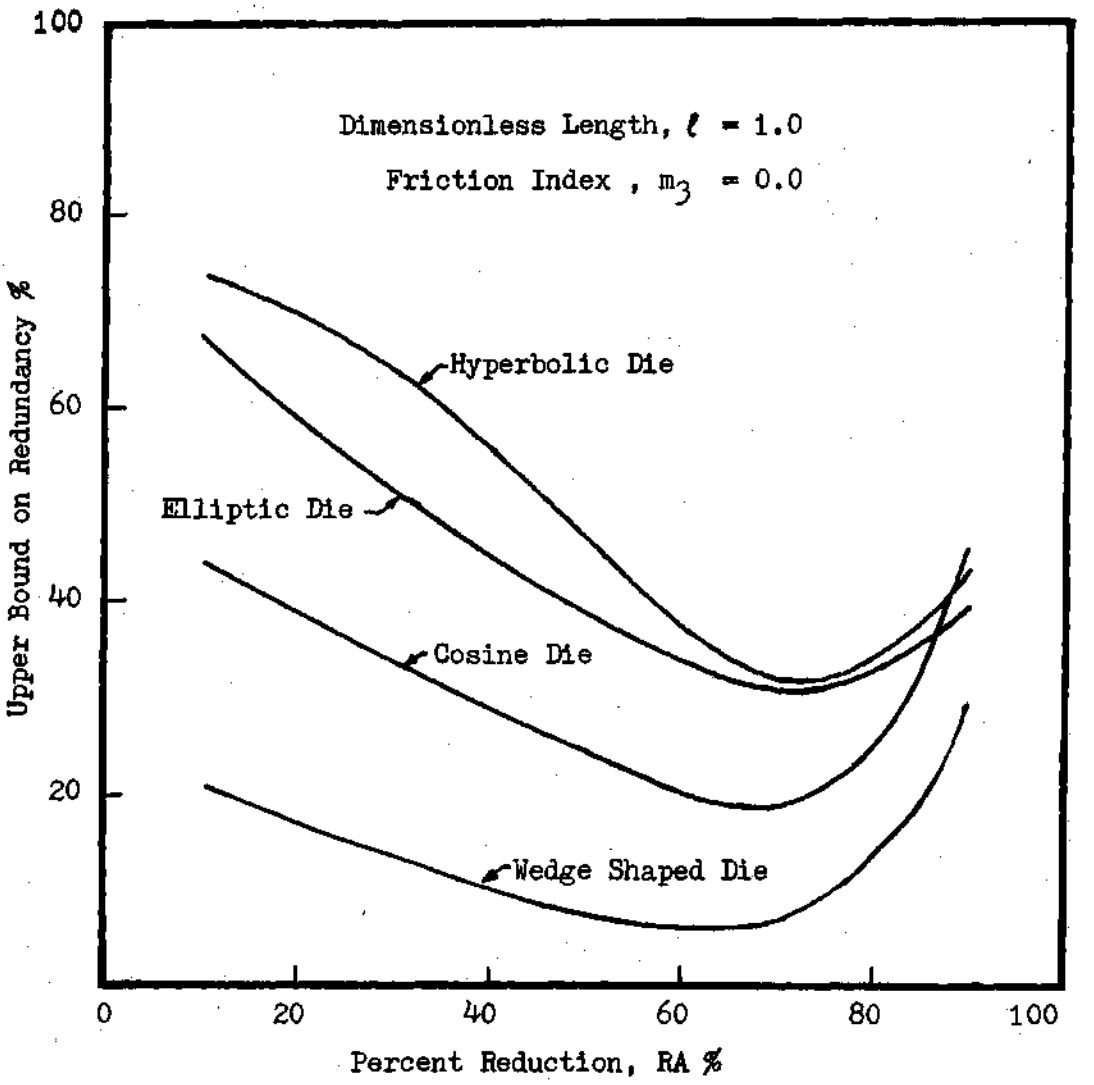


Figure 23. Effect of Reduction on Redundancy in Extrusion through Various Dies when the Dimensionless Length of the Dies is Equal to One

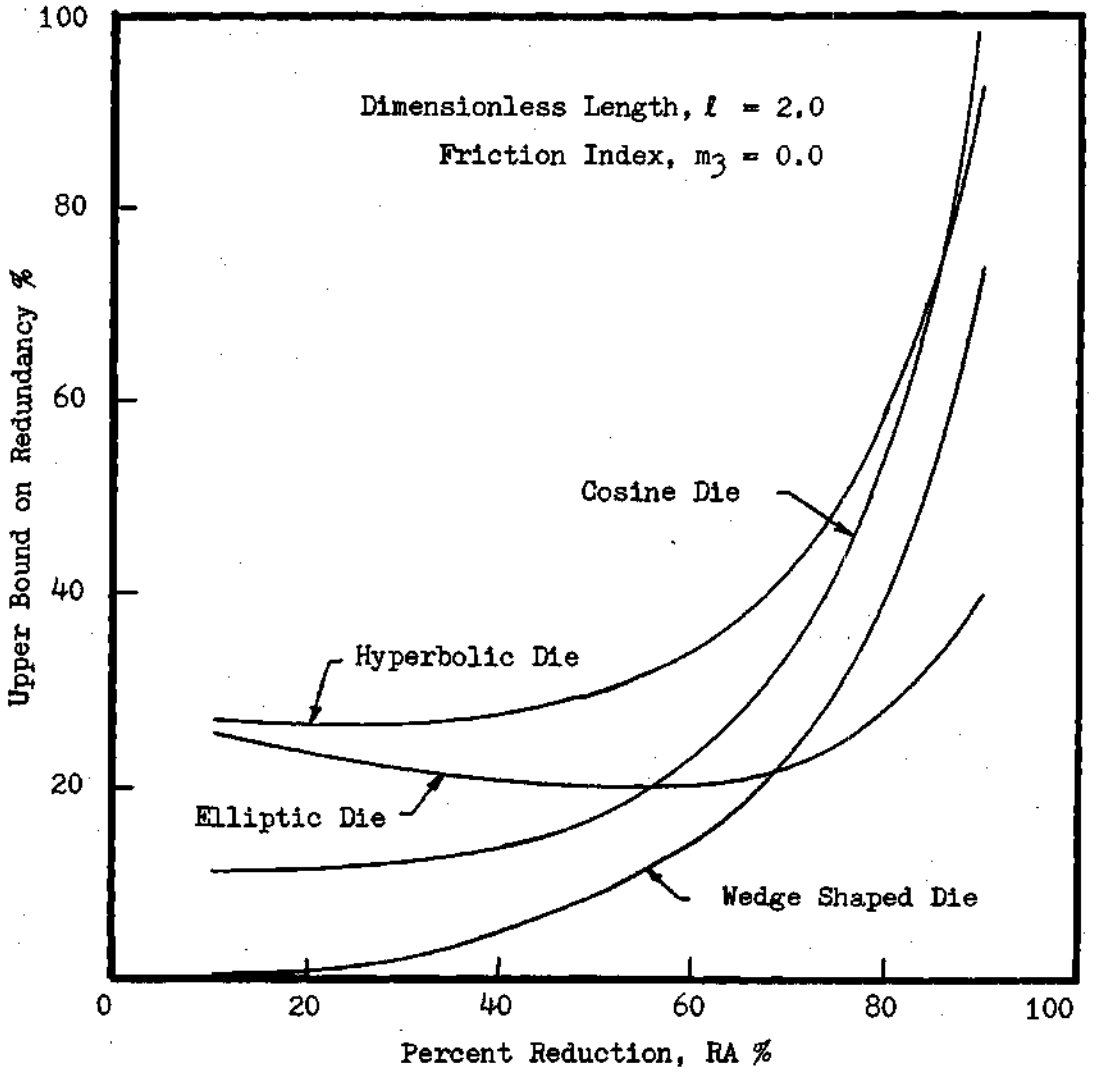


Figure 24. Effect of Reduction on Redundancy in Extrusion through Various Dies when the Dimensionless Length of the Dies is Equal to Two

pressure in equation (3.55). The results thus show that for small reductions, the wedge shaped die approaches the ideal dies proposed by Richmond and Devenpeck [45] and Morrison [73] in efficiency for a frictionless process.

An evaluation of the usefulness of the proposed lower upper-bound analysis is made by comparing results with Chen's simple upper bound solution [35]. Comparison of values for redundancy of the various dies, shown in Figure 25, indicates that except for the hyperbolic die, much lower upper-bounds on redundancy and hence on extrusion pressure are obtained with the current analysis when the reduction and the die length are small. For longer dies and larger reductions the present solution does not give better results mainly because the assumption of a triangular shaped plastic zone fails to approximate the actual deformation under these process conditions. For hyperbolic dies, triangular plastic zone is not suitable under most conditions because of the extreme angle of the die at the entrance. In actual practice, the die length is kept small to reduce the loss of useful power due to friction at the die surface. Also the percentage reduction is limited by the tendency of the material to buckle under high compressive extrusion pressure. For practical conditions of small die lengths ($\ell$) and reductions, the proposed analysis presents better solution.

## Dies With Discontinuities

In formulating the deformation models shown in Figures 17 and 18, the assumption was made that the function $h(s)$ representing the die contour had no discontinuities in its first and second derivatives. Extrusion

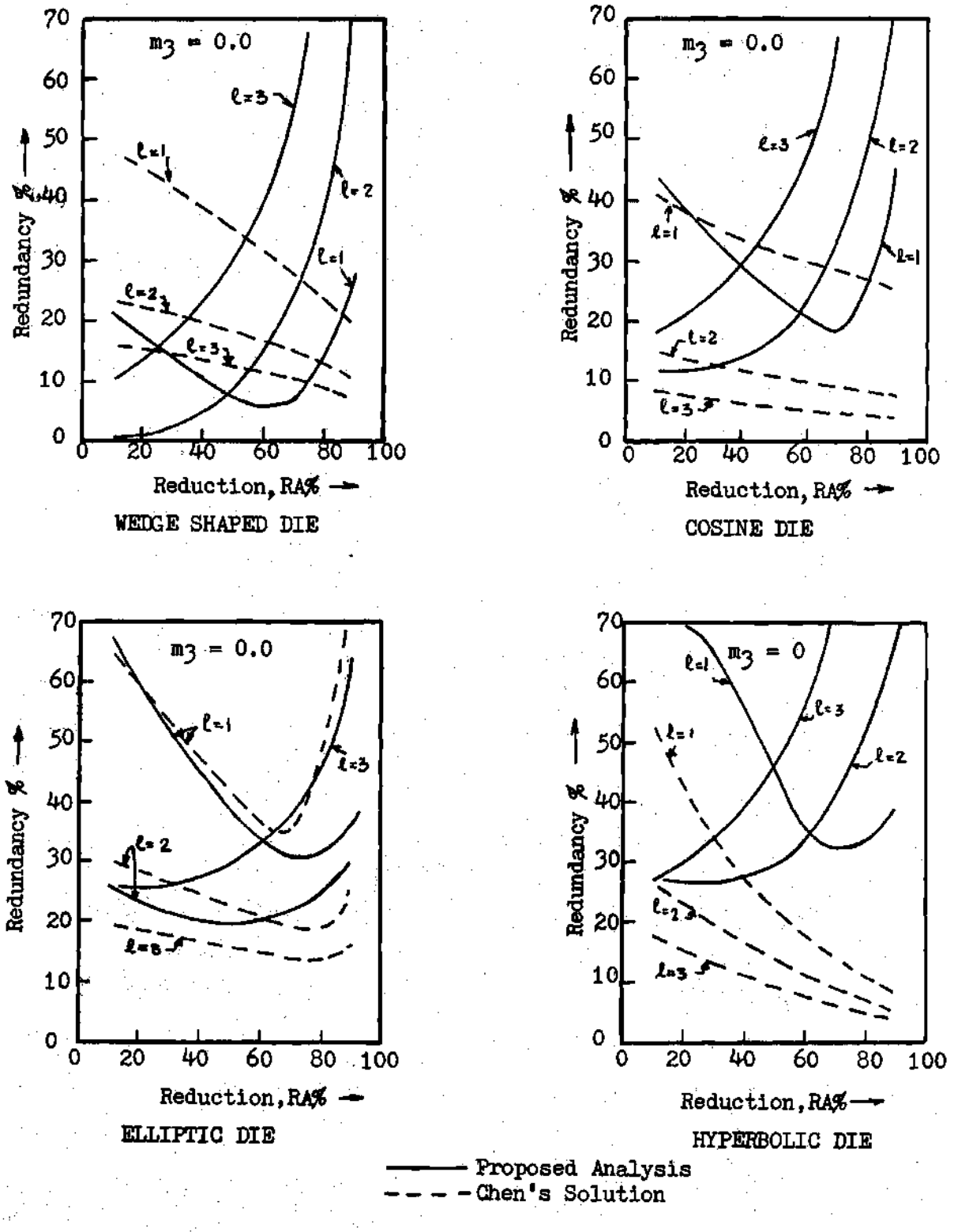


Figure 25. Comparison with Simple Upper Bound Solution Proposed by Chen [35]

through dies with discontinuities in $h(\varsigma)$, $h'(\varsigma)$ and $h''(\varsigma)$ can easily be treated as follows. A discontinuity is either removed by assuming a suitable dead zone surface as the rigid tool boundary or one or two surfaces of velocity discontinuity are assumed to start from this discontinuity thus excluding it from the plastic zone. As an example, consider extrusion through a square die. The discontinuity in $h(\varsigma)$ is removed by assuming suitable dead zone (see Figure 26a). Another example where discontinuity in slope is removed by assuming a dead zone is shown in Figure 26b. For these dies the upper bound on extrusion pressure can easily be calculated by treating the dead zone as perfectly rough ($m_3 = 1.0$).

Figure 26c shows how a discontinuity in $h'(\varsigma)$ or $h''(\varsigma)$ can be avoided by assuming two surfaces of tangential velocity discontinuity. The zone bounded by these surfaces may be considered rigid or non-deforming. It should be noted that this choice of the deformation model simply makes the extrusion of any material through the die with discontinuities equivalent to extrusion through a number of dies with no discontinuities. As shown in Figure 26d, assumption of a single surface of velocity discontinuity can also avoid the discontinuity in die profile. The plastic zone is divided into two zones and continuous velocity field as well as strain rate field can be determined for each plastic zone from flow function concepts.

## High Efficiency Dies for Plane Strain Extrusion

As stated before, a problem of great industrial importance is the determination of the die profiles that are most efficient for plane strain

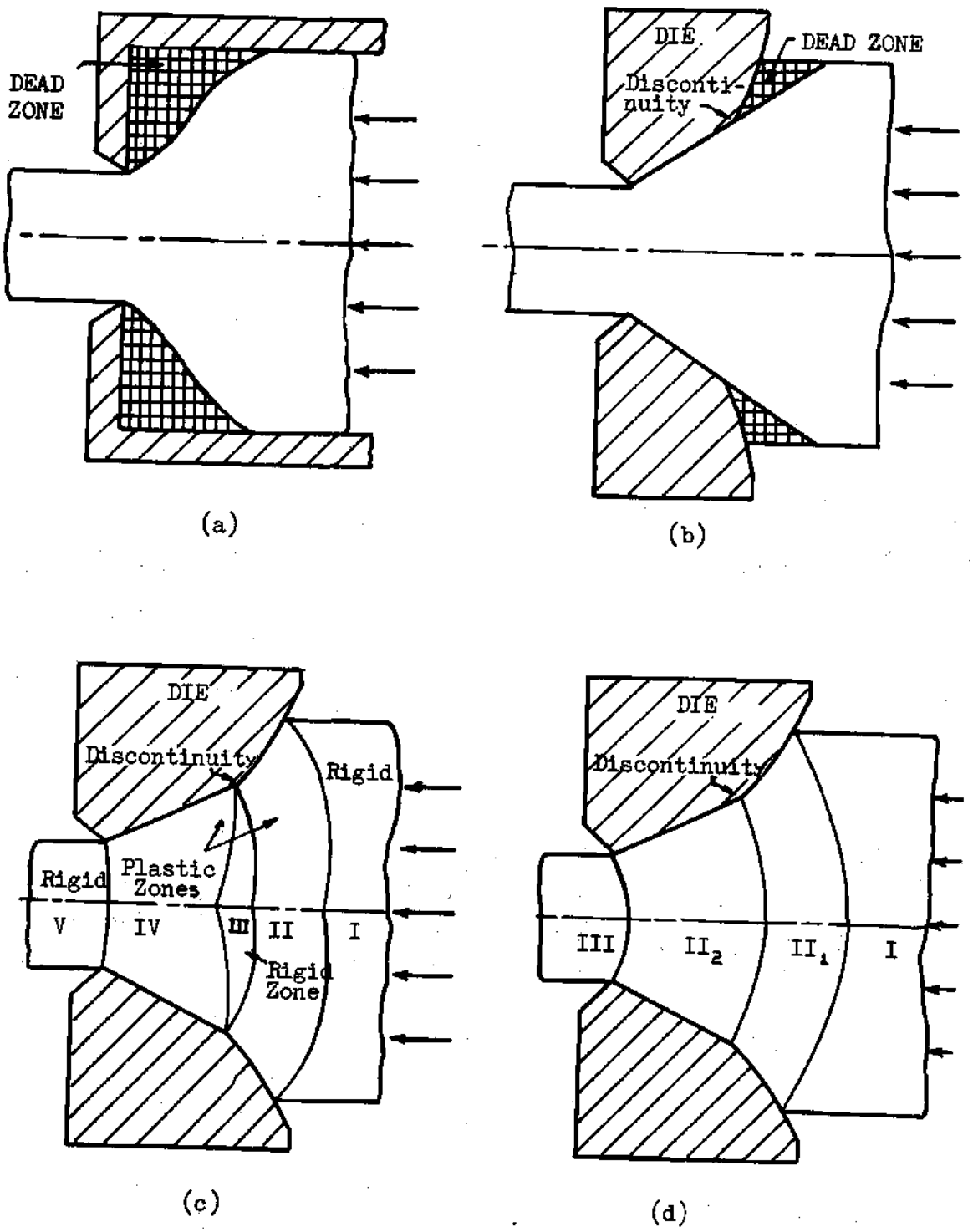


Figure 26. Dies with Discontinuities

extrusion or drawing under frictional conditions. For frictionless extrusion, ideal dies which require the minimum work for uniform deformation have been proposed by Richmond and Devenpeck [45] who used slip field theory and a semi-inverse technique. For extrusion under frictional conditions, the most efficient die profiles have not yet been determined. Here, in this work, an attempt is made to solve this problem by utilizing the proposed lower upper-bound approach. Clearly the approximate nature of the method itself rules out the possibility of finding the exact profiles. However, within the limitation of the proposed approach, die profiles which show quite high efficiency are determined.

Using the deformation model shown in Figure 18, expression (3.44) gives the upper bound on extrusion pressure in extrusion of a rigid-perfectly plastic material through an arbitrarily shaped die. This relation for $\bar{p}$ may be written in functional form as

$$\bar{p} = \bar{p}\left(h(s), \ell, \ell_1, h_f, m_s\right) \tag{3.56}$$

where the parameters inside the bracket are the variables. For a given reduction and friction index, the interest is to find the die profile $h(s)$ and the length of die ($\ell$) which gives a minimum $\bar{p}$. Due to the complexity of the expression (3.44), it is unlikely that the exact extremizing function $h(s)$ and the parameters $\ell$, and $\ell_1$ can be obtained through variational principles. Therefore approximate solution is attempted. As done in the direct methods of calculus of variations, the function $h(s)$ is approximated as a linear combination of some known functions. In the proposed analysis, two different forms for $h(s)$ were

tried.

In one case, the die profile was assumed to have a parabolic shape given by

$$\psi = h(s) = \sum_{i=0}^{2} a_i x^i \qquad (3.57)$$

For a given reduction, the coefficients $a_1$ are related and the die profile may be represented by

$$\psi = h(s) = h_f + ax + bx^2 \qquad (3.58)$$

where $a = \left( \frac{1-h_f}{\ell} - b\ell \right)$

The slope of the die should not be negative with the choice of coordinate axes shown in Figure 18. This requires

$$-\left( \frac{1-h_f}{\ell^2} \right) \leq b \leq \left( \frac{1-h_f}{\ell^2} \right)$$

For this die

$$I_1(\ell_1) = a^2 \ell_1 + \frac{4}{3} b^2 \ell_1^3 + 2ab\ell_1^2$$

$$I_2(\ell,\ell_1) = a^2(\ell-\ell_1) + \frac{4}{3} b^2(\ell^3-\ell_1^3) + 2ab(\ell^2-\ell_1^2)$$

Substituting for $h(s)$, $I_1(\ell_1)$, $I_2(\ell, \ell_1)$ in equation (3.44), one obtains, for a given reduction and friction index ($m_3$), an expression for the extrusion pressure of form

$$\bar{p} = \bar{p}(b, \ell, \ell_1)$$

The extrusion pressure is thus obtained as a function of three independent coefficients $(b, \ell, \ell_1)$. The problem is accordingly reduced to finding the values of these coefficients which make $\bar{p}$ a minimum. The previously written computer program (Appendix A) was slightly modified and was used to obtain the value of $\ell_1$ that gave the least pressure for any given b and $\ell$. b and $\ell$ were then varied and their values which gave the minimum pressure were obtained by trial and error. The optimal values of b and $\ell$, when substituted in equation (3.58), defined that die profile which requires the least extrusion pressure.

The other form assumed for $h(s)$ had a cosine contour represented by

$$\psi = h(s) = \frac{h_f - \cos(\pi c \ell)}{1 - \cos(\pi c \ell)} + \frac{1 - h_f}{1 - \cos(\pi c \ell)} \cos[\pi c (\ell - s)] \qquad (3.59)$$

$$\text{where} \quad 0 < c \leq \frac{1}{\ell}$$

For this die

$$I_1(\ell_1) = \left[\frac{(1-h_f)\pi c}{1-\cos(\pi c \ell)}\right]^2 \left[\frac{\ell_1}{2} + \frac{1}{4\pi c}\left\{\sin[2\pi c(\ell - \ell_1)] - \sin(2\pi c \ell)\right\}\right]$$

$$I_2(\ell, \ell_1) = \left[\frac{(1-h_f)\pi c}{1-\cos(\pi c \ell)}\right]^2 \left[\left(\frac{\ell - \ell_1}{2}\right) - \frac{1}{4\pi c}\sin[2\pi c(\ell - \ell_1)]\right]$$

Substituting for $h(\varsigma)$, $I_1(\ell_1)$, and $I_2(\ell, \ell_1)$, one obtains an expression for extrusion pressure of the form

$$\bar{p} = \bar{p}(c, \ell, \ell_1)$$

Optimal values of c and $\ell$, and the corresponding die profiles, were obtained in a similar manner.

Numerical results showed that the parabolic form (3.58) gave lower values for extrusion pressure compared to cosine shape (3.59) for any given reduction and frictional condition. Table 1 gives the die parameters which define the shapes of the high efficiency dies obtained through proposed approach. It may be noted that when b = 0 in equation (3.58), the die takes a wedge shape. For frictionless extrusion and for small reductions, wedge shaped dies have efficiencies approaching the ideal efficiency of 100% . Efficiency is defined here as

$$\text{Efficiency } \% = \frac{p_{ideal}}{p_{actual}} \times 100$$

For larger reductions, the optimal die profiles have a concave shape for all frictional conditions considered. The profiles for RA = 70% and RA = 90% are shown in Figure 27 for frictionless extrusion ($m_3 = 0.0$) and when the friction index $m_3 = 0.1$. The optimal length of dies decreases with increase in friction as shown in Table 1.

## Discussion

The flow function can be applied readily to form general

Table 1. High Efficiency Dies

Die Profile: $h(S) = h_f + \left(\frac{1-h_f}{\ell} - b\ell\right)x + bx^2$

| Process Parameters | | Die Parameters | | Extrusion Pressure $\bar{p}/(2/\sqrt{3})\sigma_o$ | Extrusion Efficiency % |
|---|---|---|---|---|---|
| Reduction | Friction Index, $m_3$ | Length ($\ell$) | b | | |
| 10 | 0.0 | 1.9 | 0.0 | 0.1054 | 99.963 |
| 30 | 0.0 | 1.7 | 0.0 | 0.3586 | 99.462 |
| 50 | 0.0 | 1.4 | 0.0 | 0.7071 | 98.027 |
| 70 | 0.0 | 1.1 | -0.058 | 1.2768 | 94.296 |
| 90 | 0.0 | 0.8 | -0.984 | 2.7046 | 85.136 |
| 10 | 0.1 | 1.1 | 0.0 | 0.1795 | 58.697 |
| 30 | 0.1 | 1.3 | 0.0 | 0.4490 | 79.436 |
| 50 | 0.1 | 1.2 | 0.0 | 0.8066 | 85.935 |
| 70 | 0.1 | 1.0 | -0.070 | 1.3893 | 86.666 |
| 90 | 0.1 | 0.7 | -1.194 | 2.8728 | 80.151 |
| 10 | 0.2 | 0.9 | 0.0 | 0.2311 | 45.59 |
| 30 | 0.2 | 1.1 | 0.0 | 0.5241 | 68.054 |
| 50 | 0.2 | 1.1 | 0.0 | 0.8945 | 77.490 |
| 70 | 0.2 | 1.0 | -0.140 | 1.4941 | 80.582 |
| 90 | 0.2 | 0.7 | -1.010 | 3.0372 | 75.812 |

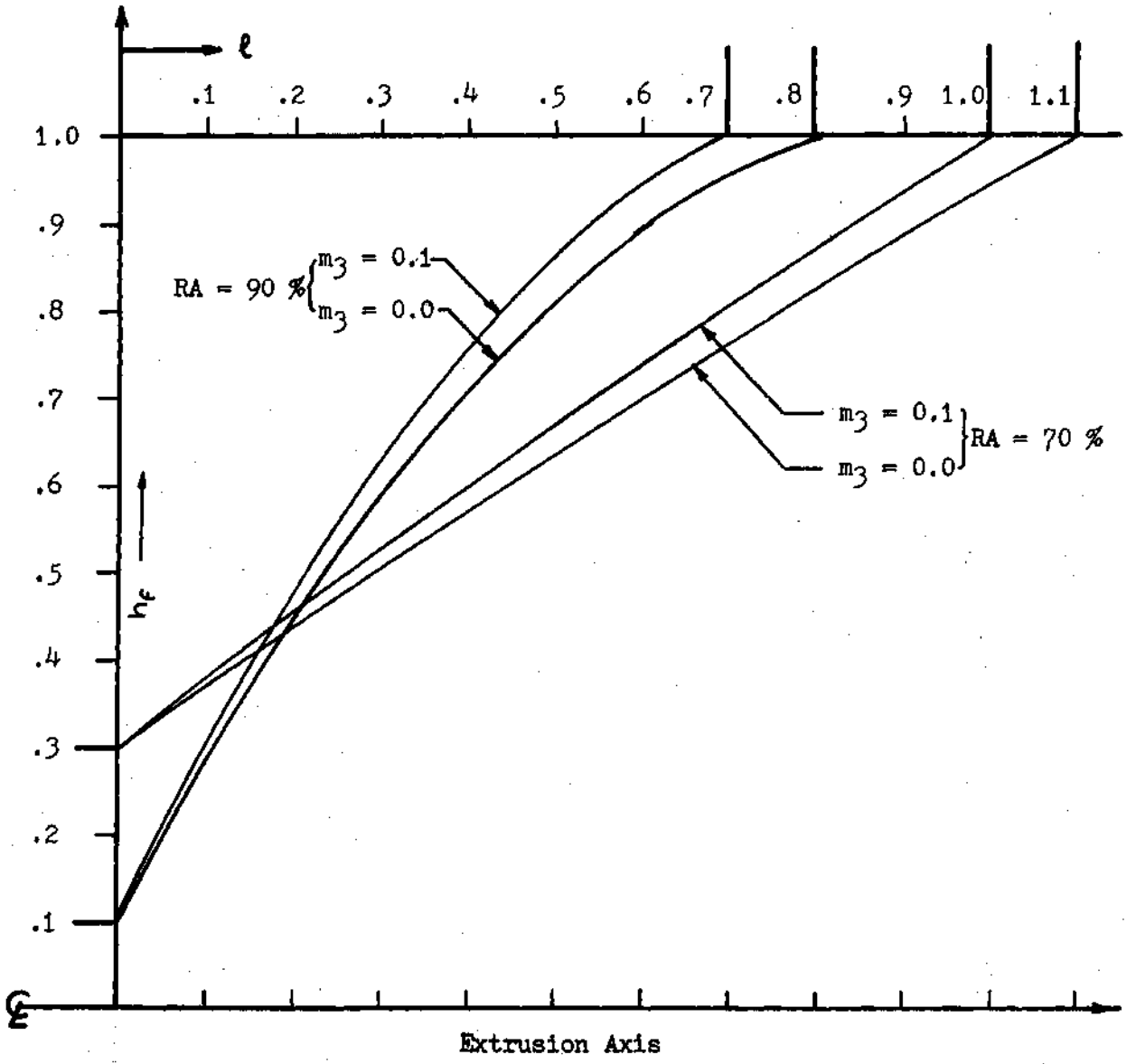


Figure 27. Profiles of High Efficiency Dies

kinematically admissible model for any extrusion process. It appears unlikely that an exact solution can be obtained through this approach because of the complexity of the expression for extrusion pressure. Useful but approximate solution may be obtained by restricting the general flow function. As done in proposed lower upper-bound analysis, with the assumption of the model that has a triangular shaped plastic zone (Figure 18), a simple closed form expression for $\bar{p}$ is obtained. However, the model gives useful results only when the die length ($\ell$) and percent reduction (RA) are small. For long dies and larger reductions, model shown in Figure 17 must be used to obtain close approximate solution.

The results obtained by assuming the model shown in Figure 18 seem to indicate that wedge shaped dies are more efficient compared to other dies considered, in the sense that less pressure is required to extrude a material through these dies. Undoubtedly, it can be asserted that wedge shaped dies have very high efficiency. However its comparison with other dies in regard to the extrusion efficiency must be made keeping in mind the approximate nature of the upper bound solution. The validity of the comparison between different dies can be asserted only when all possible kinematic models are tried and also when the formation of dead zone is investigated. The same discussion applies to the proposed analysis of high efficiency dies. The results give the die profiles that have efficiences atleast as high as shown in Table 1. Yet, by no means, these dies are the most efficient dies.

# CHAPTER IV

# IRONING OF CUPS IN DEEP DRAWING

## Definition of the Problem

Deep drawing with simultaneous ironing is performed with essentially the same equipment as is used for ordinary deep drawing. The clearance between the punch and the die is kept smaller than the nominal thickness of the blank which results in a forced reduction of the cup wall. Figure 4 shows deformation of the blank at a stage of the process when the punch has moved well into the die. At this stage, a portion of the blank in region A is radially drawn towards the center of the punch. In region B, radial drawing and bending of the blank under tension occurs and in region C, the bent material is ironed. The processes of radial drawing and plastic bending in regions A and B are common to the ordinary deep drawing process. Complete analyses for these two regions have been presented [54] and therefore are not treated here. As stated in Chapter I, no satisfactory solution has been presented for the ironing process taking place in region C. The present work analyzes only the ironing process occurring in region C.

The initial stage of the deep drawing process in which the punch just bends the flat blank but has not yet entered the die is similar to the corresponding initial stage in ordinary deep drawing process analyzed by Swift and Chung [54]. This portion of the process is, therefore, also excluded from the current work. The problem thus posed is to determine

the contribution of the ironing process occurring in region C to the total punch load required for the process of deep drawing with simultaneous ironing.

## Upper Bound Analysis

It is of importance to realize the following characteristic features of the ironing process occurring in region C:

1. The process is unsteady. The thickness of the blank entering region C is continuously changing during the deep drawing process due to the radial drawing and plastic bending of the blank in regions A and B.

2. The material entering region C has a certain curvature due to bending over the die profile under tension in region B.

3. The initially curved blank, after getting ironed between the punch and the die, leaves the die in a axial direction. Also the ironed cup has the same velocity as the punch.

Here, an upper bound analysis which utilizes the flow function concepts discussed in Chapter II is developed. This analysis presents a solution at any particular instance of time when the thickness of the entering blank is $t_o$ and the final thickness of the ironed blank is $t_f$ (see Figure 28). Since in the unsteady process the only parameter changing with time is $t_o$, the variation of the component of the punch load due to ironing with time or downward movement of the punch can easily be obtained by means of a step by step solution.

### Kinematically Admissible Model

The following assumptions are made in the analysis:

1. The deformation in region C (Figure 4) occurs under plane

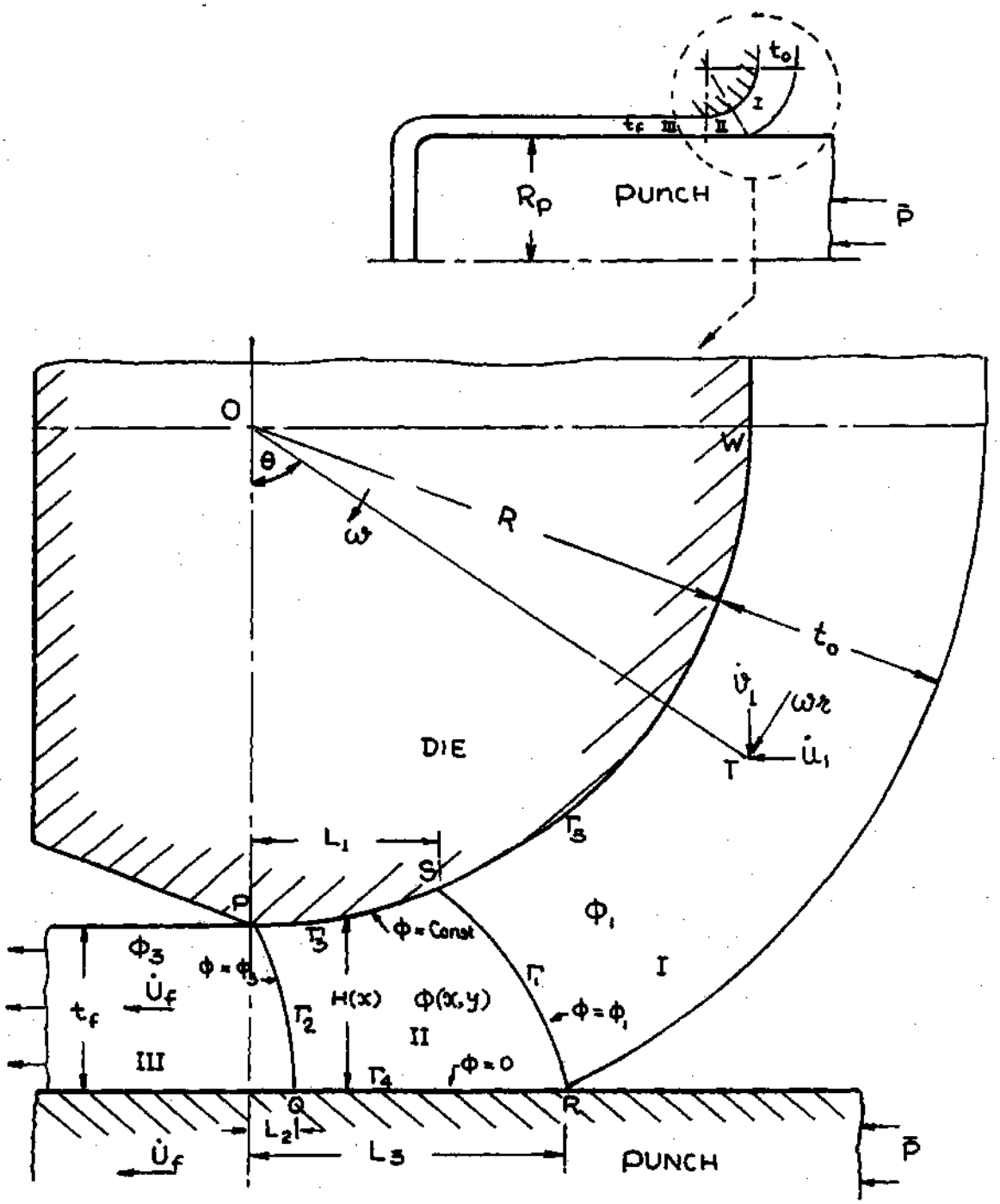


**Figure 28.** Deformation Model for the Ironing Process

strain conditions. This assumption is justified as the thickness of the blank is usually much less than the diameter of the punch. The hoop strain can thus be neglected [1] and the process can be considered as taking place under plane strain conditions.

2. The material entering region C has an initial radius of curvature. This, together with the assumption of plane strain deformation, implies that the entering material has a rigid body rotational motion.

Due to rotational symmetry, deformation in the upper half portion only of a meridian plane is considered and shown in Figure 28. To determine the ironing load at any instance of the process, let the initial thickness of the blank be $t_o$ and let $t_f$ represent the thickness of ironed cup. To obtain a kinematically admissible model for this ironing process, the deforming body is divided into three zones as shown in Figure 28. The body of material in zone I has a rigid body rotational motion about the axis O of the circular die. In zone II, the blank undergoes plastic deformation and its thickness is reduced from $t_o$ to $t_f$. The deformed material in zone III has a uniform axial velocity ($\dot{U}_f$) equal to the velocity of the moving punch. The necessary kinematic conditions are satisfied in zones I and III. A kinematically admissible velocity field ($\dot{U}_x, \dot{U}_y$) for zone II together with admissible shapes of boundaries $\Gamma_1$ and $\Gamma_2$ of the plastic zone has to be determined to complete the kinematically admissible model for the process.

The circular profile of the die is represented by

$$y = H(x) = R + t_f - \sqrt{R^2 - x^2} \qquad (4.1)$$

R is the radius of the die. $\phi(x,y)$ represents the flow function for the velocity field in zone II and is defined by

$$\left.\begin{aligned} \dot{U}_x &= \frac{\partial \phi}{\partial y} \\ \dot{U}_y &= -\frac{\partial \phi}{\partial x} \end{aligned}\right\} \qquad (4.2)$$

Let the boundaries $\Gamma_1$ and $\Gamma_2$ be represented as

$$\begin{aligned} \Gamma_1 &: \quad y = y_{\Gamma_1}(x) \\ \Gamma_2 &: \quad y = y_{\Gamma_2}(x) \end{aligned} \qquad (4.3)$$

The components $(\dot{u}_1, \dot{v}_1)$ of the velocity vector in the x and y directions respectively for any point T in zone I are

$$\left.\begin{aligned} \dot{u}_1 &= -\omega r \cos\theta = -\omega(R + t_f - y) \\ \dot{v}_1 &= -\omega r \sin\theta = -\omega x \end{aligned}\right\} \qquad (4.4)$$

where $\omega$ is the angular speed of zone I about 0, r is the distance of point T from point 0 and $\theta$ is the angle as shown in Figure 28. It can be easily verified that the flow function $\phi_1(x,y)$ defined by equations

$$\dot{u}_1 = \frac{\partial \phi_1}{\partial y} \quad , \quad \dot{v}_1 = -\frac{\partial \phi_1}{\partial x} \qquad (4.5)$$

is $$\phi_1(x,y) = \frac{\omega}{2}\left[x^2 + (R + t_f - y)^2\right] + \text{Const} \qquad (4.6)$$

Following Chapter II, the kinematic boundary conditions on $\phi$ for zone II are

$$\phi(x,y) = -\dot{U}_f t_f \quad \text{at} \quad y = H(x) \qquad (4.7)$$

$$\phi(x,y) = 0 \quad \text{at} \quad y = 0 \qquad (4.8)$$

$$\phi(x,y) = -\dot{U}_f y \quad \text{at} \quad y = y_{\pi_2} \qquad (4.9)$$

$$\phi(x,y) = \frac{\omega}{2}\left[x^2 + (R + t_f - y)^2\right] + \text{Const} \quad \text{at} \quad y = y_{\pi_1} \qquad (4.10)$$

The constant in equation (4.10) can be determined from the condition

$$\phi(x,y) = \phi_1(x,y) = 0 \quad \text{at} \quad \text{point} \quad R$$

which yields

$$\text{Const} = -\frac{\omega}{2}(R + t_0)^2 \qquad (4.11)$$

Substituting in equation (4.10), one obtains

$$\phi(x,y) = \frac{\omega}{2}\left[x^2 + (R + t_f - y)^2\right] - \frac{\omega}{2}(R + t_0)^2 \quad \text{at} \quad y = y_{\pi_1} \qquad (4.12)$$

The model shown in Figure 28 would be kinematically admissible if a flow function $\phi(x,y)$ can be determined which satisfies equations (4.7), (4.8), (4.9) and (4.12). Equations (4.9) and (4.12) do not restrict $\phi$ because the shapes of boundaries $\Gamma_1$ and $\Gamma_2$ are not fixed by the geometry of the problem. The conditions on the flow function due to continuity at these surfaces can always be satisfied by choosing the equations of the boundaries to be

$$\Gamma_2 : \qquad \Phi(x,y) = -\dot{U}_F\, y \tag{4.13}$$

$$\text{and} \quad \Gamma_1 : \qquad \Phi(x,y) = \frac{\omega}{2}\left[x^2 + (R + t_f - y)^2\right] - \frac{\omega}{2}(R+t_o)^2$$

The whole problem is, therefore, reduced to finding a flow function which satisfies equations (4.7) and (4.8). Clearly, there are infinite admissible flow functions which would satisfy equations (4.7) and (4.8). Therefore the determination of the actual flow function which would yield the mathematically exact model requires an additional condition. This condition comes from the principle of the Upper Bound Theorem that the actual velocity field and hence the actual flow function minimizes the upper bound. Due to the complexity of the expression for the upper bound on the punch load, an exact solution for $\phi(x,y)$ cannot be obtained by variational methods. An approximate lower upper-bound solution is therefore attempted by approximating the actual flow function by a linear combination of some known functions $\Lambda(x,y)$

$$\Phi(x,y) = \sum_{i=1}^{N} b_i \Lambda_i(x,y) \tag{4.14}$$

The coefficients $b_i$ can then be determined so that the upper bound on the component of punch load due to ironing is a minimum.

Lower Upper-Bound Solution

In this analysis, the $\Lambda_i(x,y)$ are chosen to be of the form

$$\Lambda_i(x,y) = \eta^i \tag{4.15}$$

where $\eta(x,y) = y/H(x)$

Numerical formulation of the problem requires further simplification. In equation (4.14), all coefficients except $b_1$ and $b_2$ are taken to be equal to zero. The flow function is thus approximated by

$$\Phi(x,y) = b_1(y/H(x)) + b_2(y/H(x))^2 \tag{4.16}$$

Applying equation (4.7) and the condition that the boundary $\Gamma_2$ represented by equation (4.13) passes through point Q yields

$$b_1 + b_2 = -\dot{U}_f t_f$$

$$\text{and} \qquad b_1 = -\dot{U}_f H(L_2) \tag{4.17}$$

$H(L_2)$ is the value of $H(x)$ at $x = L_2$. Solving for $b_1$ and $b_2$ and substituting in equation (4.16) gives the following equation for the assumed flow function.

$$\phi(x,y) = \dot{U}_f t_f \left[-C\eta + (C-1)\eta^2\right] \tag{4.18}$$

where $C = \frac{H(L_2)}{t_f}$ and $\eta = y/H(x)$

From equations (4.2) and (4.18), the velocity field in zone II can be determined. Boundaries of plastic zone II can be determined by substituting equation (4.18) in (4.13). Knowing the velocity field in the different zones and the equations of the various boundaries, various components of the total rate of energy dissipation can be calculated. Appendix B gives the details of the derivation. Only the final expressions for these quantities are given here. To nondimensionalize, let

$$y/t_o = \Psi \;,\; x/t_o = S \;,\; t_f/t_o = h_f \;,\; R/t_o = R_d,\; L_2/t_o = \ell_2$$

$$L_1/t_o = \ell_1 \;,\; L_3/t_o = \ell_3 \;,\; H(L_2)/t_o = h(\ell_2) \;,\; H(x)/t_o = h(S) \tag{4.19}$$

Then one obtains the following expressions:

Die profile:

$$\Psi = h(S) = R_d + h_f - \sqrt{R_d^2 - e^2} \tag{4.20}$$

Boundaries of the plastic zone:

$$\Gamma_1: \quad \Psi + h(S) - 2(R_d + h_f) - 2\frac{(R_d + .5)}{h(S)}\left[-C + (C-1)X\left(\frac{\Psi}{h(S)} + 1\right)\right] = 0 \qquad (4.21)$$

$$\Gamma_2: \quad \Psi = \frac{h(S)}{(C-1)}\left[C - \frac{h(S)}{h_f}\right] \qquad \text{when } \ell_2 \neq 0$$

$$S = 0 \qquad \text{for } \ell_2 = 0 \qquad (4.22)$$

Velocity field in zone II:

$$\dot{U}_x = t_o(\dot{U}_f t_f)\left[-C + 2(C-1)\frac{\Psi}{h(S)}\right]\frac{1}{h(S)}$$

$$\dot{U}_y = t_o(\dot{U}_f t_f)\left[-C + 2(C-1)\frac{\Psi}{h(S)}\right]\frac{\Psi}{h^2(S)}h'(S) \qquad (4.23)$$

The internal power of deformation in zone I and III is zero. In zone II, the internal power of deformation ($\dot{W}_i$) is given by

$$\frac{\dot{W}_i}{(2\sigma_o/\sqrt{3})\dot{U}_f t_f} = \int_{\Psi}\int_{S}\left\{\frac{h'^2(S)}{h^4(S)}\left[-C + 4(C-1)\left(\frac{\Psi}{h(S)}\right)\right]^2 +\right.$$

$$\frac{1}{4}\left[\frac{2(C-1)}{h^2(S)} + \Psi\frac{h''(S)}{h^2(S)}\left(-C+2(C-1)\frac{\Psi}{h(S)}\right) - \frac{\Psi}{h^3(S)}h'^2(S)\left(-2C+6(C-1)\frac{\Psi}{h(S)}\right)\right]^2\Bigg\}^{1/2} dS\,d\Psi \qquad (4.24)$$

The double integration is to be performed over the area PQRS of the plastic zone. The shear power loss along the entrance boundary ($\dot{W}_{Sr_1}$) is

$$\frac{\dot{W}_{Sr_1}}{(2\sigma_0/\sqrt{3})\dot{U}_f t_f} = \frac{1}{2}\left|\int_{l_3}^{l_1}\left\{\left(\frac{R_d+h_f-\Psi}{R_d+0.5}\right)+\left(-C+2(C-1)\frac{\Psi}{h(S)}\right)\frac{1}{h(S)}\right\}dS + \int_0^{h(l_1)}\left\{\frac{S}{(R_d+0.5)}+\left(-C+2(C-1)\frac{\Psi}{h(S)}\right)\frac{\Psi}{h^2(S)}h'(S)\right\}d\Psi\right| \qquad (4.25)$$

The shear power loss along the exit boundary $\Gamma_2$ ($\dot{W}_{Sr_2}$) is

$$\frac{\dot{W}_{Sr_2}}{(2\sigma_0/\sqrt{3})\dot{U}_f t_f} = \frac{1}{2}\left|\int_{l_2}^{0}\left\{\frac{1}{h_f}+\left(-C+2(C-1)\frac{\Psi}{h(S)}\right)\frac{1}{h(S)}\right\}dS + \int_0^{h_f}\left(-C+2(C-1)\frac{\Psi}{h(S)}\right)\frac{\Psi}{h^2(S)}h'(S)\,d\Psi\right| \quad (\text{for } l_2=0)$$

$$= \frac{h'(0)}{4} = 0 \quad \text{for } l_2 = 0 \qquad (4.26)$$

The friction power losses over the surfaces $\Gamma_3$, $\Gamma_4$ and $\Gamma_5$ are calculated

assuming constant interfacial friction stresses ($\tau_i$) at these surfaces of the form

$$\tau_i = m_i \frac{\sigma_o}{\sqrt{3}} \tag{4.27}$$

where $m_i$ is the friction index. The friction loss ($\dot{W}_{S\Gamma_3}$) over portion PS of the die profile ($\Gamma_3$) is

$$\frac{\dot{W}_{S\Gamma_3}}{(2\sigma_o/\sqrt{3})\dot{U}_f t_f} = \frac{m_3}{2}\left|(c-2)\int_0^{\ell_1}\left(\frac{1+h'^2(s)}{h(s)}\right)ds\right| \tag{4.28}$$

The friction power loss ($\dot{W}_{S\Gamma_4}$) over portion QR of punch surface ($\Gamma_4$) included by the plastic zone II is

$$\frac{\dot{W}_{S\Gamma_4}}{(2\sigma_o/\sqrt{3})\dot{U}_f t_f} = \frac{m_4}{2}\left|\int_{\ell_2}^{\ell_3}\left(-\frac{c}{h(s)}\right)ds + \frac{1}{h_f}(\ell_3-\ell_2)\right| \tag{4.29}$$

It may be noted that the remaining surface of contact between punch and material does not contribute to any friction loss because the relative velocity at this surface is zero. The friction loss ($\dot{W}_{S\Gamma_5}$) over portion SW of the die profile ($\Gamma_5$) is

$$\frac{\dot{W}_{S\Gamma_5}}{(2\sigma_o/\sqrt{3})\dot{U}_f t_f} = \frac{m_3}{2}\frac{R_d^2}{(R_d+0.5)}\left[\frac{\pi}{2} - \sin^{-1}\left(\frac{\ell_1}{R_d}\right)\right] \tag{4.30}$$

Let $P_a$ represent the component of the punch load required to perform ironing and to overcome friction at the die surface. $P_a$ is

called the 'Ironing Load' in this work to distinguish it from the total punch load. From the Upper Bound Theorem, the upper bound on $P_a$ (P) is obtained by equating the rate of energy supplied by P to the total rate of energy expended due to the internal deformation, the shear loss over surfaces of velocity discontinuity, and the friction loss. This gives

$$P = \frac{2\pi R_p}{\dot{U}_f}\left[\dot{W}_i + \dot{W}_{s\Gamma_1} + \dot{W}_{s\Gamma_2} + \left(\dot{W}_{s\Gamma_3} + \dot{W}_{s\Gamma_6}\right) + \dot{W}_{s\Gamma_4}\right]$$

or

$$p^* = \frac{P}{(2\sigma_o/\sqrt{3})(2\pi R_p)t_f} = \frac{1}{(2\sigma_o/\sqrt{3})\dot{U}_f t_f}\left[\dot{W}_i + \sum_{i=1}^{5}\dot{W}_{s\Gamma_i}\right] \qquad (4.31)$$

$p^*$ is termed 'Reduced Ironing Load' in this work. Substituting equations (4.24), (4.25), (4.26), (4.28), (4.29) and (4.30), one obtains the upper bound on p* of the form

$$p^* = p^*(R_d, h_f, m_3, m_4, C) \qquad (4.32)$$

For a given set of process parameters ($R_d$,$h_f$,$m_3$,$m_4$), the coefficient C can be varied arbitrarily within certain limits and independent of the kinematic conditions of the problem. The best approximate solution to the ironing process is thus obtained by selecting an optimal value of C ($C_{opt}$) which gives the lowest upper-bound (p*) for any given set of parameters.

A computer program was written to determine p* numerically from equation (4.31) for given values of $R_d$, $h_f$, $m_3$, $m_4$ and C. Details of the program are given in Appendix C. To determine the lowest upper-bound for a given set of parameters ($R_d$,$h_f$,$m_3$,$m_4$), values of p* were obtained

for different values of C and the lowest upper bound together with $C_{opt}$ was obtained. This optimum C thus defines the best deformation model for the given set of process parameters.

Results

To put the upper bound analysis presented here in the proper perspective, a comparison is made with the approximate analysis of Kasuga, et al. [60] . These authors assumed a Coulomb friction behavior at the die and punch surfaces, whereas in this analysis, the friction is taken into account by assuming a constant interfacial friction stress at these surfaces. To make a valid comparison, the analysis of Kasuga, et al. was rederived assuming constant friction stress at the die and punch surfaces. The analysis is presented in Appendix D and is called the 'Modified Kasuga's Analysis'. According to this modified analysis, the reduced punch load due to the ironing process and friction at the die surface, termed 'Reduced Ironing Load', is

$$p_k^* = \frac{P}{(2\pi R_p)(2\sigma_o/\sqrt{3})t_f} = \frac{p_e}{2\sigma_o/\sqrt{3}} + \frac{m_4}{2h_f}\left[(R_d+1)^2-(R_d+h_f)^2\right]^{1/2}$$

$$\text{where} \quad \frac{p_e}{2\sigma_o/\sqrt{3}} = \left\{1 + \left(\frac{m_3-m_4}{2\alpha}\right)\ln\left(\frac{1}{h_f}\right) + \frac{\alpha}{2}\right\}$$

$$\text{and} \quad \alpha = \tan^{-1}\sqrt{\frac{1-h_f}{2R_d+1}+h_f} \qquad (4.33)$$

The subscript k in $p_k^*$ distinguishes this reduced ironing load from $p^*$

obtained through the analysis proposed here.

As stated in the introduction, Johnson [33] has analyzed extrusion through a circular die using circular arcs as surfaces of velocity discontinuity. Using a similar analysis, Alexander and Whitlock [74] analyzed the process of bimetallic extrusion. There is a similarity between the deformation processes of bimetallic extrusion and ironing considered here. Using the approach suggested by Johnson and Alexander et al., expression for the upper bound on the punch load due to ironing is derived here using a model shown in Figure 29. The complete analysis is given in Appendix D and is called the 'Modified Johnson's Analysis'. According to this modified analysis, the reduced ironing load $p_j^*$ is given by

$$p_j^* = \frac{p}{(2\sigma_o/\sqrt{3})(2\pi R_p)t_f} = \frac{1}{t_o(R+0.5t_o)}\left[\frac{r_1^2}{2}(\pi - 2\theta_1) + m_3\frac{\pi}{4}R^2\right]$$

$$\text{where} \quad r_1 = \left(\frac{L_3^2}{2t_f} + \frac{t_f}{2}\right), \quad \theta_1 = \tan^{-1}\left(\frac{L_3}{t_f}\right)$$

$$\text{and} \quad L_3 = \left[(R+t_o)^2 - (R+t_f)^2\right]^{1/2} \qquad (4.34)$$

The results obtained with the present analysis are now presented.

Effect of Parameter C. It is instructive to look at the effect of the parameter C on the various components of the reduced ironing load $(\overset{*}{p})$ and on the assumed deformation model. Figure 30 shows typical variations of components of the reduced ironing load $(\overset{*}{p})$ with the parameter C. An

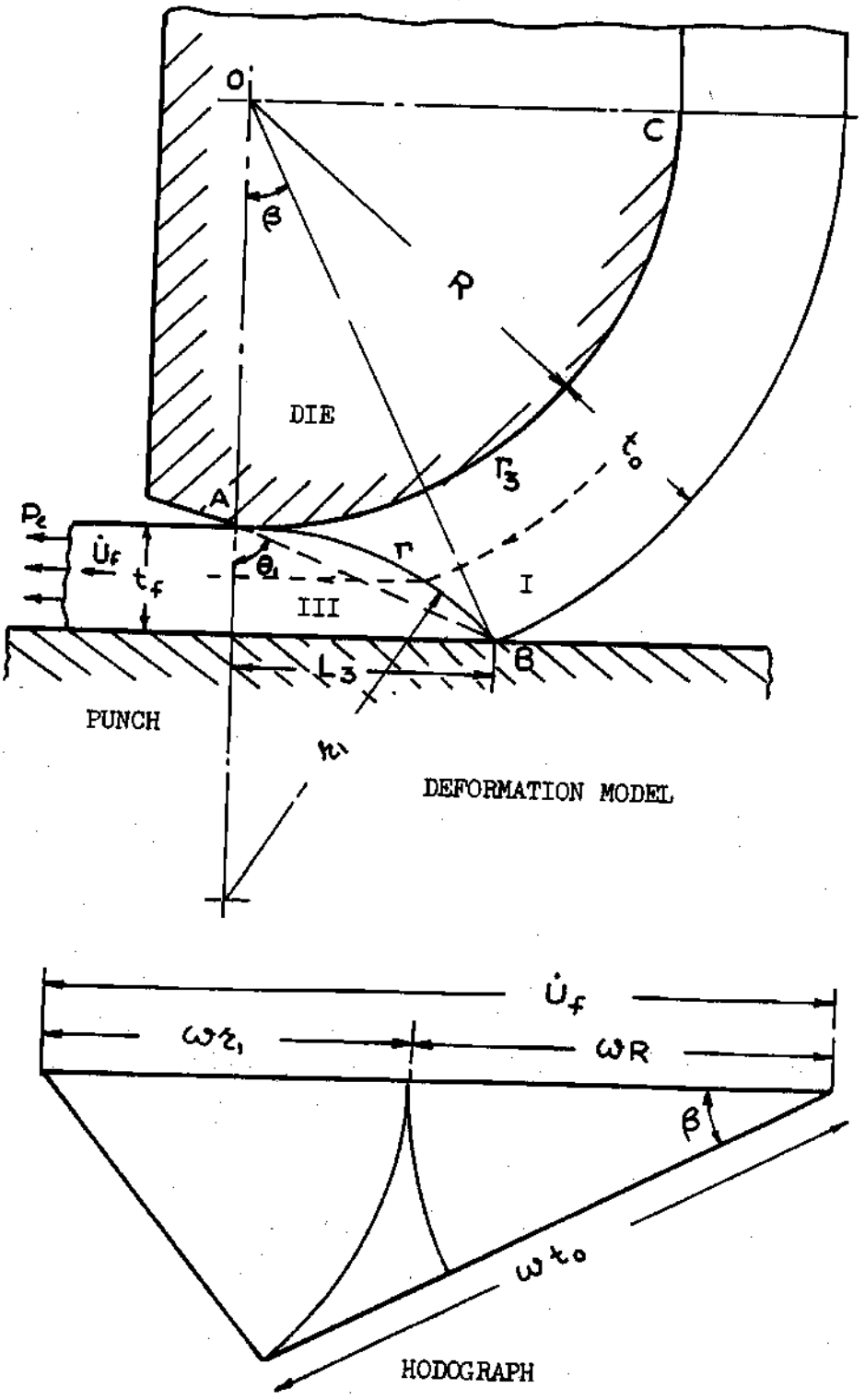


Figure 29. Deformation Model and Corresponding Hodograph — Modified Johnson's Analysis

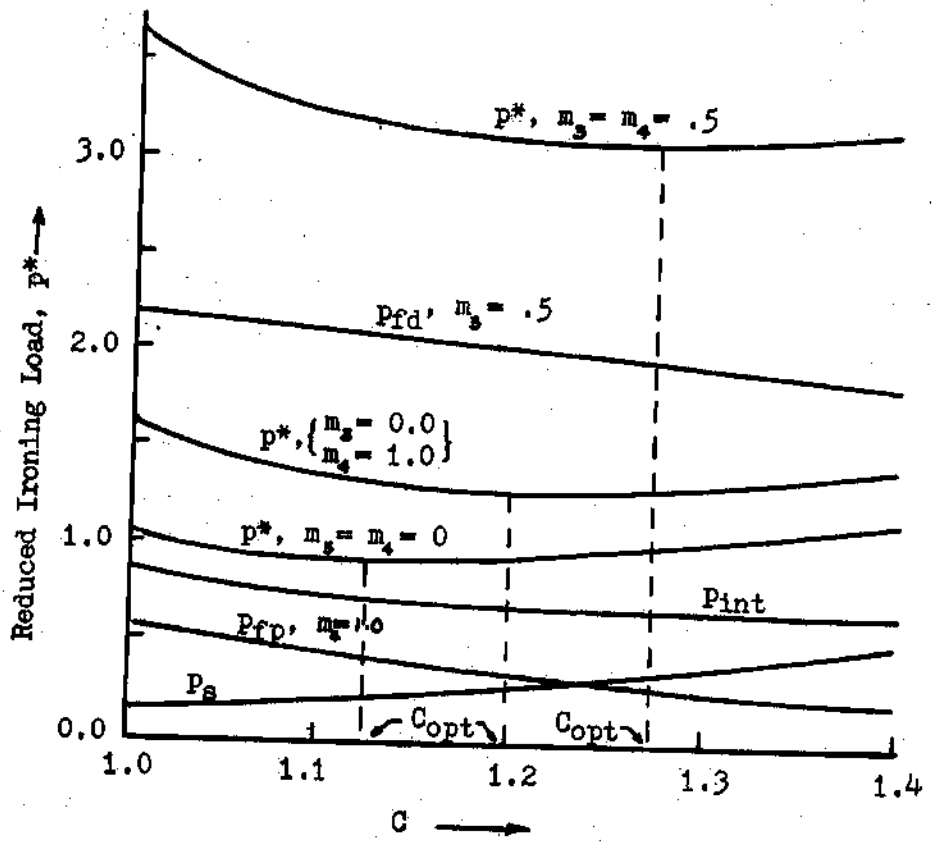


Figure 30. Effect of Parameter C on Various Components of Ironing Load, $R_d = 5.0$, $h_f = 0.5$

increase in C results in a decrease in the components due to internal deformation ( $p_{int}$ ) in zone II as well as friction at the punch and die surfaces ( $p_{fp}$ and $p_{fd}$ ). The component due to shear deformation at surfaces $\Gamma_1$ and $\Gamma_2$ , however, increases with increasing C. The net effect of these components is that the upper bound on reduced ironing load ($\bar{p}^*$) goes through a minimum. This least upper bound is obtained for a certain optimal value of C ($C_{opt}$). Comparing the variation of $\bar{p}^*$ for different frictional conditions, one notices that the effect of interfacial friction at the die and punch surfaces is to increase the value of $C_{opt}$. The reason for this dependence of various components of ironing load on C can best be understood fron Figure 31 which shows the change in deformation model with the parameter C.

From equation (4.18), it is obvious that an increase in C would result in an increase in $L_2$. Hence boundary $\Gamma_2$ would move opposite to the direction of flow with an increase in C. Equation (B.6) of Appendix B gives the dependence of $L_1$ on C. Numerical calculations show that an increase in C results in a decrease in $L_1$ and thus boundary $\Gamma_1$ moves towards the direction of flow. The combined effect is that the plastic zone II reduces in size with an increase in C. This is probably the reason why the component due to internal deformation, which is dependent on the size of the plastic zone, decreases with C. An increase in $L_2$ decreases the area of surface $\Gamma_4$ and thereby the contribution of friction at the punch. Thus the component due to friction at the punch decreases with increase in C as noted in Figure 30. An increase in $L_2$ and decrease in $L_1$ increases the slope of the boundaries $\Gamma_2$ and $\Gamma_1$ . The shear deformation at these boundaries and its component in $\bar{p}^*$ increase with increase in C. The

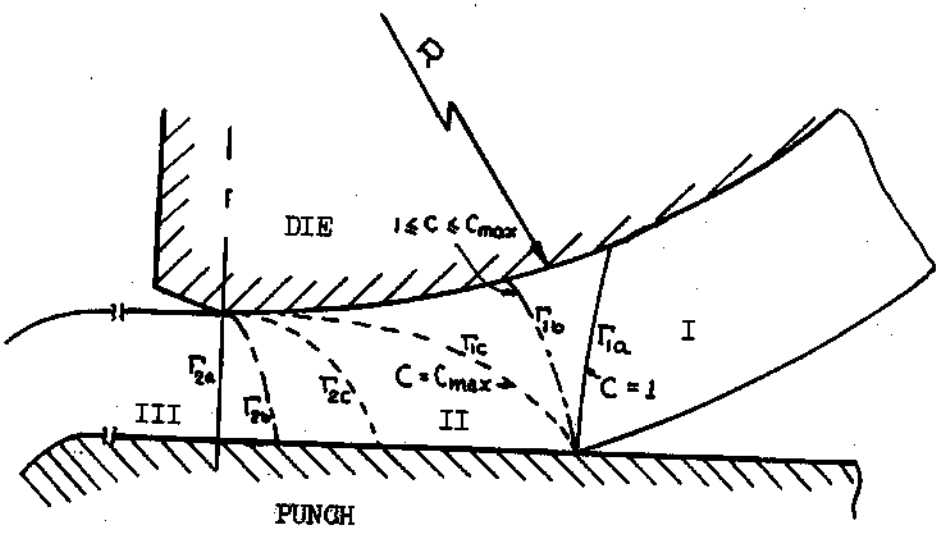


Figure 31. Effect of Parameter C on the Kinematically Admissible Deformation Model

dependence of the component due to die friction on C is similar to that of the component due to punch friction. An increase in C reduces $L_1$ and thereby the area of the boundary $\Gamma_3$ at which a greater velocity discontinuity exists compared to the velocity discontinuity at $\Gamma_5$ . Thus when the friction is high at the die and / or punch surface, the deformation model adjusts, through an increase in C, to reduce the rate of energy dissipation. $C_{opt}$ thus increases with an increase in friction.

Ironing Load. Figures 32 and 33 show for different die radii ($R_d$), the least upper bounds on ironing load obtained as a function of ironing reduction. The die is taken to be frictionless and the curves are plotted for the cases when the punch is frictionless ($m_4 = 0$) and when the punch is perfectly rough ($m_4 = 1.0$). For comparison, the results obtained from the modified Kasuga's analysis and from the modified Johnson's analysis are also shown. The ironing reduction as used here is the reduction in thickness and is defined as

$$\text{Ironing Reduction, RA\%} = \left(\frac{t_o - t_f}{t_o}\right) \times 100$$

As Figures 32 and 33 show, the ironing load increases with an increase in reduction. Also the effect of friction at the punch is to increase the ironing load. This dependence of ironing load on reduction is observed for all die radii.

Comparison of the results indicates that when the punch is frictionless, the modified Kasuga's analysis gives lower values for ironing loads compared to the least upper bounds obtained here. The difference, however, diminishes for larger dies. This seems to indicate

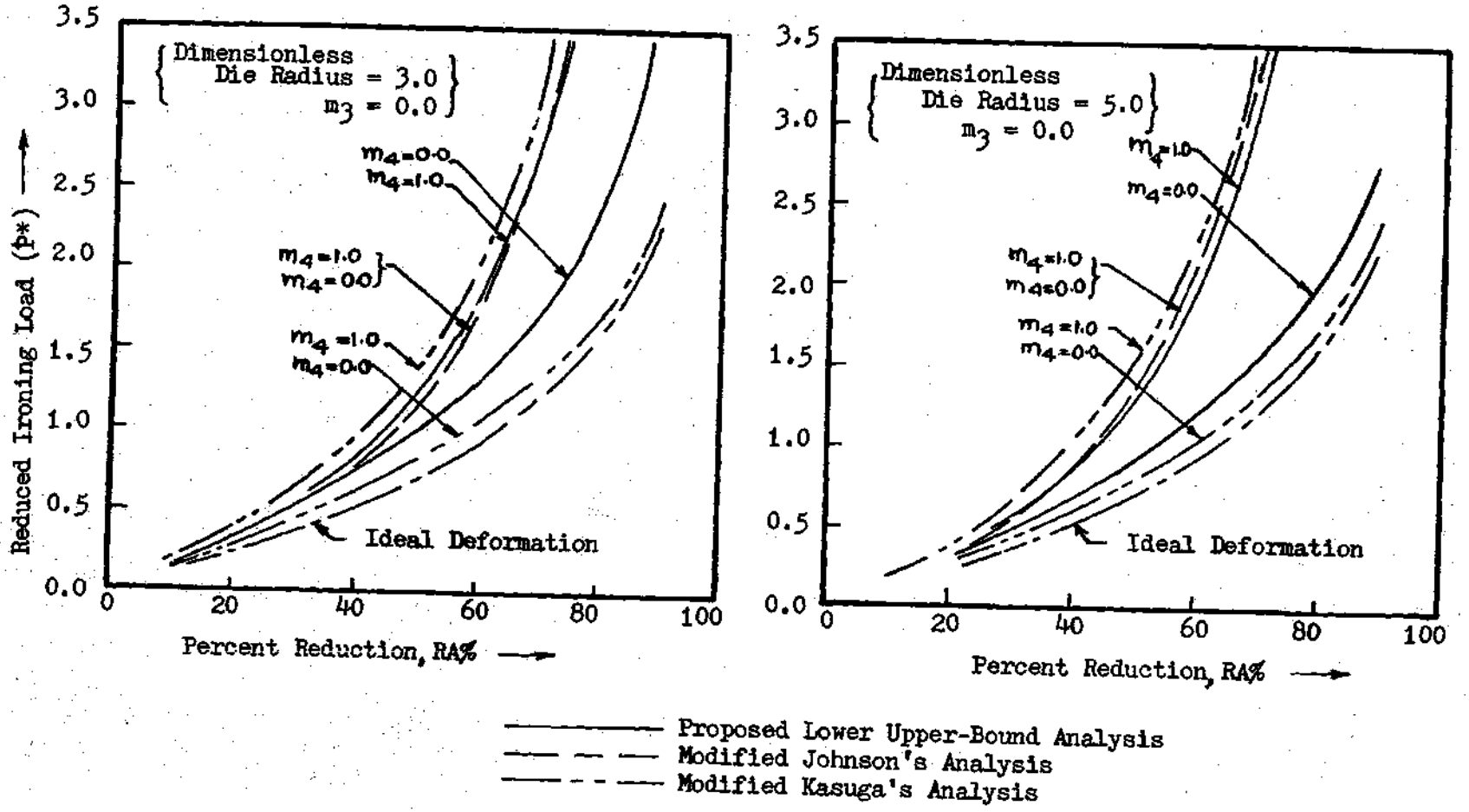


Figure 32. Reduced Ironing Load (P*) as a Function of Ironing Reduction

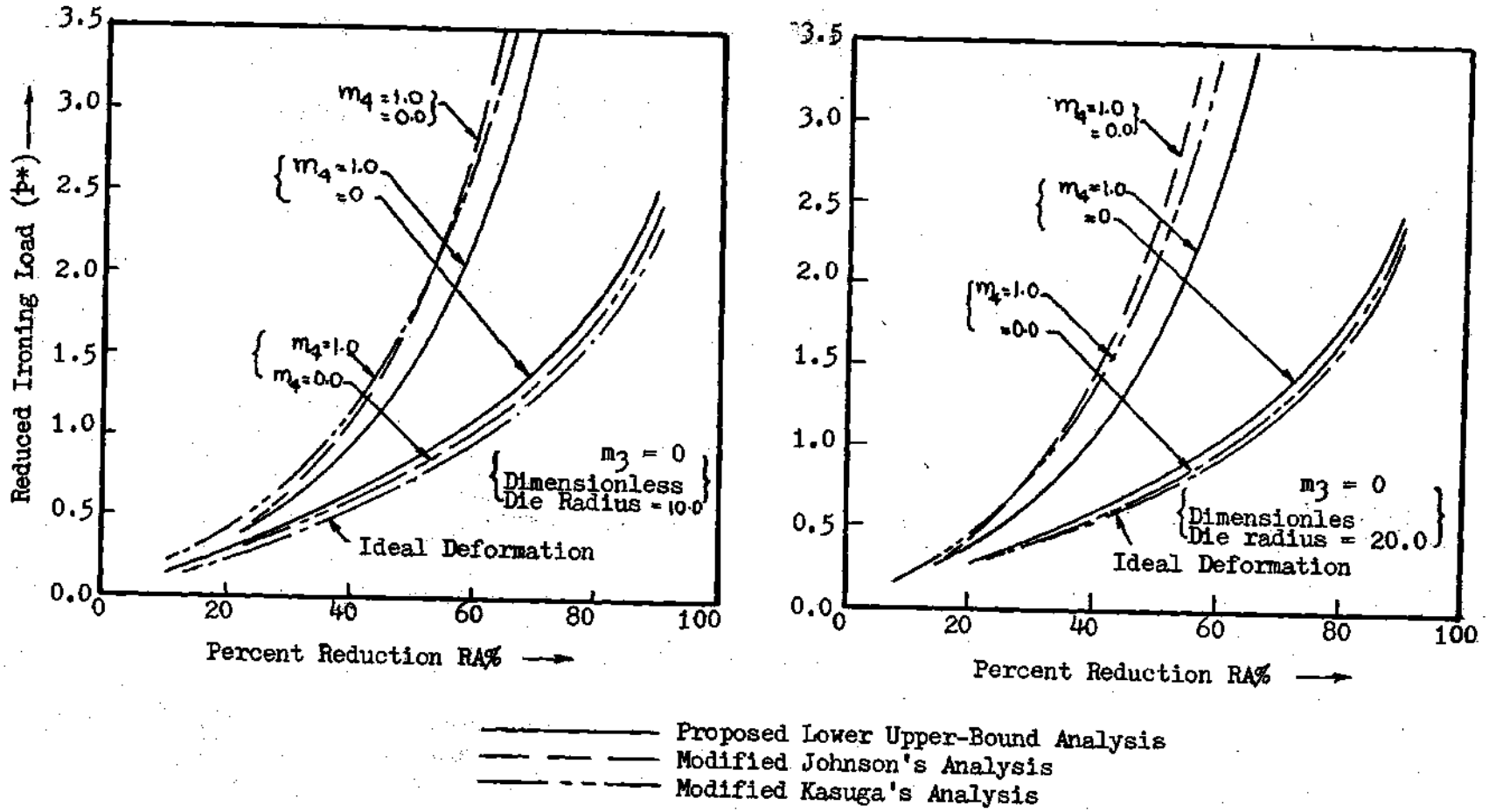


Figure 33. Reduced Ironing Load (p*) as a Function of Ironing Reduction

that the difference in values for ironing load is due to the error in Kasuga's analysis introduced by approximating the circular profile of the die by a straight tapering shape. For larger die radii, the difference in circular profile and straight taper is small and can be neglected. However for dies of small radius, the difference in profile can introduce large errors in the calculated ironing load. For the perfectly rough punch, Kasuga's results are higher than those obtained here with the lower upper-bound solution. Since the actual values for the ironing load must lie below the lower upper-bounds, the current analysis given better results compared to Kasuga's analysis.

The modified Johnson's analysis gives the same ironing loads for all frictional conditions of the punch. Clearly the analysis and hence the the assumed deformation model is not accurate for the case where friction at the punch surface is small. Comparison of ironing load values for the rough punch indicates that except for small die radii and reductions, the analysis proposed here gives lower upper-bounds. The present analysis, therefore, seems to give better results in comparison with existing solutions for the ironing load.

Figure 34 shows the least upper-bounds obtained on reduced ironing load as a function of the ironing reduction (RA) when the die friction index ($m_3$) is 0.1. The results obtained with the modified Johnson's analysis are also shown. Except for the case when the die radius is small and the punch surface is rough, our analysis gives lower upper-bounds compared to the modified Johnson's analysis. On the whole, the analysis presented here gives better solution with regard to the load requirement.

Figures 35 and 36 show the ironing load as a function of the

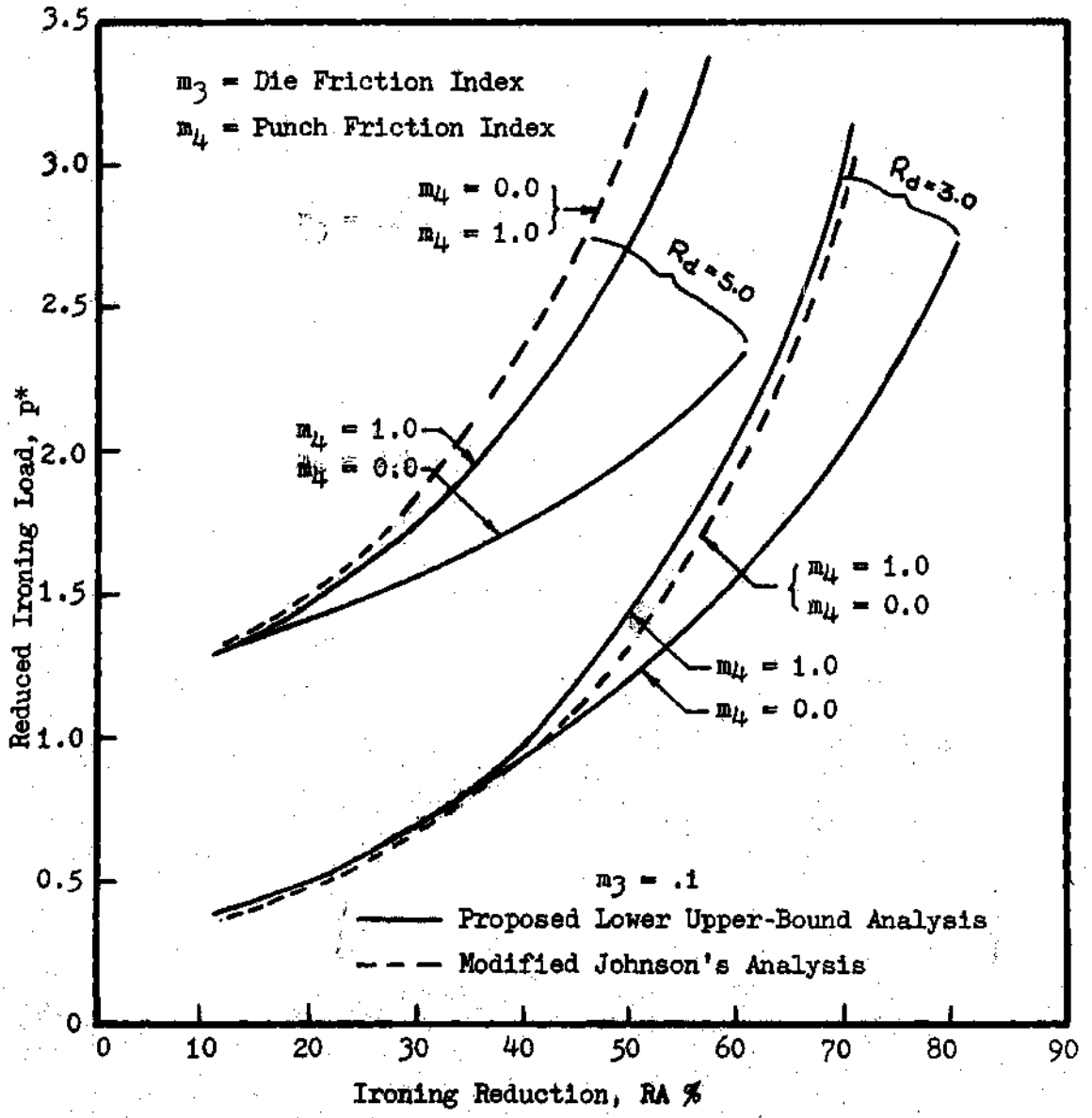


Figure 34. Reduced Ironing Load (p*) VS Reduction (RA)

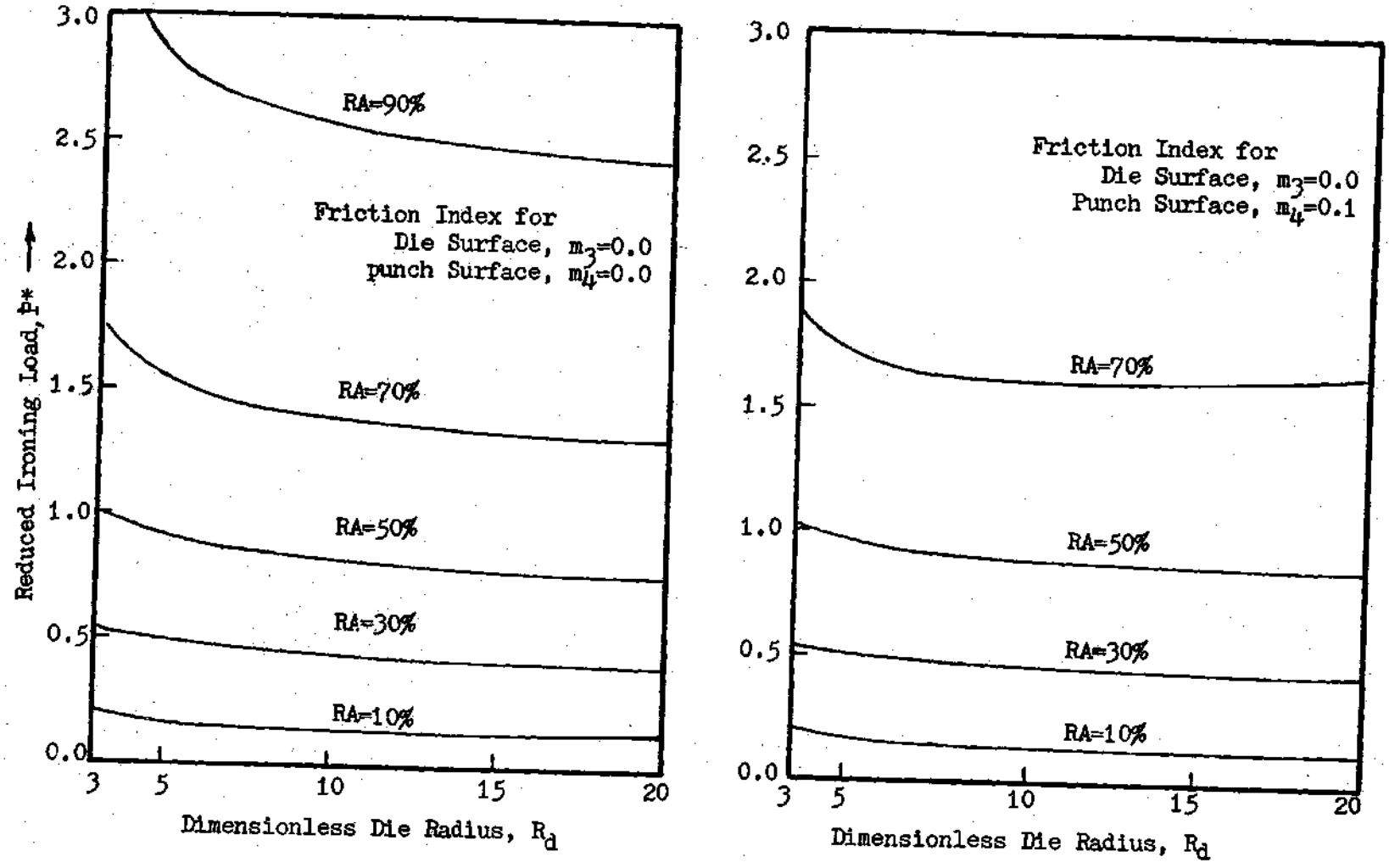


Figure 35. Reduced Ironing Load (P*) as a Function of Dimensionless Die Radius ($R_d$)

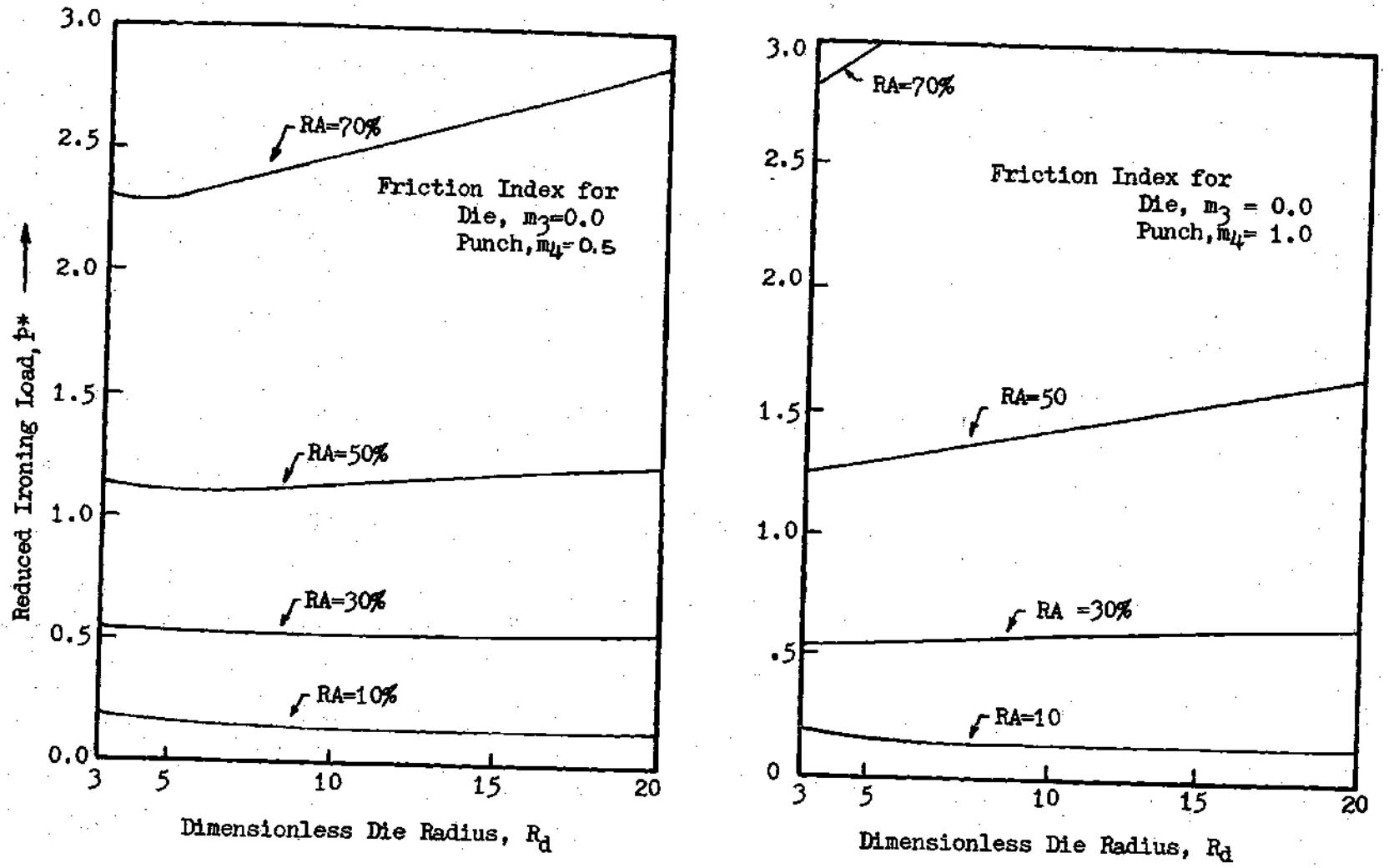


Figure 36. Reduced Ironing Load (P*) as a Function of Dimensionless Die Radius ($R_d$)

dimensionless die radius ($R_d$), for different ironing reductions and frictional conditions at the punch. For a frictionless ironing process ($m_3=m_4=0$), the ironing load decreases with an increase in die radius. This is due to the increase in effective length over which the reduction in thickness takes place. Thus the redundant work of deformation is reduced and results in a decrease in the ironing load. This behavior is observed at all reductions. The decrease in load is however small for $R_d \geq 10$. In practice, there is an upper limit set on the die radius because of a greater tendency of cups to wrinkle with larger dies. This tendency is due to the early removal of the guiding influence of the blank holder [17]. When the punch is not frictionless, an increase in the die radius reduces the redundant work but increases the contribution due to punch friction. The minimum in reduced ironing load is thus obtained for a certain optimal die radius to thickness ratio ($R_d$).

Deformation Model. For any given set of process parameters, the optimal value of C defines the best approximate deformation model. Figure 37 shows the predicted shape of the plastic zone for different ironing reductions when the die is frictionless and its dimensionless radius ($R_d$) is equal to five. With 10% reduction, the plastic zone of the deformation model takes a triangular shape. The exit boundary $r_2$ has moved its maximum and the point Q of $r_2$ has coincided with point R of the boundary $r_1$. With 20% reduction, the plastic zone is very narrow and the deformation model is quite similar to that assumed in the modified Johnson's analysis. It is of interest to note that friction at the punch surface does not affect the deformation model for these reductions because the parameter C has already reached its maximum limit. As the reduction is increased further,

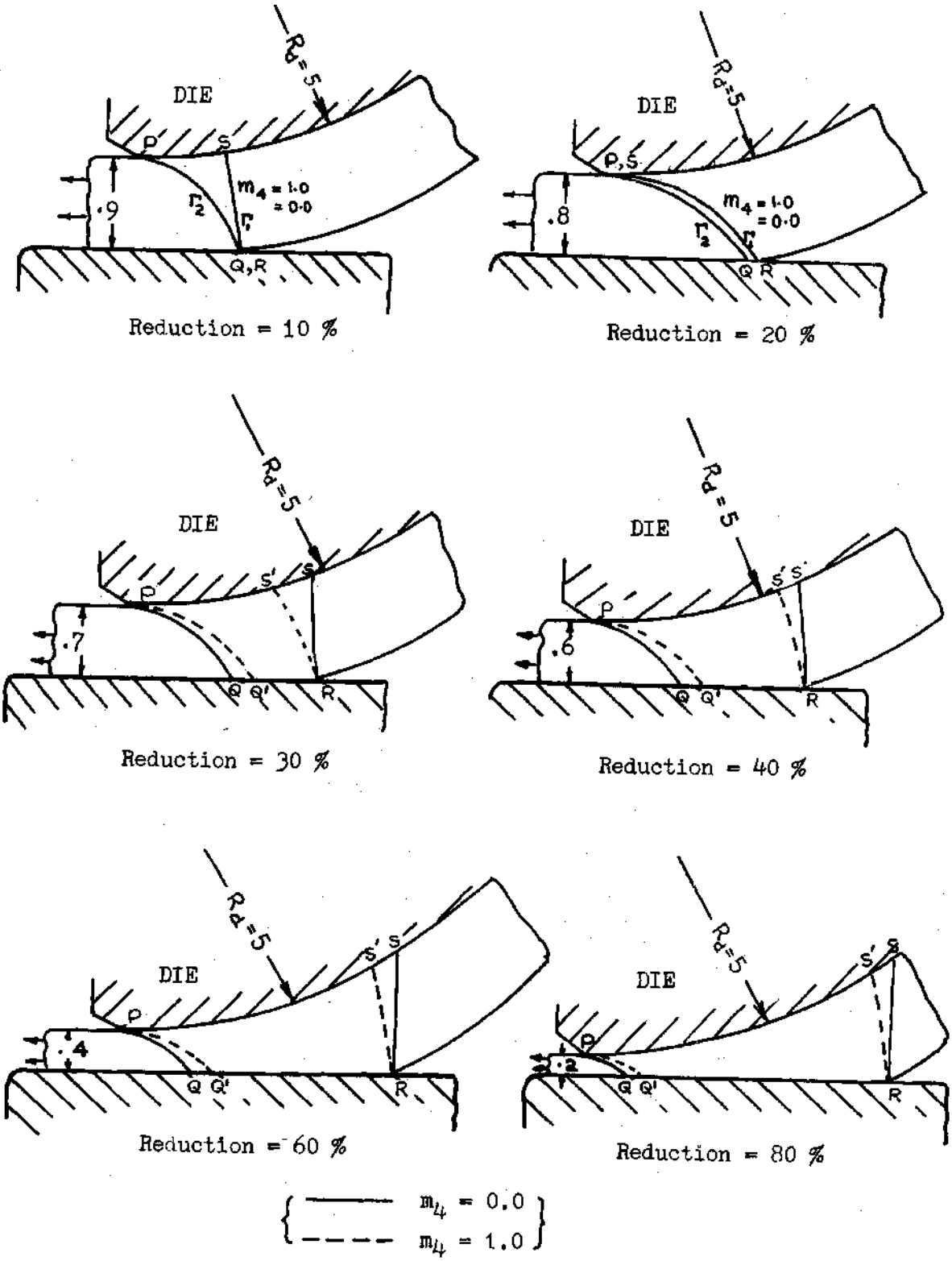


Figure 37. Deformation Models for Different Reductions and Punch Frictional Conditions, $R_d = 5.0$, $m_3 = 0.0$

the plastic zone covers a finite portion of the die as well as the punch surface. At these reductions, the effect of friction at the punch is to decrease the size of the plastic zone.

Figure 38 shows the predicted deformation model for different reductions when the punch is frictionless. As is obvious from this Figure, the effect of die friction is similar to that of punch friction. Die friction also reduces the size of the plastic zone.

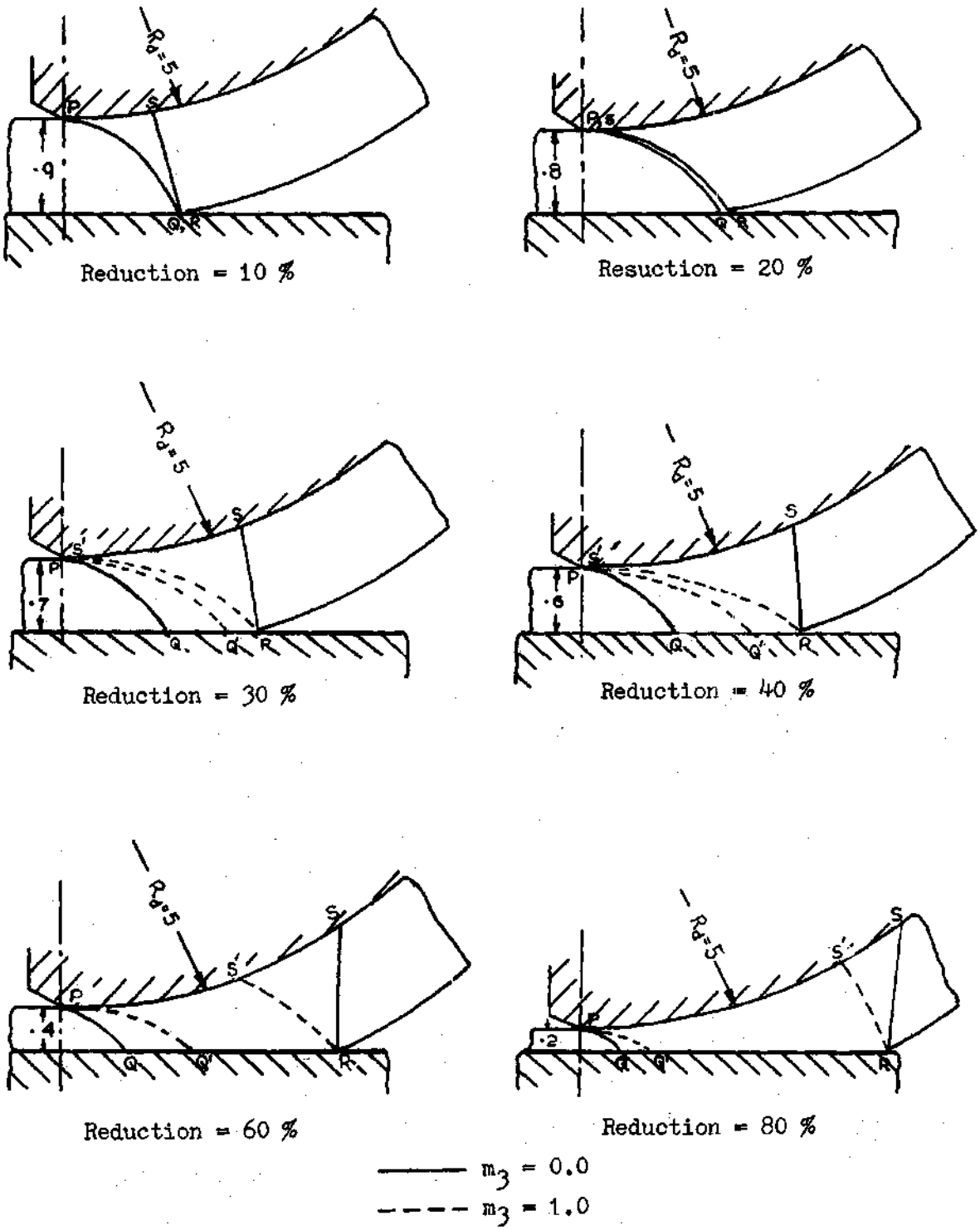


Figure 38. Deformation Models for Different Reductions and Die Frictional Conditions, $R_d$ = 5.0, $m_4$ = 0.0

# CHAPTER V

## AXISYMMETRIC FLOW THROUGH ARBITRARILY SHAPED DIE

The operations called wire drawing, rod extrusion, hydrostatic extrusion and tube sinking are all performed through similar dies. Identical flow patterns are assumed in the analytical study of these different processes. Analysis is presented in this Chapter for direct extrusion of a rod through an arbitrarily shaped die. With slight modification, the analysis can be extended to other processes.

The problem posed is to determine the pressure required to extrude a rigid-perfectly plastic material through a die of an arbitrary shape and to obtain the characteristics of flow of such a material and its final deformation in extruded stage. This problem is analyzed using a generalized upper bound approach. Only steady state extrusion is considered.

### General Kinematically Admissible Model

For this process of extrusion through arbitrarily shaped die, general kinematically admissible model was obtained in Chapter II and is shown in full detail in Figure 39. Due to symmetry, only upper half portion of the flow in meridian plane is shown. The die profile is represented by equation

$$r = R(z) \tag{5.1}$$

and $\quad R(0) = R_f \quad , \quad R(L) = R_o$

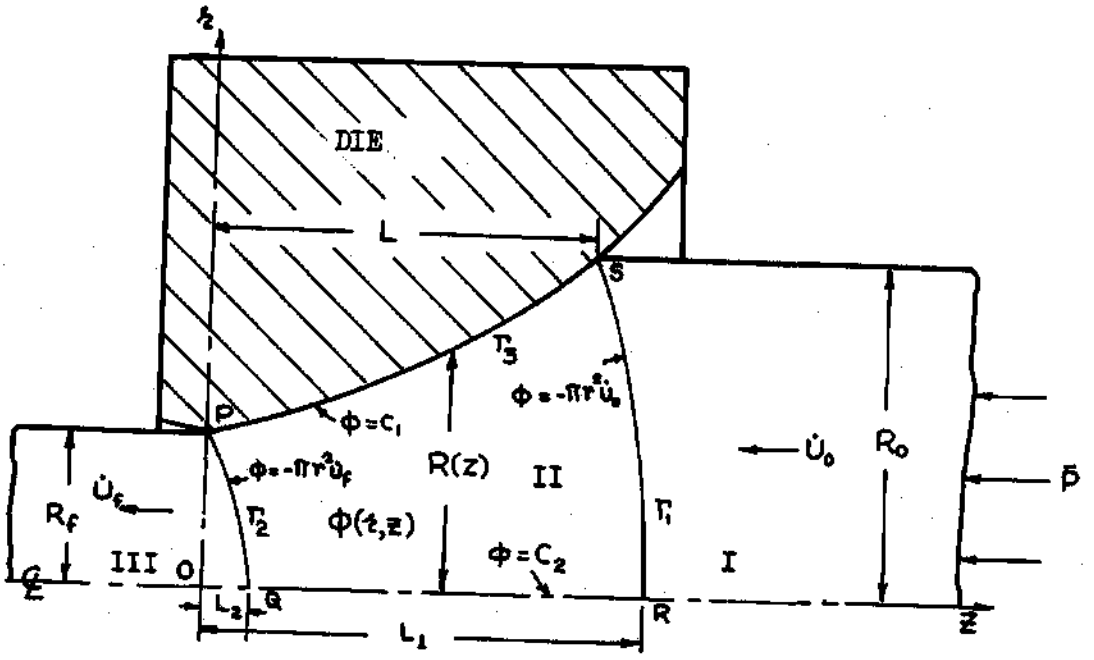


Figure 39. General Kinematically Admissible Deformation Model for Axisymmetric Extrusion through An Arbitrarily Shaped Die

$R_o$ is the initial radius of the rod and $R_f$ is its final radius. The function $R(z)$ has continuous first and second derivatives in the range considered. The current analysis can easily be extended to die shapes that do not have a continuous slope and / or curvature and is therefore applicable for an arbitrarily shaped die.

In the admissible deformation model for the steady state process, the deforming bar is divided into three zones. In zone I, the undeformed region, a rigid body motion in the negative z direction is described by uniform velocity $\dot{U}_o$, and in zone III, the already deformed region, no further deformation occurs and the rigid body motion is described by uniform velocity $\dot{U}_f$ in negative z direction. Because of volume constancy

$$\dot{U}_f = \dot{U}_o \frac{R_o^2}{R_f^2} \tag{5.2}$$

Let $(\dot{U}_r, \dot{U}_z)$ represent the components of velocity field in zone II in r and z directions of a cylindrical coordinate system $(r,\theta,z)$ and $\hat{\phi}(r,z)$ represent the corresponding flow function given by relations

$$\dot{U}_r = -\frac{1}{2\pi r}\frac{\partial \hat{\phi}}{\partial z} \quad , \quad \dot{U}_z = \frac{1}{2\pi r}\frac{\partial \hat{\phi}}{\partial r} \tag{5.3}$$

The admissibility conditions on flow function which are derived from the velocity boundary conditions are shown in Figure 39 and these are

$$\hat{\phi}(r,z) = C_1 \quad \text{at} \quad r = R(z) \tag{5.4}$$

$$\hat{\phi}(r,z) = C_2 \quad \text{at} \quad r = 0 \tag{5.5}$$

$$\hat{\Phi}(r,z) = -\pi r^2 \dot{U}_0 \quad \text{at} \quad r = r_{\Gamma_1}(z) \tag{5.6}$$

$$\hat{\Phi}(r,z) = -\pi r^2 \dot{U}_f \quad \text{at} \quad r = r_{\Gamma_2}(z) \tag{5.7}$$

$C_1$ and $C_2$ are some constants. $r = r_{\Gamma_1}(z)$ and $r = r_{\Gamma_2}(z)$ represent, in explicit form, the boundaries $\Gamma_1$ and $\Gamma_2$ respectively of zone II. The constants $C_1$ and $C_2$ can be determined as follows. At point $S(R_0,L)$, $\hat{\Phi}(r,z)$ from equations (5.4) and (5.6) is

$$\hat{\Phi}(R_0,L) = C_1 = -\pi R_0^2 \dot{U}_0 \tag{5.8}$$

and at point $R(0,L_1)$

$$\hat{\Phi}(0,L_1) = C_2 = 0 \tag{5.9}$$

Substituting for $C_1$ and $C_2$ in equations (5.4) and (5.5), one obtains

$$\hat{\Phi}(r,z) = -\pi R_0^2 \dot{U}_0 \quad \text{at} \quad r = R(z) \tag{5.10}$$

$$\hat{\Phi}(r,z) = 0 \quad \text{at} \quad r = 0 \tag{5.11}$$

A further restriction on flow function comes from the compatibility condition that shear strain rate $\dot{\epsilon}_{rz}$ should vanish at the axis of symmetry. The strain rate tensor $\dot{\epsilon}_{ij}$ is given by

$$\dot{\epsilon}_{ij} = \frac{1}{2}\left(\dot{U}_{i,j} + \dot{U}_{j,i}\right) \tag{5.12}$$

where $\dot{U}_i$ is the velocity component in i direction. Therefore

$$\dot{\epsilon}_{rz} = \frac{1}{2}\left( \frac{\partial \dot{U}_r}{\partial z} + \frac{\partial \dot{U}_z}{\partial r} \right) \tag{5.13}$$

Substituting for $\dot{U}_r$ and $\dot{U}_z$ in equation (5.13), and setting $\dot{\epsilon}_{rz}$ equal to zero, gives

$$\frac{\partial}{\partial z}\left( \frac{1}{r} \frac{\partial \hat{\Phi}}{\partial z} \right) - \frac{\partial}{\partial r}\left( \frac{1}{r} \frac{\partial \hat{\Phi}}{\partial r} \right) = 0 \quad \text{at } r = 0 \tag{5.14}$$

Component $\dot{U}_r = 0$ at $r = 0$, therefore

$$\frac{\partial}{\partial z}\left( \frac{1}{r} \frac{\partial \hat{\Phi}}{\partial z} \right) = 0 \tag{5.15}$$

Condition (5.14) thus becomes

$$\frac{\partial}{\partial r}\left( \frac{1}{r} \frac{\partial \hat{\Phi}}{\partial r} \right) = 0 \quad \text{at} \quad r = 0 \tag{5.16}$$

The conditions (5.6) and (5.7) can be satisfied by letting the boundaries $r_1$ and $r_2$ of plastic zone be represented by these equations. It can be easily verified that a general flow function which satisfies the remaining boundary conditions (5.10), (5.11) and (5.16) is

$$\hat{\Phi}(r, z) = f(\hat{\eta}) \quad , \quad \text{where} \quad \hat{\eta} = r/R(z) \tag{5.17}$$

and $$\frac{\partial}{\partial r}\left( \frac{1}{r} f'(\hat{\eta}) \frac{\partial \hat{\eta}}{\partial r} \right) = 0 \quad \text{at} \quad r = 0$$

The physical interpretation of this form of flow function is that equation of the streamlines is

$$\hat{\phi}(r,z) = f(r/R(z)) = \text{Const} \qquad (5.18)$$

$$\text{or} \quad r/R(z) = \text{Constant}$$

Equally spaced streamlines thus remain equally spaced at all vertical sections. Substituting for $\hat{\phi}$ in equation (5.3), a general admissible velocity field for plastic zone II is

$$\dot{U}_r = \frac{1}{2\pi} f'(\hat{\eta}) \frac{R'(z)}{R^2(z)} \quad , \quad \dot{U}_z = \frac{1}{2\pi} f'(\hat{\eta}) \frac{1}{r R(z)} \qquad (5.19)$$

where $f'(\hat{\eta}) = \frac{df}{d\hat{\eta}}$ and $\hat{\eta}(r,z) = r/R(z)$

From equations (5.6), (5.7) and (5.17), the boundaries of plastic zone are given by

$$\Gamma_1 : \qquad f(\hat{\eta}) = -\pi r^2 \dot{U}_0 \quad \text{at} \quad r = r_{\Gamma_1}(z) \qquad (5.20)$$

$$\Gamma_2 : \qquad f(\hat{\eta}) = -\pi r^2 \dot{U}_f \quad \text{at} \quad r = r_{\Gamma_2}(z) \qquad (5.21)$$

Velocity field (5.19) together with generalized boundaries of plastic zone represented by equations (5.20) and (5.21) defines a general kinematically admissible model.

The general velocity field can also be represented as a function of the shape of the boundaries of plastic zone. To accomplish this, differentiate equations (5.20) and (5.21) and obtain along

$$\Gamma_1 : \qquad f'(\hat{\eta}) = -2\pi \dot{U}_0 \, z \frac{dz}{d\hat{\eta}} \qquad \text{at} \quad z = z_{\Gamma_1}(r) \tag{5.22}$$

$$\Gamma_2 : \qquad f'(\hat{\eta}) = -2\pi \dot{U}_f \, z \frac{dz}{d\hat{\eta}} \qquad \text{at} \quad z = z_{\Gamma_2}(r) \tag{5.23}$$

Flow function $f(\hat{\eta})$ can only be a function of $\hat{\eta}$ , it therefore can be written, from equations (5.22) and (5.23), as

$$\begin{aligned} f'(\hat{\eta}) &= -2\pi \dot{U}_0 \, z_{\Gamma_1}(r) \frac{dz_{\Gamma_1}}{d\hat{\eta}} \\ &= -2\pi \dot{U}_f \, z_{\Gamma_2}(r) \cdot \frac{dz_{\Gamma_2}}{d\hat{\eta}} \end{aligned} \tag{5.24}$$

Using equations (5.24) and (5.19), the general velocity field for zone II expressed as a function of the shape of the boundary $\Gamma_1$ is

$$\begin{aligned} \dot{U}_z &= -\left( \dot{U}_0 \, z_{\Gamma_1}(r) \frac{dz_{\Gamma_1}}{d\hat{\eta}} \right) \frac{R'(r)}{R^2(r)} \\ \dot{U}_r &= -\left( \dot{U}_0 \, z_{\Gamma_1}(r) \frac{dz_{\Gamma_1}}{d\hat{\eta}} \right)_z \frac{1}{R(r)} \end{aligned} \tag{5.25}$$

From equation (5.24), it can be derived that the two boundaries are related by expression

$$\frac{r_1^2(z)}{r_2^2(z)} = \frac{\dot{U}_f}{\dot{U}_o}$$

which can be derived directly from incompressibility condition as well. Some special cases of this general model which present rather interesting results are now investigated.

Model for Curved Die When $f(\hat{\eta}) \propto \eta^2$

Consider the special case when

$$f(\hat{\eta}) = -\pi R_o^2 \dot{U}_o \hat{\eta}^2 \tag{5.26}$$

Equations (5.20) and (5.21) for boundaries $\Gamma_1$ and $\Gamma_2$ reduce to

$$\Gamma_1 : \quad R(z) = R_o \quad \text{or} \quad z = L \tag{5.27}$$

$$\Gamma_2 : \quad R(z) = R_f \quad \text{or} \quad z = 0 \tag{5.28}$$

which means that the boundaries are vertical surfaces. From equations (5.17), (5.19) and (5.26), it follows that the velocity field in zone II is given by

$$\dot{U}_z = -\dot{U}_o R_o^2 \frac{z R'(z)}{R^3(z)}$$

$$\dot{U}_\theta = 0 \tag{5.29}$$

$$\dot{U}_z = -\dot{U}_o R_o^2 \frac{1}{R^2(z)}$$

The foregoing velocity field is the same as presented by Chang and Choi [36] for extrusion through curved dies. The velocity field proposed by Chang and Choi is therefore only a special case of a more general velocity field presented here by equation (5.19).

Model for Extrusion through Conical Die

Consider the special case of extrusion through a conical die (see Figure 2 ). The apex of the die cone is taken as origin of the coordinate axes. The conical die profile is represented by

$$R(z) = z \tan\alpha \tag{5.30}$$

Substituting for R(z) in equation (5.25), a general velocity field in plastic zone for extrusion through a conical die is

$$\dot{U}_z = -\left(\dot{U}_o r_n(z) \frac{dr_n}{d\hat{\eta}}\right) \frac{1}{z^2 \tan\alpha} \quad , \quad \dot{U}_\theta = 0$$

$$\dot{U}_z = -\left(\dot{U}_o r_n(z) \frac{dr_n}{d\hat{\eta}}\right) \frac{1}{r z \tan\alpha} \tag{5.31}$$

where $\hat{\eta}(r,z) = r/z\tan\alpha$

To write equation (5.31) in spherical coordinates $(\rho_1, \theta_1, \phi_1)$,

transformation rule is applied that

$$r = \rho_1 \sin\theta_1 \quad , \quad z = \rho_1 \cos\theta_1 \tag{5.32}$$

then

$$\hat{\eta}(r,z) = \tan\theta_1/\tan\alpha \tag{5.33}$$

$$\text{and} \quad \frac{d\xi_\Pi}{d\hat{\eta}} = \frac{d}{d\hat{\eta}}\left(\rho_{\Gamma_1}(\theta_1)\sin\theta_1\right) = \frac{d}{d\theta_1}\left(\rho_{\Gamma_1}(\theta_1)\sin\theta_1\right)\frac{\tan\alpha}{\sec^2\theta_1}$$

where $\rho_1 = \rho_{\Gamma_1}(\theta_1)$ represents the entrance boundary $\Gamma_1$. Substituting equations (5.32) and (5.33) in equation (5.31), one obtains

$$\begin{aligned} \dot{U}_r &= -\dot{U}_0 \sin\theta_1 \frac{\rho_\Pi(\theta_1)}{\rho_1^2}\left[\frac{d}{d\theta_1}\left(\rho_{\Gamma_1}(\theta_1)\sin\theta_1\right)\right] \\ \dot{U}_z &= -\dot{U}_0 \cos\theta_1 \frac{\rho_{\Gamma_1}(\theta_1)}{\rho_1^2}\left[\frac{d}{d\theta_1}\left(\rho_{\Gamma_1}(\theta_1)\sin\theta_1\right)\right] \end{aligned} \tag{5.34}$$

If $(\dot{U}_{\rho_1}, \dot{U}_{\theta_1}, \dot{U}_{\phi_1})$ are the components of velocity field in spherical coordinate system $(\rho_1, \theta_1, \phi_1)$, then from equation (5.34), the velocity field in zone II reduces to

$$\begin{aligned} \dot{U}_{\rho_1} &= -\dot{U}_0 \frac{\rho_\Pi(\theta_1)}{\rho_1^2}\left[\frac{d}{d\theta_1}\left(\rho_{\Gamma_1}(\theta_1)\sin\theta_1\right)\right] \\ \dot{U}_{\theta_1} &= \dot{U}_{\phi_1} = 0 \end{aligned} \tag{5.35}$$

which is same as suggested by Stepanskii [31] and later used by Zimerman and Avitzur [32] and by Tirosh [75]. The proposed general velocity field for extrusion through an arbitrarily shaped die thus reduces, for a conical die, to that presented by Stepanskii [31]. When it is assumed that $\rho_{r_i}$ is not a function of $\theta_i$, expression (5.35) reduces to

$$\dot{U}_{\rho_i} = -\dot{U}_o \left( \frac{\rho_c}{\rho_i} \right)^2 \cos \theta_i$$

$$\dot{U}_{\theta_i} = \dot{U}_{\phi_i} = 0 \qquad (5.36)$$

$\rho_c$ is a constant. This is the radial velocity field with spherical boundaries used by Avitzur [50]. His model therefore is also only a special case of the general model presented here.

## Lower Upper-Bound Analysis

### Optimal Flow Function and Upper Bound

From the general kinematically admissible model, that particular model has to be selected which results in minimum upper bound on extrusion pressure. Since the generality in the kinematic model is due to the flow function $\hat{\Phi}(r,z)$, the problem is to find the extremizing flow function. Complexity of the expression for upper bound on pressure, however, excludes the possibility of finding the exact function by variational techniques except for some trivial cases. An approximate solution to this variational problem is thus sought here.

A method similar to Rayleigh-Ritz method [77] shall be used to find approximatly the extremizing $\hat{\phi}(r,z)$ and corresponding lower upper

bound on extrusion pressure for a given set of process parameters. In this analysis, the actual flow function is approximated by linear combination of known functions $\hat{\eta}^i$

$$\hat{\phi}(r,z) = \sum_{i=0}^{N} b_i \hat{\eta}^i \quad , \quad \text{where } \hat{\eta} = r/R(z) \tag{5.37}$$

Coefficients $b_i$ are constants and shall be chosen so that the form (5.37) is admissible and that least upper bound on extrusion pressure is obtained. From admissibility conditions (5.10), (5.11) and (5.16), one obtains

$$\sum_{i=0}^{N} b_i = -\pi R_0^2 \dot{U}_0 \tag{5.38}$$

$$\text{and} \qquad b_0 = b_1 = b_3 = 0$$

Numerical formulation of the solution, however, requires further simplification. All coefficients except $b_2$ and $b_4$ are assumed equal to zero. Using equations (5.37) and (5.38), the admissible flow function assumed in this analysis is

$$\hat{\phi}(r,z) = b_2 \left(r/R(z)\right)^2 - \left(b_2 + \pi R_0^2 \dot{U}_0\right)\left(r/R(z)\right)^4 \tag{5.39}$$

From equation (5.6), the boundary $\Gamma_i$ is given by

$$b_2 \left(r/R(z)\right)^2 - \left(b_2 + \pi R_0^2 \dot{U}_0\right)\left(r/R(z)\right)^4 = -\pi r^2 \dot{U}_0 \tag{5.40}$$

$\Gamma_1$ passes through $(0,L_1)$ which yields

$$b_2 = -\pi R^2(L_1)\dot{U}_o \tag{5.41}$$

Similarly from equation (5.7) and the condition that $\Gamma_2$ passes through $(0,L_2)$, one obtains

$$b_2 = -\pi R^2(L_2)\dot{U}_f$$

The points at which the plastic zone boundaries meet the extrusion axis are thus related by

$$\frac{R^2(L_1)}{R^2(L_2)} = \frac{\dot{U}_f}{\dot{U}_o} = \frac{R_o^2}{R_f^2} \tag{5.42}$$

Substituting for $b_2$ in equation (5.39), one obtains

$$\hat{\Phi}(r,z) = \pi R_o^2 \dot{U}_o \left[-C^2\left(r/R(z)\right)^2 + (C^2-1)\left(r/R(z)\right)^4\right] \tag{5.43}$$

where $C = \dfrac{R(L_1)}{R_o} = \dfrac{R(L_2)}{R_f}$

The general kinematic model chosen to obtain lower upper-bound solution is shown in Figure 39 with flow function defined by equation (5.43). The model has only one coefficient 'C' which can be varied independently of the kinematic conditions and this coefficient is related to the location of boundaries $\Gamma_1$ and $\Gamma_2$ of the plastic zone II and the shape of the die.

From the assumed flow function, following expressions are derived

for velocity field in zone II, shape of boundaries $\Gamma_1$ and $\Gamma_2$ of plastic zone, and reduced extrusion pressure $(\bar{p}/\sigma_o)$ (see Appendix E):

Velocity field:

$$\dot{U}_r = \dot{U}_o \left[ -\frac{c^2 \rho}{r_d} + \frac{2(c^2-1)\rho^3}{r_d^3} \right] \frac{r_d'}{r_d^2}$$

$$\dot{U}_z = \dot{U}_o \left[ -\frac{c^2 \rho}{r_d} + \frac{2(c^2-1)\rho^3}{r_d^3} \right] \frac{1}{\rho r_d} \qquad (5.44)$$

Boundaries:

$$\Gamma_1 : \quad \rho = \left[ r_d^2 \left( \frac{c^2 - r_d^2}{c^2 - 1} \right) \right]^{1/2} \quad \text{for } c \neq 1$$

$$\xi = 1 \quad \text{for } c = 1 \qquad (5.45)$$

$$\Gamma_2 : \quad \rho = \left[ \frac{r_d^2}{r_f^2} \left( \frac{c^2 r_f^2 - r_d^2}{c^2 - 1} \right) \right]^{1/2} \quad \text{for } c \neq 1$$

$$\xi = 0 \quad \text{for } c = 1$$

Reduced extrusion pressure:

$$\frac{\bar{p}}{\sigma_o} = \frac{2}{\sqrt{3}} \left[ 2\, G(r_d, l, r_f, c) + \left\{ H_1(r_d, l, r_f, c) + H_2(r_d, r_f, c) + m\, H_3(r_d, l, r_f, c) \right\} \right] \qquad (5.46)$$

where $\frac{R_{(L_1)}}{R_0} = c$ , $\frac{\xi}{R_0} = \rho$ , $\frac{\eta}{R_0} = \xi$ , $\frac{R_f}{R_0} = r_f$ , $\frac{L}{R_0} = \ell$ , $\frac{R_{(\xi)}}{R_0} = r_d$

(5.47)

Function G in equation (5.46) represents the contribution due to internal deformation in zone II and is given by

$$G(r_d, \ell, r_f, c) = \iint g(r_d, \rho, \xi, \ell, r_f, c)\, d\rho\, d\xi$$

where
$$g = \left[ \tfrac{1}{2} (r_d'/r_d^2)^2 \left\{ (a\hat{\eta} + 6b\hat{\eta}^3)^2 + (a\hat{\eta} + 2b\hat{\eta}^3)^2 + (2a\hat{\eta} + 8b\hat{\eta}^3)^2 \right\} + \tfrac{1}{4}\rho^2 \left[ (a\hat{\eta} + 2b\hat{\eta}^3) \frac{r_d''}{r_d^2} - (3a\hat{\eta} + 10b\hat{\eta}^3) \frac{r_d'^2}{r_d^3} + 4b\hat{\eta} \frac{1}{r_d^3} \right]^2 \right]^{1/2}$$

and $a = -c^2$ , $b = (c^2 - 1)$ (5.48)

Functions $H_1$ and $H_2$ define the contribution due to shear deformation along surfaces of velocity discontinuity $\Gamma_1$ and $\Gamma_2$ respectively. These functions are given by

$$H_1 = \int_{\ell}^{\ell_1} \left( h/r_d + \rho \right) d\xi + \int_{1}^{0} \left( h\, r_d'\, \rho / r_d^2 \right) d\rho$$

$$H_2 = \int_{0}^{\ell_2} \left( h/r_d + \rho/r_f^2 \right) d\xi + \int_{r_f}^{0} \left( h\, r_d'\, \rho / r_d^2 \right) d\rho$$

$$\text{where} \qquad h = \left[ -C^2\eta + 2(C^2-1)\eta^3 \right] , \quad \ell_1 = L_1/R_0 , \quad \ell_2 = L_2/R_0$$

In equation (5.46), the contribution of friction at the die surface is included by assuming a constant interfacial friction stress ($\tau = m\,\sigma_0/\sqrt{3}$), where m is the friction index. The function $H_3$ which represents the component due to friction, is given by

$$H_3 = \int_0^{\ell} \left[ (C^2-2)(1+z_d'^2)/z_d \right] d\xi$$

A computer program similar to that in Appendix C was written to determine the reduced extrusion pressure numerically for given values of reduction ratio ($r_f$), length of the die ($\ell$), interfacial friction index (m) and parameter C. To determine the best deformation model for a given set of process parameters ($r_f, \ell, m$), the surfaces $\Gamma_1$ and $\Gamma_2$ were moved by varying C and the location which resulted in lowest upper bound on pressure was determined. For the sake of generality, the computer program is written for an arbitrarily shaped die so that results can be obtained for any particular die by including a small subprogram defining the die shape. Numerical results of extrusion through two particular dies, one concave and other convex in shape are obtained.

Die Shapes

As shown in Appendix E, for C = 1, i.e., when the boundaries $\Gamma_1$ and $\Gamma_2$ are vertical surfaces, the expression (5.46) for extrusion

pressure reduces to

$$\left.\frac{\bar{p}}{\sigma_o}\right|_{C=1} = \left| \frac{4}{\sqrt{3}} \int_0^{\ell} \int_0^{z_d} \frac{\rho}{z_d^3} \sqrt{3 z_d'^2 + \frac{\rho^2}{4 z_d^2}\left(3 z_d'^2 - z_d z_d''\right)^2}\; d\rho\, d\xi \right.$$

$$\left. + \frac{2}{3\sqrt{3}}\left[z_d'(0) + z_d'(\ell)\right] + \frac{2}{\sqrt{3}} m \int_0^{\ell} \frac{(1+z_d'^2)}{z_d} d\xi \right| \qquad (5.49)$$

The first term on right hand side is the component due to internal deformation ( $p_{int}/\sigma_o$ ) in zone II. It can be easily verified that when contribution due to shear strain is zero, i.e.,

$$\left(3 z_d'^2 - z_d z_d''\right) = 0 \qquad (5.50)$$

$p_{int}$ reduces to

$$\left. p_{int}/\sigma_o \right|_{C=1} = 2 \ln(1/z_f) \qquad (5.51)$$

which is the ideal power of deformation. Solving the differential equation (5.50), one obtains

$$z_d = 1/(A_o \xi + B_o)^{1/2} \qquad (5.52)$$

Thus a die profile represented by equation (5.52) gives an internal power of deformation equal to the ideal power of deformation, when C = 1. This die which has a convex shape was first introduced by Samanta [53] as a high efficiency die. He derived this shape by solving simultaneously

the incompressibility condition and the condition that shear strain be zero throughout the plastic zone. His solution, however, allowed surfaces of velocity discontinuity and thus redundant work due to shear deforma - tion along these surfaces remained unchecked. This is obvious from expression (5.49) where substituting equation (5.52) does not necessarily reduce the total extrusion pressure $\bar{p}$. Samanta's conclusion that such a die has necessarily a high efficiency is erroneous. As shown later, the results indicate that this convex die has rather a low efficiency particularly at high reductions because of high redundant work of shear deformation. In this study, results are obtained for extrusion through this convex die represented by equation (5.52) and written in complete form as

$$R(z) = 1/(A_1 z + B_1)^{1/2}$$

$$\text{where} \quad A_1 = -(R_o^2 - R_f^2)/L R_o^2 R_f^2 , \quad B = 1/R_f^2 \tag{5.53}$$

Numerical results are also obtained for a concave die represented by equation

$$R(z) = (A_2 z + B_2)^{1/2}$$

$$\text{where} \quad A_2 = (R_o^2 - R_f^2)/L , \quad B_2 = R_f^2 \tag{5.54}$$

This die was first investigated by Chang and Choi [36] who presented a

simple upper bound solution assuming plane vertical boundaries of plastic zone. Comparison shall be made of results obtained using lower upper-bound analysis presented here with those presented by Samanta [53] and Chang and Choi [36].

Results

Qualitative effect of parameter C on boundaries of the plastic zone, velocity field and the various components of extrusion pressure is discussed first.

Effect of Parameter 'C'. As derived before, the locations of the entrance boundary $\Gamma_1$ and exit boundary $\Gamma_2$ are related by

$$\frac{R^2(L_1)}{R^2(L_2)} = \frac{\dot{U}_f}{\dot{U}_o} = \frac{R_o^2}{R_f^2} \qquad (5.42)$$

The above relation imposes certain restrictions on the possible shape of plastic zone boundaries. These restrictions are best illustrated by some examples.

For a die with cosine or sine profile which has zero entrance and exit angles, as shown in Figure 40a , relation (5.42) can be satisfied only when C = 1 i.e., when the boundaries are vertical plane surfaces. Thus the lower upper-bound analysis degenerates to a simple upper bound solution for dies of this shape. When the die has a zero entrance angle but a non-zero exit angle as for a elliptic die, relation (5.42) can be satisfied only when $L_2$ is negative as shown in Figure 40b. For each negative value of $L_2$, there are two values of $L_1$ according to equation (5.42), one greater than L and one less than L. When the die has a zero

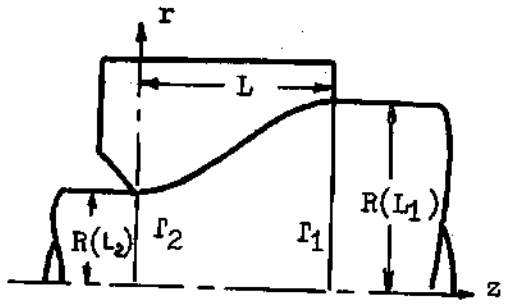


(a) COSINE DIE

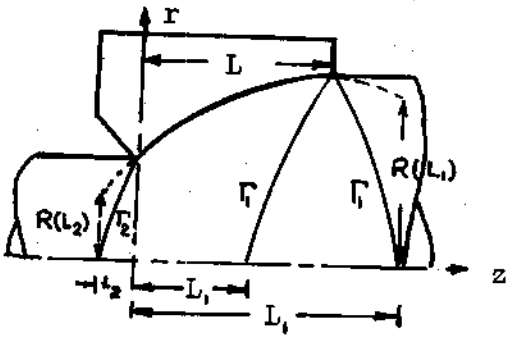


(b) ELLIPTIC DIE

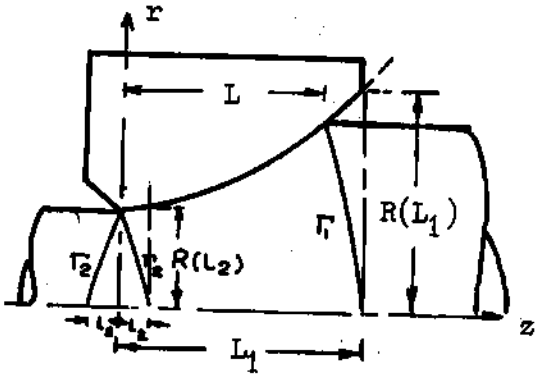


(c) HYPERBOLIC DIE

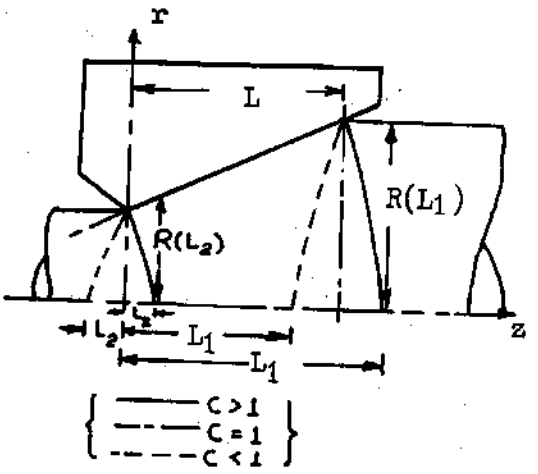


(d) CONICAL DIE

Figure 40. Possible Location of the Plastic Zone Boundaries in Extrusion through Some Dies

exit angle and a non-zero entrance angle as shown in Figure 40c for a hyperbolic die, relation (5.42) can be satisfied only when $L_1$ is greater than L and for each value of $L_1$, $L_2$ has two values, one positive and one negative. The possible shape of boundaries is thus as shown in Figure 40c. For a die with non-zero exit and entrance angles, $L_2$ can be positive or negative. For positive $L_2$, $L_1$ will be greater than L and for negative $L_2$, $L_1$ would be less than L. This is shown in Figure 40d. Convex and concave dies analyzed in present work, and conical dies fall in this last category.

From the definition of parameter 'C', equation (5.43), it is obvious that an increase in C shifts the entrance boundary in a direction opposite to metal flow. For dies with non-zero entrance and exit angles, the exit boundary $\Gamma_2$ also moves in the same direction as $\Gamma_1$. Henceforth we shall limit our discussion to such dies only. For C = 1, the boundaries are vertical surfaces and for C less than one or greater than one, the boundaries will be as shown in Figure 40d. The maximum value of C is $\sqrt{2}$. This is derived from the consideration that boundary $\Gamma_1$ should not fall outside of the bar radius $R_o$. Differentiating equation (5.45), the slope of entrance boundary $\Gamma_1$ is

$$\Gamma_1: \quad \frac{d\rho}{d\xi} = \frac{1}{2}\left[z_d^2\left(\frac{C^2 - z_d^2}{C^2-1}\right)\right]^{-\frac{1}{2}} \cdot 2\, z_d\left(\frac{C^2 - 2z_d^2}{C^2-1}\right)$$

$$\text{At} \qquad \rho = z_d = 1\,, \quad \xi = l$$

$$\Gamma_1: \quad \frac{d\rho}{d\xi} = \left(\frac{C^2-2}{C^2-1}\right) \tag{5.55}$$

Therefore along $\Gamma_1$

$$\left.\frac{d\rho}{d\xi}\right|_{\xi=l} = \begin{cases} -\infty & \text{for } 1 < C < \sqrt{2} \\ 0 & \text{for } C = \sqrt{2} \\ +\infty & \text{for } C > \sqrt{2} \end{cases} \tag{5.56}$$

For $C > 1$, $\left.\frac{d\rho}{d\xi}\right|_{\xi=l}$ can be zero or negative. Thus the value of C is limited to

$$C \leq \sqrt{2} \tag{5.57}$$

The effect of factor C on velocity field can be judged from equation (5.44). An increase in C would tend to increase the absolute value of velocity components ($\dot{U}_r$, $\dot{U}_z$) at small ($\rho/\ell_d$) ratios, that is near the axis of extrusion and would decrease the absolute value of velocity components at large ($\rho/\ell_d$) ratios, i.e. near the die surface. It is interesting to observe the variation of velocity at die surface with parameter C.

Along die surface $\Gamma_3$, $\rho = r_d$

$$\left.\begin{aligned} \dot{U}_t &= \dot{U}_0 (C^2-2) \frac{\ell_d'(\xi)}{\ell_d^2} \\ \dot{U}_z &= \dot{U}_0 (C^2-2) \frac{1}{\ell_d^2} \end{aligned}\right\} = 0 \quad \text{for } C = \sqrt{2} \tag{5.58}$$

From equation (5.58), it is evident that an increase in C reduces the absolute value of velocity components at the die surface and for $C = \sqrt{2}$,

velocity along die surface is zero throughout. The combined effect of change in boundaries and velocity field with C is reflected in variation of extrusion pressure with C.

Figure 41 shows a typical variation of various components of reduced extrusion pressure ( $\bar{P}/\sigma_o$ ) with parameter C for a given reduction ratio ($r_f$), length of die ($\ell$), and friction index (m). Results shown are for concave die but similar pattern was obtained for convex die. Components of pressure due to internal deformation and shear power loss over boundaries $\Gamma_1$ and $\Gamma_2$ go through a minimum. The component due to friction at die-material interface, however, decreases with increase in C and is equal to zero for C equal to $\sqrt{2}$. This dependence is evident from the expression for friction component ( $P_f/\sigma_o$ ) of reduced extrusion pressure given below (see Appendix E)

$$\frac{P_f}{\sigma_o} = \frac{2}{\sqrt{3}} m(C^2-2) \left| \int_0^{\ell} \frac{1}{t_d} \left[1 + t_d'^2(\xi)\right] d\xi \right| \tag{5.59}$$

$$\text{or} \quad \frac{P_f}{\sigma_o} = \text{Const.}\,(C^2-2) \quad \text{for given } t_d, \ell, m$$

An increase in C decreases the relative velocity between die and material and thereby decreases the friction loss. The combined effect of these components is that the least upper bound on reduced extrusion pressure is obtained for a certain optimal value of C, termed $C_{opt}$, less than or equal to $\sqrt{2}$.

It is interesting to note that a increase in interfacial friction results in an increase in the value of $C_{opt}$ which means that the

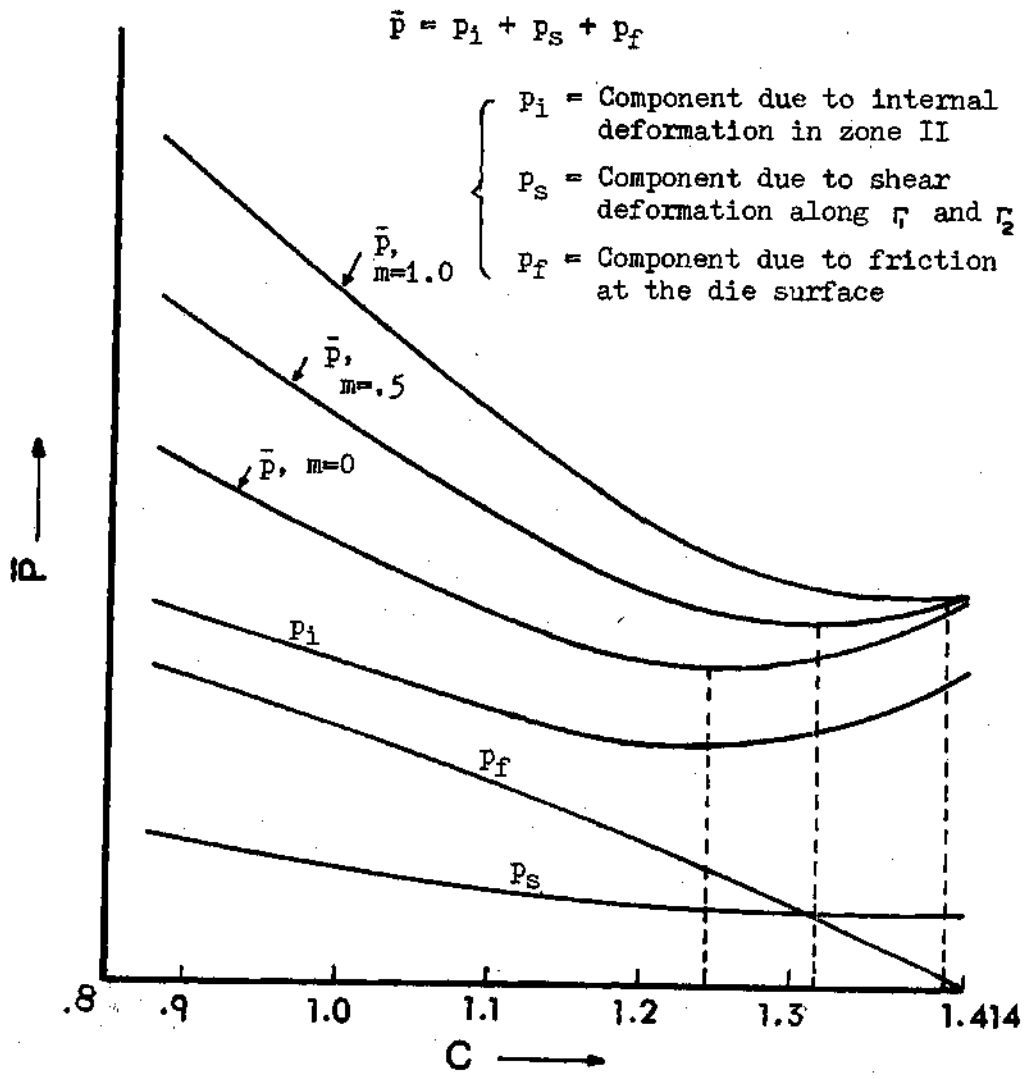


Figure 41. Typical Effect of Parameter C on Various Components of Extrusion Pressure ($\bar{p}$)

deformation model adjusts itself to reduce the velocity along the die surface and thereby decrease the rate of energy dissipation due to friction.

Lower Upper-Bound on Extrusion Pressure. Figures 42 and 43 show, for concave die and convex die respectively, the least upper bounds obtained on the extrusion pressure as a function of reduction ratio, length of the die and friction index. The pressure required to extrude the material increases with an increase in area reduction (RA) for any given $\ell$ and m. The effect of friction is to increase the extrusion pressure for a given reduction and length of the die. For a frictionless extrusion, an increase in length ($\ell$) of the die reduces the extrusion pressure. For comparison, pressure required to ideally deform the material is also shown. This curve forms a lower bound on the actual extrusion pressure as the actual pressure can never be less than the ideal pressure. The difference in the lower bound and the upper bound on extrusion pressure when $\ell = 3$ is small which indicates that the analysis presented here forms a close upper bound on the actual pressure. It may be stated here that for other dies, similar variation of the extrusion pressure with reduction, length and friction index has been observed [16,34].

Comparison of numerical values shows that up to 50 % reduction, the extrusion pressures are almost equal for the concave die and the convex die. However, above 50 % reduction, extrusion pressures for concave die are less than those for convex die. From results for conical die reported by Zimerman and Avitzur [32] and Avitzur [50], it seems that extrusion pressures for conical die of equal length are nearly equal

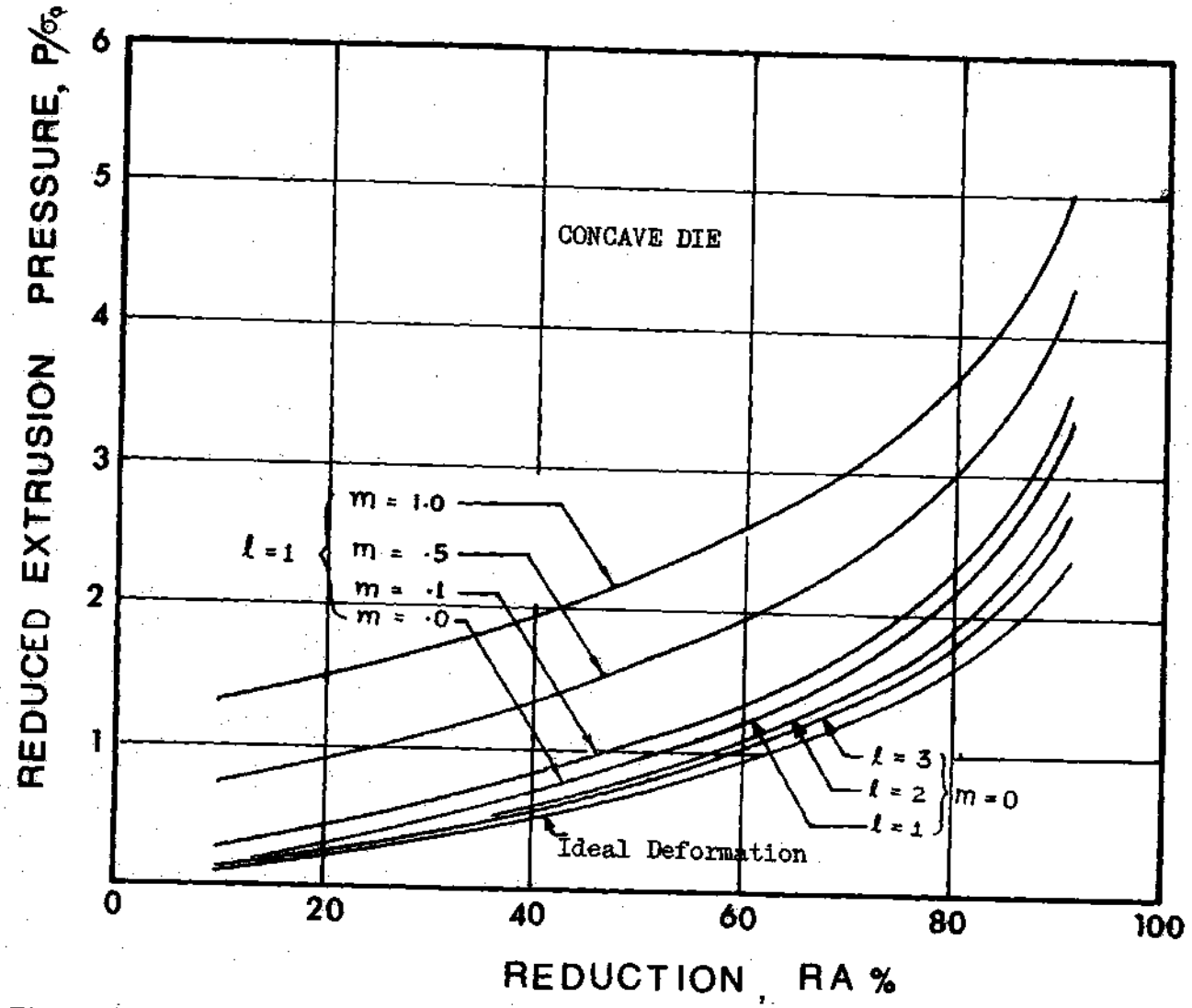


Figure 42. Effect of Reduction, Length, and Friction on Reduced Extrusion Pressure (Concave Die)

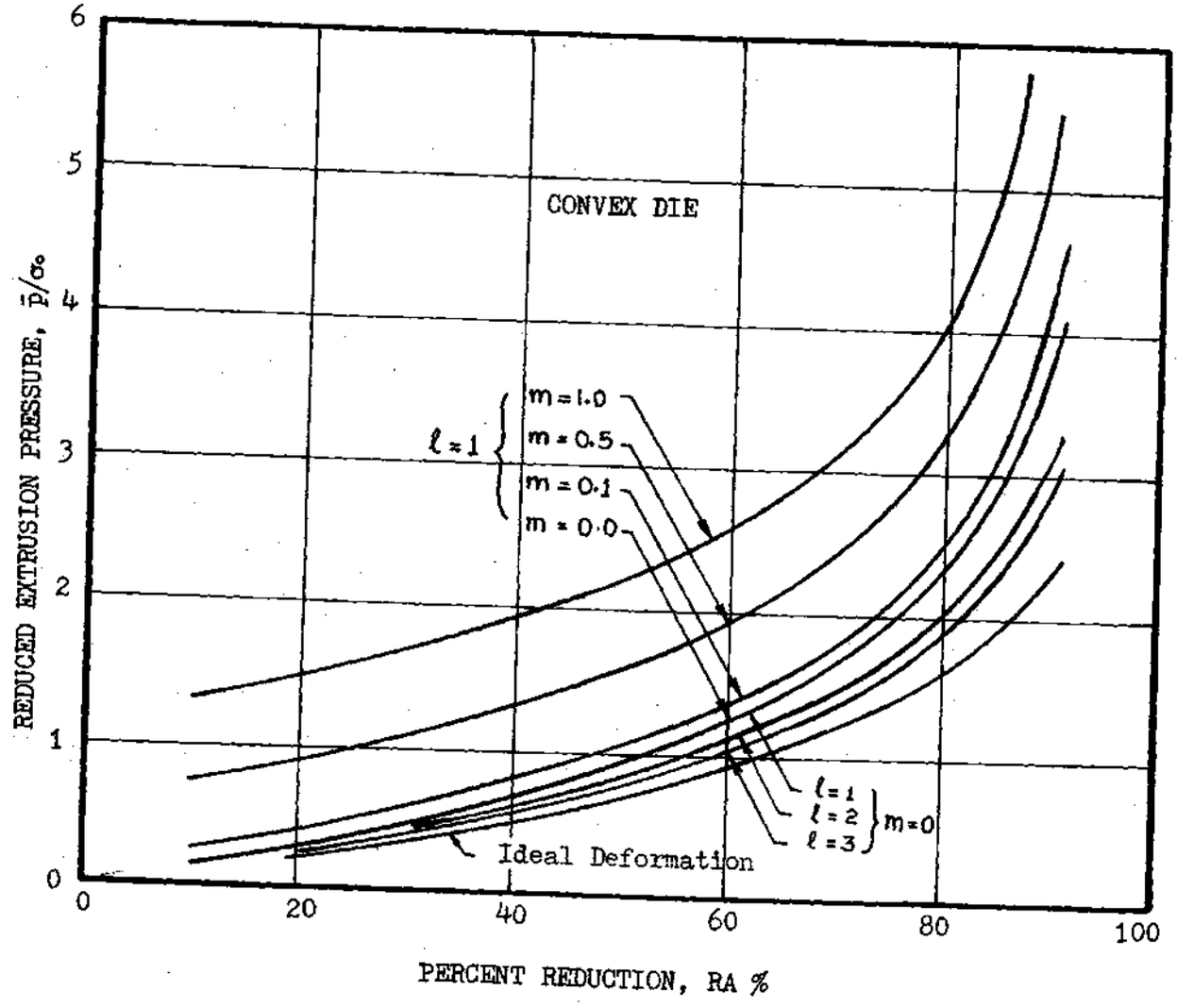


Figure 43. Effect of Reduction, Length, and Friction on Reduced Extrusion Pressure (Convex Die)

to those for concave die and convex die for reductions up to 40% and above this reduction, the extrusion pressures for conical die are slightly lower than those for concave die.

A typical variation of various components of the extrusion pressure with length of die in extrusion through a concave die is shown in Figure 44. The effect of length on component due to internal deformation in zone II is moderate. The shear losses over surfaces of velocity discontinuity $\Gamma_1$ and $\Gamma_2$ decrease with an increase in length due to decrease in the magnitude of velocity discontinuity. An increase in length increases the contribution due to friction because of increase in contact area over which friction occurs. Summing the partial contributions, the total extrusion pressure is presented in Figure 44. This curve exhibits a a minimum where the compromise is found between friction and excessive distortion or shear. The length of die at which the pressure is minimum is termed optimal length ($\ell_{opt}$).

For concave dies, Figures 45 and 46 show the least upper bounds on reduced extrusion pressure as a function of length ($\ell$) of die for different frictional conditions. When the extrusion process is frictionless, the required extrusion pressure theoretically reaches its minimum value of ideal deformation for $\ell \to \infty$. This behavior is apparent in Figure 45 for concave dies. If some die friction is to be included, a finite optimal length ($\ell_{opt}$) exists at which the extrusion pressure is minimum. This is observed for concave as well as convex die and is shown in Figures 45b and 46. The Figures for convex dies are included in Appendix E. The optimal lengths and corresponding extrusion pressures are obtained with different frictional factors. Table 2 shows the results. It

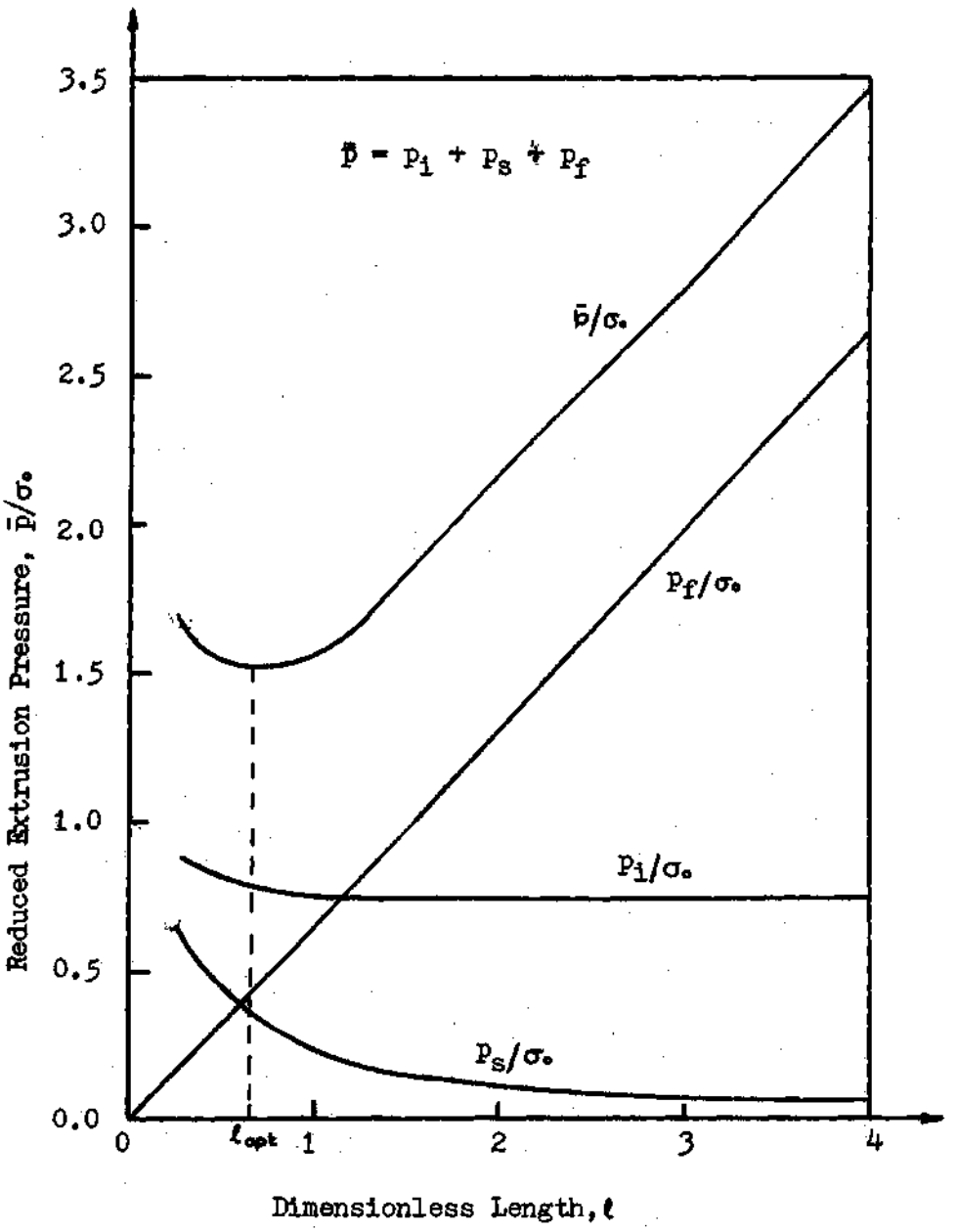


Figure 44. Typical Variation of the Various Components of Extrusion Pressure with Dimensionless Length ($\ell$) of Concave Die, $r_f = 0.7$, $m = 0.5$

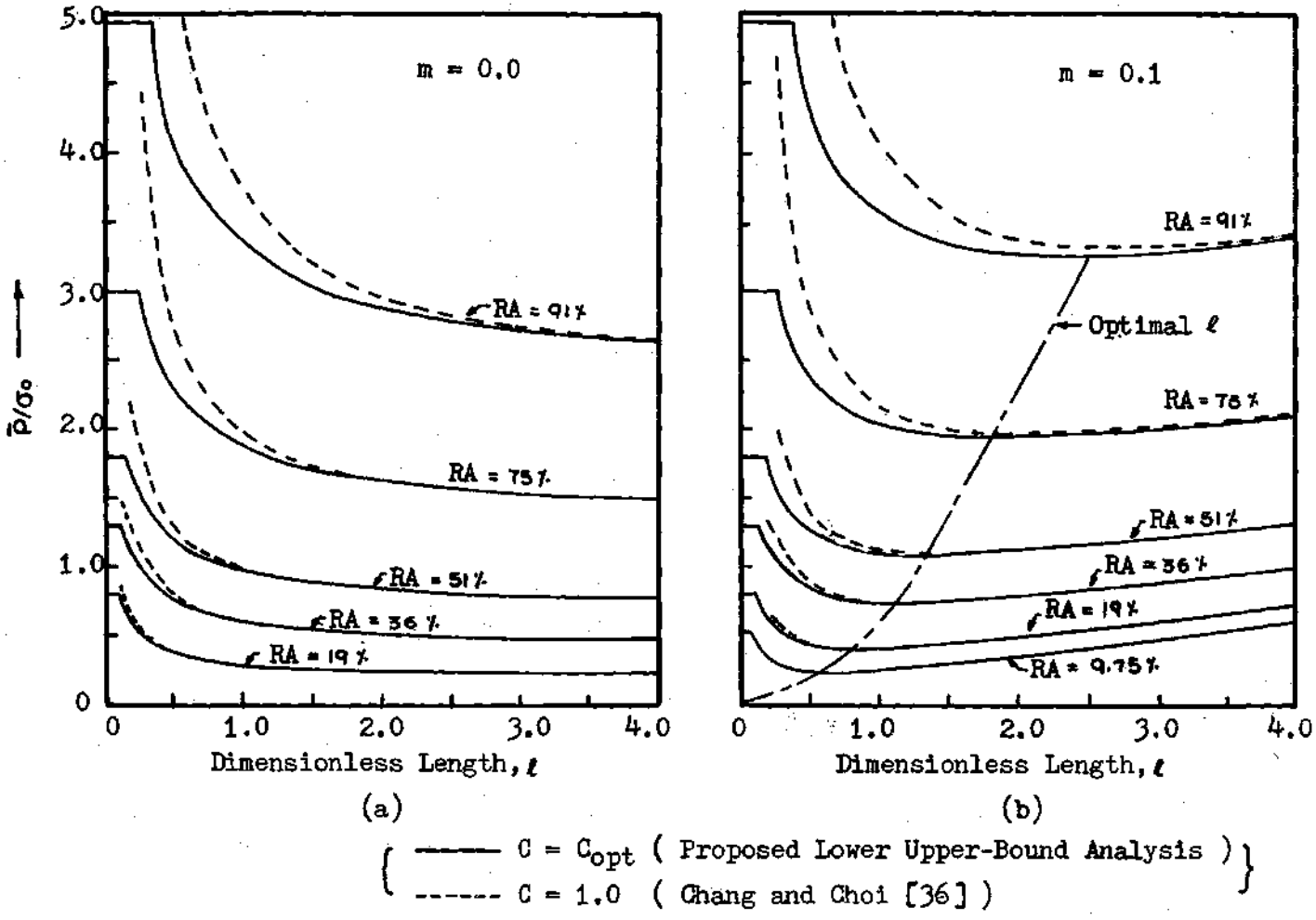


Figure 45. Effect of Dimensionless Length ($\ell$) on Reduced Extrusion Pressure ($\bar{p}/\sigma_o$) in Extrusion through Concave Die

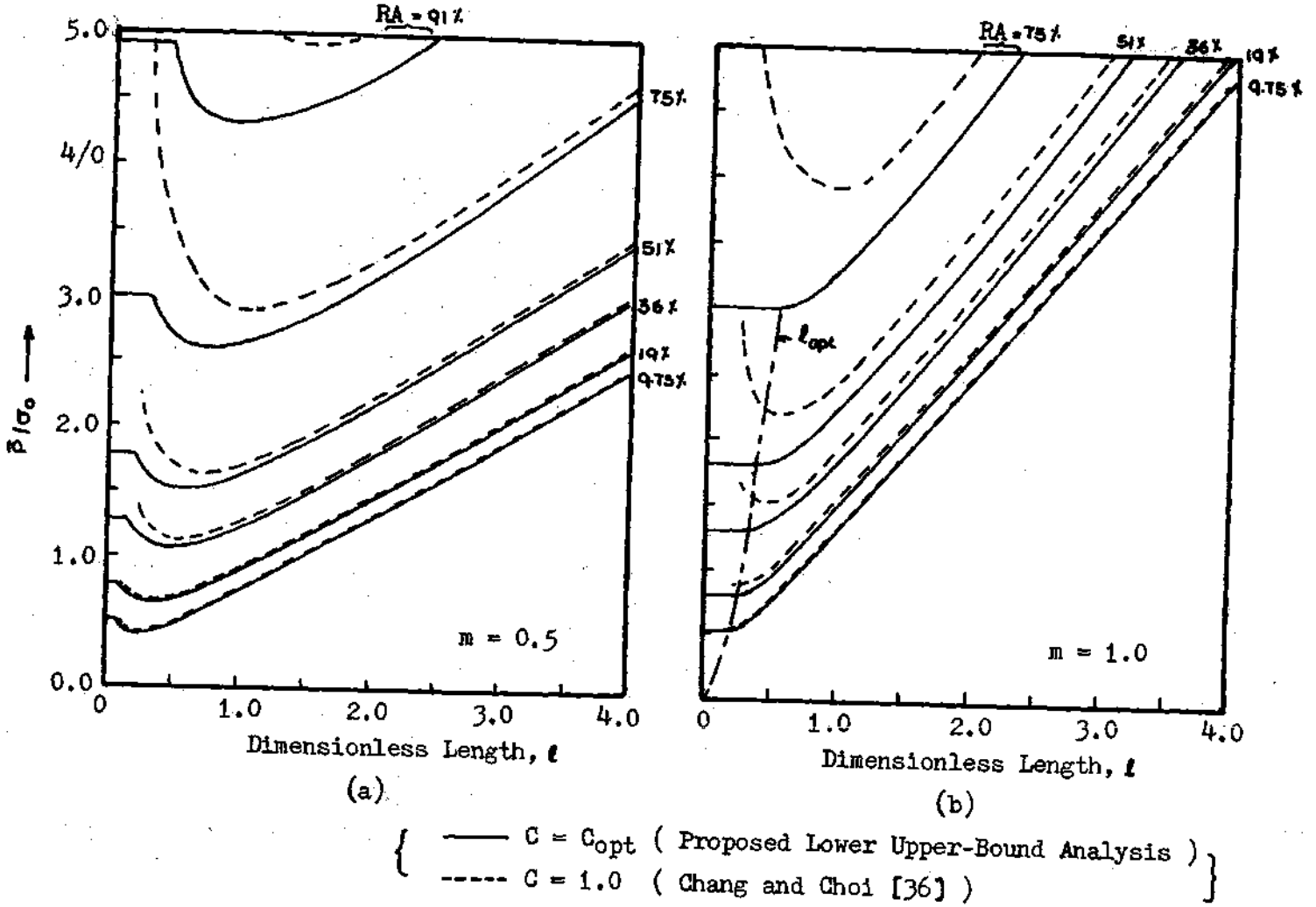


Figure 46. Effect of Dimensionless Length ($\ell$) on Reduced Extrusion Pressure ($\bar{p}/\sigma_o$) in Extrusion through Concave Die

Table 2. Optimal Lengths and Corresponding Extrusion Pressures for Concave and Convex Dies

| Friction Index (m) | Reduction (Area) % | Concave Die | | Convex Die | |
|---|---|---|---|---|---|
| | | $\ell_{opt}$ | $\bar{p}/\sigma_o$ | $\ell_{opt}$ | $\bar{p}/\sigma_o$ |
| 1. | 9.75 | 0.55 | .238 | 0.55 | 0.238 |
| | 19 | 0.80 | .405 | 0.80 | 0.404 |
| | 36 | 1.10 | .732 | 1.10 | 0.731 |
| | 51 | 1.35 | 1.082 | 1.30 | 1.085 |
| | 75 | 1.80 | 1.936 | 1.70 | 2.032 |
| | 91 | 2.50 | 3.259 | 2.65 | 3.910 |
| 1.0 | 9.75 | 0.175 | .524 | 0.17 | 0.531 |
| | 19 | 0.250 | .809 | 0.27 | 0.817 |
| | 36 | 0.325 | 1.309 | 0.37 | 1.303 |
| | 51 | 0.375 | 1.808 | 0.47 | 1.814 |
| | 75 | 0.525 | 3.010 | 0.75 | 3.377 |
| | 91 | 0.700 | 4.931 | 1.15 | 7.527 |

is evident that for small reductions and low friction factors, the optimal lengths and pressures are almost equal; however, for large reductions, the optimal lengths and extrusion pressures are smaller for the concave die. The present theoretical analysis therefore seems to indicate that a concave shaped die is in general more efficient with regard to the rate of energy dissipation than a convex shaped die. A similar observation has been made by Devenpeck [73]. For small die lengths, a mode of deformation which assumes a dead zone at the die surface requires less rate of energy dissipation than a mode which assumes no dead zone. The pressure does not change with length of the die when dead zone forms. This is the reason why the curves show a flat portion at small lengths.

The dependence of optimal value of C ($C_{opt}$) on dimensionless length ($\ell$) and friction index (m) is shown in Figures 47 and 48 for concave and convex dies, respectively. It can be argued that for $\ell \to 0$, the $C_{opt}$ will approach one. The value of $C_{opt}$ first rises very rapidly and then drops off in a exponential manner with increase in length ($\ell$). For concave die, an increase in $C_{opt}$ was observed with an increase in reduction and friction index. For convex die, as the Figure 48 shows, at large reductions, the $C_{opt}$ decreases for certain range of die lengths.

Flow Characteristics. When C is replaced by $C_{opt}$ in equation (4.43), the flow function represents the best approximation to the actual flow function for any given set of process parameters. Along a streamline, this flow function is constant. Thus

$$\hat{\Phi} = f(C_{opt}, \hat{\eta}) = C_o \qquad (5.60)$$

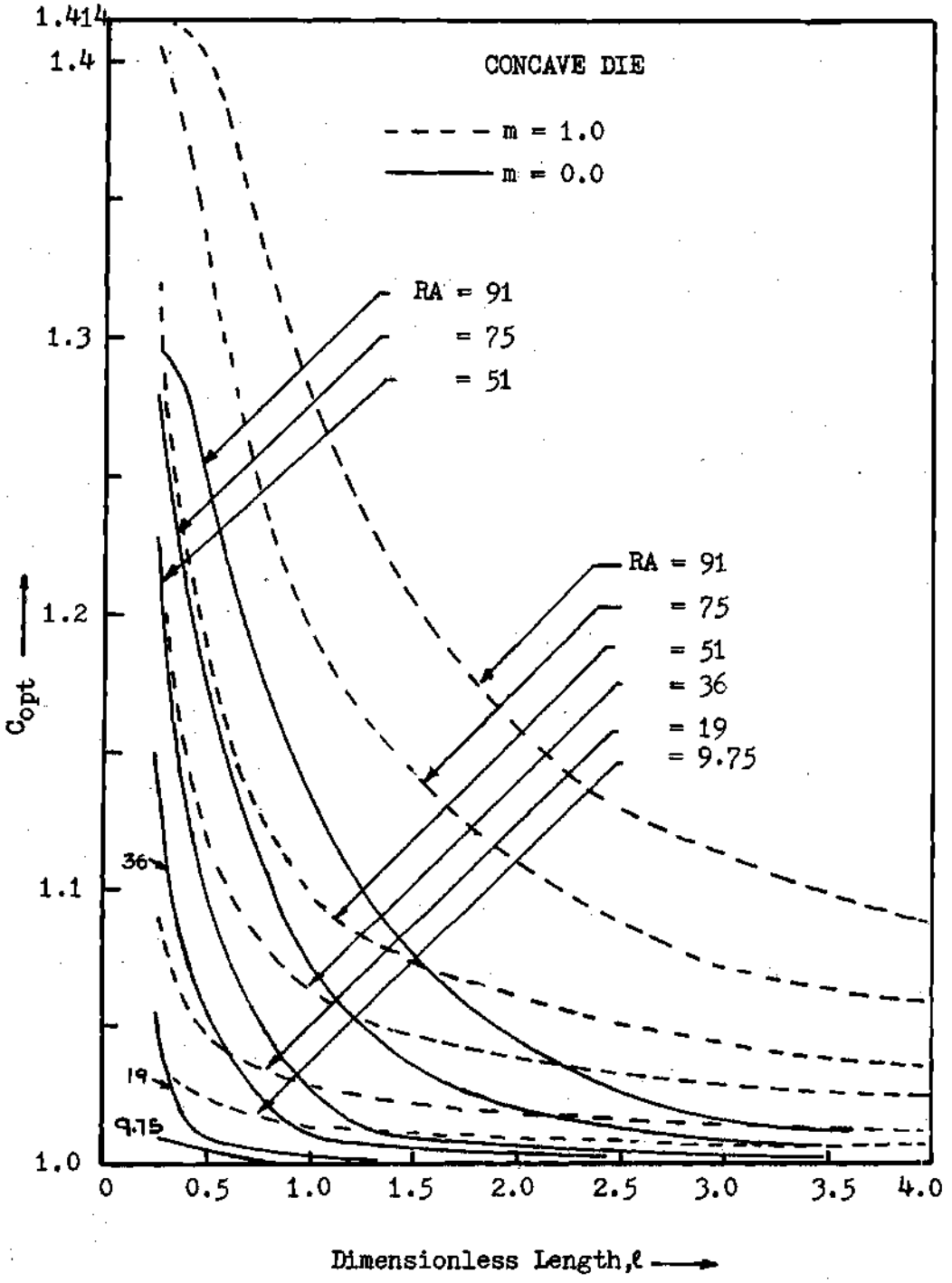


Figure 47. $C_{opt}$ as Function of the Dimensionless Length, (Concave Die)

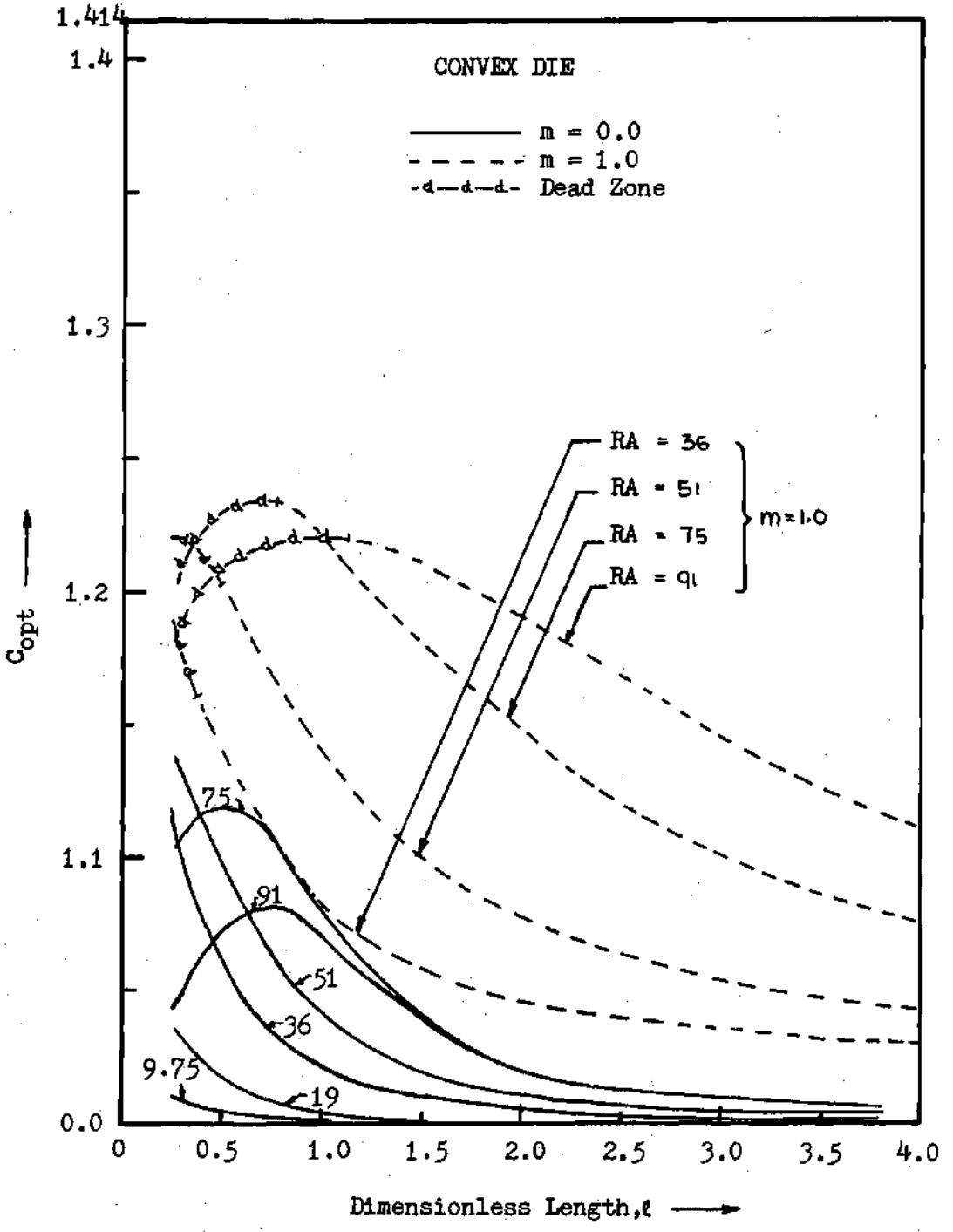


Figure 48. $C_{opt}$ as Function of Dimensionless Length, (Convex Die)

$C_o$ is a constant whose value is proportional to the volume of material passing through the tube bounded by surface $\hat{\phi} = C_o$ . Solving equation (5.60) for $\hat{\eta}$ , one obtains the equation for streamlines

$$r/R(z) = S(C_{opt}, C_o) = \text{Const} \tag{5.61}$$

where $S(C_{opt}, C_o)$ is some combination of constants $C_{opt}$ and $C_o$. From equation (5.61) one can notice that the effect of $C_{opt}$ is to move the streamlines in zone II towards or away from the extrusion axis. Calculations show that an increase in $C_{opt}$ results in a displacement of streamlines towards the extrusion axis. Figure 49 shows the shape and location of flow lines in extrusion through concave die for different frictional conditions at the die-material interface. The effect of interfacial friction is to displace the flow lines towards the extrusion axis. Also the entire flow field is altered and not just the region near the die surface. Such effect of friction on flow field has been observed experimentally in extrusion through conical die by Shabaik and Thomsen [78]. It may be pointed out that solutions presented by Samanta [53] and others [36, 34] for this problem would fail to predict the difference in flow pattern due to friction since the velocity fields and hence the flow functions assumed in their analyses are not affected by friction. Figure 49b shows the flow lines in extrusion through convex die.

The effect of displacement of flow lines towards extrusion axis is to move the boundaries of plastic zone II in a direction opposite to metal flow. It is interesting to compare the individual displacement of boundaries $r_1$ and $r_2$ for the two dies. Due to friction, $r_1$ is displaced

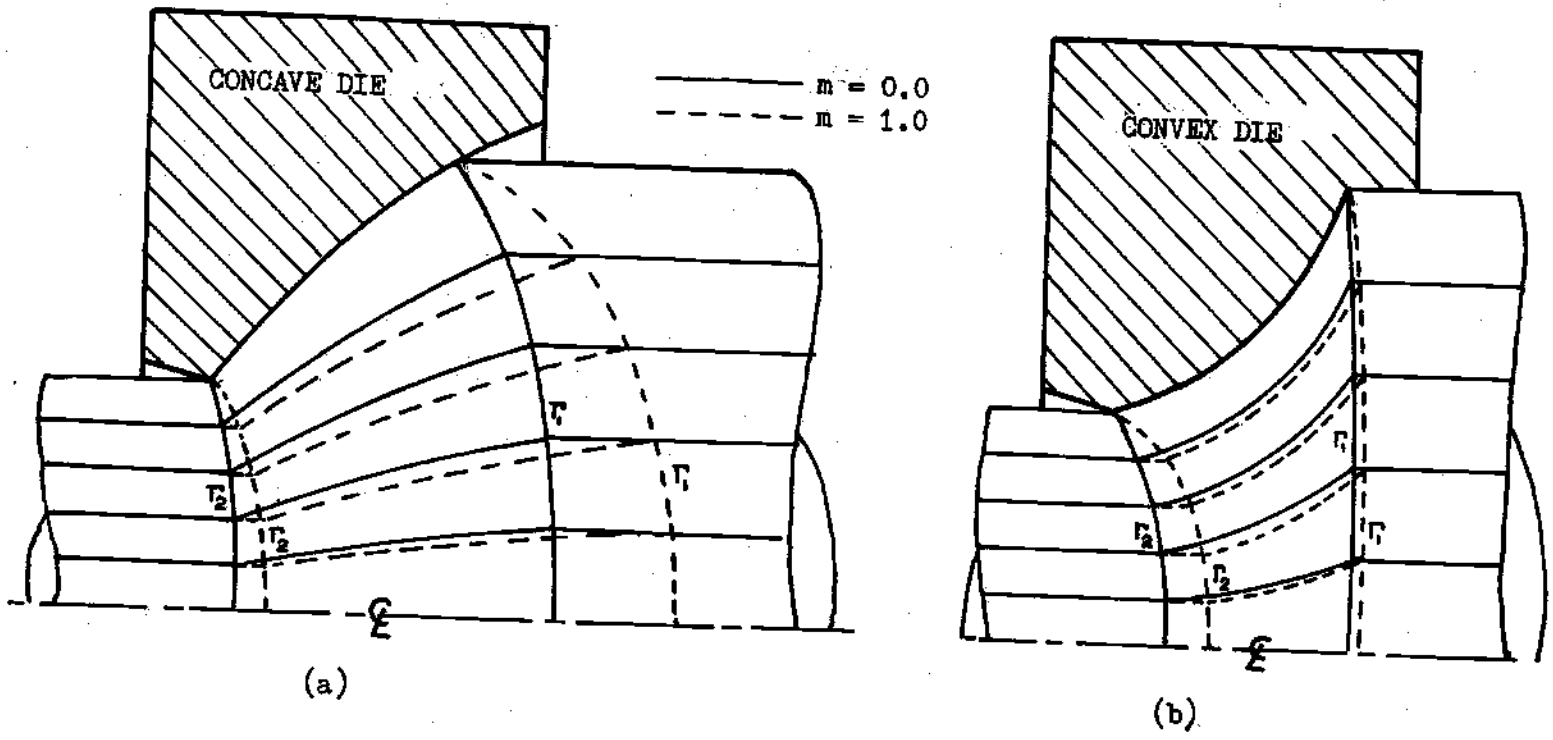


Figure 49. Flow Lines with Different Friction Conditions in Extrusion through Concave and Convex Dies

more than $r_2$ for concave shaped die whereas opposite effect is noted for the convex die. As the Figure 49 shows, the net effect is that for convex die the flow field is not affected as much as for concave die by the friction factor (m). This is probably the reason why extrusion through convex die requires much higher pressures under high frictional conditions. It may be pointed out that the predicted displacement of boundaries of plastic zone is in qualitative agreement with visioplasticity studies [79] and theoretical findings of Zimerman and Avitzur [32] for conical dies.

Figure 50 shows the resultant velocities along the axis of extrusion and along die surface in extrusion through a concave die. The effect of friction is to reduce the velocity along the die profile and increase it along the axis. Comparison with velocities obtained for conical die of equal axial length, experimentally by visioplasticity method [79], shows good qualitative agreement. Theoretical velocities show an abrupt discontinuity at surfaces $r_1$ and $r_2$ which is admissible for the assumed rigid-perfectly plastic material. The experimental curves, however, show a gradual change because the material tested is not perfectly rigid-plastic material.

The effect of process variables on flow field is reflected in the distortion of an originally square or rectangular grid. Predicted grid distortions in extrusion through concave dies are shown in Figure 51.

## Conclusions

The analysis presents a generalized upper bound approach to the solution of axisymmetric extrusion through a curved die. As shown, the problem is reduced to approximating the actual flow function by a function which satisfies certain simple boundary conditions. For the purpose of

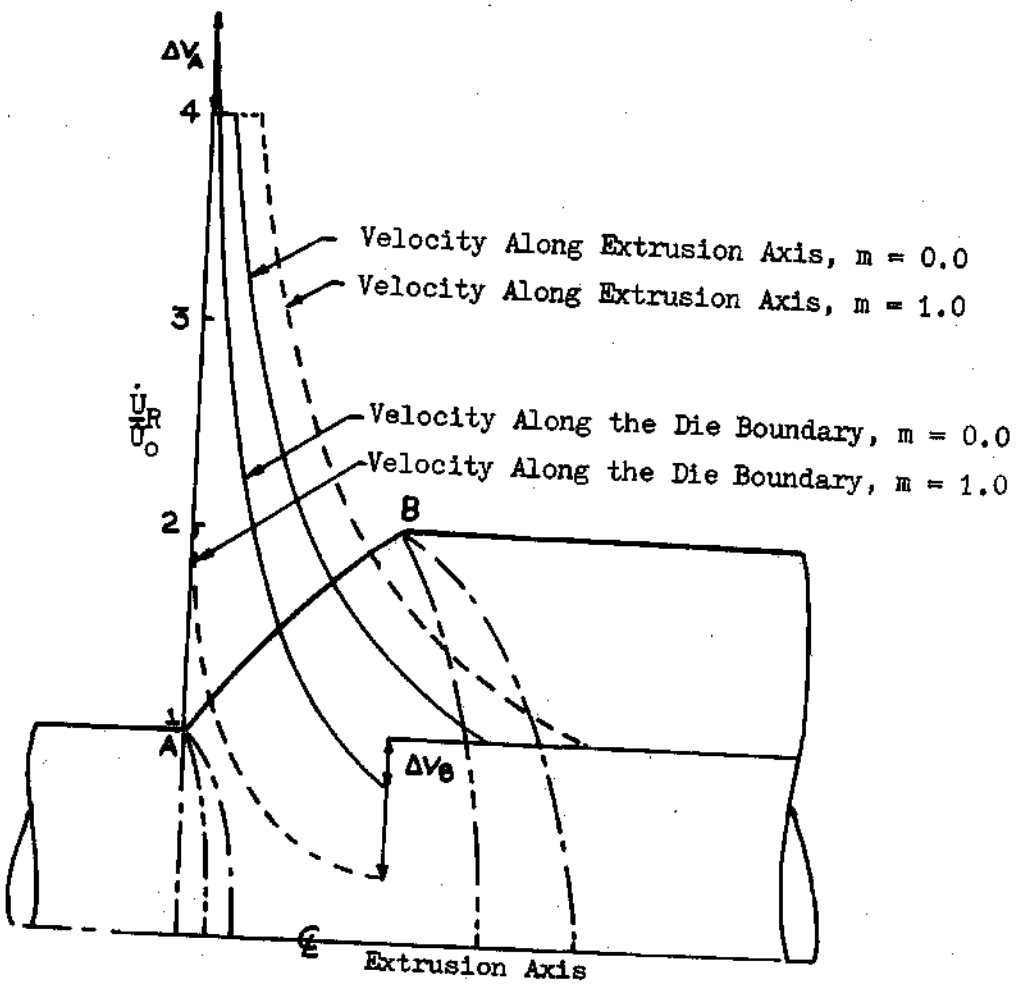


Figure 50. Resultant Velocities along the Die Surface and the Extrusion Axis in Extrusion through Concave Die, $r_f = 0.5$, $\ell = 0.5$

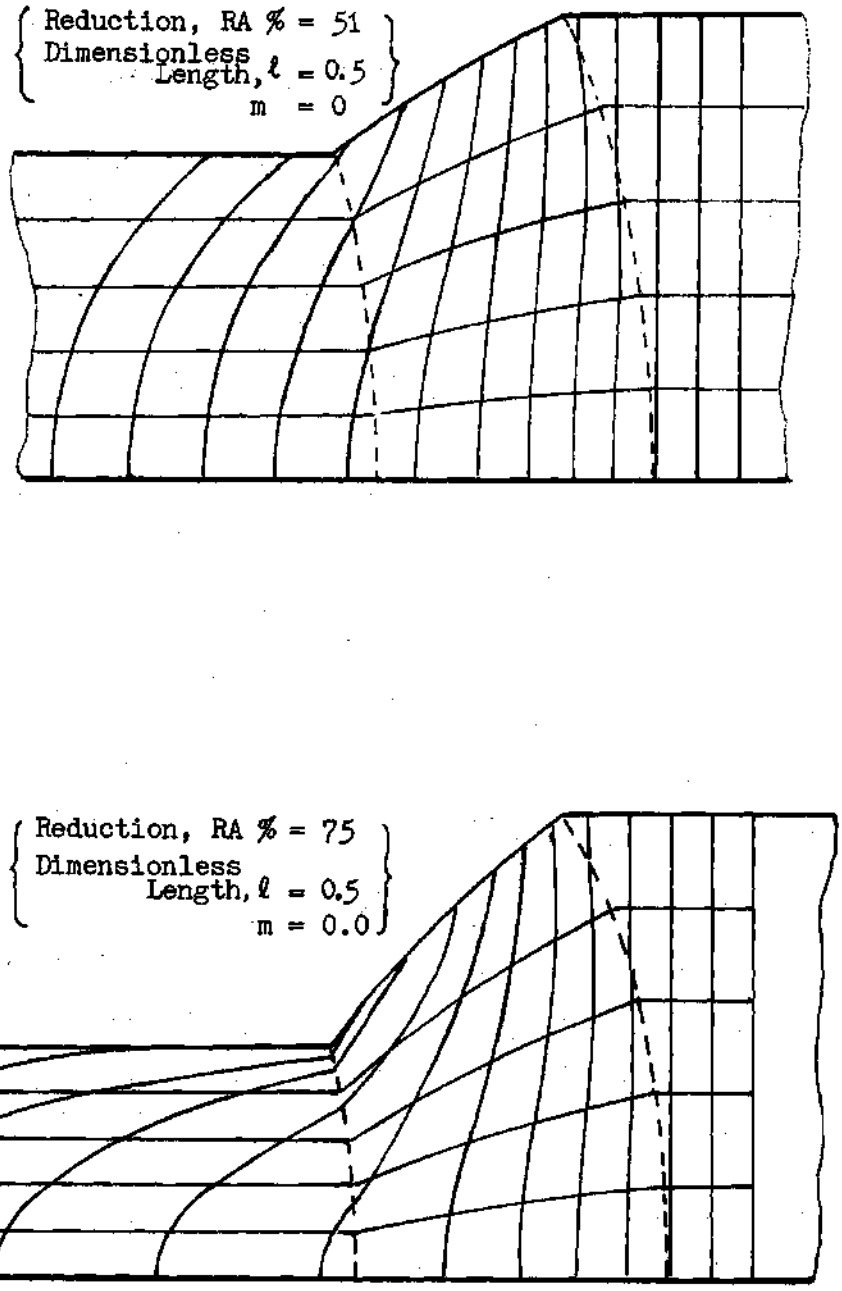


Figure 51. Expected Grid Distortion in Extrusion through Concave Die

generality and with numerical simplicity in mind, an admissible function is chosen which has only one arbitrary parameter that is not defined by kinematic conditions of the problem. Upper Bound Theorem is used to get the optimal value of this parameter for a given set of process parameters. This defines the approximate flow function which in turn gives the approximate solution to the problem. Results for two particular types of dies show that a close approximate solution is obtained which not only gives better upper bounds on pressure but also is able to predict qualitatively the characteristics of flow.

At high reductions and under high frictional conditions, the convex die showed low efficiency. This is due to high redundant work of shear deformation at surface $\Gamma_1$ . Since the high shear deformation is due to the extreme entrance angle of the convex die at these reductions, the results indicate the necessity of keeping the entrance angle small.

Comparison of the curved dies considered in this analysis with conical dies indicates that the fabrication of curved dies is not warranted becuase no marked improvement in efficiency is expected.

# CHAPTER VI

## PLANE STRAIN AND AXISYMMETRIC FORGING

### Plane Strain Forging

In this Chapter, the problem of forging a rectangular strip under plane strain conditions is analyzed. The concept of flow function, discussed in Chapter II, is again used to form a general kinematically admissible model.

#### General

The axes of rectangular coordinates are chosen as shown in Figure 12b. The platens are considered rigid bodies. The top platen moves at a velocity of $-\dot{U}$ while the bottom platen moves at a velocity of $\dot{U}$. It is assumed that the length of strip is very large compared to its thickness and width so that strain in the z direction is negligible.

An admissible model for this process of forging was presented in Chapter II (Figure 12). Because of symmetry, only the upper right half of the strip is considered. A general velocity field for zone I, which satisfies the incompressibility condition is

$$\dot{U}_x = f'(\eta)\frac{\partial \eta}{\partial y}$$
$$\dot{U}_y = -f'(\eta)\frac{\partial \eta}{\partial x} \qquad (6.1)$$

where $f(\eta) = \Phi$ , $f'(\eta) = \frac{df(\eta)}{d\eta}$

For the velocity field, and hence the flow function $\phi$, to be kinematically admissible, the following conditions need to be satisfied:

$$\Phi(x,y) = f(\eta) = 0 \quad \text{at} \quad y = 0 \tag{6.2}$$

$$\Phi(x,y) = f(\eta) = 0 \quad \text{at} \quad x = 0 \tag{6.3}$$

$$\Phi(x,y) = \dot{U}x \quad \text{at} \quad y = y_r \tag{6.4}$$

$y = y_r$ represents the boundary r of the dead zone between platen and deforming strip, or if no dead zone is formed, then it defines the platen surface, i.e., y = t. It should be noted that the physical problem does not define the existence of a dead zone. The solution must define whether or not a dead zone would form for the given process conditions (friction at platen surface, width and thickness of strip). The criterion, ofcourse, is the total rate of energy dissipation. The kinematically admissible mode of deformation which requires less rate of energy to deform would be applicable. To analyze this type of problem by an upper bound approach, it is essential that both possible modes of deformation are considered. The case where the assumption is made that no dead zone is formed between platens and strip is considered first.

Strip Forging-No Dead Zone

To form kinematically admissible model for this case, let the streamlines be of the following form

$$\Phi(x,y) = h(x)\,g(y) \tag{6.5}$$

where h(x) and g(y) are some arbitrary but increasing functions of x and y, respectively. From equations (6.2) and (6.3), the admissibility conditions on h(x) and g(y) are

$$\begin{aligned} h(x) &= 0 \quad \text{at} \quad x = 0 \\ g(y) &= 0 \quad \text{at} \quad y = 0 \end{aligned} \tag{6.6}$$

From equation (6.4)

$$h(x)\,g(y) = \dot{U}x \quad \text{at} \quad y = t$$

Therefore,

$$h(x) = \frac{\dot{U}x}{g(t)}$$

Thus a general admissible flow function is

$$\Phi(x,y) = \frac{\dot{U}}{g(t)}\,x\,g(y) \tag{6.7}$$

where $g(y) = 0$ at $y = 0$

The velocity field for the plastic zone I is

$$\left.\begin{aligned} \dot{U}_x &= \frac{\dot{U}}{g(t)}\, x\, g'(y) \\ \dot{U}_y &= -\frac{\dot{U}}{g(t)}\, g(y) \end{aligned}\right\} \tag{6.8}$$

The velocity field given by equation (6.8) together with the boundary $y = t$ forms a general kinematically admissible model. This model is termed "Model I" here to distinguish it from another kinematically admissible model proposed later.

The following expression for upper bound on average forging pressure ($P_{av}$) is obtained using this model (see Appendix F)

$$\frac{P_{av}}{2/\sqrt{3}\,\sigma_o} = \frac{1}{4}\left[\frac{1}{g(t)}\int_0^t g''(y)\left\{\sqrt{4\left(\frac{g'(y)}{g''(y)}\right)^2+\omega^2} + \frac{4}{\omega}\left(\frac{g'(y)}{g''(y)}\right)^2 \ln\left|\left(\frac{\omega+\sqrt{4\left(\frac{g'(y)}{g''(y)}\right)^2+\omega^2}}{2\,\frac{g'(y)}{g''(y)}}\right)\right|\right\} dy + m_p\,\omega\left|\frac{g'(t)}{g(t)}\right|\right] \tag{6.9}$$

$$\text{where} \quad g(y) = g''(y) = 0 \quad \text{at} \quad y = 0 \tag{6.10}$$

The condition that the second derivative of $g(y)$ be zero at $y = 0$ comes from the requirement that the shear strain be zero at $y = 0$. It is obvious from equation (6.10) that the function $g(y)$ is not completly restricted by the kinematic conditions of the problem. In principle, an infinite number

of different forms for g(y) which would satisfy equation (6.10) can be selected. Rather interesting results are obtained with some particular admissible forms of g(y).

Let g(y) be of the form

$$g(y) = 1 - e^{-by/t} \tag{6.11}$$

From equation (6.7)

$$\phi(x,y) = \frac{\dot{U}}{(1-e^{-b})} \cdot x \left(1 - e^{-by/t}\right)$$

and the velocity field in zone I becomes

$$\begin{aligned} \dot{U}_x &= \frac{\partial \phi}{\partial y} = \frac{b}{t} \frac{\dot{U}}{(1-e^{-b})} x\, e^{-by/t} \\ \dot{U}_y &= -\frac{\partial \phi}{\partial x} = -\frac{\dot{U}}{(1-e^{-b})}\left(1 - e^{-by/t}\right) \end{aligned} \tag{6.12}$$

The velocity component $\dot{U}_x$ is a function of y and therefore the free surfaces of the strip, according to this velocity field, would bulge upon forging. By substituting for g(y) in equation (6.9), one obtains the same expression for $\dot{P}_{av}$ as proposed by Avitzur [16]. Avitzur's solution is therefore only a special case of the general solution formed with arbitrary function g(y) in this analysis. It should be noted that g(y) given by equation (6.11) does not satisfy the condition (6.10) that

$$g''(y) = 0 \quad \text{at} \quad y = 0$$

Avitzur's solution thus does not satisfy all compatibility conditions.

Consider another special form of $g(y)$

$$g(y) = y \tag{6.13}$$

which gives

$$\Phi(x,y) = \frac{\dot{U}}{t} xy$$

$$\left.\begin{aligned} \text{and} \quad \dot{U}_x &= \frac{\dot{U}}{t} x \\ \dot{U}_y &= -\frac{\dot{U}}{t} y \end{aligned}\right\} \tag{6.14}$$

The velocity component $\dot{U}_x$ is not a function of y and therefore the free surfaces according to this assumed flow function, would not bulge. This kinematically admissible velocity field (6.14) was first proposed by Avitzur [16] who termed it the "Uniform Parallel Velocity Field". Again Avitzur's solution turns out to be only a special case of the proposed general upper bound solution.

In actual practice, bulging of free surfaces of the strip is normally observed when friction is present at the platen-material interface. The flow of material is restricted more at the region near the platen surfaces because of interfacial friction. This results in a bulgy appearance of the free surfaces. In the kinematic model, the assumption of a velocity field which incorporates bulging is therefore more realistic.

In the proposed lower upper-bound solution, a kinematically admissible velocity field which satisfies equation (6.10) and includes bulging is assumed.

It is of importance to understand that forging is a non-steady process. If bulging occurs, then the shape of the body undergoing plastic deformation changes as deformation proceeds. Most all solutions therefore give only the pressure required at any particular instant when the strip has some known dimensions. Also the analyses are usually based on the assumption that the strip is rectangular and thus the solution gives only the 'Yield Point Load', i.e., the load required to initiate the plastic flow. Once the body has undergone large plastic flow, its configuration changes and therefore the original analysis can no longer be applied. The proposed lower upper-bound analysis is also restricted in these respects.

Proposed Lower Upper-Bound Solution. From expression (6.9), it is apparent that for given process parameters $(w,t,m_p)$, the value of the upper bound $p_{av}$ is dependent on an arbitrary function $g(y)$ which is restricted only by condition (6.10). The problem is thus to find that admissible form for $g(y)$ which yields the least upper bound. It is unlikely that an exact extremizing function can be determined from variational methods. An approximate solution is thus sought.

Choose $g(y)$ of the form

$$g(y) = y\left(1 - A\frac{y^2}{t^2}\right)$$

It can be easily verified that this form for $g(y)$ satisfies equation (6.10). Upon substituting $g(y)$ in equation (6.9), one obtains the

expression for upper bound on forging pressure

$$\frac{p_{av}}{2/\sqrt{3}\,\sigma_o} = \frac{3}{2}\frac{A}{1-A}\int_0^1 \psi\left\{\sqrt{\frac{(1-3A\psi^2)^2}{9A^2\psi^2}+W^2}\right. \tag{6.15}$$

$$\left. + \frac{1}{W}\frac{(1-3A\psi^2)^2}{9A^2\psi^2}\ln\left|\frac{W+\sqrt{\frac{(1-3A\psi^2)^2}{9A^2\psi^2}+W^2}}{\left(\frac{1-3A\psi^2}{3A\psi}\right)}\right|\right\} d\psi$$

$$+ \frac{m_p}{4} W \frac{1-3A}{1-A} \qquad \text{where} \quad \psi = y/t \;,\; W = \omega/t$$

In Appendix (F), a simpler but approximate expression for $p_{av}$ which maintains the upper bound property is derived. This expression is

$$\frac{p_{av}}{2/\sqrt{3}\,\sigma_o} = 1 + \frac{\omega^2}{24\,g(t)}\int_0^t \frac{g''^2(y)}{g'(y)}\,dy + \frac{m_p}{4}\omega\frac{g'(t)}{g(t)} \tag{6.16}$$

$$\text{provided} \quad \frac{\omega^2}{4}\frac{g''^2(y)}{g'^2(y)} < 1$$

Substituting g(y) in equation (6.16) yields

$$\frac{p_{av}}{2/\sqrt{3}\,\sigma_o} = 1 + \frac{1}{2}\left(\frac{\omega}{t}\right)^2\frac{A}{1-A}\left\{-1+\frac{1}{2\sqrt{3A}}\ln\left(\frac{1+\sqrt{3A}}{1-\sqrt{3A}}\right)\right\} + \frac{m_p}{4}\frac{\omega}{t}\left(\frac{1-3A}{1-A}\right) \tag{6.17}$$

The value of A which gives minimum $\bar{p}_{av}$ for any given w/t and $m_p$ is obtained by setting

$$\frac{\partial \bar{p}_{av}}{\partial A} = 0$$

which yields the following equation for optimum A

$$\frac{3A-1}{2(1-3A)} + \frac{A+1}{4\sqrt{3A}} \ln\left(\frac{1+\sqrt{3A}}{1-\sqrt{3A}}\right) = m_p \frac{t}{w} \tag{6.18}$$

The Newton Raphson method [80] was used to solve equation (6.18) for optimal A. Substituting the obtained value of optimal A in equation (6.17) yielded the least upper bound. Figure 52 shows the least upper-bound on average forging pressures as well as the value of optimal A for various values of friction index $m_p$ and w/t ratios. As the results indicate, the average forging pressure increases almost linearly with increase in w/t ratio. Greater pressure is thus required to forge thinner strips. The effect of interfacial friction at the platen surfaces is to increase the pressure required to forge.

The assumed velocity field for the plastic zone I is

$$\left.\begin{aligned} \dot{U}_x &= \frac{\partial \phi}{\partial y} = \frac{\dot{U}}{t(1-A)} x\left(1 - 3A\frac{y^2}{t^2}\right) \\ \dot{U}_y &= -\frac{\partial \phi}{\partial x} = -\frac{\dot{U}}{t(1-A)} y\left(1 - A\frac{y^2}{t^2}\right) \end{aligned}\right\} \tag{6.19}$$

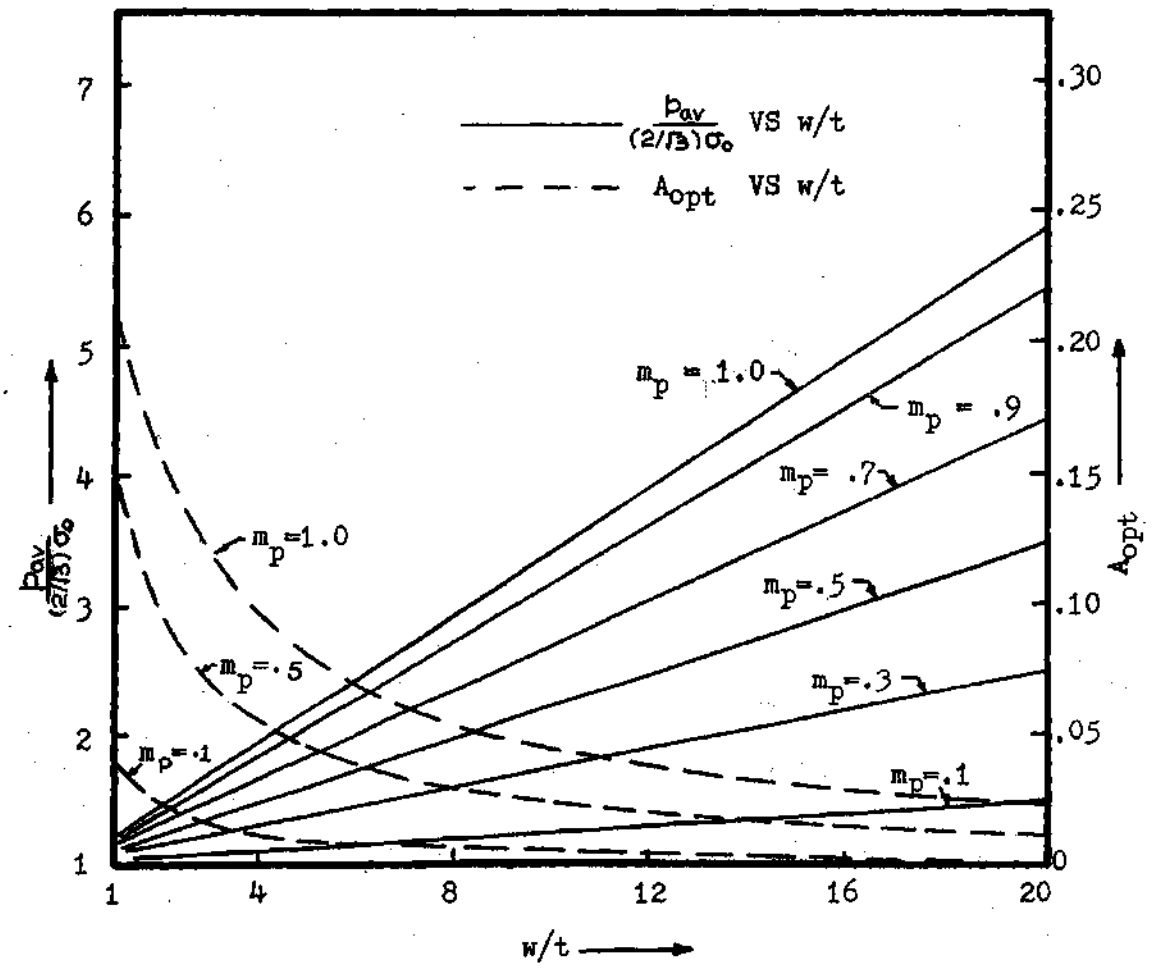


Figure 52. Reduced Forging Pressure and Optimal A as Functions of w/t Ratio and Friction Index ($m_p$)

From equation (6.19), one can observe that an increase in A , in effect, increases velocity component $\dot{U}_x$ along x axis but results in a decrease in $\dot{U}_x$ along platen surface. From Figure 52, notice that the friction increases the optimal value of A and thereby decreases the velocity component $\dot{U}_x$ along the platen surface. The proposed model therefore predicts a decrease in flow velocity near the platen surface, as is observed in practice [81]. Since a decrease of velocity component $\dot{U}_x$ at the platen surface reduces the contribution of friction, the model is actually adjusting itself so as to require the least rate of energy for deformation.

For the case of plane strain forging, the average pressure corresponding to a uniform parallel velocity field suggested by Avitzur [16] is

$$\frac{p_{av}}{(2/\sqrt{3})\sigma_o} = 1 + \frac{m_p}{4}\frac{\omega}{t} \qquad (6.20)$$

The improvement of the proposed equations (6.15) and (6.17) over equation (6.20) is calculated using the following relation.

$$\xi\ \% = \frac{p_{av}\big|_{eq.(6.20)} - p_{av}\big|_{eq.(6.15)\ or\ eq.(6.17)}}{p_{av}\big|_{eq.(6.20)}} \qquad (6.21)$$

The results are plotted in Figure 53. Corresponding data from the analysis proposed by Avitzur [16], using the velocity field (6.12) which accounts for bulging, is also plotted. The improvement due to the present analysis over Avitzur's solution is quite apparent. It is interesting to note that equation (6.17) gives a good approximation to results obtained with

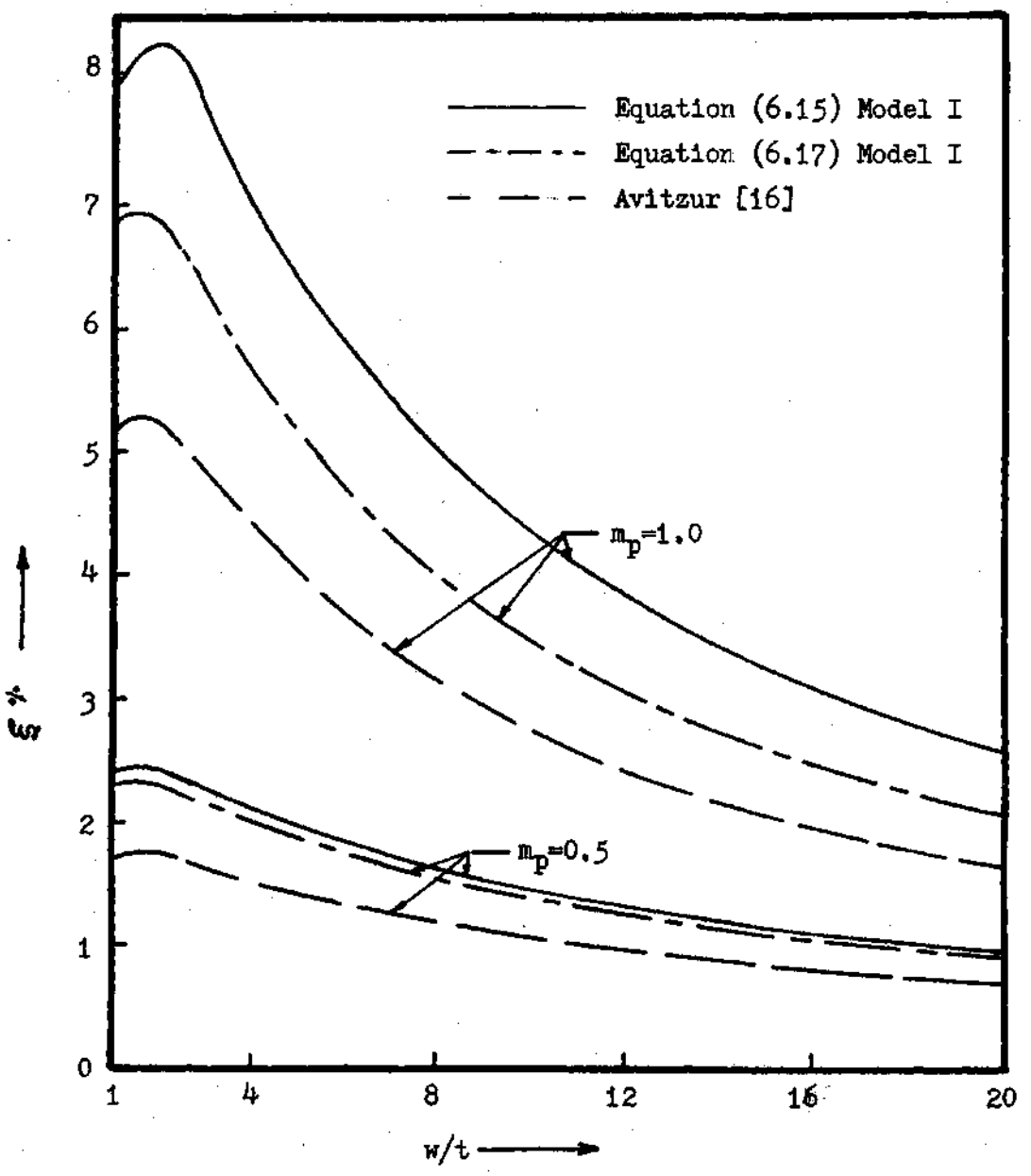


Figure 53. Comparison of Results Obtained with Model I with Avitzur's Solutions

equation (6.15).

Strip Forging-With Dead Zone

When the assumption is made that a dead zone which extends over the complete boundary of the platen is formed, condition (6.4) does not restrict the choice of a kinematically admissible flow function $\phi$. This is because the new boundary $\Gamma$ is not defined by the geometry of the problem and can be selected arbitrarily. The choice of an admissible function is thus restricted only by equations (6.2) and (6.3), which are rewritten here:

$$\phi(x,y) = 0 \quad \text{at} \quad y = 0 \tag{6.2}$$

$$\phi(x,y) = 0 \quad \text{at} \quad x = 0 \tag{6.3}$$

The condition (6.3) needs to be satisfied only if plastic zone I covers a finite portion of the y axis. In case the y axis is excluded from the plastic zone by a rigid zone which extends to the origin, this condition is not required to be satisfied.

Consider the following form for $\phi(x,y)$

$$\phi(x,y) = \sum_{i=1}^{N} a_i \left[ h_1(x)\, g_1(y) \right]^i \tag{6.22}$$

where $g_1(y) = 0 \quad \text{at} \quad y = 0$

$h_1(x)$ and $g_1(y)$ are some arbitrary but increasing functions of x and y respectively. The assumption is made that a rigid zone extends to the origin as shown in Figure 54. The flow function given by (6.22) is kinematically admissible as it satisfies the only remaining requirement (6.2). A general kinematically admissible model can thus be formed from this flow function. Again an exact solution to the variational problem of selecting extremizing functions for $h_1(x)$ and $g_1(y)$ such that the upper bound on forging pressure is minimum cannot be obtained. Of necessity, an approximate solution which would give only a lower upper-bound is therefore sought.

Lower Upper-Bound Solution. The following special form of general flow function given by equation (6.22) is chosen to obtain a lower upper-bound solution

$$\Phi(x,y) = a_0(a+bx)y \tag{6.23}$$

$a_0$, a and b are some constants. The velocity field for zone I is

$$\dot{U}_x = \partial\Phi/\partial y = a_0(a+bx) \quad , \quad \dot{U}_y = -\partial\Phi/\partial x = -a_0 b y \tag{6.24}$$

Substituting for $\Phi(x,y)$ in equation (6.4), the following equation for dead zone boundary Γ is obtained

$$y_\Gamma = \frac{t}{\omega} x \left[\frac{\beta+1}{\beta + x/\omega}\right] \quad , \quad \beta = \frac{a}{b\omega} \tag{6.25}$$

$\dot{U}_x$ is not a function of y and therefore the assumed velocity field does not take into account the bulging effect. This model shown in Figure 54

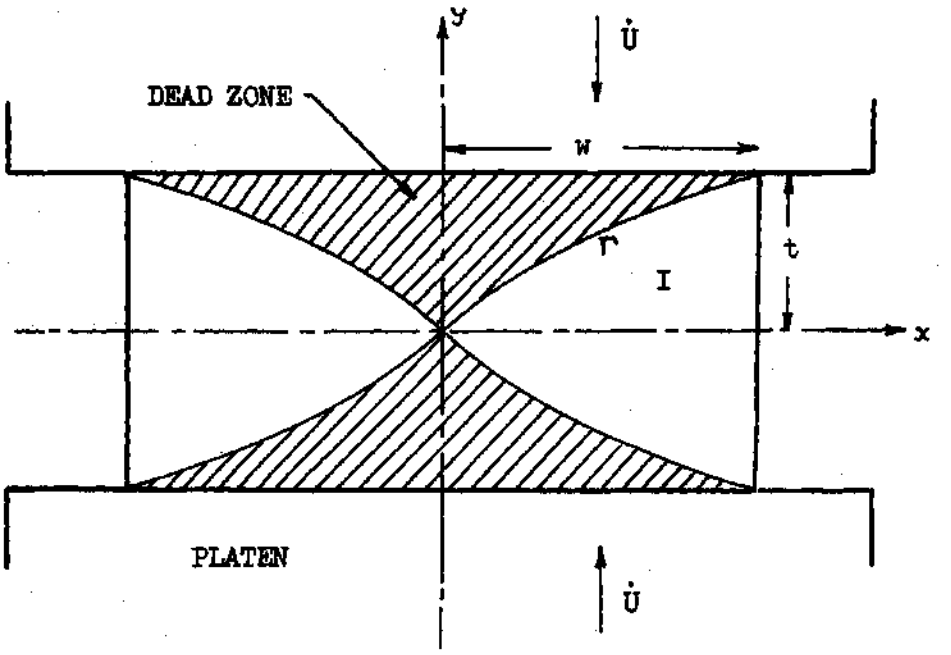


Figure 54. Deformation Model II for Plane Strain Forging

is termed "Model II" to distinguish it from the 'Model I' in which no dead zone was assumed.

From the velocity field given by equation (6.24), the following expression for $\bar{p}_{av}$ is obtained (see Appendix F)

$$\frac{p_{av}}{(2/\sqrt{3})\sigma_o} = 1 - B \ln\left(\frac{1+B}{B}\right) + \frac{1}{2}\left[\frac{\omega}{t}\left(\frac{B+.5}{B+1}\right) + \frac{t}{\omega} - \frac{t}{2\omega}\left(\frac{1}{B+1}\right)\right] \tag{6.26}$$

The above expression is independent of the friction at the platen surfaces ($m_p$) as there is no relative movement between the dead zone and the platen. The analysis of this section is therefore essentially applicable to forging with rough platens ($m_p = 1$).

The optimum value of B which gives the minimum $\bar{p}_{av}$ is obtained by setting

$$\frac{\partial p_{av}}{\partial B} = 0$$

which yields the following equation for optimum B

$$(B+1)^2 \ln\left(\frac{1+B}{B}\right) - B = 1 + \frac{1}{4}\frac{\omega}{t} + \frac{1}{4}\frac{t}{\omega} \tag{6.27}$$

The Newton Raphson method [80] was used to determine the optimum B from equation (6.26). The values of $\bar{p}_{av}$ obtained from equation (6.26) with optimum B are plotted in Figure 55 for various w/t ratios.

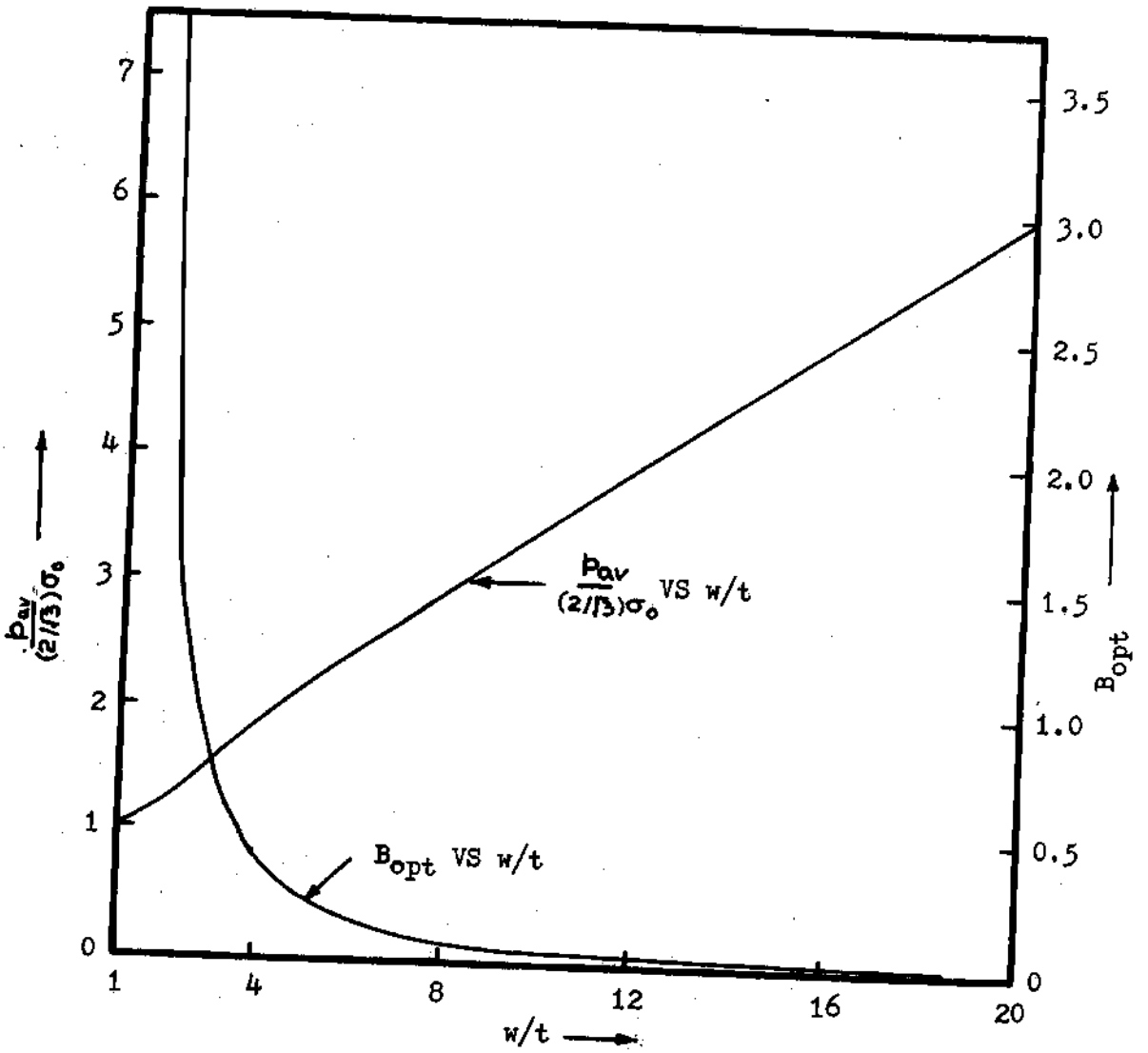


Figure 55. Forging Pressure and $B_{opt}$ as Function of w/t Ratio — Model II

It is interesting to note that for w/t = 1, the least upper-bound on forging pressure $\bar{P}_{av}$ is equal to $(\frac{2}{\sqrt{3}}\sigma_o)$. Also the optimum value of B is $\infty$ or 1/B = 0 for this particular case. From equation (6.25), the dead zone boundary r is given by

$$y_r = \frac{t}{\omega} x \tag{6.28}$$

i.e., the boundary r is a plane surface. This deformation model is exactly the same as derived through slip field theory [1] and is therefore mathematically exact. Thus for this particular case (w/t = 1), the proposed lower upper-bound approach gives the exact solution.

Figure 55 indicates that the forging pressure increases almost linearly with the w/t ratio. Also according to this assumed model II, the forging pressure remains the same for all frictional conditions at the platen surfaces which is true only for w/t = 1. The value of optimum B decreases rapidly with increase in w/t ratio. For $w/t > 12$, $B_{opt}$ is very nearly equal to zero. When $B \to 0$, the velocity field reduces to

$$\left.\begin{aligned} \dot{U}_x &= Ax \\ \dot{U}_y &= -Ay \end{aligned}\right\}$$

which is the parallel velocity field proposed by Avitzur. The dead zone disappears for this limiting case. For large w/t ratios, this lower upper-bound solution gives almost identical results to those obtained from

equation (6.20) with $m_p = 1$.

Comparison with Existing Solutions

Comparison of results obtained through the proposed Model I with Avitzur's results [16] has been shown in Figure 53. Kudo [27] has proposed a model assuming rigid zones separated by plane surfaces of velocity discontinuity. The improvement ($\xi$) obtained with the models proposed here and Kudo's analysis over the parallel velocity field [16] are calculated using the relation (6.21) for rough platens ($m_p = 1$). The results are tabulated in Table 3. It is interesting to note that equation (6.26), obtained by assuming a curved dead zone, gives lower upper-bounds than all the existing upper bound solutions for small w/t ratios. For w/t ratios greater than 12, model I gives lower upper-bounds and for w/t ratios between 3 and 12, the analysis proposed by Kudo [27], assuming unit rigid blocks, gives better results.

For some limited process parameters (w/t, $m_p$), results of exact solutions obtained by slip field theory are available [1]. The improvement ($\xi$) obtained with the exact solution is plotted in Figure 56 together with the improvement obtained with the models proposed here for rough platens ($m_p = 1.0$). As the results show, the proposed upper bound results are only higher by a maximum of 5% from the exact values.

It is of interest to note that for $1 \leq w/t \leq 3.8$, model II, which assumes a curved dead zone, gives lower values for forging pressure and therefore for the rate of energy required for deformation compared to model I which does not assume any dead zone. From energy considerations, model II is the applicable deformation model for $1 \leq w/t \leq 3.8$, while for $w/t > 3.8$, model I defines the deformation mode. Exact slip field solution

Table 3. Comparison of Proposed Solutions for Plane Strain Forging with Kudo's Solution

| w/t | | 1 | 2 | 3 | 4 | 6 | 12 | 20 |
|---|---|---|---|---|---|---|---|---|
| Improvement § % | Model II Equation (6.26) | 20.00 | 17.984 | 11.146 | 6.752 | 2.511 | -.035 | -.167 |
| | Kudo [27] | 20.00 | 16.667 | 10.204 | 9.821 | 6.970 | 3.783 | 2.440 |
| | Model I Equation (6.15) | 7.906 | 8.253 | 7.685 | 6.96 | 5.855 | 3.817 | 2.588 |

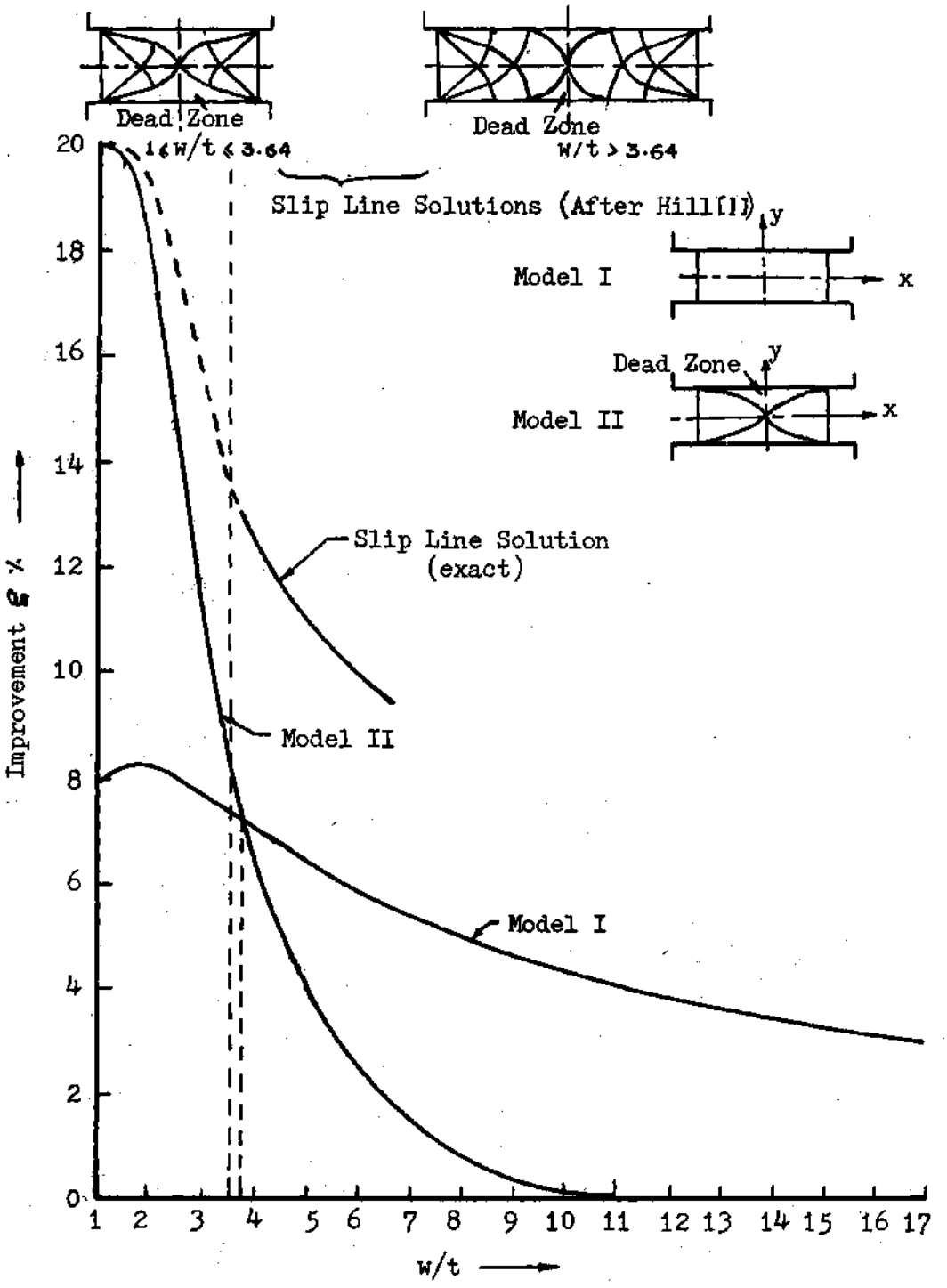


Figure 56. Comparison of Proposed Upper Bound Solutions with Slip-Line Field Solutions, $m_p = 1.0$

confirm this conclusion. Results from the slip field solution show that for $1 \leq w/t \leq 3.64$, a dead zone is formed which covers the platen surfaces completly and extends to the center of the forging. For $w/t > 3.64$, the dead zone forms but only over a portion of platen surfaces. For large w/t ratios, the dead zone is very small compared to the deforming zone and thus approaches the condition when there is no dead zone.

The proposed upper bound solution thus predicts closely the pressure required to forge and also the deformation modes. The advantage of the proposed solution lies in the ease with which numerical results can be obtained. Also results can be obtained for those process parameters for which exact solutions have not been proposed.

## Axisymmetric Forging

The problem of forging a cylindrical workpiece is treated in a manner similar to plane strain forging. Use is again made of the flow function to form a general kinematically admissible model for this forming process.

### General Kinematically Admissible Model

Forging of a cylindrical workpiece by two moving platens is shown in Figure 57. The axes are chosen as shown with the origin of the cylindrical coordinate system at the center of the workpiece. The top platen moves at a velocity of $-\dot{U}/2$ while the bottom platen moves at a velocity of $\dot{U}/2$. Because of symmetry, the upper right half of the workpiece is only considered. A general kinematically admissible model can be formed by assuming the streamlines in the plastic zone to be of the form

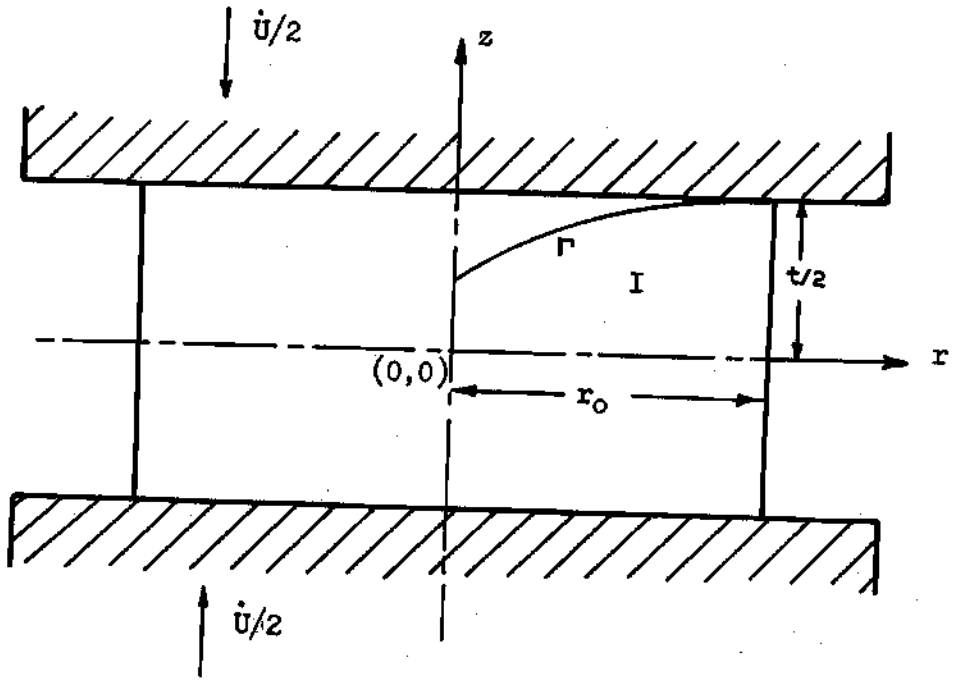


Figure 57. Axisymmetric Forging

$$\hat{\eta} = \hat{h}(r)\,\hat{g}(z) = \text{Constant} \tag{6.29}$$

where $\hat{h}(r)$ and $\hat{g}(z)$ are some arbitrary but increasing functions of r and z, respectively. Admissibility conditions on $\hat{g}(z)$ and $\hat{h}(r)$ are

$$\hat{g}(z) = 0 \quad \text{at} \quad z = 0 \tag{6.30}$$

$$\text{and} \qquad \hat{h}(r) = 0 \quad \text{at} \quad r = 0 \tag{6.31}$$

Equation (6.31) needs to be satisfied only if the dead zone does not cover the z axis completely. The general velocity field in the deforming zone is

$$\left.\begin{aligned} \dot{U}_r &= -\frac{1}{r} f_1'(\hat{\eta})\,\hat{h}(r)\,\hat{g}'(z) \\ \dot{U}_z &= \frac{1}{r} f_1'(\hat{\eta})\,\hat{h}'(r)\,\hat{g}(z) \\ \dot{U}_\theta &= 0 \end{aligned}\right\} \qquad \dot{U}_r = -\frac{1}{r}\frac{\partial \hat{\phi}}{\partial z}, \quad \dot{U}_z = \frac{1}{r}\frac{\partial \hat{\phi}}{\partial r} \tag{6.32}$$

where $\hat{\phi} = f_1(\hat{\eta})$ is the flow function. The equation of the boundary $\Gamma$ of any dead zone, if assumed, is

$$\Gamma: \qquad f_1(\hat{\eta}) = -\frac{\dot{U}}{4} r^2 + \text{Const.} \tag{6.33}$$

The velocity given by equation (6.32), together with generalized boundary $\Gamma$

of the plastic zone, defines a general kinematically admissible model for the axisymmetric forging process. The kinematic model can be altered arbitrarily by choosing different functions for $\hat{h}(r)$ and $\hat{g}(z)$ which satisfy equations (6.30) and (6.31). That kinematic model which gives the least upper-bound on forging pressure would present the best approximate solution. Since the problem does not define whether the dead zone would form or not for any given conditions, kinematic models which assume dead zones and models which do not assume any dead zone must necessarily be tried to predict the applicable mode of deformation from energy considerations. The model which does not assume any dead zone is considered first.

1. Kinematic Model with No Dead Zone. It can be easily apprehended that when no dead zone is assumed, equation (6.33) will reduce to

$$\Gamma: \qquad z = t/2$$

The condition that

$$\dot{U}_z = -\dot{U}/2 \qquad \text{at} \qquad z = t/2$$

requires that

$$\hat{h}(z) = z^2 \quad \text{and} \quad f_1'(\hat{\eta}) = -\dot{U}/4\,\hat{g}(t/2) \tag{6.34}$$

Thus for the case when no dead zone forms, the flow function and the velocity field are given by

$$\hat{\phi}(z,r) = -\frac{\dot{U}}{4\,\hat{g}(t/2)}\,r^2\,\hat{g}(z) \tag{6.35}$$

$$\text{and} \quad \dot{U}_r = \frac{\dot{U}}{4\,\hat{g}(t/2)}\,r\,\hat{g}'(z) \;, \quad \dot{U}_z = -\frac{\dot{U}}{2\,\hat{g}(t/2)}\,\hat{g}(z) \;, \quad \dot{U}_\theta = 0 \tag{6.36}$$

The corresponding strain rate field is

$$\dot{\epsilon}_{rr} = \frac{\dot{U}}{4\hat{g}(t/2)}\hat{g}'(z)$$

$$\dot{\epsilon}_{\theta\theta} = \frac{\dot{U}}{4\hat{g}(t/2)}\hat{g}'(z)$$

$$\dot{\epsilon}_{zz} = -\frac{\dot{U}}{2\hat{g}(t/2)}\hat{g}'(z)$$

$$\dot{\epsilon}_{rz} = \frac{1}{2}\left(\frac{\partial \dot{U}_r}{\partial z} + \frac{\partial \dot{U}_z}{\partial r}\right) = \frac{\dot{U}}{8} r\,\hat{g}''(z)/\hat{g}(t/2)$$

Note that the incompressibility condition ( $\dot{\epsilon}_{rr} + \dot{\epsilon}_{\theta\theta} + \dot{\epsilon}_{zz} = 0$) is satisfied. The shear strain rate $\dot{\epsilon}_{rz}$ should equal zero at z = 0. This requires

$$\hat{g}''(z) = 0 \quad \text{at} \quad z = 0$$

Proceeding in a similar manner as for plane strain forging, the external power is equated to the sum of the internal power of deformation plus the frictional loss at the surface of the velocity discontinuity $\Gamma$. This yields

$$\pi r_o^2 p_i \dot{U} = \frac{2\sigma_o}{\sqrt{3}} \int_V \sqrt{\tfrac{1}{2}\dot{\epsilon}_{ij}\dot{\epsilon}_{ij}}\, dV + m_p \frac{\sigma_o}{\sqrt{3}} \int_\Gamma |\dot{U}_r|_{z=t/2}\, ds$$

Substituting for various terms and simplifying gives the following

expression for the general upper bound on forging pressure

$$\frac{p}{\sigma_o} = \left| \frac{8}{t_o \hat{g}(t/2)} \int_0^{t/2} \frac{\hat{g}'^3(z)}{\hat{g}''^2(z)} \left\{ \left[ 1 + \frac{t_o^2}{12} \left( \frac{\hat{g}''(z)}{\hat{g}'(z)} \right)^2 \right]^{3/2} - 1 \right\} dz \right|$$

$$+ \left| \frac{m_p}{3\sqrt{3}} t_o \frac{\hat{g}'(t/2)}{\hat{g}(t/2)} \right| \qquad (6.37)$$

$$\text{where} \quad \hat{g}(z) = \hat{g}''(z) = 0 \quad \text{at} \quad z = 0 \qquad (6.38)$$

$r_o$ is the outside diameter of the workpiece. An approximate but simpler expression for $p_1$ which maintains the upper bound property is

$$\frac{p_1}{\sigma_o} = \left| 1 + \frac{t_o^2}{48 \hat{g}(t/2)} \int_0^t \frac{\hat{g}''^2(z)}{\hat{g}'(z)} dz \right| + \left| \frac{m_p t_o}{3\sqrt{3}} \frac{\hat{g}'(t/2)}{\hat{g}(t/2)} \right| \qquad (6.39)$$

It is apparent that for a given set of process parameters ($r_o$, $m_p$), the upper bound on the forging pressure can be varied independently by selecting different functions for $\hat{g}(z)$, the choice of which is restricted only by condition (6.38). The problem thus is to find the extremizing function $\hat{g}(z)$. An exact extremizing function cannot be derived from variational methods due to the complexity of the expression (6.37). Of necessity, an approximate extremizing function is sought.

Let $\hat{g}(z)$ be of the form

$$\hat{g}(z) = C_o z \quad , \qquad (6.40)$$

where $C_o$ is some constant. The velocity field given by equation (6.36)

reduces to

$$\left.\begin{aligned} \dot{U}_r &= -C_2\, r \\ \dot{U}_z &= 2\,C_2\, z \end{aligned}\right\} \tag{6.41}$$

where $C_2$ is some constant. This so-called 'Parallel Velocity Field' was proposed by Kudo [29].

Consider another special form for $\hat{g}(z)$

$$\hat{g}(z) = C_3\left(z - \frac{\lambda}{3a^2} z^3\right) \tag{6.42}$$

where $C_3$, $\lambda$ and $a$ are constants. The velocity field for this case becomes

$$\left.\begin{aligned} \dot{U}_r &= -C_4\, r\left(1-\lambda\frac{z^2}{a^2}\right) \\ \dot{U}_z &= 2\,C_4\left(z - \frac{\lambda}{3a^2} z^3\right) \end{aligned}\right\} \tag{6.43}$$

which was used by Тарновский[82] in his solution for axisymmetric forging.

Let $\hat{g}(z)$ be

$$\hat{g}(z) = b_1 \sin(\pi z/t) + b_2 \sin(3\pi z/t) \tag{6.44}$$

The velocity field obtained from this choice of flow function is the same as suggested by Tarnovskii, et al. [83].

Choose another particular form for $\hat{g}(z)$

$$\hat{g}(z) = C_5\left(1 - e^{-b_3 z/t}\right) \tag{6.45}$$

where $C_5$, $b_3$ are constants. Equation (6.36) gives the velocity field

$$\left.\begin{aligned} \dot{U}_r &= C_6\, r\, e^{-b_3 z/t} \\ \dot{U}_z &= C_7\left(1 - e^{-b_3 z/t}\right) \end{aligned}\right\} \tag{6.46}$$

where $C_6$ and $C_7$ are constants. This velocity field was used by Avitzur [16] in his analysis of axisymmetric forging. It may be noted here that this form of $\hat{g}(z)$ does not satisfy condition (6.38). Thus Avitzur's solution does not satisfy all compatibility conditions.

Consider another special form for $\hat{g}(z)$

$$\hat{g}(z) = C_8 \sin\left(b_4 \frac{\pi z}{t}\right) \tag{6.47}$$

where $C_8$ and $b_4$ are constants. The velocity field that is obtained by this choice of flow function is the same as proposed by Liu [69].

It is obvious from the above examples that solutions presented by Kudo, Tarnovskii, et al., Avitzur and Liu are only special cases of the general solution formed with the flow function concept in this analysis. Since the exact extremizing function cannot be derived, no attempt is made in the present work to obtain numerical results with the assumption

of a special form for $\hat{g}(z)$. Numerous solutions of this nature have already been presented and no advantage would be gained by proposing yet another approximate solution. It is of significance, however, to derive the general flow function, since many proposed upper bound solutions actually can be shown to be only special cases of one single general kinematically admissible solution. The foregoing discussion refers to the kinematic model which assumes no dead zone. The general model which assumes a dead zone is treated next.

2. Kinematic Model With Dead Zone. The assumption of a dead zone allows additional flexibility in forming the kinematic model since the choice of the shape for the dead zone is now arbitrary. If the assumption is made that the dead zone completly separates the deforming (plastic) zone from the platen surfaces, a general flow function for the plastic zone which is kinematically admissible is

$$\hat{\phi}(r,z) = \hat{F}_1(\hat{\eta}_1) \tag{6.48}$$

$$\left.\begin{aligned} &\text{where} \quad \hat{\eta}_1 = \hat{h}_1(r)\,\hat{g}_1(z) \\ &\text{and} \quad \hat{h}_1(r) = 0 \quad \text{at} \quad r = 0 \\ &\qquad\quad \hat{g}_1(z) = 0 \quad \text{at} \quad z = 0 \end{aligned}\right\}$$

The general velocity field for this case is given by

$$\left.\begin{aligned} \dot{U}_r &= -\tfrac{1}{r}\hat{F}_1'(\hat{\eta}_1)\,\hat{h}_1(r)\,\hat{g}_1'(z) \\ \dot{U}_z &= \tfrac{1}{r}\hat{F}_1'(\hat{\eta}_1)\,\hat{h}_1'(r)\,\hat{g}_1(z) \end{aligned}\right\} \quad \left.\begin{aligned} \dot{U}_r &= -\tfrac{1}{r}\frac{\partial\hat{\phi}}{\partial z} \\ \dot{U}_z &= \tfrac{1}{r}\frac{\partial\hat{\phi}}{\partial r} \end{aligned}\right. \tag{6.49}$$

To determine the actual deformation model, it is necessary now to find the functions $\hat{h}_1(r)$, $\hat{g}_1(z)$ and $\hat{f}_1$ such that the minimum value of forging pressure is obtained. Obviously, only an approximate solution at best can be attempted by assuming some special forms for these functions. As an example, choose

$$\hat{f}_1'(\hat{\eta}) = C \quad , \quad \hat{h}_1(r) = r, \quad \hat{g}_1(z) = z \tag{6.50}$$

where C is a constant. From equation (6.49), the velocity field for this special case is given as

$$\left.\begin{aligned} \dot{U}_r &= -C \\ \dot{U}_z &= C\,\frac{z}{r} \end{aligned}\right\} \tag{6.51}$$

This is the triangular velocity field proposed by Kudo [29]. Numerical results have already been presented by Kudo with this choice of velocity field.

Consider another form for these functions where

$$\hat{f}_1'(\hat{\eta}) = C \quad , \quad \hat{h}_1(r) = r^{m+1} \quad , \quad \hat{g}_1(z) = z \tag{6.52}$$

and m is some constant. The velocity field corresponding to this choice of functions is

$$\left.\begin{aligned} \dot{U}_r &= -C\,r^m \\ \dot{U}_z &= C\,(1+m)\,z/r^{1-m} \end{aligned}\right\} \tag{6.53}$$

This velocity field was proposed by Koboyashi [84] who used it to obtain results for an axisymmetric forging process. There are other existing solutions [20] which can also be shown to be only special cases of the general solution given by equation (6.48). In the presence of so many existing solutions, which are in principle only special cases of the proposed general kinematic model, no improvement in upper bound analysis is expected by considering yet another special form of the general flow function. Therefore, no numerical results are derived from this model as well.

## Discussion

Like other problems, general kinematically admissible models for the forging problem can readily be formed by using a flow function and its characteristic features. Kinematic conditions impose only simple boundary conditions on the flow function and as shown, a flow function which satisfies these conditions and still can be varied arbitrarily is easily selected. The assumption of a dead zone makes the selection even simpler since the restriction on the flow function due to continuity requirement at one particular boundary can be satisfied merely by a suitable choice of dead zone.

The general kinematically admissible models proposed in this work allow a large variation in velocity fields and thus, in principle, one should be able to obtain very close approximate solutions. The complexity of the expression of forging pressure excludes the possibility of finding an exact flow function and therefore only an approximate flow function can be obtained. As a consequence, different particular forms

must be tried for the flow function. A survey of the existing literature shows that many admissible forms of the flow function have already been tried by other authors. Apparently these authors did not realize that they were merely presenting solutions by using special cases of the general admissible velocity field for the plastic zone. Thus these solutions were not different in principle. As shown, many of the solutions of these authors turn out to be only special cases of the general solution formed in this work. Since many special cases have already been tried, no particular lower upper-bound solution is presented in this work for axisymmetric forging problem.

# CHAPTER VII

# CONCLUSIONS AND RECOMMENDATIONS FOR FURTHER RESEARCH

## Conclusions

The theoretical analyses made in this study and the results point to the conclusion that the suggested approach of using flow function to obtain a general kinematically admissible velocity field or deformation model is very useful. It has the advantage that the velocity field is selected from the shape of streamlines that are consistent with the deformation. Also this approach gives a systematic method of obtaining admissible models in place of guessing them from the incompressibility and velocity boundary conditions. Introduction of the flow function automatically satisfies the incompressibility condition. Conversion of the velocity boundary conditions and continuity requirements to admissibility conditions on flow function (as discussed in Chapter II) further simplifies the formulation of kinematically admissible models. In many instances, the admissibility requirements can be satisfied without restricting the choice of flow function. In effect, therefore, a general kinematically admissible model for any forming problem can be selected which allows an infinite number of variations in admissible velocity field or strain rate field. Thus upper bound solutions which give much lower upper-bounds on forming pressure and also closer approximation to actual deformation are obtained.

The upper bound approach proposed in this study allows formulation of very general kinematic models. It is repeatedly shown in solutions of

specific metal forming problems that many of the solutions presented by other authors are actually special cases of the general models formed in this study through the use of flow functions.

Because of the ease with which the kinematic conditions can be satisfied by the use of flow functions, it should be possible to formulate upper bound solutions to other forming problems, the solution of which have not been attempted by an upper bound approach. An example is the analysis of the problem of simultaneous ironing in deep drawing made in this study.

In addition to the above general conclusions, solutions of specific metal forming problems have yielded many interesting conclusions which have been stated in the preceding Chapters.

## Recommendations

The following recommendations are presented concerning further research on the solution of metal forming problems by upper bound approach using flow function:

1. In this study, the general models formed satisfy all the kinematic conditions which are required for formulating an upper bound solution. Static conditions, however, are not satisfied. Using the flow function, kinematically admissible models should be formed which also satisfy atleast some of the given static conditions, if not all. Such models should give solutions very close to the exact solutions.

2. The effects of work-hardening, strain rate, and temperature should be included in the analysis. It would, however, be necessary to devise models without any velocity discontinuities.

3. Using the analysis presented in this study for extrusion through any arbitrarily shaped die, other possible die shapes should be evaluated with regard to their extrusion efficiency. A systematic approach should then be followed to obtain die shapes which are most efficient under various frictional conditions.

4. Collins [86] has shown that an upper bound solution can be formed even with the assumption of Coulomb friction behavior provided some additional velocity boundary conditions are satisfied. The approach of using flow functions should be extended to formulate general models that would give upper bound solutions with Coulomb friction.

5. The flow function concept should be extended to forming problems which do not occur under plane strain or axisymmetric conditions. It would indeed be interesting to apply the flow function approach to non-steady problems where the change of boundary conditions with time may be built in the formulation of the solution.

# APPENDIX A

## COMPUTER PROGRAM FOR DETERMINING LEAST UPPER BOUND

This program is written to determine, numerically, the least value of upper bound on extrusion pressure $\bar{p}$ given by equation (3.44) with respect to the parameter $\ell_1$. The purpose of devising this special program is to eliminate the necessity of differentiating $\bar{p}$ with respect to $\ell_1$ and then solving the resulting transcendental equation for optimal $\ell_1$, by Newton Raphson method, separately for each die shape. Instead this same program can be used for all dies to determine optimal $\ell_1$ and corresponding least upper bound.

In principle, the program uses the numerical method of interval halving. This method is commonly employed for finding solution of an algebraic equation [80]. In this work, the interest is to determine minimum $\bar{p}$ and hence in the solution of equation

$$\frac{d\bar{P}(\ell_1)}{d\ell_1} = 0 = F(\ell_1)$$

Therefore the same basic program as used for finding roots of an equation can be employed with the difference that now the function to be determined at any value of $\ell_1$, say at $x_m$, is the slope of $\bar{p}$, i.e., $d\bar{p}/d\ell_1$. This value was determined numerically by using the relation

$$\left.\frac{d\bar{P}}{d\ell_1}\right|_{\ell_1 = x_m} = \frac{\left.\bar{P}(\ell_1)\right|_{\ell_1 = x_m + \frac{\Delta}{2}} - \left.\bar{P}(\ell_1)\right|_{\ell_1 = x_m - \frac{\Delta}{2}}}{\Delta}$$

where interval $\Delta$ is very small compared to $\ell_i$ .

A flow chart for the program is included here. This flow chart uses the basic approach given in the text book by Dorn and McCracken [80], which may be referred for further explanation.

## FLOW CHART

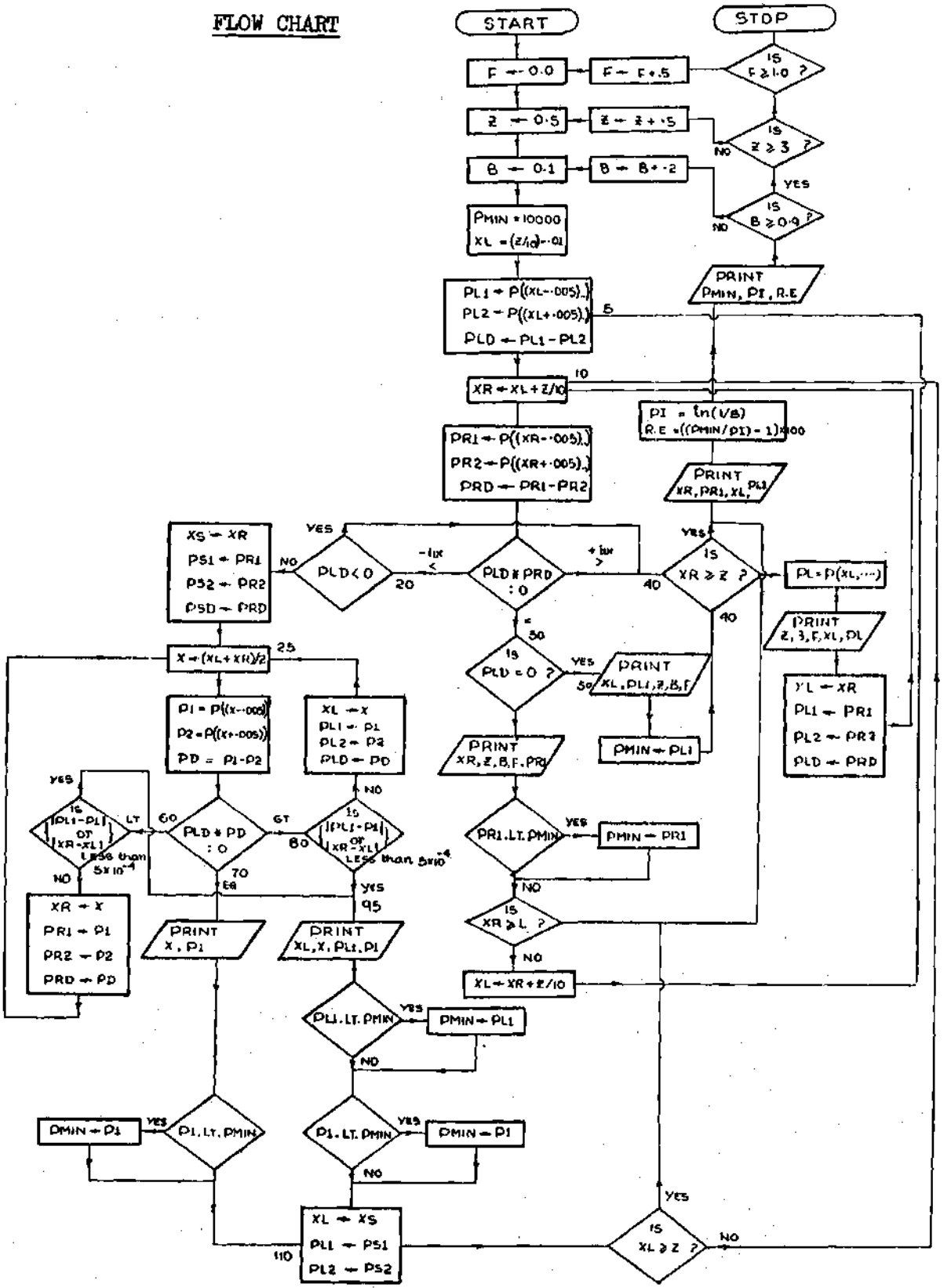
START
STOP
F ← 0.0
F ← F+.5
IS F ≥ 1.0 ?
Z ← 0.5
Z ← Z+.5
IS Z ≥ 3 ?
NO
YES
B ← 0.1
B ← B+.2
IS B ≥ 0.9 ?
NO
PMIN = 10000
XL = (Z/10)-.01
PRINT PMIN, PI, R.E
PL1 ← P((XL-.005),)
PL2 ← P((XL+.005),)
PLD ← PL1 - PL2
5
10
XR ← XL + Z/10
PI = ln(1/B)
R.E = ((PMIN/PI) - 1)*100
PR1 ← P((XR-.005),)
PR2 ← P((XR+.005),)
PRD ← PR1 - PR2
PRINT XR, PR1, XL, PL1
XS ← XR
PS1 ← PR1
PS2 ← PR2
PSD ← PRD
YES
NO
PLD < 0
20
-ive <
PLD ≠ PRD : 0
+ive >
40
IS XR ≥ Z ?
YES
PL = P(XL,---)
PRINT Z, B, F, XL, PL
YL ← XR
PL1 ← PR1
PL2 ← PR2
PLD ← PRD
40
=
50
IS PLD = 0 ?
YES
PRINT XL, PL1, Z, B, F
50
PMIN ← PL1
PRINT XR, Z, B, F, PR1
X ← (XL+XR)/2
25
P1 = P((X-.005),)
P2 = P((X+.005),)
PD = P1 - P2
XL ← X
PL1 ← PL
PL2 ← P2
PLD ← PD
YES
NO
IS |PL1 - PL| OR |XR - XL| LESS than 5x10^-4
LT
60
PLD ≠ PD : 0
GT
80
IS |PL1 - PL| OR |XR - XL| LESS than 5x10^-4
70
EQ
95
YES
NO
XR ← X
PR1 ← P1
PR2 ← P2
PRD ← PD
PRINT X, P1
PRINT XL, X, PL1, P1
PR1 .LT. PMIN
YES
PMIN ← PR1
NO
IS XR ≥ L ?
NO
XL ← XR + Z/10
PL1 .LT. PMIN
YES
PMIN ← PL1
NO
PMIN ← P1
P1 .LT. PMIN
YES
P1 .LT. PMIN
YES
PMIN ← P1
NO
XL ← XS
PL1 ← PS1
PL2 ← PS2
110
YES
IS XL ≥ Z ?
NO

## COMPUTER PROGRAM

```
1*      C THIS IS THE MAIN PROGRAM TO EVALUATE LOWER UPPER BOUND
2*      C ON PRESSURE REQUIRED TO EXTRUDE A MATERIAL THRU CURVED DIE
3*      C
4*      C THE DIE FOR THIS PARTICULAR CASE HAS A WEDGE SHAPE PROFILE
5*      C
6*      C THE THICKNESS OF STRIP AT ENTRANCE IS UNITY
7*      C THE THICKNESS OF STRIP AT EXIT IS B
8*      C F = FRICTION INDEX(M), Z = DIE LENGTH.
9*      C THE REDUCED PRESSURE IS (P/2K)
10*     C
11*     C
12*     C MINIMUM EXTRUSION PRESSURE IS DETERMINED BY NUMERICAL
13*     C METHOD OF INTERVAL HALVING
14*     C
15*           DO 190 I=1,11,5
16*           F = I
17*           F =(F-1.0)/10.0
18*           DO 190 J=1,6
19*           Z = J
20*           Z = Z+0.5
21*           DO 190 K=1,9,2
22*           B = K
23*           B = B/10.0
24*           PMIN=10000.0
25*           WRITE(6,12)
26*        12 FORMAT(1H ,' LENGTH(Z)      B      F.INDEX(F)      X1      RED. PRESS
27*          1URE',/)
28*           XL = 0.01
29*         5 PL1 = P((XL-.0005),Z,B,F)
30*           PL2 = P((XL+.0005),Z,B,F)
31*           PLD = PL1-PL2
32*        10 XR = XL + Z/10.0
33*           PR1 = P((XR-.0005),Z,B,F)
34*           PR2 = P((XR+.0005),Z,B,F)
35*           PRD = PR1-PR2
36*     C
37*     C TEST WHETHER XL AND XR BRACKET A MIN
38*           IF (PLD*PRD) 20,30,40
39*     C
40*     C HERE IF XL AND XR DO NOT BRACKET A MIN
41*        40 IF (XR.GE.Z) GO TO 185
42*     C PREPARE TO EXAMINE NEXT INTERVAL
43*           PL=P(XL,Z,B,F)
44*           WRITE(6,500) Z,B,F,XL,PL
45*       500 FORMAT(5F10.6)
46*           XL =XR
47*           PL1 = PR1
48*           PL2 = PR2
49*           PLD = PRD
50*           GO TO 10
51*     C
52*     C IF XL OR XR IS A MINIMUM
53*        30 IF(PLD.EQ.0.0) GO TO 50
54*           WRITE(6,500) Z,B,F,XR,PR1
55*           IF(PR1.LT.PMIN)PMIN=PR1
56*           IF(XR.GE.Z) GO TO 185
57*           XL = XR+Z/10.0
58*           GO TO 5
```

```
   50  WRITE(6,500) Z,B,F,XL,PL1
       IF (PL1.LT.PMIN)PMIN=PL1
       GO TO 40
C
C HERE IF XL AND XR MAY BRACKET A MIN
   20  IF (PLD.LE.0.0) GO TO 40
       WRITE(6,22)
   22  FORMAT(1H ,'OPTIMUM X1 LIES BETWEEN XL AND XR.',/)
       XS =XR
       PS1 = PR1
       PS2 = PR2
       PSD = PRD
   25  X = (XL+XR)/2.0
       P1 = P((X-.0005),Z,B,F)
       P2= P((X+.0005),Z,B,F)
       PD= P1-P2
       IF (PLD*PD) 60,70,80
C
C HERE IF X IS A MIN
   70 WRITE(6,500)Z,B,F,X,P1
       IF(P1.LT.PMIN)PMIN=P1
       GO TO 110
C
C HERE IF MIN IS BETWEEN XL AND X
   60 IF(ABS(PL1-P1).LE.0.00001) GO TO 95
       IF(ABS(XR-XL) .LE.0.0001) GO TO 95
       XR = X
       PR1=P1
       PR2=P2
       PRD=PD
       GO TO 25
C
C HERE IF ROOT IS BETWEEN X AND XR
   80  IF (ABS(PL1-P1).LE.0.00001)GO TO 95
       IF (ABS(XR-XL).LE.0.0005) GO TO 95
       XL=X
       PL1 = P1
       PL2 = P2
       PLD = PD
       GO TO 25
C
C CLOSE ENOUGH - PRINT THE MIN
   95  WRITE(6,500)Z,B,F,XL,PL1
       IF (PL1.LT.PMIN) PMIN=PL1
       WRITE(6,500)Z,B,F,X,P1
       IF (P1.LT.PMIN) PMIN=P1
C
C GO TO EXAMINE NEXT INTERVAL
  110 XL=XS
       PL1 = PS1
       PL2=PS2
       PLD=PSD
       IF(XL.GE.Z) GO TO 185
       GO TO 10
  185 PL=P(XL,Z,B,F)
       PR=P(XR,Z,B,F)
       WRITE(6,500)Z,B,F,XL,PL
       WRITE(6,500)Z,B,F,XR,PR
       PIDEAL=ALOG(1.0/B)
       REDEFF=(PMIN/PIDEAL -1.0)*100.0
       WRITE (6,520) PMIN,PIDEAL,REDEFF
  520 FORMAT(1H ,'PMIN= ',F10.6,3X,'PIDEAL= ',F10.6,3X,
     1'REDUNDANCY =',F10.6,///)
  190  CONTINUE
       STOP
       END
```

```
C THE DIE HAS A WEDGE SHAPE PROFILE
C
C THIS IS THE FUNCTION SUBPROGRAM FOR FINDING THE REDUCED
C PRESSURE FOR PLANE STRAIN EXTRUSION THROUGH CURVED DIES
      FUNCTION P(X,Z,B,F)
C HERE H(X)= DIE PROFILE, XINT=I(X), XLINT=I(L,X),Z=LENGTH
C OF THE DIE, B IS STRIP THICKNESS AT EXIT, P(X,Z,B,F) IS RED.
C PRESSURE (P/2K), F IS FRICTION INDEX,M..
C FOLLOWING PROGRAM WILL CHANGE WITH CHANGE IN DIE PROFILE
      AA=(1.0-B)/Z
      AB=AA**2.0
      XINT=AB*X
      XLINT=AB*(Z-X)
      H=B+AA*X
C FOLLOWING PROGRAM WILL NOT CHANGE WITH CHANGE IN DIE PROFILE
      HB = H-B
      H1 = 1.0-H
C PINT,PSHR,PFRIC ARE THE STRESS COMPONENTS DUE TO INTERNAL
C DEFORMATION, SHEAR RESISTANCE, AND FRICTION LOSSES.
      PINT=0.0
      PSHR = 0.5*ABS((HB*X)/(B*H) + (B*XINT)/(H*HB))
     1     + 0.5*ABS((H1*(Z-X)/H) + XLINT/(H*H1))
      PFRIC = 0.5*F*ABS( Z/H + (XINT+XLINT)/H)
      P = PINT+PSHR+PFRIC
      RETURN
      END
```

# APPENDIX B

## UPPER BOUND ON IRONING LOAD

An expression for the upper bound on the component of punch load due to ironing in the deep drawing process is derived here. The assumed deformation model is shown in Figure 28.

Boundaries of the Plastic Zone II

From equation (4.16), the flow function is assumed to be of the form

$$\phi(x,y) = b_1 \left( y/H(x) \right) + b_2 \left( y/H(x) \right)^2 \qquad (B.1)$$

From equation (4.13), the equation of the boundary $\Gamma_2$ is

$$\Gamma_2 : \qquad b_1 \frac{y}{H(x)} + b_2 \left( \frac{y}{H(x)} \right)^2 = -\dot{U}_f y$$

$$\text{or} \qquad b_1 \frac{1}{H(x)} + b_2 \frac{y}{H^2(x)} = -\dot{U}_f \qquad (B.2)$$

The boundary $\Gamma_2$ passes through points $Q(0,L_2)$ and $P(0,t_f)$ which yields

$$b_1 = -\dot{U}_f H(L_2)$$

$$\text{and} \qquad b_1 + b_2 = -\dot{U}_f t_f$$

Solving for $b_2$, one obtains

$$b_1 = -\dot{U}_f t_f C \quad , \quad b_2 = \dot{U}_f t_f (C-1) \tag{B.3}$$

where $C = H(L_2)/t_f$

To nondimensionalize with respect to the initial thickness ($t_o$), let

$$y/t_o = \psi \ , \ x/t_o = \varsigma \ , \ t_f/t_o = h_f \ , \ R/t_o = R_d$$

$$L_1/t_o = \ell_1 \ , \ L_2/t_o = \ell_2 \ , \ L_3/t_o = \ell_3 \ , \ H(x)/t_o = h(\varsigma)$$

Substituting for $b_1$ and $b_2$ in equation (B.2) and rearranging gives

$$\Gamma_2 : \qquad y = H(x)\left[\frac{H(L_2) - H(x)}{H(L_2) - t_f}\right] \tag{B.4}$$

or

$$\psi = h(\varsigma)\left[\frac{h(\ell_2) - h(\varsigma)}{h(\ell_2) - h_f}\right] \quad \text{when } \ell_2 \neq 0$$

When $\ell_2 = 0$, the boundary $\Gamma_2$ becomes a vertical plane surface passing through the origin $(0,0)$ and point $P(0,t_f)$. Thus

$$\Gamma_2 : \qquad \varsigma = 0 \qquad \text{when } \ell_2 = 0 \tag{B.4}$$

The equation of the plastic boundary $\Gamma_1$, given by equation (4.13), is

$$\Gamma_1 : \ \frac{\omega^2}{2}\left[x^2 + (R + t_f - y)^2\right] - \frac{\omega^2}{2}(R + t_o)^2 = -\dot{U}_f H(L_2)\frac{y}{H(x)} + \dot{U}_f\left[H(L_2) - t_f\right]\left(\frac{y}{H(x)}\right)^2$$

From the condition of volume constancy

$$\dot{U}_f = \omega \frac{t_o}{t_f} (R + 0.5\, t_o) \tag{B.5}$$

Substituting for $\dot{U}_f$ and rearranging gives

$$\frac{1}{2}\left[y^2 - H^2(x)\right] - (R+t_f)\left[y - H(x)\right] = t_o (R + 0.5\, t_o)\, X$$

$$\left\{ - \frac{H(L_2)}{t_f}\left(\frac{y}{H(x)}\right) + \frac{H(L_2)}{t_f} + \frac{H(L_2)}{t_f}\left(\frac{y}{H(x)}\right)^2 - \frac{H(L_2)}{t_f} - \left(\frac{y}{H(x)}\right)^2 + 1 \right\}$$

Dividing both sides by $\left[y - H(x)\right]$, and simplifying yields the following expression for the plastic boundary $\Gamma_1$

$$\Gamma_1 : \quad y + H(x) - 2(R + t_f) - \frac{2t_o}{H(x)}(R + 0.5\, t_o)\, X$$

$$\left\{ - \frac{H(L_2)}{t_f} + \left( \frac{H(L_2)}{t_f} - 1 \right)\left( \frac{y}{H(x)} + 1 \right) \right\} = 0$$

Nondimensionalizing the above equation yields equation (4.21). $\Gamma_1$ meets the die at point $S(L_1, H(L_1))$ which gives

$$h^2(\ell_1) - (R_d + h_f)\, h(\ell_1) - \left[ (R_d + 0.5)\left( \frac{h(\ell_2)}{h_f} - 2 \right) \right] = 0 \tag{B.6}$$

Solution of the above equation for real $\ell_1$ requires that

$$(R_d + h_f)^2 + 4(R_d + 0.5)(C - 2) \geq 0$$

$$\text{or} \quad C \geq 2 - \frac{(R_d + h_f)^2}{4(R_d + 0.5)}$$

The minimum value of $h(\ell_1)$ is $h_f$. This requires that

$$C \leq 2 - \frac{R_d h_f}{(R_d + 0.5)}$$

Thus the condition that the boundary $\Gamma_1$ must meet the die profile at some point defines the limits on the parameter C

$$\left[ 2 - \frac{(R_d + h_f)^2}{4(R_d + 0.5)} \right] \leq C \leq \left[ 2 - \frac{R_d h_f}{(R_d + 0.5)} \right] \qquad (B.7)$$

Velocity Field in Zone II

$$\dot{U}_x = \frac{\partial \phi}{\partial y} = (b_1 + 2 b_2 \eta) \frac{1}{H(x)}$$

$$\dot{U}_y = -\frac{\partial \phi}{\partial x} = (b_1 + 2 b_2 \eta) \frac{y}{H^2(x)} H'(x) \qquad (B.8)$$

By rewriting in dimensionless form, one obtains equation (4.23) for the velocity field. It may be noted that

$$\dot{U}_y / \dot{U}_x = H'(x) \quad \text{at} \quad y = H(x)$$

Thus the resultant velocity vector is tangential to the die surface. The condition that the velocity normal to the die surface be zero is therefore satisfied.

Strain Rate Field in Zone II

$$\dot{\epsilon}_{xx} = \frac{\partial \dot{U}_x}{\partial x} = -\frac{H'(x)}{H^2(x)}\left[b_1 + 4 b_2 \eta\right]$$

$$\dot{\epsilon}_{yy} = \frac{\partial \dot{U}_y}{\partial y} = \frac{H'(x)}{H^2(x)}\left[b_1 + 4 b_2 \eta\right] \qquad \text{(B.9)}$$

$$\dot{\epsilon}_{xy} = \frac{1}{2}\left(\frac{\partial \dot{U}_x}{\partial y} + \frac{\partial \dot{U}_y}{\partial x}\right)$$

$$= \frac{1}{2}\left[\frac{2 b_2}{H^2(x)} + \frac{y H''(x)}{H^2(x)}(b_1 + 2 b_2 \eta) - \frac{y H'^2(x)}{H^3(x)}(2 b_1 + 6 b_2 \eta)\right]$$

It is evident that the incompressibility condition ( $\dot{\epsilon}_{xx} + \dot{\epsilon}_{yy} = 0$) is satisfied by the selected velocity field.

Internal Power of Deformation in Zone II

The body in zone II is getting plastically deformed. The rate of energy dissipation is given by

$$\dot{W}_i = \frac{2}{\sqrt{3}} \sigma_0 \iiint_V \sqrt{\frac{1}{2} \dot{\epsilon}_{ij} \dot{\epsilon}_{ij}}\, dV$$

$$= \frac{2}{\sqrt{3}} \sigma_0 \iint_{x\,y} \sqrt{\dot{\epsilon}_{xx}^2 + \dot{\epsilon}_{xy}^2}\, dx\, dy$$

By substituting for strain rates and simplifying, one obtains

$$\dot{W}_i = \frac{2}{\sqrt{3}}\sigma_o \iint_{S\,\psi} \left\{ \frac{h'^2(s)}{h^4(s)}\left[b_1 + 4b_2\left(\psi/h(s)\right)\right]^2 \right.$$

$$+ \frac{1}{4}\left[\frac{2b_2}{h^2(s)} + \psi\,\frac{h''(s)}{h^2(s)}\left(b_1 + 2b_2\left(\psi/h(s)\right)\right)\right.$$

$$\left.\left. - \frac{\psi}{h^3(s)}h'^2(s)\left(2b_1 + 6b_2\left(\psi/h(s)\right)\right)\right]^2 \right\}^{1/2} d\psi\, ds \qquad \text{(B.10)}$$

Shear Power Loss along Entrance Boundary $\Gamma_1$

The shear power loss is given by

$$\dot{W}_{s_{\Gamma_1}} = \int \tau_1 |\Delta v_1|\, dA$$

where $\tau_1$ is the shear stress at the boundary $\Gamma_1$ and is not more than the shear stress at yield $(\sigma_o/\sqrt{3})$. $\Delta v_1$ is the tangential velocity discontinuity along $\Gamma_1$ and is given by

$$|\Delta v_1| = \left|\left[\omega(R + t_f - y) + \dot{U}_x\right]\frac{dx}{ds} + \left(\omega x + \dot{U}_y\right)\frac{dy}{ds}\right|$$

where ds is an infinitely small length of the curve $\Gamma_1$. Substituting for $\Delta v_1$, $\dot{U}_x$, and $\dot{U}_y$, one obtains on simplification

$$\dot{W}_{s_{\Gamma_1}} = \frac{\sigma_o}{\sqrt{3}}\left|\int_{\ell_3}^{\ell_1}\left\{\dot{U}_f t_f\left(\frac{R_d + h_f - \psi}{R_d + 0.5}\right) + \left(b_1 + 2b_2\frac{\psi}{h(s)}\right)\frac{1}{h(s)}\right\} ds\right. +$$

(B.11)

$$\int_0^{h(\ell_1)} \left\{ \dot{U}_f t_f \frac{5}{(R_d + 0.5)} + \left( b_1 + 2 b_2 \frac{\psi}{h(5)} \right) \frac{\psi}{h^2(5)} h'(5) \right\} d\psi \Bigg|$$

Shear Power Loss along Exit Boundary $\Gamma_2$

The shear power loss along $\Gamma_2$ due to a tangential velocity discontinuity along this surface is

$$\dot{W}_{s_{\Gamma_2}} = \int \tau_2 |\Delta v_2| \, dA$$

where $\tau_2$ is the shear stress at the boundary $\Gamma_2$ and is not more than the shear stress at yield ($\sigma_0/\sqrt{3}$). $\Delta v_2$ is the tangential velocity discontinuity along $\Gamma_2$ and is given by

$$\Delta v_2 = (\dot{U}_x + \dot{U}_f) \frac{dx}{ds} + \dot{U}_y \frac{dy}{ds}$$

Substituting for $\Delta \dot{v}_2$, $\dot{U}_x$ and $\dot{U}_y$, yields

$$\dot{W}_{s_{\Gamma_2}} = \frac{\sigma_0}{\sqrt{3}} \left| \int_{\ell_2}^{0} \left\{ \dot{U}_f t_f \cdot \frac{1}{h_f} + \left( b_1 + 2 b_2 \frac{\psi}{h(5)} \right) \frac{1}{h(5)} \right\} ds \right.$$

$$\left. + \int_0^{h_f} \left( b_1 + 2 b_2 \frac{\psi}{h(5)} \right) \frac{\psi}{h^2(5)} h'(5) \, d\psi \right| \qquad \text{(B.12)}$$

for $\ell_2 \neq 0$

When $\ell_2 = 0$, the above expression simplifies to

$$\dot{W}_{s_{\Gamma_2}} = \frac{\sigma_0}{\sqrt{3}} \dot{U}_f t_f \left| \frac{h'(0)}{2} \right| = 0 \quad , \qquad \ell_2 = 0 \qquad \text{(B.12)}$$

Friction Power Loss over Die Surface $\Gamma_3$

The assumption is made that the interfacial shear stress ($\tau_3$) due to friction is constant along the boundary and is expressed as

$$\tau_3 = m_3(\sigma_0/\sqrt{3})$$

where $m_3$ is defined as the friction index. The power loss due to friction is

$$\dot{W}_{S\Gamma_3} = \int \tau_3 |\Delta v_3| dA$$

$\Delta v_3$ is the tangential velocity discontinuity at the surface $\Gamma_3$ and is given by

$$\Delta v_3 = \left(\dot{U}_x^2 + \dot{U}_y^2\right)^{1/2} \Big|_{y=H(x)}$$

$$\text{also} \qquad dA = \left(dx^2 + dy^2\right)^{1/2} \Big|_{y=H(x)} = dx\left[1 + H'^2(x)\right]^{1/2}$$

Substituting for $\Delta v_3$, $\dot{U}_x$, $\dot{U}_y$ and dA, one obtains on simplification

$$\dot{W}_{S\Gamma_3} = m_3 \frac{\sigma_0}{\sqrt{3}} \left|(b_1+2b_2)\right| \int_0^{\ell_1} \left(\frac{1+h'^2(s)}{h(s)}\right) ds \qquad \text{(B.13)}$$

Friction Power Loss over Punch Surface $\Gamma_4$

Again assuming a constant interfacial shear stress, the friction power loss over $\Gamma_4$ is written as

$$\dot{W}_{S\Gamma_4} = m_4 \frac{\sigma_o}{\sqrt{3}} \int |\Delta v_4| \, dA$$

where $m_4$ is the friction index for the punch surface. The tangential velocity discontinuity $\Delta v_4$ is

$$|\Delta v_4| = |\dot{U}_x + \dot{U}_y|_{y=0} \quad , \quad \text{also} \quad dA = dx$$

Substituting for $\Delta v_4$, $\dot{U}_x$ and dA, and upon simplification, results in

$$\dot{W}_{S\Gamma_4} = m_4 \frac{\sigma_o}{\sqrt{3}} \left| \left\{ \int_{\ell_2}^{\ell_3} \left( \frac{b_1}{h(s)} \right) ds + \dot{U}_f t_f \left( \frac{\ell_3 - \ell_2}{h_f} \right) \right\} \right| \qquad (B.14)$$

Friction Power Loss over Die Surface $\Gamma_5$

The friction power loss over the die surface $\Gamma_5$ is

$$\dot{W}_{S\Gamma_5} = m_5 \frac{\sigma_o}{\sqrt{3}} \int |\Delta v_5| \, dA$$

The tangential velocity discontinuity $\Delta v_5$ is

$$\Delta v_5 = \omega R$$

Substituting for $\Delta v_5$ and $\omega$, one obtains

$$\dot{W}_{S\Gamma_5} = m_5 \frac{\sigma_o}{\sqrt{3}} \dot{U}_f t_f \frac{R_d^2}{(R_d + 0.5)} \left[ \frac{\pi}{2} - \sin^{-1}\left( \frac{\ell_1}{R_d} \right) \right] \qquad (B.15)$$

Upper Bound

The sum of the rates of energy dissipation in internal deformation,

shear along the surfaces of velocity discontinuity and friction gives an upper bound on the rate of energy supplied by external traction, which in this case is the punch load. Equation (4.31) thus gives an upper bound on the component of punch load required for the ironing process.

# APPENDIX C

## COMPUTER PROGRAM FOR UPPER BOUND ON IRONING LOAD

The computer program used to obtain, numerically, the upper bound on reduced ironing load (p*) is included in this Appendix. The program is written in Fortran for the Univac 1108 computer at the Rich Electronic Center at Georgia Tech. Determination of p* given by equation (4.31) involves evaluation of integrals, single and double, with a finite range of integration. Single integrals are evaluated by the well known Trapezoidal Rule and Simpson Rule. The mathematical basis and computer programs for these Rules can be found in standard text books on numerical analysis [80]. Expression for $\dot{W}_i$ involves double integration with variable limits as the region II in Figure 28 over which the integrand is summed is defined by the shapes of the plastic boundaries and the die profile, and is not rectangular. Gerald [85] has outlined a procedure and his approach is basically followed in this computer program.

The error involved in calculating the reduced ironing load (p*) numerically is related directly to the accuracy with which the individual integrals are calculated. This in turn depends on the number of divisions in which the limits of that integral are divided. Selection of the number of divisions for each integral was made separately by relating it to the accuracy of calculation. The overall error in the determination of the upper bound on ironing load was kept less than 2%. The upper bound property was still maintained, however, since the error gave a higher

value for p* than the actual.

To obtain least upper bound for a given set of process parameters, p* was calculated for different values of the coefficient C. The difference in successive values of C at which p* was calculated was selected such that the minimum p* did not differ more than 2% from the adjoining p* values. This accuracy was considered sufficient in view of the upper bound quality of the solution.

The symbols used in the program necessarily differed from those used elsewhere; therefore, the definitions of the program symbols are given below.

| Computer Symbols | | Definition |
|---|---|---|
| R | = | Ratio of the die radius to initial thickness (defined as $R_d$ in Chapter IV) |
| HF | = | $t_f/t_o$ (see Figure 28) |
| L1, L2, L3 | = | $\ell_1$, $\ell_2$, $\ell_3$ as defined in Chapter IV |
| HD | = | $h(\varsigma)$ (see Figure 28) |
| HD1 | = | $h'(\varsigma)$ |
| HD2 | = | $h''(\varsigma)$ |
| HL1, HL2, HL3 | = | $H(x)/t_o$ at $x = L_1$, $L_2$, and $L_3$ respectively |
| C | = | $H(L_2)/t_f$ (see Figure 28) |
| CMAX | = | Maximum admissible value of C |
| CMIN | = | Minimum admissible value of C |
| DIV | = | Number of divisions in which the range of C is divided |
| T1, T2 | = | Boundaries $\Gamma_1$ and $\Gamma_2$ of the plastic zone II |

WST1 $= \dfrac{\dot{W}_{sr_1}}{2(\sigma_o/\sqrt{3})\dot{U}_f t_f}$ (terms defined in Chapter IV)

WST2 $= \dfrac{\dot{W}_{sr_2}}{2(\sigma_o/\sqrt{3})\dot{U}_f t_f}$ " " "

WINT $= \dfrac{\dot{W}_i}{2(\sigma_o/\sqrt{3})\dot{U}_f t_f}$ " " "

WFDA $= \dfrac{\dot{W}_{sr_3}}{2(\sigma_o/\sqrt{3})\dot{U}_f t_f}$ " " "

WFDB $= \dfrac{\dot{W}_{sr_3}}{2(\sigma_o/\sqrt{3})\dot{U}_f t_f}$ " " "

WFRICP $= \dfrac{\dot{W}_{sr_4}}{2(\sigma_o/\sqrt{3})\dot{U}_f t_f}$ " " "

```
C THIS PROGRAM DETERMINES THE COMPONENT OF PUNCH LOAD
C DUE TO IRONING IN A DEEP DRAWING PROCESS. PROCESS
C IS CONSIDERED TO BE OCCURING UNDER PLANE STRAIN
C CONDITIONS.   FRICTION IS TAKEN INTO ACCOUNT BY
C ASSUMING A CONSTANT INTERFACIAL FRICTION STRESS AT
C DIE AND PUNCH SURFACES.
C
C
C THE DIE HAS A CIRCULAR PROFILE OF RADIUS R WITH
C ZERO EXIT ANGLE.
C HF = FINAL THICKNESS OF DRAWN CUP
C L1,L2,L3 AND HL2 ARE AS SHOWN IN SKETCH
C COEFFICIENT C = HL2/HF
C M3 AND M4 ARE FRICTION FACTORS FOR DIE SURFACE
C AND PUNCH SURFACE RESPECTIVELY
C
C SUBPROGRAMS ARE WRITTEN FOR FUNCTIONS HD,HD1,HD2
C WHICH DEFINE THE SHAPE,SLOPE AND CURVATURE OF CIRCULAR DIE
C     **********************************
C
C
C DEFINE FUNCTION XD TO DETERMINE COORDINATE X FROM
C A KNOWN VALUE OF HD.
      XD(HDIE,R,HF) = SQRT(R**2.0-(R+HF-HDIE)**2.0)
C
C
      DIMENSION Y1(50),Y2(50),X1(50),X2(50),F1(50),F2(50)
C     N CAN ONLY BE A MULTIPLE OF SIXTEEN(16)
      N = 48
      COMMON R,HF,C
      REAL L1,L2,L3,M3,M4
      WRITE(6,480)
      DO 320 KK=1,61
      WRITE(6,705)
      READ(5,500) R,HF,M3,M4,CMIN,CMAX,DIV
      CMINT=2.0-(R+HF)**2.0/(4.0*(R+.5))
      CMAXT=CMAX
      IF(CMINT.GT.CMAXT)GO TO 320
      IF(CMINT.GT.CMIN)CMIN=CMINT
      II = 1
      MA=2
      MB=2
      MC=2
      C=CMIN
   10 HL2 = C*HF
      L2 = XD(HL2,R,HF)
      WRITE(6,505) R,HF,M3,M4,L2,C
   15 FN = N
      N1 = N+1
C     **********************************
C
C
C DETERMINE POINTS ON BOUNDARIES T1 AND T2
C ENTRANCE BOUNDARY T1
      IF(L2.GT.L3) GO TO 320
      L3 = SQRT((R+1.0)**2.0-(R+HF)**2.0)
      IF(L2.GT.L3) GO TO 320
      E1 = (R+.5)*(C-2.0)
      HL1 = ((R+HF)-SQRT((R+HF)**2.0+4.0*E1))/2.0
      IF(HL1.LT.HF) GO TO 240
      L1 = XD(HL1,R,HF)
      I = 1
      X = L1
      DELXB = (L3-L1)/FN
      A0 = -(R+.5)*C
      A1 = (R+.5)*(C-1.0)
```

```
   20  HDIE = HD(X,R,HF)
       Y = (2.0*(R+HF)-HDIE+2.0*(A0+A1)/HDIE)/(1.0-2.0*A1/HDIE**2.0)
       IF(Y.GT.(HDIE+1.0E-4))GO TO 220
       X1(I) = X
       Y1(I) = Y
C
C DEFINE FUNCTIONS TO EVALUATE SHEAR POWER LOSS OVER T1
       HDIE1 = HD1(X,R)
       F1(I) = (R+HF-Y)/(R+.5) + (-C+2.0*(C-1.0)*(Y/HDIE))/HDIE
       F2(I) = X/(R+.5) + (-C+2.0*(C-1.0)*(Y/HDIE))*Y*HDIE1/HDIE**2.0
       IF(I.GE.N1) GO TO 40
       X = X+DELXB
       I = I+1
       GO TO 20
C
C COMPONENT OF LOAD DUE TO SHEAR DEFORMATION ALONG T1
C
   40  CALL SIMP(1,N1,N1,DELXB,F1,P1)
       CALL TRAP(1,N1,N1,Y1,F2,P2)
       WST1 = .5*ABS(P1+P2)
       WRITE(6,530)
  530 FORMAT(1H ,'          BOUNDARY T1            FUNCTIONS DEFINING SHEA
      1R DEFORMATION ALONG T1',/,'        X1            Y1            F1
      2        F2')
       WRITE(6,540)(X1(I),Y1(I),F1(I),F2(I),I=1,N1)
C
C
C EXIT BOUNDARY T2
C
       IF(ABS(L2).LT.1.0E-4) GO TO 100
C HERE IF L2 IS NOT EQUAL TO ZERO
       I = 1
       X = 0
       DELXB = L2/FN
   60  HDIE = HD(X,R,HF)
       Y = HDIE*(C-HDIE/HF)/(C-1.0)
       IF (L2.GT.0.0.AND.Y.GT.(HDIE+1.0E-4)) GO TO 220
       IF (L2.LT.0.0.AND.Y.GT.(HF+1.0E-4)) GO TO 220
       X2(I) = X
       Y2(I) = Y
C
C
C DEFINE FUNCTIONS TO CALCULATE SHEAR POWER LOSS ALONG T2
       HDIE1 = HD1(X,R)
       F1(I) = 1.0/HF + (-C+2.0*(C-1.0)*(Y/HDIE))/HDIE
       F2(I) = (-C+2.*(C-1.0)*(Y/HDIE))*Y*HDIE1/HDIE**2.0
       IF(I.GE.N1) GO TO 80
       X = X+DELXB
       I = I+1
       GO TO 60
C
C COMPONENT OF LOAD DUE TO SHEAR DEFORMATION ALONG T2
C
   80  CALL SIMP(1,N1,N1,DELXB,F1,P1)
       CALL TRAP(1,N1,N1,Y2,F2,P2)
       WST2 = .5*ABS(P1+P2)
       GO TO 110
C HERE IF L2 IS EQUAL TO ZERO
  100 HDIE1 = HD1(0.0,R)
       WST2 = .5*ABS(HDIE1/2.0)
       WRITE(6,535)
  535 FORMAT(1H ,'          BOUNDARY T2            FUNCTIONS DEFINING SHE
      1AR DEFORMATION ALONG T2',/,'        X2            Y2            F1
      2        F2')
       WRITE(6,540)(X2(I),Y2(I),F1(I),F2(I),I=1,N1)
  110 CONTINUE
```

```
C     ***********************************
C
C
C COMPONENT OF LOAD DUE TO INTERNAL DEFORMATION
C
      IF (ABS(L1-L3).LT.1.0E-4) GO TO 125
      FNOT=FN/4.0
      K = FNOT
      K1 = K+1
      DO 120 I=1,K1
      F1(I)=0.0
      F2(I) = Y1(4*I-3)
  120 X1(I) = X1(4*I-3)
      WINT1 = DOUBLE(X1,F1,F2,K,K1)
      GO TO 130
  125 WINT1 = 0.0
  130 CONTINUE
C
      IF(ABS(L2).LT.1.0E-4) GO TO 136
      DO 135 I=1,K1
      F1(I)=0.0
      F2(I) = Y2(4*I-3)
  135 X2(I) = X2(4*I-3)
      WINT2 = DOUBLE(X2,F1,F2,K,K1)
      GO TO 137
  136 WINT2 = 0.0
  137 CONTINUE
      IF(L1.LT.1.0E-4) GO TO 145
      X1(1) = 0.0
      F1(I) = 0.0
      F2(1) = HF
      X = 0.0
      DO 140 I=2,K1
      X = X+4.0*L1/FN
      X1(I) = X

      F1(I) = 0.0
  140 F2(I) = HD(X,R,HF)
      WINT3 = DOUBLE(X1,F1,F2,K,K1)
      GO TO 150
  145 WINT3 = 0.0
  150 CONTINUE
      WINT = ABS(WINT1-WINT2+WINT3)
C     ***********************************
C
C
C COMPONENT OF PUNCH LOAD DUE TO FRICTION AT DIE SURFACE
      X = 0.0
      X1(1) = 0.0
      HDIE = HD(X,R,HF)
      F2(1) = HDIE
      HDIE1 = HD1(X,R)
      X2(1) = (1.0+HDIE1**2.0)/HDIE
      DO 160 I=2,K1
      X = X+4.0*L1/FN
      X1(I) = X
      HDIE = HD(X,R,HF)
      F2(I) = HDIE
      HDIE1 = HD1(X,R)
```

```
  160 X2(I) = (1.0+HDIE1**2.0)/HDIE
      SPACE1 = 4.0*L1/FN
      CALL SIMP(1,K1,K1,SPACE1,X2,P3)
  180 WFDA = .5*M3*(2.0-C)*P3
      ALFA = ATAN(L1/SQRT(R**2.0-L1**2.0))
      WFDB = .5*M3*R**2.0*(1.570796-ALFA)/(P+.5)
C     ***********************************
C
C
C COMPONENT OF LOAD DUE TO FRICTION AT PUNCH SURFACE
      X = L2
      X1(1) = L2
      HDIE = HD(X,R,HF)
      X2(1) = -C/HDIE
      DO 190 I=2,K1
      X = X  + 4.0*(L3-L2)/FN
      HDIE = HD(X,R,HF)
      X1(I) = X
  190 X2(I) = -C/HDIE
      SPACE2 = 4.0*(L3-L2)/FN
      CALL SIMP(1,K1,K1,SPACE2,X2,P4)
      WFRICP = .5*M4*(P4+(L3-L2)/HF)
C     ***********************************
C
C
      W = WINT + WST1 + WST2 + WFDA + WFDB + WFRICP
      WRITE(6,630) WINT,WST1,WST2,WFDA,WFDB,WFRICP,W,C,L2,L1
      WI = WINT + WST1 + WST2
      W1 = WI
      W2 = WI+.05*WFRICP
      W3 = WI+.1*WFRICP
      W4 = WI+.15*WFRICP
      W5 = WI+.2*WFRICP
      W6 = WI+.3*WFRICP
      W7 = WI+.5*WFRICP
      W8 = WI+.75*WFRICP
      W9 = WI+WFRICP
      WFD = WFDA+WFDB
      W10 = WI+.05*WFD
      W11 = WI+.1*WFD
      W12 = WI+.15*WFD
      W13 = WI+.2*WFD
      W14 = WI+.3*WFD
      W15 = WI+.5*WFD
      W16 = WI+.75*WFD
      W17 = WI+WFD
      WFDP = WFRICP+WFD
      W18 = WI+.1*WFDP
      W19 = WI+.2*WFDP
      W20 = WI+.3*WFDP
      W21 = WI+.4*WFDP
      W22 = WI+.5*WFDP
      WRITE(6,640)W1,W2,W3,W4,W5,W6,W7,W8,W9,W10,W11,W12,W13,W14,W15,W16
     1,W17,W18,W19,W20,W21,W22
  640 FORMAT(1H ,1F6.3,4X,8F6.3,4X,8F6.3,/,5F6.3,/)
      DO 210 I=1,50
      X1(I) = 0.0
      X2(I) = 0.0
      Y1(I) = 0.0
      Y2(I) = 0.0
      F1(I) = 0.0
      F2(I) = 0.0
  210 CONTINUE
      GO TO 300
```

```
  240 WRITE(6,710) L2,HL1
      GO TO 300
  220 GO TO 250
  250 WRITE(6,520) X,Y
      IF(C.GE.CMAX) GO TO 320
      GO TO 306
  300 IF(C.GE.CMAX)GO TO 320
      IF(ABS(C-CMAX).LE.1.0*E-4)GO TO 320
      IF(II.EQ.1)GO TO 305
      IF(W9.GE.WM9)MA=1
      IF(W17.GE.WM17)MB=1
      IF(W22.GE.WM22)MC=1
      IF((MA*MB*MC).EQ.1)GO TO 320
      IF(MA.EQ.2)WM9=W9
      IF(MB.EQ.2)WM17=W17
      IF(MC.EQ.2)WM22=W22
      MA=2
      MB=2
      MC=2
      C = C+(CMAX-CMIN)/DIV
      II=II+1
      GO TO 10
  305 WM9 = W9
      WM17 = W17
      WM22 = W22
      II=II+1
  306 C = C+(CMAX-CMIN)/DIV
      GO TO 10
  320 CONTINUE
      STOP
  480 FORMAT(1H ,'        IRONING OF CUP IN A DEEP DRAWING PROCESS'//)
  500 FORMAT(7F10.6)
  505 FORMAT(6F10.6)
  520 FORMAT(1H ,'    BOUNDARY OF ZONE II HAS GONE BEYOND THE LIMITS OF
     1CUP THICKNESS AT X=',F7.3,'    Y=',F7.3,/)
  540 FORMAT(4F14.6)
  630 FORMAT(10F10.6)
  705 FORMAT(1H ,'-----------------------------------------------------
     1-----------')
  710 FORMAT(1H ,'  HL1 IS LESS THAN HF FOR L2 =',F10.5,' .  HL1=',F10.
     15,/)
      END
C     ************************************

C HD DEFINES THE SHAPE OF THE DIE
      FUNCTION HD(X,R,HF)
      HD = R+HF-SQRT(R**2.0-X**2.0)
      RETURN
      END
C     ************************************

C HD1 DEFINES SLOPE OF THE DIE PROFILE
      FUNCTION HD1(X,R)
      HD1 = X/SQRT(R**2.0-X**2.0)
      RETURN
      END
C     ************************************
```

```
C HD2 DEFINES THE SECOND DERIVATIVE OF DIE PROFILE
      FUNCTION HD2(X,R)
      HD2 = R**2.0/(R**2.0-X**2.0)**1.5
      RETURN
      END
C     ***********************************
```

```
C THIS IS THE SUBROUTINE TO INTEGRATE NUMERICALLY
C BY SIMPSON RULE
      SUBROUTINE SIMP(IINT,IFINAL,ISIZE,H,F,SUM)
      DIMENSION F(ISIZE)
      SUM4 = 0.0
      SUM2 = 0.0
      K1 = IINT+1
      K2= IFINAL-3
      DO 10 I=K1,K2,2
      SUM4 = SUM4 + F(I)
 10   SUM2 = SUM2 + F(I+1)
      SUM = (H/3.0)*(F(IINT)+4.0*SUM4+2.0*SUM2+
     14.0*F(IFINAL-1) + F(IFINAL))
      RETURN
      END
C     ***********************************
```

```
C SUBROUTINE TO INTEGRATE NUMERICALLY BY TRAPEZOIDAL RULE
      SUBROUTINE TRAP(IINIT,IFINAL,ISIZE,Y,F,SUM)
      DIMENSION Y(ISIZE),F(ISIZE)
      I=IINIT
      SUM = 0.0
   10 SUM = SUM + 0.5*(Y(I+1)-Y(I))*(F(I+1)+F(I))
      IF(I.GE.(IFINAL-1)) GO TO 20
      I=I+1
      GO TO 10
   20 RETURN
      END
C     ***********************************
```

```
      FUNCTION FRZ(X,Y)
      COMMON R,HF,C
      D = HD(X,R,HF)
      D1 = HD1(X,R)
      D2 = HD2(X,R)
      C1 = C-1
      YOD = Y/D
      EXX = -D1*(-C+4.0*C1*YOD)/D**2.0
      EXY = 0.5*( 2.0*C1/D**2.0 + Y*D2*(-C+2.0*C1*YOD)/D**2.0
     1 - Y*D1**2.0*(-2.0*C+6.0*C1*YOD)/D**3.0)
      FRZ = SQRT(EXX**2.0+EXY**2.0)
      RETURN
      END
C     ***********************************
```

```
      FUNCTION SUM(Z,RINIT,RFINAL,N)
C THIS FUNCTION PROGRAM SUMS ACROSS ONE COLUMN BY SIMPSON S RULE
C A FUNCTION SUBPROGRAM CALLED FRZ IS USED WITH THIS PROGRAM
      FN=N
      H=(RFINAL-RINIT)/FN
      TWOH=H+H
      SUM4 = 0.0
      SUM2= 0.0
      R = RINIT + H
      I = 1
   10 SUM4 = SUM4 + FRZ(Z,R)
      SUM2 = SUM2 + FRZ(Z,(R+H))
      IF (I.GE.(N-3)) GO TO 20
      I = I+2
      R = R+TWOH
      GO TO 10
   20 SUM = (H/3.0)*(4.0*SUM4 + 2.0*SUM2 + FRZ(Z,RINIT)
     1    + 4.0*FRZ(Z,(RFINAL-H)) + FRZ(Z,RFINAL))
      RETURN
      END
C     ***********************************



      FUNCTION DOUBLE(Z1,R1,R2,N,N1)
      DIMENSION Z1(N1),R1(N1),R2(N1)
      H = Z1(2)-Z1(1)
      I = 1
      Z = Z1(I)
      RINIT = R1(I)
      RFINAL = R2(I)
      SUM1 = SUM(Z,RINIT,RFINAL,N)
      I = N
      Z = Z1(I)
      RINIT = R1(I)
      RFINAL = R2(I)
      SUMN = SUM(Z,RINIT,RFINAL,N)
      I = N+1
      Z = Z1(I)
      RINIT = R1(I)
      RFINAL = R2(I)
      SUMF = SUM(Z,RINIT,RFINAL,N)
      I = 2
      SUM4 = 0.0
      SUM2 = 0.0
   10 Z = Z1(I)
      RINIT = R1(I)
      RFINAL = R2(I)
      SUM4 = SUM4 + SUM(Z,RINIT,RFINAL,N)
      Z = Z1(I+1)
      RINIT = R1(I+1)
      RFINAL = R2(I+1)
      SUM2 = SUM2 + SUM(Z,RINIT,RFINAL,N)
      IF (I.GE.(N-2)) GO TO 20
      I = I+2
      GO TO 10
   20 DOUBLE = (H/3.0)*(SUM1 + 4.0*SUM4 + 2.0*SUM2 + 4.0*SUMN + SUMF)
      RETURN
      END
C     ***********************************
C     ***********************************
```

# APPENDIX D

## MODIFIED KASUGA'S ANALYSIS AND MODIFIED JOHNSON'S ANALYSIS

### Modified Kasuga's Analysis

The original analysis presented by Kasuga, et al. [60] assumed Coulomb friction at the die and punch surfaces. The analysis is rederived here assuming instead constant frictional stresses at these surfaces. The basic approach used by Kasuga, et al. is followed and the reader is referred to the original work [60] for further details.

The analysis approximates the circular die by a straight wedge shaped die (see Figure 21, Ref. [60]). Using the slab method, the equilibrium condition along the radial direction gives

$$p + g + s\frac{dp}{ds} - \left(\frac{\tau_4 - \tau_3}{\alpha}\right) = 0 \qquad (D.1)$$

where $p$ is the radial stress, $g$ is the circumferencial compressive stress, $\tau_3$ and $\tau_4$ are the constant frictional stresses at the die-material interface and punch-material interface respectively. From the von Mises yield criterion

$$p + g = 2\sigma_o/\sqrt{3} \qquad (D.2)$$

Substituting equation (D.2) in (D.1), integrating and applying the conditions

$$p = \sigma_t \quad \text{at} \quad s = s_o$$

$$p = p_e \quad \text{at} \quad s = s_e$$

yields

$$\frac{p_e}{2\sigma_o/\sqrt{3}} = \left[1 + \frac{m_3 - m_4}{2\alpha}\right] \ln\left(\frac{s_o}{s_e}\right) + \frac{\alpha}{2} + \frac{\sigma_t}{2\sigma_o/\sqrt{3}} \qquad (D.3)$$

where $\tau_3 = m_3 \sigma_o/\sqrt{3}$

$\tau_4 = m_4 \sigma_o/\sqrt{3}$

$\sigma_t$ is the back tension caused by radial drawing. $(\alpha/2)$ is added on to the right side of the above equation to account for redundant work due to shear deformation at the entrance and exit [60]. The punch load $(P_1)$ due to back tension $(\sigma_t)$ and ironing is

$$P_1 = p_e 2\pi R_p t_f + \tau_4 (s_o - s_e) 2\pi R_p$$

The component of punch load (P) due to ironing alone ( $\sigma_t = 0$), which is termed the ironing load, is given by

$$p''_h = \frac{P}{(2\pi R_p)(2\sigma_o/\sqrt{3})t_f} = \frac{p_e}{(2\sigma_o/\sqrt{3})} + \frac{m_4}{2t_f}\left[(R+t_o)^2 - (R+t_f)^2\right]^{1/2} \qquad (D.4)$$

$$\text{where} \quad \frac{p_c}{2\sigma_o/\sqrt{3}} = \left\{ 1 + \left( \frac{m_3 - m_4}{2\alpha} \right) \ln \left( \frac{t_o}{t_f} \right) + \frac{\alpha}{2} \right\}$$

$$\text{and} \quad \alpha = \tan^{-1} \sqrt{\frac{t_o - t_f}{2R + t_o + t_f}}$$

Non-dimensionalizing the above equation gives equation (4.33). It may be noted that the above expression does not account for friction at the die surface not included in the plastic zone. To avoid confusion, comparison of the results obtained with the proposed upper bound solution and with the modified Kasuga's analysis is made only when the die friction is zero.

## Modified Johnson's Analysis

Johnson [33] has presented an upper bound analysis for extrusion through a circular die. His solution is extended to an analysis of the ironing process. The deformation model assumed is shown in Figure 29. This model contains a single surface of velocity discontinuity $\Gamma$ and has no plastic zone unlike the proposed deformation model shown in Figure 28. In zone I, the body of the material has a rigid rotational motion about point O. In crossing surface $\Gamma$, it suffers a tangential velocity discontinuity. The resultant velocity in zone III is uniform and axial, and is equal to the velocity of the punch. Since there is no velocity discontinuity at the punch-material interface, the ironing load, according to this model, is independent of the interfacial friction at the punch.

An admissible hodograph or velocity diagram for this model is shown in Figure 29. From the Upper Bound Theorem

$$P\dot{U}_f = 2\pi R_f \left[ (\sigma_o/\sqrt{3})\, \widehat{AB}\, |\Delta v_r| + m_3 (\sigma_o/\sqrt{3})\, \widehat{AC}\, |\Delta v_d| \right] \qquad (D.5)$$

where $\Delta v_r$ is the velocity discontinuity at surface r, $\widehat{AB}$ is the arc length of surface r, $\Delta v_d$ is the velocity discontinuity at die surface and $\widehat{AC}$ is the arc length of the die surface as shown in Figure 29.

From the hodograph

$$\Delta v_r = \omega t_1 \quad , \quad \Delta v_d = \omega R$$

$$\text{also} \qquad \widehat{AB} = t_1 (\pi - 2\theta_1) \quad , \quad \widehat{AC} = \pi R/2$$

From the condition of volume constancy

$$\dot{U}_f t_f = \omega t_o (R + .5 t_o)$$

Substituting for $\omega$, $\Delta v_r$, $\Delta v_d$, $\widehat{AB}$, $\widehat{AC}$ in (D.5), the following expression for ironing load can be written

$$P_J^* = \frac{P}{(2\pi R_f)(2\sigma_o/\sqrt{3})t_f} = \frac{1}{t_o(R + .5t_o)} \left[ \frac{t_1^2}{2} (\pi - 2\theta_1) + m_3 \frac{\pi}{4} R^2 \right] \qquad (D.6)$$

From the geometry of the model

$$t_1 = \left( \frac{L_3^2}{2t_f} + \frac{t_f}{2} \right) \quad , \quad \theta_1 = \tan^{-1} \left( \frac{L_3}{t_f} \right)$$

$$\text{and} \qquad L_3 = \left[ (R + t_o)^2 - (R + t_f)^2 \right]^{1/2} \qquad (D.7)$$

# APPENDIX E

## UPPER BOUND ON EXTRUSION PRESSURE-AXISYMMETRIC EXTRUSION

An expression for upper bound on extrusion pressure can be derived as follows:

Flow Function

The flow function is assumed to be

$$\hat{\Phi}(r,z) = \pi R_o^2 \dot{U}_o \left[ -C^2 \left( r/R(z) \right)^2 + (C^2-1) \left( r/R(z) \right)^4 \right] \qquad (5.43)$$

where $C = \frac{R(L_1)}{R_o} = \frac{R(L_2)}{R_f}$

Boundaries of Plastic Zone II

Continuity across the boundary $r_i$ requires that this boundary be represented by equation

$$r_i : \qquad \hat{\Phi}(r,z) = -\pi r^2 \dot{U}_o \qquad (5.20)$$

Substituting for $\hat{\Phi}(r,z)$ from equation (5.43), and nondimensionlizing, the following equation for $r_i$ is obtained

$$\left.\begin{aligned} \rho &= \kappa_d \left[ \frac{C^2 - \kappa_d^2}{C^2-1} \right]^{1/2} \quad \text{for} \quad C \neq 1 \\ \text{and} \quad \xi &= \ell \qquad\qquad\quad \text{for} \quad C = 1 \end{aligned}\right\} \qquad (E.1)$$

where $r/R_o = \rho$, $R(z)/R_o = r_d$, $R(L_1)/R_o = C$, $r_f = \frac{R_f}{R_o}$

Proceeding in a similar manner, the following equation for the exit boundary $\Gamma_2$ is obtained

$$\left.\begin{aligned} \rho &= \frac{r_d}{r_f}\left[\frac{C^2 r_f^2 - r_d^2}{C^2 - 1}\right]^{1/2} \quad \text{for } C \neq 1 \\ \xi &= 0 \qquad\qquad\qquad\quad \text{for } C = 1 \end{aligned}\right\} \tag{E.2}$$

Velocity field for Zone II

$$\left.\begin{aligned} \dot{U}_r &= -\frac{1}{2\pi r}\frac{\partial \hat{\Phi}}{\partial z} \\ \dot{U}_z &= \frac{1}{2\pi r}\frac{\partial \hat{\Phi}}{\partial r} \end{aligned}\right\}$$

Substituting for $\hat{\Phi}(r,z)$ from equation (5.43), one obtains after simplification

$$\left.\begin{aligned} \dot{U}_r &= \dot{U}_o\left(-\frac{C^2\rho}{r_d} + 2(C^2-1)\frac{\rho^3}{r_d^3}\right)\frac{r_d'}{r_d^2} \\ \dot{U}_z &= \dot{U}_o\left(-\frac{C^2\rho}{r_d} + 2(C^2-1)\frac{\rho^3}{r_d^3}\right)\frac{1}{\rho r_d} \end{aligned}\right\} \tag{E.3}$$

Internal Power of Deformation:

In regions I and III, no deformation occurs and therefore no internal power of deformation is involved. In zone II, the power of deformation $\dot{W}_i$ is given by

$$\dot{W}_i = \frac{2}{\sqrt{3}} \sigma_o \iiint_V \sqrt{\tfrac{1}{2} \dot{\epsilon}_{ij} \dot{\epsilon}_{ij}} \, dV \qquad (E.4)$$

The strain rate components in terms of velocity components are given by relations

$$\dot{\epsilon}_{rr} = \frac{\partial \dot{U}_r}{\partial r} \;, \quad \dot{\epsilon}_{\theta\theta} = \frac{\dot{U}_r}{r} \;, \quad \dot{\epsilon}_{zz} = \frac{\partial \dot{U}_z}{\partial z}$$

$$\text{and} \quad \dot{\epsilon}_{rz} = \frac{1}{2}\left[ \frac{\partial \dot{U}_r}{\partial z} + \frac{\partial \dot{U}_z}{\partial r} \right] \;, \quad \dot{\epsilon}_{r\theta} = \dot{\epsilon}_{\theta z} = 0$$

Substituting for strain rate components in (E.4) and simplifying yields

$$\dot{W}_i = \left( \frac{4}{\sqrt{3}} \sigma_o \pi R_o^2 \dot{U}_o \right) G(r_d, \ell, r_f, C) \qquad (E.5)$$

$$\text{where} \quad G(r_d, \ell, r_f, C) = \int_{\xi} \int_{\rho} g(r_d, \rho, \xi, \ell, r_f, C) \, d\rho \, d\xi$$

$$\text{and} \quad g(r_d, \rho, \xi, \ell, r_f, C) = \rho \left[ \frac{1}{2} \left( \frac{r_d'}{r_d^2} \right)^2 \left\{ \left( -\frac{C^2}{r_d} + 6 \frac{(C^2-1)\rho^2}{r_d^3} \right)^2 + \right. \right.$$

$$\left(-\frac{c^2}{r_d}+2\frac{(c^2-1)\rho^2}{r_d^3}\right)^2+\left(-2\frac{c^2}{r_d}+8\frac{(c^2-1)\rho^2}{r_d^3}\right)^2\Bigg\}+\frac{1}{4}\,X$$

$$\left[\left(-\frac{c^2\rho}{r_d}+2\frac{(c^2-1)\rho^3}{r_d^3}\right)\frac{r_d''}{r_d^2}-\left(-3\frac{c^2\rho}{r_d^4}+10\frac{(c^2-1)\rho^3}{r_d^6}\right)r_d'^2+4\frac{(c^2-1)\rho}{r_d^4}\right]^2\Bigg]^{1/2} \tag{E.6}$$

The limit of integration is determined by shape of the die and the boundaries $r_1$ and $r_2$.

Shear Power Loss over Surfaces $r_1$ and $r_2$

Normal velocity across surfaces $r_1$ and $r_2$ is continuous but tangential velocity discontinuity exists, in general, along these surfaces. The power consumed ($\dot{W}_{S_{r_1}}$) along $r_1$ is no more than

$$\dot{W}_{S_{r_1}} = \int k\,|\Delta v_t|\,dA \tag{E.7}$$

k is the yield stress in shear. The velocity discontinuity along $r_1$ is

$$\Delta v_t = (\dot{U}_z + \dot{U}_0)\frac{dz}{ds} + \dot{U}_r\frac{dr}{ds}$$

Substituting for velocity components in equation (E.7), one obtains

$$\dot{W}_{S_{r_1}} = \frac{2}{\sqrt{3}}\sigma_0\,\pi R_0^2\,\dot{U}_0\,H_1(r_d, l, r_f, C) \tag{E.8}$$

where $$H_1 = \left|\int_{l}^{l_1}\left[\left(-\frac{c^2\rho}{r_d}+2\frac{(c^2-1)\rho^3}{r_d^3}\right)\frac{1}{r_d}+\rho\right]d\xi+\int_{1}^{0}\left(-\frac{c^2\rho}{r_d}+2\frac{(c^2-1)\rho^3}{r_d^3}\right)\frac{r_d'}{r_d^2}\rho\,d\rho\right|$$

and $L_1/R_o = \ell_1$ , $L/R_o = \ell$

Proceeding in a similar manner, one obtains following expression for shear power loss over surface $\Gamma_2$.

$$\dot{W}_{s\Gamma_2} = \frac{2}{\sqrt{3}} \sigma_o \pi R_o^2 \dot{U}_o H_2 \qquad (E.9)$$

$$\text{where } H_2 = \left| \int_0^{\ell_2} \left[ \left( -\frac{c^2\rho}{r_d} + 2(c^2-1)\frac{\rho^3}{r_d^3} \right) \frac{1}{r_d} + \frac{\rho}{r_f^2} \right] d\xi + \right.$$

$$\left. \int_{r_f}^{0} \left( -\frac{c^2\rho}{r_d} + 2(c^2-1)\frac{\rho^3}{r_d^3} \right) \frac{r_d'}{r_d^2} \rho \, d\rho \right| , \quad \frac{L_2}{R_o} = \ell_2$$

Friction Loss over Die Surface

The friction power loss ($\dot{W}_{s\Gamma_3}$) over the die surface is given by

$$\dot{W}_{s\Gamma_3} = \int \tau_3 |\Delta v_3| \, dA \qquad (E.10)$$

The velocity discontinuity is given by

$$\Delta v_3 = \left[ \dot{U}_r^2 + \dot{U}_z^2 \right]^{1/2} \Big|_{r = R(z)}$$

and the infinitesimal area dA by

$$dA = 2\pi r \left[ dr^2 + dz^2 \right]^{1/2} \Big|_{r = R(z)}$$

Assuming a constant interfacial friction stress ( $\tau_3 = m\sigma_0/\sqrt{3}$ ), the following expression for $\dot{W}_{S\tau_3}$ is obtained

$$\dot{W}_{S\tau_3} = \frac{2}{\sqrt{3}}\sigma_0 \pi R_0^2 \dot{U}_0 m H_3(z_d, \ell, z_f, C) \qquad (E.11)$$

where $$H_3 = (C^2-2)\left|\int_0^{\ell} \frac{1}{z_d}(1+z_d'^2)\, d\xi\right|$$

Upper Bound on Extrusion Pressure

Equating the external applied power to the total power expended in deformation, shear, and friction, one obtains for extrusion process

$$\pi R_0^2 \dot{U}_0 \bar{P} = \frac{4}{\sqrt{3}}\sigma_0 \pi R_0^2 \dot{U}_0 G + \frac{2}{\sqrt{3}}\sigma_0 \pi R_0^2 \dot{U}_0 (H_1 + H_2 + m H_3)$$

or

$$\frac{\bar{P}}{\sigma_0} = \frac{2}{\sqrt{3}}\left[2G(z_d, \ell, z_f, C) + H_1(z_d, z_f, \ell, C) + H_2(z_d, z_f, C) + m H_3(z_d, \ell, z_f, C)\right] \qquad (E.12)$$

where G, $H_1$, $H_2$, and $H_3$ are given by the equations (E.6), (E.8), (E.9) and (E.10) respectively. For C = 1, the above expression reduces to equation (5.49).

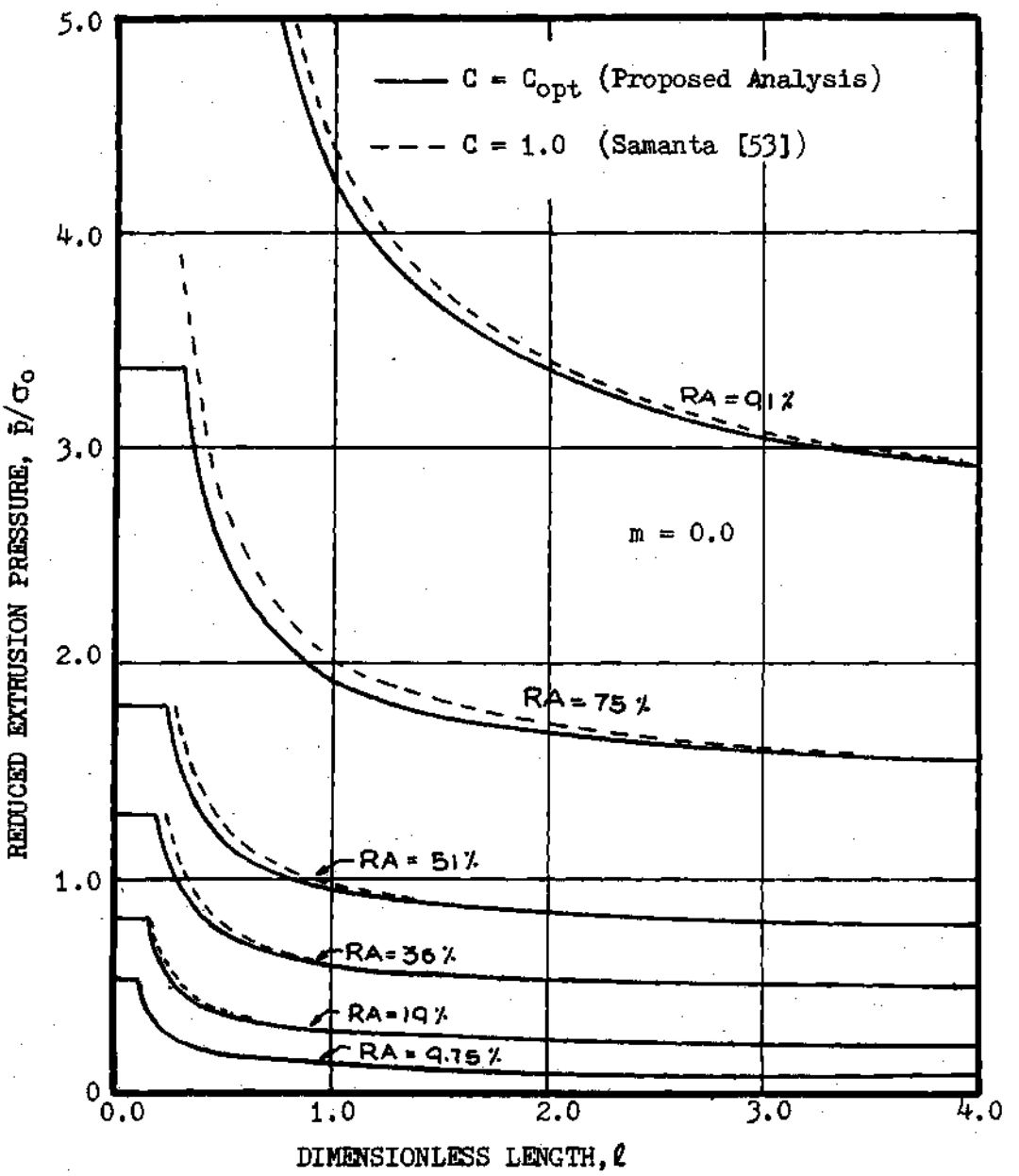


Figure 58. Effect of Dimensionless Length ($\ell$) on Reduced Extrusion Pressure in Extrusion through Convex Die, m = 0.0

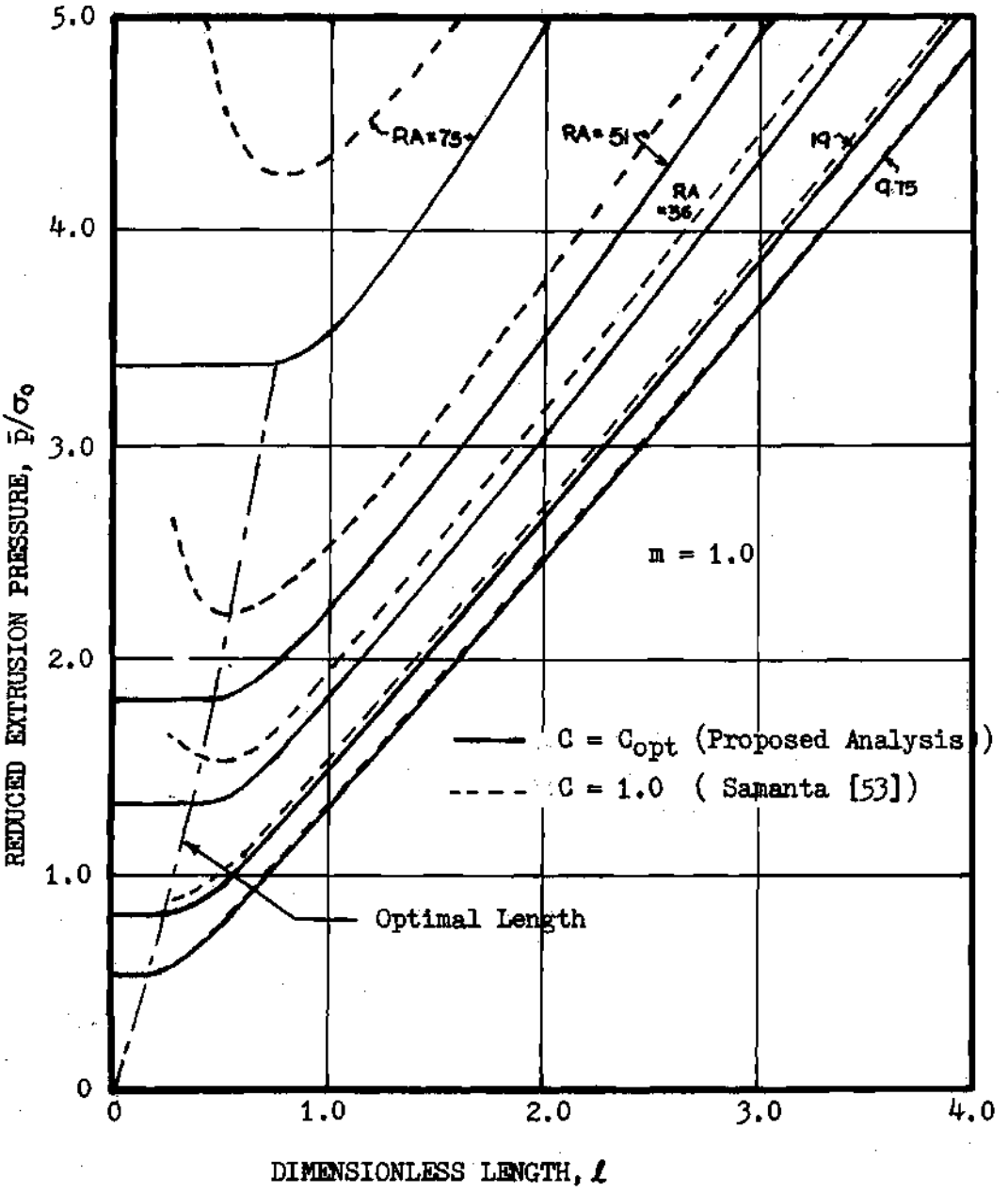


Figure 59. Effect of Dimensionless Length ($\ell$) on Reduced Extrusion Pressure in Extrusion through Convex Die, m = 1.0

# APPENDIX F

## UPPER BOUND ON FORGING PRESSURE - PLANE STRAIN FORGING

### Model I

Model I is shown in Figure 12c. No dead zone is assumed and the flow function for zone I is assumed to be

$$\Phi(x,y) = \frac{\dot{U}}{g(t)} x\, g(y) \tag{F.1}$$

Velocity field in zone I:

$$\left.\begin{aligned} \dot{U}_x &= \frac{\partial \Phi}{\partial y} = \frac{\dot{U}}{g(t)} x\, g'(y) \\ \dot{U}_y &= -\frac{\partial \Phi}{\partial x} = -\frac{\dot{U}}{g(t)} g(y) \end{aligned}\right\} \tag{F.2}$$

Strain rates in zone I:

$$\dot{\epsilon}_{xx} = \frac{\partial \dot{U}_x}{\partial x} = \frac{\dot{U}}{g(t)} g'(y)$$

$$\dot{\epsilon}_{yy} = \frac{\partial \dot{U}_y}{\partial y} = -\frac{\dot{U}}{g(t)} g'(y) = -\dot{\epsilon}_{xx} \tag{F.3}$$

$$\dot{\epsilon}_{xy} = \frac{1}{2}\left(\frac{\partial \dot{U}_x}{\partial y} + \frac{\partial \dot{U}_y}{\partial x}\right) = \frac{1}{2}\frac{\dot{U}}{g(t)} x\, g''(y)$$

$$\dot{\epsilon}_{xz} = \dot{\epsilon}_{yz} = \dot{\epsilon}_{zz} = 0$$

The incompressibility condition ($\dot{\epsilon}_{xx} + \dot{\epsilon}_{yy} = 0$) is satisfied. The shear strain should be zero at $y = 0$, this requires

$$g''(y) = 0 \quad \text{at} \quad y = 0 \tag{F.4}$$

Internal power of deformation, $\dot{W}_i$:

$$\dot{W}_i = \frac{2}{\sqrt{3}}\sigma_0 \int_V \sqrt{\tfrac{1}{2}\dot{\epsilon}_{ij}\dot{\epsilon}_{ij}}\, dV$$

Substituting for strain rates and simplifying, one obtains

$$\dot{W}_i = \frac{4\sigma_0}{\sqrt{3}} \frac{\dot{U}}{g(t)} \left| \int_0^t g''(y) \left[ \int_0^w \left[ 4 \frac{g'^2(y)}{g''^2(y)} + x^2 \right]^{1/2} dx \right] dy \right| \tag{F.5}$$

Integrating and simplifying yields

$$\dot{W}_i = \frac{2\sigma_0}{\sqrt{3}} \frac{\dot{U}}{g(t)} \left| \int_0^t g''(y) \left\{ w \left[ 4 \frac{g'^2(y)}{g''^2(y)} + w^2 \right]^{1/2} + 4 \frac{g'^2(y)}{g''^2(y)} \ln \left| \frac{w + \left[ 4 \frac{g'^2(y)}{g''^2(y)} + w^2 \right]^{1/2}}{2 \frac{g'(y)}{g''(y)}} \right| \right\} dy \right| \tag{F.6}$$

Friction loss between platens and strip, $\dot{W}_f$:

$$\dot{W}_f = \int \tau_p |\Delta v| \, ds$$

Assuming constant interfacial friction stress ($\tau_p = m_p \sigma_o/\sqrt{3}$) and substituting for tangential velocity discontinuity $\Delta v$ which in this case is equal to $\dot{U}_x$, one obtains

$$\dot{W}_f = \frac{4}{\sqrt{3}} m_p \sigma_o \int_0^{\omega} |\dot{U}_x|_{y=t} \, ds$$

Substituting for $\dot{U}_x$ and integrating yields

$$\dot{W}_f = \frac{2\dot{U}}{\sqrt{3}} \sigma_o \, m \, \omega^2 \left| \frac{g'(t)}{g(t)} \right| \tag{F.7}$$

External power supplied by platens, J:

$$J = 4 \omega p_{av} \dot{U} \tag{F.8}$$

Upper bound on forging pressure, $p_{av}$:

By equating the external power with the internal power of deformation plus friction loss, one obtains the following equation for $p_{av}$ after simplification

$$\frac{p_{av}}{(2/\sqrt{3})\sigma_o} = \frac{1}{4}\left[ \frac{1}{g(t)} \int_0^t g''(y) \left\{ \left[ 4 \frac{g'^2(y)}{g''^2(y)} + \omega^2 \right]^{1/2} + \right. \right. \tag{F.9}$$

$$\left. \left. \frac{4}{\omega} \frac{g'^2(y)}{g''^2(y)} \ln \left| \frac{\omega + \left[ 4 \frac{g'^2(y)}{g''^2(y)} + \omega^2 \right]^{1/2}}{2 \frac{g'(y)}{g''(y)}} \right| \right\} dy + m_p \omega \left| \frac{g'(t)}{g(t)} \right| \right]$$

where $g(y) = 0$ at $y = 0$

$g''(y) = 0$ at $y = 0$

An approximate but simpler expression for $p_{av}$ can be obtained as follows: Since the shear strain is usually less than the normal strain throughout most of the deforming zone, equation (F.5) may be written as

$$\dot{W}_i = \frac{2}{\sqrt{3}} \sigma_o \frac{\dot{U}}{g(t)} \iint g'(y) \left[ 1 + \frac{1}{2} \frac{g''^2(y)}{4 g'^2(y)} x^2 - \frac{1}{8} \left( \frac{g''^2(y)}{4 g'^2(y)} x^2 \right)^2 + - - - - - \right] dx\, dy$$

$$\text{provided } \frac{\omega^2}{4} \frac{g''^2(y)}{g'^2(y)} < 1$$

Neglecting terms of $\frac{x^2}{4}\left[\frac{g''(y)}{g'(y)}\right]^2$ of order higher than unity which maintains the upper bound property, and integrating, one obtains

$$\dot{W}_i = \frac{8\sigma_o}{\sqrt{3}} \dot{U} \omega + \frac{1}{3\sqrt{3}} \sigma_o \dot{U} \frac{\omega^3}{g(t)} \int_0^t \frac{g''^2(y)}{g'(y)} dy \qquad \text{(F.10)}$$

Equating the external power with the internal power of deformation given by equation (F.10) plus friction loss yields

$$\frac{p_{av}}{(2/\sqrt{3})\sigma_o} = \left| 1 + \frac{\omega^2}{24\, g(t)} \int_0^t \frac{g''^2(y)}{g'(y)} dy \right| + \frac{m_\rho}{4} \omega \left| \frac{g'(t)}{g(t)} \right|, \quad \left(\text{provided } \frac{\omega^2}{4} \frac{g''^2(y)}{g'^2(y)} < 1\right) \qquad \text{(F.11)}$$

## Model II

Deformation model II for plane strain forging assumes the formation of a dead zone at the platen surfaces. The model is shown in Figure 54. The flow function for zone I is chosen to be

$$\Phi(x,y) = a_o(a+bx)y \tag{F.12}$$

where $a_o$, a and b are constants. The velocity field for zone I is

$$\left.\begin{aligned} \dot{U}_x &= \frac{\partial \Phi}{\partial y} = a_o(a+bx) \\ \dot{U}_y &= -\frac{\partial \Phi}{\partial x} = -a_o b y \end{aligned}\right\} \tag{F.13}$$

The strain rates are

$$\left.\begin{aligned} \dot{\epsilon}_{xx} &= a_o b \\ \dot{\epsilon}_{yy} &= -a_o b \end{aligned}\right\} \tag{F.14}$$

$$\dot{\epsilon}_{xy} = \dot{\epsilon}_{yz} = \dot{\epsilon}_{xz} = \dot{\epsilon}_{zz} = 0$$

The dead zone surface $\Gamma$ is given by equation (6.4) as

$$a_o(a+bx)y_\Gamma = \dot{U}x \tag{F.15}$$

$\Gamma$ passes through points (0,0) and (w,t) which gives

$$a_o = \frac{\dot{U}\,\omega}{(a+b\omega)t} \tag{F.16}$$

The internal power of deformation for zone I is

$$\dot{W}_i = \frac{2}{\sqrt{3}}\,\sigma_o \iint \sqrt{\tfrac{1}{2}\,\dot{\epsilon}_{ij}\,\dot{\epsilon}_{ij}}\;dx\,dy$$

Substituting for strain rates yields upon simplification

$$\dot{W}_i = \frac{8\sigma_o}{\sqrt{3}}\,a_o\,b \int_0^{\omega}\int_0^{y_\Gamma} dy\,dx \tag{F.17}$$

By substituting for $y_\Gamma$ from equation (F.15) and integrating, one obtains

$$\dot{W}_i = \frac{8\sigma_o}{\sqrt{3}}\,\dot{U}\left[\omega - \frac{a}{b}\ln\left(1+\frac{b}{a}\omega\right)\right] \tag{F.18}$$

The shear power loss due to tangential velocity discontinuity along $\Gamma$ is

$$\dot{W}_f = \frac{\sigma_o}{\sqrt{3}}\int_\Gamma |\Delta v|\,ds$$

$$= \frac{4\sigma_o}{\sqrt{3}}\left[\int_0^{\omega}\dot{U}_x\,dx + \int_0^{t}(\dot{U}+\dot{U}_y)\,dy\right]$$

Substituting for $\dot{U}_x$ and $\dot{U}_y$, and integrating gives

$$\dot{W}_f = \frac{4\sigma_o}{\sqrt{3}}\left[a_o\left(a\omega + \frac{b\omega^2}{2}\right) + \dot{U}t - \frac{a_o}{2}bt^2\right] \qquad (F.19)$$

Again equating external power to internal power of deformation plus friction loss and simplifying yields

$$\frac{P_{av}}{(2/\sqrt{3})\sigma_o} = 1 - \frac{1}{\omega}\frac{a}{b}\ln\left(1 + \frac{b\omega}{a}\right) + \frac{1}{2}X$$

$$\left[\frac{\omega}{t}\frac{\left(a + \frac{b}{2}\omega\right)}{a + b\omega} + \frac{t}{\omega} - \frac{bt}{2(a+b\omega)}\right] \qquad (F.20)$$

By substituting $\left(B = \frac{a}{b\omega}\right)$ in the above equation, one obtains equation (6.26).

# BIBLIOGRAPHY


1. Hill, R., The Mathematical Theory of Plasticity, Oxford University Press, London, 1950.

2. Hencky, H., "Ueber einige statisch bestimmte faelle des Gleichgewichts in plastischen Koerpern," Z. Angew. Math. Mechanik, Vol. 3, 1923, pp. 241-251.

3. Geiringer, H., "Fondements mathematiques de la theorie des corps plastiques isotropes," Memorial Sci. Math., No. 86, Gauthiers-Villars, Paris, 1937.

4. Oxley, P. L. B., and Palmer, W. B., "Mechanics of Orthogonal Machining," Proc. Instn. Mech. Engrs., 173, 1959, p. 623.

5. Hill, R., "A Theoretical Analysis of Stresses and Strains in Extrusion and Piercing," Journal of the Iron and Steel Institute, Vol. 158, 1948, pp. 177-185.

6. Thomsen, E. G., Yang, C. T., and Kobayashi, S., Mechanics of Plastic Deformation in Metal Processing, Macmillan, New York, 1965.

7. Ishlinsky, A., Prikladnaia Matematika i Mekhanika, 8, 1944, p. 201.

8. Shield R. T., "On the Plastic Flow of Metals Under Conditions of Axial Symmetry," Proc. R. Soc., A, 233, 1955, p. 267.

9. Thomsen, E.G., and Lapsley, J.T., Jr., "Experimental Stress Determination Within a Metal During Plastic Flow," Proceedings of the Society of Experimental Stress Analysis, Vol. 11, 1954, pp. 59-68.

10. Thomsen , E. G., Yang, C. T., and Bierbower, J. B., "An Experimental Investigation of the Mechanics of Plastic Deformation in Metals," University of California Publication in Engineering, Vol. 5, 1954, pp. 89-144.

11. Shabaik, A., and Kobayashi, S., "Computer Application to the Visioplasticity Method," Journal of Engineering for Industry, Trans. ASME, Series B, Vol. 89, No. 2, May 1967, pp. 339-346.

12. Sachs, G., Spanlose Formung der Metalle, Springer Verlag, Berlin, 1931.

13. Siebel, E., Die Formgebung im bildsamen Zustande, Verlag Stahleisen Duesseldorff, 1932.

14. Kobayashi, S., "Theories and Experiments on Friction, Deformation, and Fracture in Plastic Deformation Processes," Metal Forming ; Interrela-

tion Between Theory and Practice, Plenum Press, New York, 1971, pp. 325-347.

15. Gorden, J. L., and Weinstein, A. S., "A Finite Element Analysis of the Plane Strain Drawing Problem," Proceedings of The North American Metalworking Research Conference, University of Wisconsin at Madison, May 1974, pp. 194-208.

16. Avitzur, B., Metal Forming: Processes and Analysis, McGraw-Hill Book Company, New York, 1968.

17. Prager, W., and Hodge, P. G., Theory of Perfectly Plastic Solids, John Wiley and Sons, Inc., 1951.

18. Drucker, D. C., Greenberg, H. J., and Prager, W., "The Safety Factor of an Elastic-Plastic Body in Plane Strain," Trans. ASME, Journal of Applied Mechanics, 73, 1951, p. 371.

19. Drucker, D. C., Prager, W., and Greenberg, H. J., "Extended Limit Design Theorems for Continuous Media," Quarterly of Applied Mathematics, Vol. 9, 1952, pp. 381-389.

20. Kobayashi, S., and Thomsen, E. G., "Upper and Lower Bound Solutions to Axisymmetric Compression and Extrusion Problems," International Journal of Mechanical Science , Vol. 7, 1965, p. 127.

21. Hill, R., "On the State of Stress in a Plastic-Rigid Body at the Yield Point," Philosophical Magazine, Vol. 42, 1951, p. 868.

22. Hill, R., "A Variational Principle of Maximum Plastic Work in Classical Plasticity," Quarterly Journal of Mechanics and Applied Mathematics, Vol. 1, 1948, p. 18.

23. Green, A. P., "A Theoretical Investigation of the Compression of a Ductile Material Between Smooth Flat Dies," Philosophical Magazine, Vol. 42, 1951, pp. 900-918.

24. Johnson, W., "Over-Estimates of Load for Some Two-Dimensional Forging Operations," Proceedings of The Third U.S. Congress of Applied Mechanics, 1958, pp. 571-579.

25. Johnson, W., "Estimation of Upper Bound Loads for Extrusion and Coining Operations," Proceedings of The Institution of Mechanical Engineers, Vol. 173, 1959, p. 61.

26. Johnson, W., Mellor, P. B., and Woo, D. M., "Single-Hole Staggered and Multi-Hole Extrusion," J. Mech. Phys. Solids, Vol. 6, 1958, p. 203.

27. Kudo, H., "An Upper Bound Approach to Plane Strain Forging and Extrusion," Parts I, II and III, Intern. J. Mech. Sci., Vol. 1, p. 57, p. 229, p. 366, 1960.

28. Lambert, E. R., Mehta, H. S., and Kobayashi, S., "A New Upper Bound Method for Analysis of Some Steady-State Plastic Deformation Processes," Paper No 68-WA/ Prod-10, Trans. ASME, 1968.

29. Kudo, H., "Some Analytical and Experimental Studies of Axisymmetric Cold Forging and Extrusion-I," International Journal of Mechanical Sciences, Vol. 2, 1960, pp. 102-127.

30. Kobayashi, S., "Upper-Bound Solutions of Axisymmetric Forming Problems," Part II, Journal of Engineering for Industry, Vol. 86, 1964, pp. 326-332.

31. Stepanskii, L. G., "The Boundaries of the Area of Plastic Deformation in Extrusion," Russian Engineering Journal , Vol. 43, No. 9, 1963, pp. 40-42.

32. Zimerman, Z., and Avitzur, B., "Metal Flow through Conical Converging Dies - A Lower Upper Bound Approach Using Generalized Boundaries of the Plastic Zone," Journal of Engineering for Industry, Vol. 92, 1970, pp. 119-129.

33. Johnson, W., "Upper Bound Loads for Extrusion through Circular Dies," Appl. Sci. Res., Series A, Vol. 7, 1958, p. 437.

34. Chen, P. C. T., and Ling. F. F., "Upper Bound Solutions to Axisymmetric Extrusion Problems," Intern. J. Mech. Sci., Vol. 10, 1968, p. 863.

35. Chen, P. C. T., "Upper Bound Solutions to Plane Strain Extrusion Problems," Journal of Engineering for Industry, 1970, p. 158.

36. Chang, K. T., and Choi, J. C., "Upper Bound Solutions to Extrusion Problems through Curved Dies," Proceedings of the 12th Midwestern Mechanics Conference, University of Notre Dame, Aug. 1971.

37. Green, A. P., and Hill, R. "Calculation on the Influence of Friction and Die Geometry in Sheet Drawing," J. Mech. Phys. Solids, Vol. 1, 1952, p. 31.

38. Avitzur, B., Fueyo, J., and Thompson, J. R., "Analysis of Plastic Flow through Inclined Planes in Plane Strain," J. of Eng. for Ind., Trans. ASME, Vol. 89, 1967, pp. 361-375.

39. Shabaik, A., Kobayashi, S., and Thomsen, E. G., "Application of Potential Flow Theory to Plane Strain Extrusion," Journal of Engineering for Industry, Vol. 89, 1967, pp. 503-513.

40. Sokolovskii, V. V., "Complete Plane Problems of Plastic Flow," J. Mech. Phys. Solids, Vol. 10, 1962, p. 353.

41. Johnson, W., and Hillier, M. J., "Plane Strain Extrusion through

Partly Rough Dies," Int. J. Mech. Sci., Vol. 5, 1963, p. 191.

42. Kronsjö, L. I., and Mellor, P. B., "Plane Strain Extrusion through Concave Dies," International Journal of Mechanical Sciences, Vol. 8, 1966, p. 515.

43. Sowerby, R., Johnson, W., and Samanta, S. K., "Plane Strain Drawing and Extrusion of a Rigid-Perfectly Plastic Material through Concave Dies," Int. J. Mech. Sci., Vol. 10, 1968, p. 231.

44. Samanta, S. K., "Slip-Line Field for Extrusion through Cosine-Shaped Dies," J. Mech. Phys. Solids, Vol. 18, 1970, pp. 311-318.

45. Richmond, O., and Devenpeck, M. L., "A Die Profile for Maximum Efficiency in Strip Drawing," Proc. 4th U.S. Congr. Appl. Mech., ASME, 1962, p. 1053.

46. Sortais, H. C., and Kobayashi, "An Optimum Die Profile for Axisymmetric Extrusion," Int. J. Mach. Tool Des. Res., Vol. 8, 1968, p. 61.

47. Richmond, O., and Morrison, H. L., "Streamlined Wire Drawing Dies of Minimum Length," J. Mech. Phys. Solids, Vol. 15, 1967, pp. 195-203.

48. Yang, C. T., "The Upper-Bound Solution as Applied to Three Dimensional Extrusion and Piercing Problems," Journal of Engineering for Industry, Trans. ASME, 1962, pp. 397-404.

49. Halling, J., and Mitchell, L. A., "The Solution of Axisymmetric Plastic Deformation Problems from Equilibrium Force Diagram Consideration and the Application of the Method to the Extrusion Process," The Inter. J. of Prod. Research, Vol. 4, 1965, p. 141.

50. Avitzur, B., "Analysis of Wire Drawing and Extrusion through Conical Dies of Small Cone Angle," J. of Eng. Ind., Trans. ASME, Vol. 85, 1963, pp. 86-96.

51. Avitzur, B., "Analysis of Wire Drawing and Extrusion through Conical Dies of Large Cone Angle," J. of Eng. Ind., Trans. ASME, 1964, pp. 305-316.

52. Lambert, E. R., "A New Upper Bound Approach to the Mechanics of Plastic Flow through Converging Dies," Ph.D. Dissertation, University of California, Berkeley, June 1967.

53. Samanta, S. K., "A New Die Profile with High Process Efficiency," Appl. Sci. Res., Vol. 25, 1971, pp. 54-64.

54. Chung, S. Y., and Swift, H. W., "Cup Drawing from a Flat Blank; Part I-Experimental Investigation; Part II - Analytical Investigation," Proc. Instn. Mech. Engrs., Vol. 165, 1951, p. 199.

55. Chiang, D., and Kobayashi, S., "The Effect of Anisotrophy and Work-Hardening Characteristics on the Stress and Strain Distribution in Deep Drawing," Journal of Engineering for Industry, Trans. ASME, 1966, pp. 443-448.

56. Ray, R., and Berry, J. T., "Prediction of Press Loads in Deep Drawing Ti-6AL-4V, 304 Stainless and Inconel X Under Various Conditions of Lubrication at Room Temperature," J. of Eng. Ind., Vol. 92, 1970, p. 413.

57. Berry, J. T., and Pope, M. H., "Force Requirements and Friction in Warm Working Operations," Metal Forming; Interrelation Between Theory and Practice," Plenum Press, New York, 1971, pp. 307-325.

58. Barlow, D. A., "The Formability of Aluminum Alloys," Engineering, Vol. 181, 1956, p. 329, 366, 393.

59. Alexander, J. M., "An Appraisal of the Theory of Deep Drawing," Metallurgical Reviews, Vol. 5, 1960, p. 349.

60. Yasuo Kasuga, Ichizo Otoda and Ryozo Sugiyama, " Investigation into the Deep Drawing with Particular Consideration of Simultaneous Ironing," La Metallurgia Italiana, n. 8, 1968, pp. 745-756.

61. Prandtl, L., "Anwendungsbeispiele Zu einem Henckyschen satz über das Plastische Gleichgewicht," Z. Angew. Math. Mech., Vol. 3, 1923, pp. 401-406.

62. Hill, R., Lee, E. H., and Tupper, S. J., "A Method of Numerical Analysis of Plastic Flow in Plane Strain and Its Application to the Compression of a Ductile Material Between Rough Plates, " Trans. ASME, J. Appl. Mech., Vol. 18, 1951, pp. 46-52.

63. Alexander, J. M., "The Effect of Coulomb Friction in the Plane Strain Compression of Plastic-Rigid Material," J. Mech. Phys. Solids, Vol. 3, 1955, pp. 233-245.

64. Bishop, J. F. W., "On the Effect of Friction on Compression and Indentation Between Flat Dies," Journal of Mechanics and Physics of Solids, Vol. 6, 1958, pp. 132-144.

65. Kulkarni, K. M., and Kalpakjian, S., "A Study of Barreling as an Example of Free Deformation in Plastic Working," Trans. ASME, Dec. 1968, Paper No. 68-WA/Prod-6.

66. Siebel, E., "The Application of Shaping Processes of Hencky's Laws of Equilibrium," Journal of Iron and Steel Institute, Vol. 155, 1947, pp. 526-534.

67. Stone, M., and Greenberger, J. L., "Rolling Pressures in Strip Mill," Iron Steel Engr., Vol. 20, 1943, p. 61.

68. Hoffman, O., and Sachs, G., Introduction to the Theory of Plasticity for Engineers, McGraw Hill, New York, Chapter 21, pp. 240-245.

69. Liu, J. Y., "Upper-Bound Solutions of Some Axisymmetric Cold Forging Problems," J. Eng. Ind., Trans. ASME, Vol. 93, 1971, pp. 1134-1144.

70. Johnson, W., Sowerby, R., and Haddow, J. B., "Plane-Strain Slip-Line Fields: Theory and Bibliography," American Elsevier Publishing Co., Inc., New York, 1970.

71. Kachanov, L. M., Foundations of the Theory of Plasticity, (English Translation from the Second Edition), American Elsevier Publishing Company, Inc., New York, 1971.

72. Bachrach, B. I., and Samanta, S. K., "Plane Strain Sheet and Tube Extrusion through Cosine-Shaped Dies with Friction," Proceedings of the Second North American Metalworking Research Conference, University of Wisconsin at Madison, May 1974, pp. 179-193.

73. Devenpeck, M. L., "Experimental Evaluation of Theoretically Ideal Drawing Dies," Metal Forming; Interrelation Between Theory and Practice, Plenum Press, New York, 1971, pp. 215-234.

74. Alexander, J. M., and Whitlock, B. C., "Extrusion of a Bi-Metallic Strip from Separate Containers," Appl. Mech. Conv., Proc. Instn. Mech. Engrs., 1965-1966, Vol. 180, pt. 3I, p. 250.

75. Tirosh, J., "On the Dead-Zone Formation in Plastic Axially-Symmetric Converging Flow," J. Mech. Phys. Solids, Vol. 19, 1971, p. 39.

76. Nadai, A., Theory of Flow and Fracture of Solids, Volume I, Second Edition, McGraw-Hill Book Company, Inc., New York, 1950, Chapters 20 and 37.

77. Fung, Y. C., Foundations of Solid Mechanics, Prentice-Hall, Inc., Englewood Cliffs, New Jersey, 1965.

78. Shabaik, A. H., and Thomsen, E. G., "Flow Studies in Extrusion," CIRP Annals, 1969.

79. Sohrabpour, S., Shabaik, A. H., and Thomsen, E. G., "Local Friction Coefficients in Axisymmetric Extrusions of Aluminum," Journal of Engineering for Industry, Trans. ASME, 1970, pp. 461-468.

80. Dorn, W. S., and McCracken, D. D., Numerical Methods with Fortran IV Case Studies, John Wiley & Sons, Inc., New York, 1972.

81. Schey, J. A., Metal Deformation Processes: Friction and Lubrication, Marcel Dekker Inc., New York, 1970.

82. И.Я. ТАРНОВСКИЙ, et al., " ДЕФОРМАЦИИ И УСИЛИЙ ПРИ ОБРАБОТКЕ

МЕТАЛЛОВ ДАВЛЕНИЕМ," МОСКВА, 1959.

83. Tarnovskii, I. Ya., Pozdeyev, A. A., and Lyashkov, V. B., Deformation of Metals During Rolling, Pergamon Press, New York, 1965.

84. Kobayashi, S., "Upper-Bound Solutions of Axisymmetric Forming Problems - I," Trans. ASME, Journal of Engineering for Industry, May 1964, pp. 122-126.

85. Gerald, C. F., Applied Numerical Analysis, Addison-Wesley Publishing Company, Reading, Massachusetts, 1970.

86. Collins, I. F., "The Upper Bound Theorem for Rigid-Plastic Solids Generalized to Include Coulomb Friction," J. Mech. Phy. Solids, Vol. 17, 1969, pp. 323-327.

# VITA

Vijay Nagpal was born in Amritsar, India, on October 4, 1944, the son of Mr. and Mrs. Devki N. Nagpal. He attended elementary School in Amritsar and passed the Matriculation examination at the Cambridge School, Amritsar. Vijay attended Hindu College from 1958 to 1960 where he was awarded an Intermediate degree. He attended Panjab Engineering College, Chandigarh, India, from 1960 to 1964, where he was awarded the degree Bachelor of Science in Mechanical Engineering with honor in March, 1964. During the fall of 1969 Vijay entered the Graduate Division of the Georgia Institute of Technology, Atlanta, and began graduate work in the School of Mechanical Engineering. In December, 1970, he received a M.S. in Mechanical Engineering and continued his work towards a Doctor of Philosophy in the School of Mechanical Engineering.

After graduating in 1964, Vijay joined Tata Engineering and Locomotive Company (TELCO), Jamshedpur, India, as a graduate trainee. Upon completion of his training in 1966, he was appointed Assistant Engineer in the tool room of TELCO's General Engineering Division, where he worked till 1969. Vijay worked with Livsey and Company, Charlotte from July 1971 to March 1972. During graduate studies he worked as a graduate teaching and research assistant, teaching undergraduate courses and laboratories in Materials and Design areas.

Mr. Vijay Nagpal married, in May 1969, the former Kamini Khanna, daughter of Mr. and Mrs. Kesho R. Khanna of Amritsar. The Nagpals have a three year old daughter, Radhika.